**Design of 3D-Printed, Micropatterned Scaffolds for
Tissue Engineering of Bone-Ligament Constructs
in the Oral Cavity using Gene Therapy**

by

Sophia Patricia Pilipchuk

A dissertation submitted in partial fulfillment
of the requirements for the degree of
Doctor of Philosophy
(Biomedical Engineering)
in the University of Michigan
2018

Doctoral Committee:

        Professor William V. Giannobile, Chair
        Professor Scott J. Hollister
        Professor David H. Kohn
        Adjunct Clinical Associate Professor Hector F. Rios

Sophia Patricia Pilipchuk

spilipch@umich.edu

ORCID iD: 0000-0002-5028-3956

To my mother –

I dedicate this work to you,
for everything you've seen me through
With wisdom, intellect, and grace,
the endurance of your warm embrace

No words created can quite convey
the debt of gratitude that's needed to repay
For all the time, the effort, and the pains
you have taken to help me make my gains

Your understanding, selfless love, and kindness
have been an anchor with endless guidance

Your presence and soft smile I hold so very dear
Forgive my humble gratitude, but know it is sincere:

Thank you.

– S.P.

⚓

Post scriptum:

Early in my graduate career, I was asked by my alma mater's BME newsletter spotlighting recent alumni why I had chosen to pursue graduate studies. Part of my response was: "Ultimately, I strive to make a worthwhile contribution to the field of regenerative medicine and its potential for widespread application in disease treatment."

My hope is that, in some small way, I was able to make a contribution to the field that will help push forward novel clinical applications of scaffolds for improved and more predictable patient treatment, whether it be in dentistry or related fields. More importantly, I hope that this dissertation and its contents will be of use to future students and researchers who will pave the way forward to new discoveries that will benefit human health and well-being.

TABLE OF CONTENTS

CHAPTER 3: SINGLE PATIENT CASE STUDY USING 3-D PRINTED BIORESORBABLE SCAFFOLD FOR PERIODONTAL REPAIR………………………..62

CHAPTER 4: INTEGRATION OF 3D-PRINTED AND MICROPATTERNED POLYCAPROLACTONE SCAFFOLDS FOR GUIDANCE OF ORIENTED COLLAGENOUS TISSUE FORMATION *IN VIVO*………………………………... 73

List of Figures

List of Tables

ABSTRACT

Periodontitis is a leading chronic oral inflammatory disease and primary cause of permanent tooth loss estimated to affect 47.2% of adults in the United States. Damage to the tooth-supporting apparatus, which includes periodontal ligament (PDL) fibers that anchor the tooth root to alveolar bone, subsequently initiates osseous tissue resorption. Multi-tissue morbidity is a significant challenge given lack of predictability in reconstructing tissues with physiologic functionality native to healthy periodontium. Tissue engineering strategies have potential to address existing deficiencies in clinically-induced regeneration through combinational approaches using biomaterials, growth factors, and cell-based therapy. The purpose of this work was to develop scaffolds incorporating micropatterned topography for guidance of cell growth and periodontal tissue formation, in conjunction with localized, spatiotemporally-controlled growth factor delivery via gene therapy vectors.

Micropatterned polycaprolactone (PCL) films were designed to assess PDL cell orientation *in vitro,* with incorporation of the patterned film into a 3D-printed PCL scaffold for evaluation of varying topography on oriented tissue formation in an ectopic murine model. Specifically, pillars with varying groove depths (30um, 10um) and groove widths (15um, 60um) were used for the scaffold "PDL" region in combination with human PDL (hPDL) cell seeding, while the 3D-printed base served as a region for osseous tissue formation via delivery of human gingival fibroblasts (hGFs) transduced with adenoviral bone morphogenetic protein (Ad-BMP7). Micropatterned films with pillars containing deeper grooves (30um) provided greater control over hPDL cell orientation and subsequent alignment of soft collagenous tissue compared to non-grooved pillars or an amorphous PCL film, with significant ($p<0.05$) differences in percentage of aligned cells *in vivo* observed at 6 weeks post-implantation.

In order to improve spatially-controlled delivery of BMP7 and platelet-derived growth factor (PDGF-BB) using developed 3D-printed, micropatterned scaffolds, each region of the scaffold was separately immobilized with AdBMP7 and AdPDGF-BB, respectively, using

chemical vapor deposition (CVD)-based surface modification prior to cell seeding. A separate scaffold was developed for a rat fenestration defect, with the 3D-printed scaffold region replaced by an amorphous PCL film to accommodate the 0.5mm defect thickness. Evaluation of these cell-seeded scaffolds showed significant ($p < 0.05$) bone formation in regions with immobilized AdBMP7 compared to regions immobilized with empty vectors (Ad-empty) and non-cell seeded regions immobilized with AdBMP7. A more detailed assessment of single (BMP7) and dual (BMP7 and PDGF-BB) growth factor delivery effects in combination with varying scaffold topography (i.e., patterned film versus amorphous film in the "PDL" region) was performed using the fenestration defect model. Micro-CT data showed significantly higher ($p < 0.05$) bone formation in groups with AdBMP7 immobilization and gingival fibroblast cell seeding compared to groups with Ad-empty. Collagen III and periostin expression was higher in groups with dual growth factor delivery, with significantly ($p < 0.05$) higher periostin expression in groups combining patterned film with single or dual growth factors at week 6. Nanoindentation assessment showed higher elastic moduli for regenerated bone and PDL-like tissue regions at bone-PDL interface in patterned film groups with dual growth factors (positive control) compared to amorphous films with Ad-empty at week 9 ($p < 0.05$ and $p < 0.01$, respectively). Positive control group also showed no significant differences in bone, PDL-like tissue stiffness at 3 and 9 weeks when compared to native tissues. These data indicate improvement in periodontal regeneration when combining scaffold micro-topography cues with localized growth factor expression, thereby contributing to development of next-generation scaffolds specific to periodontal regenerative medicine.

CHAPTER 1

INTRODUCTION

The "Scaffold Design and Development" section of this dissertation chapter includes excerpts from sections written as a contribution to the following book chapter:

Decker AM, **Pilipchuk SP**, Araujo-Pires AC, Giannobile WV. Bioengineering of the periodontal ligament. In: Kapila SD, Goonewardene M, eds. *Interdisciplinary Therapy: Using Contemporary Approaches for Complex Cases.* Monograph 52, Craniofacial Growth Series, Center for Human Growth and Development, The University of Michigan, Ann Arbor, 2016:195-242.

1.1   Problem Statement

Periodontitis is a leading chronic oral inflammatory disease and primary cause of permanent tooth loss estimated to affect 47.2% of adults in the United States, with a prevalence of 70% for adults aged 65 years and older [1]. Damage to the tooth-supporting apparatus, which includes periodontal ligament (PDL) fibers that anchor the tooth root to the alveolar bone, subsequently initiates osseous tissue resorption. Multi-tissue morbidity is a significant challenge for current clinical periodontal regenerative therapies, which lack predictability in reconstructing three dimensionally accurate tissues with physiologic functionality native to the healthy periodontium [2, 3]. Tissue engineering strategies have shown the potential to address existing deficiencies in clinically-induced periodontal regeneration through combinational approaches using biomaterials, growth factors, and cell-based therapy [4, 5]. Recent studies indicate that alveolar bone-PDL interface tissue regeneration can be guided using bi- and multi-phasic material scaffolds with and without bioactive factors that are developmentally-linked to periodontal tissue formation [6–10]. However, few studies have focused on whether precise topographical features can influence the physiological and functional properties of regenerated periodontal tissues through contact guidance [11, 12], and none have examined this potential affect using a 3-D hierarchical multiscale scaffold design. This research is necessary to optimize scaffold constructs to serve as guiding platforms for anatomically-native tissue formation that is required to re-

establish tissue functionality *in vivo*--thereby justifying further exploration in pre-clinical models for translational periodontal regenerative medicine.

1.2   Existing Limitations of Current Clinical Periodontal Regenerative Therapies

Damage to periodontal tissues resulting from trauma, chronic infection, congenital defects, or surgical resection requires clinical intervention. In the oral cavity, the alveolar processes of the mandible and maxilla line the tooth sockets and provide structural support and maintenance for teeth as part of the periodontium, which also consists of the periodontal ligament (PDL), cementum, and gingiva. Advanced periodontal disease alters alveolar bone morphology and destroys surrounding tooth-supporting tissues, thereby necessitating tooth extraction. Current clinical treatment for periodontal defects consist of re-establishing oral hygiene to stem progressive soft tissue and bone loss by controlling inflammation through removal of plaque and calculus. Restoration of some periodontal tissues can be achieved through tissue repair, although not necessarily regeneration, using surgical procedures, occlusive barrier membranes, and osteoconductive biomaterials in combination with recombinant growth factor proteins [13]. An autologous graft for alveolar bone restoration is considered the gold standard due to low risk of immunogenicity or disease transmission that could be associated with an allograft or xenograft. However, critical limitations of this approach include donor site morbidity and inadequate supply of graft tissue. An armamentarium of resorbable and non-resorbable commercially-available osteoconductive ceramic (i.e., calcium phosphates, bioactive glass) or polymeric (i.e., methylmethacrylate, poly-α-hydroxy acids) alloplasts and their composites are used clinically for intraoral bone maintenance and augmentation [14, 15], and in conjunction with growth factor delivery [4, 16], for dental implant stabilization in tooth extraction sockets. The capacity of bone grafts to regenerate intraoral osseous tissues predictably, however, is compromised by factors such as variability in defect type and size, growth factor instability, patient health status, and surgical technique.

Even more so than intraoral bone regeneration, the formation of physiologically functional PDL which anchors the cementum-coated tooth root to the alveolar bone remains an elusive achievement and a major clinical challenge. The PDL consists of vascularized, innervated connective tissue with highly organized fibers composed primarily of collagen type I and III. PDL fibers are perpendicularly oriented between the cementum and alveolar bone, where their ends

(Sharpey's fibers) insert into these mineralized tissues to stabilize the tooth root, transmit occlusal forces, and provide sensory function. Presence of bone and cementum is crucial for the formation of functional PDL, and regeneration of the full bone-PDL-cementum complex would negate the need to extract otherwise healthy teeth with compromised periodontal apparatus. Guided tissue regeneration (GTR) is a surgically-based technique using cell-impermeable barrier membranes to control the formation of pocket or long junctional epithelium tissue formation in place of PDL along the tooth root due to epithelial down-growths that fill periodontal defects. While regenerative periodontal surgery with GTR shows considerable reduction in probing pocket depth, radiographic evidence of increased bone fill, and clinical attachment gains that are indicative of increased collagen fiber attachment to the cemental surface, the overall quality and degree of periodontal healing varies widely [2, 17]. For example, GTR may provide space maintenance for tissue repair by endogenous progenitor cells, but PDL connective tissue repair may be disorderly or result in bone-like tissue in place of periodontal regeneration.

Periodontal wound healing can also be enhanced through the use of recombinant growth factors (GFs) and platelet rich plasma (PRP) which contains concentrated suspensions of autologous platelets that secrete bioactive GFs at the wound site. Some commonly-used bioactive agents in the clinic are derived from the following GF families: platelet derived growth factors (PDGFs), bone morphogenetic proteins (BMPs) within the β-transforming growth factor (β-TGF) superfamily, fibroblast growth factors (FGFs), among others. These are necessary biologics which regulate periodontal and mesenchymal stem cell migration, differentiation, proliferation, chemotaxis, and cell-specific extracellular matrix (ECM) production. Pre-clinical and clinical studies have shown time- and dose-dependent GF-induced regeneration of alveolar bone with BMP-2, BMP-7, PDGF-BB, and FGF-2 [18–21]; periodontal ligament with PDGF-BB [22]; and cementum with BMP-7 [23, 24] . The efficacy of these agents varies depending on delivery system, dosages, and release kinetics. Food and Drug Administration (FDA)-approved biologics used for periodontal regenerative therapies include rhPDGF-BB in the osteoconductive delivery vehicle β-tricalcium phosphate (β-TCP) (GEM-21S®) and rhBMP-2 in a collagen sponge (Infuse®). However, pharmacologic dosing is often required to mitigate the transient biological activity of GFs at local delivery sites due to short half-lives and proteolytic degradation, although use of supra-physiological doses can evoke local and systemic toxicity [25]. Localized GF delivery is therefore necessary to decrease total dosage needed without compromising function. Pre-clinical

3

studies using gene therapy indicate that this limitation may be addressed through the transduction (using viral elements) or transfection (using non-viral elements) of a target cell population to express GF-encoding genes over a period of time necessary to achieve desired therapeutic effects. This is supported by multiple studies using gene therapy for periodontal tissue regeneration: Sustained and localized PDGF-B gene expression using direct delivery in periodontal lesions was observed for up to 21-35 days after cell transduction [26], and has been shown to stimulate alveolar bone and cementum regeneration [27, 28], whereas *ex vivo* BMP-7 gene transfer using dermal fibroblast transduction resulted in predictable bridging of periodontal bone defects [29]. Safety concerns regarding risk of virus dispersion and lack of spatio-temporal control of gene expression limit the predictability of this approach and its translation into clinically-viable solutions, thereby requiring the investigation of novel methods of gene delivery. Overall, tissue engineering approaches using scaffolds alone or in combination with growth factor, cell and/or gene delivery have the potential to address existing challenges in managing periodontal tissue loss and increase clinical options for their controllable regeneration. Given the limitations of current periodontal regenerative therapies, the main goal of this research work is to design a scaffold-based delivery vehicle that can be used for the regeneration of the alveolar bone-PDL-cementum complex in conjunction with localized, controlled PDGF-BB and BMP-7 delivery using gene therapy (**Figure 1.1**).
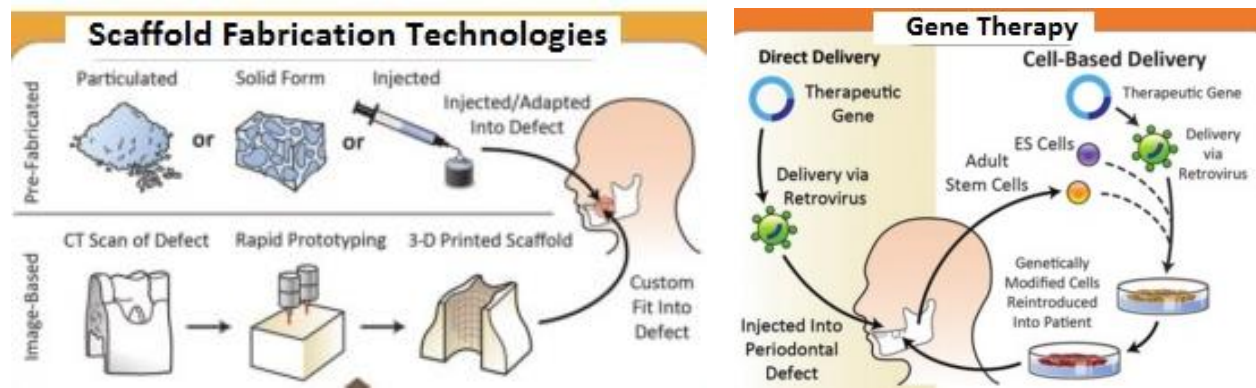
Figure 1.1 Scaffold Fabrication Techniques Combined with Gene Therapy
Areas of improvement addressed for current periodontal tissue engineering strategies: increased topographical precision of scaffold fabrication (Aim I) combined with spatiotemporally controlled gene therapy (Aim II) using the scaffold as a gene delivery vehicle to regenerate periodontal tissues in a loaded periosseous defect model (Aim III). *Figure modified from [5].*

1.2 Scaffold Design and Development for Periodontal Regeneration

A biomaterial scaffold is ideally intended to provide a cell-adhesive, three-dimensional microstructural framework for the guidance and support of physiologically functional tissue formation—reminiscent of the extracellular matrix (ECM) that provides native "scaffolding" in healthy tissue. Several important scaffold development criteria include: (1) **biological functionality** capable of supporting cell infiltration, proliferation, and differentiation, (2) ECM-mimicking **permeable microstructure** with porosity to facilitate nutrient and oxygen delivery and exchange, (3) **rate of degradation** consistent with rate of tissue regeneration and remodeling, (4) **mechanical properties** to maintain tissue defect architecture and support applied loads such as mastication-induced compressive forces on the periodontal ligament, (5) **neovascularization** for tissue homeostasis and reperfusion, and (6) targeted **cell, growth factor, and/or gene delivery** for enhanced regenerative capacity.

1.2.1 Biological, synthetic materials as scaffolds

While scaffolds formed from naturally-derived materials including proteins (i.e., collagen, fibrin, gelatin, hyaluronic acid) and polysaccharides (i.e., chitosan, alginate) have innate biological functionality, their mechanical properties and rates of degradation cannot be as precisely tailored as is possible with synthetically-derived materials. Synthetic polymers are used widely in the clinic, with members of the polyester family most prevalent due to their proven safety profile, biodegradable properties, and biocompatibility. Among these, poly(lactic acid) (PLA), poly(glycolic acid) (PGA), their co-polymer poly(lactic-co-glycolic acid) (PLGA), and polycaprolactone (PCL) have been extensively investigated in pre-clinical studies for PDL regeneration. Additionally, ceramic-based material--most commonly used as bone grafts in periodontal regeneration studies--include calcium phosphate (CaP)-derived matrices (i.e., tricalcium phosphate (TCP) and hydroxyapatite (HA)) and bioactive glass. Instead of serving as scaffolds for directed growth of periodontal ligament, these are mostly employed as barrier membranes for guided bone regeneration, and can assist in maintaining the space needed for connective tissue growth that may have PDL-like formation [30]. The method of delivering a scaffold to the site of defect varies depending on material properties, with naturally-based protein scaffolds frequently seen in the form of highly hydrated gels or particulates, whereas synthetic materials are more likely to be delivered in solid form [31-33].

Among the various candidate scaffolds for periodontal ligament regeneration, biological polymers are advantageous given their low cytotoxicity and immunogenicity, including their resemblance to an endogenous ECM. Most commonly formed as hydrogels or sponges, these polymers and polysaccharides can be used to fill irregular defects and provide a delivery vehicle with high cell-seeding efficiency. Hydrogels are typically prepared by chemically or physically crosslinking the polymer chains, using chemical crosslinkers or pH-based reactions, respectively [34]. Cell-encapsulation within hydrogels prior to transplantation can be used for cell and gene delivery into periodontal defects. Collagen scaffolds alone can still facilitate improved periodontal tissue formation as compared to a lack of treatment [35], but not to the same extent as with cell-based and growth factor-based delivery. Jin et al used a collagen matrix to deliver adenoviral PDGF-B to the periodontium, stimulating PDL formation and cementogenesis with fiber insertion, including vascularization and newly-formed periodontium not observed with collagen matrix alone. Interestingly, the majority of the collagen matrix delivered in combination with PDGF-B was resorbed by 2 weeks, with more scaffold remnants present at lesions sites with collagen matrix alone [36]. It is likely that the addition of growth factors increases the rate of tissue regrowth and invasion into the scaffold, thereby increasing its rate of degradation.

1.2.2 *Cell sheet technology as an alternative to biodegradable scaffolds*

Given the importance of biological factor delivery and retention of a viable cell population at the site of the defect, cell sheet engineering has emerged as a novel approach for targeted cell delivery without the use of biodegradable scaffolds. Cell sheet monolayers with intact cell-cell contacts and ECM can be harvested non-enzymatically using thermo-responsive polymeric surface cell culture plates that enable controlled cell adhesion [37]. In vitro cultures of human-derived hPDL cell sheets show periostin expression and high alkaline phosphatase activity [38], and several studies confirm their potential for PDL regeneration using small and large animal models [39]. Despite this scaffold-free approach, the incorporation of supporting synthetic [40] or natural membranes [41] can be useful for increased cell sheet stability and ease of transplantation. Therefore, the most promising approaches for the regeneration of PDL lie in the design and fabrication of scaffolds that can be appropriately suited to the delivery of cells and growth factors that will stimulate the regenerative process and allow for the remodeling and growth of tissue that is structurally and functionally-similar to native ligament.

1.2.3   Micropatterning and Multiphasic Scaffold Design

The complex hierarchical organization of periodontal tissues has brought into focus the need for multi-phasic biomaterial constructs that can recapitulate the structural integrity of the bone-ligament interface. Microscale technologies have been indicated for use in fabricating scaffolds that facilitate control of multiple tissue organization and positioning, as required for the regeneration of an bone-ligament interface [42, 43]. Surface topography on the micro- and nano-scale (10-100,000 nm) profoundly affects cell behavior, including adhesion, migration, alignment, intracellular signaling pathways, and ultimately tissue formation in combination with biochemical cues. This phenomenon has been explored using a variety of cell types on a diverse range of biomaterial surfaces [44-49]. Although few in number, existing studies that have investigated the effect of micropatterned surfaces on PDL cells showed high elongation and alignment relative to formed grooves and ridges on polystyrene, silicone rubber, and glass slide surfaces [50]. Among microscale technologies, soft lithography is specifically used for micro- and nano-patterning of material surfaces and has been widely applied for the study of cell behavior on topographic substrates since its transition from microelectronics industry to biologically-based research. It provides a methodology for creating 2-D and 3-D curved and ordered structures (> 500 nm) including grooves, pillars, wells, and pits, in a variety of materials--an undertaking that is not yet possible using current 3-D printing technology that is low-resolution in comparison. The most widely employed soft-lithography method is replica molding, which consist of producing an elastomeric mold, usually made of polydimethylsiloxane (PDMS), that contains a desired micro-structure pattern which is replicated on a polymer by filling the mold with the pre-polymer solution, curing it, and peeling the polymer off to obtain the patterned surface [51].

To translate microscale technology into an implant with clinical relevance, it is necessary to integrate microscale features into a three-dimensional scaffold that matches a given defect with appropriate dimensionality and bulk properties. Such an approach has already been established in dentistry with the use of nanoscale surface topology on dental implants to promote osseointegration and cell adhesion. However, the exploration of this approach for the guidance and regeneration of periodontal tissues is still nascent. Recent studies have focused on the applicability of electrospinning and additive manufacturing technology (3-D printing) as predictably reproducible methods of fabricating structures with cell-guiding features or controllable internal architectures, respectively. While electrospinning can produce linear polymer fibers on the order

7

of 5nm-1um that are structurally similar to ECM, these fibers have poor mechanical properties inconsistent with those necessary to mimic bone or ligament structure [52]. Commonly employed 3-D printing processes for the fabrication of bone scaffolds include fused deposition modeling (FDM) and selective laser sintering (SLS). Whereas FDM relies on extrusion to produce simple patterned polymeric stacks, SLS allows the processing of powdered biocompatible polymers via a focused laser beam that deposits the polymer layer by layer to create a computer-aided design (CAD)-based replica, making it useful in combination with medical imaging technology for pre-operative surgical planning and implant design. Polycaprolactone (PCL)--an FDA-approved, hydrolytically-biodegradable polyester used as a bone graft substitute--is easily manufactured into a variety of shapes, porosities, and with variable mechanical properties using SLS due to its low melting point (59-64°C) [53]. PCL, which degrades over a period of 2-4 years *in vivo*, has been the material of choice in multi-phasic scaffolds developed for the attempted regeneration of the periodontium: Park *et al.* used 3-D printed wax-based molds to cast PCL for the bone compartment of an image-based bi-phasic scaffold (6, 7); Costa *et al.* and Vaquette *et al.* employed FDM-deposited PCL for the bone compartment and electrospun PCL for the PDL region (8, 9); and Lee *et al.* used a layered 3-D printed scaffold with three PCL interphases for the cementum, PDL, and alveolar bone (10). Given PCL's malleability and ability to be formed into polymeric matrices of various physical and mechanical properties that can be designed to match tissues that are being targeted for regeneration, this research focuses on the use of PCL to develop the following bi-phasic hierarchical scaffold compartments: (1) a 3-D micropatterned PCL surface via replica molding that mimics the native dimensions of mature periodontal ligament, (2) a 3-D printed bone compartment fabricated via SLS technology.

1.4   Novel Gene Therapy-Based Approaches for Tissue Repair

Gene therapy has been shown to offer the potential for highly targeted, effective methods of growth factor delivery with reduced dosing requirements. However, these methods frequently involve use of viral vectors such adenoviruses and retroviruses, causing concerns of systemic health effects through virus dispersion and reduced transduction efficiency, thereby limiting their clinical translation. Chemical vapor deposition (CVD) has emerged as a viable surface modification technique for the bioconjugation of biomaterial surfaces with specific functional groups to immobilize viral vectors--allowing localized gene delivery directly from the biomaterial

surface [54]. CVD can be used for 2-D and 3-D surface engineering to evenly coat structures with complex geometry and porosity while conforming to surface topology. The surface polymerization occurs via monomer sublimation, activation, and subsequent deposition, negating the need for catalysts, solvents, or plasticizers, which renders the polymer coating cyto-compatible. Poly(*p*-xylylene) (PPX) polymers are selected for the CVD process given their biocompatibility and ability to accommodate various functional groups in their structure, including amines, aldehydes, alcohols, and anhydrates [55]. This technique has been used in conjunction with gene therapy to functionalize inert polymer surfaces such as that of PCL to induce spatiotemporal control of gene delivery via cell signaling adenoviral gradients for cell growth and transduction [56-58]. Two specific adenovirus binding techniques have been utilized to controllably transduce cells: Hu *et al* [56] tethered adenoviral vectors to the surface of aminated PPX-coated PCL using a sequence of virus-biotin-avidin-biotin-PCL to spatially control C4 fibroblast cell transduction; Zhang *et al* [58] simplified this technique by using an anti-adenovirus antibody immobilization on CVD-coated PCL via an amide chemical bond to transduce bone marrow stromal cells with Runx2 to drive their differentiation into an osteogenic lineage *in vitro*, resulting in 6.5-fold increases in alkaline phosphatase (ALP) activity and matrix mineralization. While this approach is promising, it is yet to be used in conjunction with growth factor gene delivery. One of the aims of this work was to investigate CVD reactive polymer coatings using PCL as a vehicle for the controlled transduction of cells with PDGF-B and BMP-7 in the PDL and bone regions, respectively, of the proposed biphasic microstructured scaffold. This novel approach allows for better containment of gene therapy vectors to the treatment site and could improve the bioavailability of these growth factors through increased transduction efficiency of the local cell population.

1.5   Thesis Aims

Current clinical periodontal regenerative therapies are limited by lack of predictable periodontal tissue regeneration, with the biggest challenge being lack of physiologically functional periodontal ligament tissue formation. Likewise, local delivery of growth factors to stimulate biologically-mediated regeneration is frequently compromised by short half-life, limited bioactivity, and proteolytic degradation. To address these limitations, this works focused on developing a novel PCL-based substrate that incorporates micropatterned topography for the guidance of cell growth and periodontal tissue formation, in conjunction with localized,

spatiotemporally controlled gene delivery to direct cellular growth factor expression. The potential of microscale technology to be used for guided 3-D periodontal tissue regeneration has not been examined, and cell guidance of patterned substrates has only been investigated on 2-D surfaces. One major challenge has been the incorporation of patterned substrates, which are often thin films without any bulk properties, into larger macroscale devices that can be used as implants. Here, this limitation is overcome by creating a bi-phasic scaffold, the foundation of which is based on a 3-D printed PCL scaffold that supports bone formation. This mimics the size ratio of alveolar bone to PDL seen *in vivo*, where the PDL region is a thin area of vascularized connective tissue that anchors the tooth root to the bone. The result of this study advances the area of scaffold fabrication and growth factor delivery for ligament-bone interface engineering and achieves a new generation of more predictable and controlled matrices for periodontal regenerative medicine.

> **AIM 1:** Design micropatterned polymer films for directed orientation of human periodontal ligament (hPDL) cells in a biphasic bone-ligament scaffold and evaluate effect of varying film topography on oriented tissue formation in an *in vivo* model.

> *Hypothesis 1: Micropatterning of PCL films will provide greater control over hPDL cell orientation and subsequent formation of aligned periodontal ligament tissue between the alveolar bone-PDL and PDL-dentin interfaces.*

> **AIM 2:** Investigate effect of spatially-controlled growth factor delivery on bone-PDL tissue complex regeneration *in vivo* using a biphasic scaffold with surface immobilization of growth factors in the PDL and bone regions of the scaffold.

> *Hypothesis 2: Spatially-controlled delivery of BMP-7 and PDGF-B will facilitate bone and PDL tissue formation, respectively, in combination with the architectural and topographical cues for cell contact guidance established for each region of the biphasic micropatterned PCL scaffold.*

AIM 3: Design micropatterned scaffolds for, and evaluate in, a mechanically-loaded *in vivo* defect model to determine tissue regeneration in combination with localized, dual growth factor delivery.

Hypothesis 3: Biphasic micropatterned scaffolds will enable the formation of periodontal tissues under biomechanical loading conditions in vivo and reactive polymer coatings formed on regions of the scaffold via CVD will facilitate BMP-7 and PDGF-B gene delivery for establishment of physiologically functional periodontium.

1.6   Dissertation Contents

Chapter 2 of this dissertation provides an in-depth review of currently-used scaffolds for bone and periodontal ligament regeneration, in addition to covering the most relevant growth factors, with an emphasis on various methods of growth factor delivery based on gene therapy in order to provide a broad understanding of the biological factors that promote soft and osseous tissue regeneration. **Chapter 3** presents the unique design of a 3D-printed scaffold for a single-patient case study, highlighting the potential of 3D printing as a means of creating customized scaffolds that mimic the necessary structural characteristics that can fit a peri-osseous defect. At the same time, this chapter also addresses some of the limitations of this approach that inform the further improvements in scaffold design and growth factor delivery that are undertaken in research presented in Chapters 4 and 5. Specifically, **Chapter 4** describes the development of 3D printed, micropatterned scaffolds that are shown to promote aligned collagenous tissue formation using an ectopic murine model, with particular focus on the identification of scaffold topography that is optimal for cellular alignment that leads to tissue alignment. **Chapter 5** focuses on the improvement of growth factor delivery using the same scaffold system and animal model through immobilization of adenoviral vectors that allow for localized growth factor delivery via transduction of the seeded cell population. This chapter further describes applying this methodology to study the formation of bone in a rat fenestration defect—a mechanically loaded site that is more representative of the conditions that are present in a true defect, except for use of athymic (T-cell deficient) animals to prevent a cross-species incompatibility response due to the presence of human-derived cells. **Chapter 6** focuses on a thorough analysis of the effects of dual (platelet-derived growth factor (PDGF-BB) and bone morphogenetic protein (BMP7)), as well as

11

single (BMP7 only) growth factor delivery in the scaffold compartments developed to guide the regeneration of PDL and alveolar bone, specific to a rat fenestration defect. This study utilizes chemical vapor deposition (CVD) in order to allow for the controlled immobilization of adenovirus encoding a specific growth factor onto a given region of the scaffold. **Chapter 7** offers concluding remarks that summarize the findings presented in Chapters 3-6, the novelty of the work, and existing limitations. Finally, a look into future applications of this work and its potential for promoting regeneration of the periodontium is presented.

1.7   References

[1]   Eke PI, Dye B a, Wei L, Thornton-Evans GO, Genco RJ. Prevalence of periodontitis in adults in the United States: 2009 and 2010. *J Dent Res* 2012;91:914–20.

[2]   Hägi TT, Laugisch O, Ivanovic A, Sculean A. Regenerative periodontal therapy. *Quintessence Int* 2014;45:185–92.

[3]   Chen F-M, Jin Y. Periodontal tissue engineering and regeneration: current approaches and expanding opportunities. *Tissue Eng Part B Rev* 2010;16:219–55.

[4]   Kaigler D, Cirelli JA, Giannobile W V. Growth factor delivery for oral and periodontal tissue engineering. *Expert Opin Drug Deliv* 2008;3:647–662.

[5]   Rios HF, Lin Z, Oh B, Park CH, Giannobile W V. Cell- and gene-based therapeutic strategies for periodontal regenerative medicine. *J Periodontol* 2011;82:1223–37.

[6]   Park CH, Rios HF, Jin Q, Bland ME, Flanagan CL, Hollister SJ, Giannobile W V. Biomimetic hybrid scaffolds for engineering human tooth-ligament interfaces. *Biomaterials* 2010;31:5945–52.

[7]   Park CH, Rios HF, Jin Q, Sugai J V, Padial-Molina M, Taut AD, Flanagan CL, Hollister SJ, Giannobile W V. Tissue engineering bone-ligament complexes using fiber-guiding scaffolds. *Biomaterials* 2012;33:137–45.

[8]   Costa PF, Vaquette C, Zhang Q, Reis RL, Ivanovski S, Hutmacher DW. Advanced Tissue Engineering Scaffold Design for Regeneration of the Complex Hierarchical Periodontal Structure. *J Clin Periodontol* 2013;doi:10.1111/jcpe.12214.

[9]   Vaquette C, Fan W, Xiao Y, Hamlet S, Hutmacher DW, Ivanovski S. A biphasic scaffold design combined with cell sheet technology for simultaneous regeneration of alveolar bone/periodontal ligament complex. *Biomaterials* 2012;33:5560–73.

[10]   Lee CH, Hajibandeh J, Suzuki T, Fan A, Shang P, Mao JJ. Three-Dimensional Printed Multiphase Scaffolds for Regeneration of Periodontium Complex. *Tissue Eng Part A* 2014;20:1342–1352.

[11]   Yu N, Prodanov L, Riet J Te, Yang F, Walboomers XF, Jansen JA. Regulation of periodontal ligament cell behavior by cyclic mechanical loading and substrate nanotexture. *J Periodontol* 2013;84:1504–13.

[12]   Hamilton DW, Oates CJ, Hasanzadeh A, Mittler S. Migration of periodontal ligament fibroblasts on nanometric topographical patterns: influence of filopodia and focal adhesions on contact guidance. *PLoS One* 2010;5:e15129.

[13]   Chen F-M, Zhang J, Zhang M, An Y, Chen F, Wu Z-F. A review on endogenous regenerative technology in periodontal regenerative medicine. *Biomaterials* 2010;31:7892–927.

[14]   Shue L, Yufeng Z, Mony U. Biomaterials for periodontal regeneration: a review of ceramics and polymers. *Biomatter* 2012;2:271–7.

[15]   Klijn RJ, Meijer GJ, Bronkhorst EM, Jansen JA. A Meta-Analysis of Histomorphometric Results and Graft Healing Time of Various Biomaterials Compared to Autologous Bone Used as Sinus Floor. *Tissue Eng Part B Rev* 2010;16:493–507.

[16]   Somerman M. Growth factors and periodontal engineering: where next? *J Dent Res* 2011;90:7–8.

[17]   Chen F-M, Jin Y. Periodontal tissue engineering and regeneration: current approaches and expanding opportunities. *Tissue Eng Part B Rev* 2010;16:219–55.

[18]   Nevins M, Kao RT, McGuire MK, McClain PK, Hinrichs JE, McAllister BS, Reddy MS, Nevins ML, Genco RJ, Lynch SE, Giannobile W V. Platelet-derived growth factor promotes periodontal regeneration in localized osseous defects: 36-month extension results from a randomized, controlled, double-masked clinical trial. *J Periodontol* 2013;84:456–64.

[19]   Kitamura M, Akamatsu M, Machigashira M, Hara Y, Sakagami R, Hirofuji T, Hamachi T, Maeda K, Yokota M, Kido J, Nagata T, Kurihara H, Takashiba S, Sibutani T, Fukuda M, Noguchi T, Yamazaki K, Yoshie H, Ioroi K, Arai T, Nakagawa T, Ito K, Oda S, Izumi Y, Ogata Y, Yamada S, Shimauchi H, Kunimatsu K, Kawanami M, *et al.* FGF-2 stimulates periodontal regeneration: results of a multi-center randomized clinical trial. *J Dent Res* 2011;90:35–40.

[20]   Wikesjö UME, Qahash M, Thomson RC, Cook AD, Rohrer MD, Wozney JM, Hardwick WR. rhBMP-2 significantly enhances guided bone regeneration. *Clin Oral Implants Res* 2004;15:194–204.

[21] Giannobile W V, Ryan S, Shih M, Kaplan PL, Chari TCK. Recombinant Human Osteogenic Wound Healing in Class III Furcation Defects. *J Periodontol* 1998;69:129–137.

[22] Nevins M, Giannobile W V, McGuire MK, Kao RT, Mellonig JT, Hinrichs JE, McAllister BS, Murphy KS, McClain PK, Nevins ML, Paquette DW, Han TJ, Reddy MS, Lavin PT, Genco RJ, Lynch SE. Platelet-derived growth factor stimulates bone fill and rate of attachment level gain: results of a large multicenter randomized controlled trial. *J Periodontol* 2005;76:2205–15.

[23] Hakki SS, Foster BL, Nagatomo KJ, Bozkurt SB, Hakki EE, Somerman MJ, Nohutcu RM. Bone morphogenetic protein-7 enhances cementoblast function in vitro. *J Periodontol* 2010;81:1663–74.

[24] Ripamonti U, Heliotis M, Rueger D, Sampath T. Induction of cementogenesis by recombinant human osteogenic protein-1 (hOP-1/BMP-7) in the baboon. *Archs Oral Biol* 1996;41:121–126.

[25] Elangovan S, Karimbux N. Review paper: DNA delivery strategies to promote periodontal regeneration. *J Biomater Appl* 2010;25:3–18.

[26] Chang P-C, Cirelli JA, Jin Q, Seol Y-J, Sugai J V, D'Silva NJ, Danciu TE, Chandler LA, Sosnowski BA, Giannobile W V. Adenovirus encoding human platelet-derived growth factor-B delivered to alveolar bone defects exhibits safety and biodistribution profiles favorable for clinical use. *Hum Gene Ther* 2009;20:486–96.

[27] Jin Q, Anusaksathien O, Webb SA, Printz MA, Giannobile W V. Engineering of tooth-supporting structures by delivery of PDGF gene therapy vectors. *Mol Ther* 2004;9:519–26.

[28] Chang P-C, Seol Y-J, Cirelli J a, Pellegrini G, Jin Q, Franco LM, Goldstein S a, Chandler L a, Sosnowski B, Giannobile W V. PDGF-B gene therapy accelerates bone engineering and oral implant osseointegration. *Gene Ther* 2010;17:95–104.

[29] Jin Q-M, Anusaksathien O, Webb S, Rutherford R, Giannobile W V. Gene Therapy of Bone Morphogenetic Protein for Periodontal Tissue Engineering. *J Periodontol* 2003;74:202–213.

[30] Hayashi C, Kinoshita A, Oda S, Mizutani K, Shirakata Y, Ishikawa I. Injectable calcium phosphate bone cement provides favorable space and a scaffold for periodontal regeneration in dogs. Journal of periodontology 2006;77:940-946.

[31] Atala A, Kasper FK, Mikos AG. Engineering complex tissues. Science translational medicine 2012;4:160rv112-160rv112.

[32] Hollister SJ. Scaffold design and manufacturing: from concept to clinic. Advanced Materials 2009;21:3330-3342.

[33] Scheller E, Krebsbach P, Kohn D. Tissue engineering: state of the art in oral rehabilitation. Journal of oral rehabilitation 2009;36:368-389.

[34] Van Vlierberghe S, Dubruel P, Schacht E. Biopolymer-based hydrogels as scaffolds for tissue engineering applications: a review. Biomacromolecules 2011;12:1387-1408.

[35] Kosen Y, Miyaji H, Kato A, Sugaya T, Kawanami M. Application of collagen hydrogel/sponge scaffold facilitates periodontal wound healing in class II furcation defects in beagle dogs. Journal of periodontal research 2012;47:626-634.

[36] Jin Q, Anusaksathien O, Webb SA, Printz MA, Giannobile WV. Engineering of tooth-supporting structures by delivery of PDGF gene therapy vectors. Molecular Therapy 2004;9:519-526.

[37] Matsuura K, Utoh R, Nagase K, Okano T. Cell sheet approach for tissue engineering and regenerative medicine. Journal of Controlled Release 2014;190:228-239.

[38] Washio K, Iwata T, Mizutani M, Ando T, Yamato M, Okano T et al. Assessment of cell sheets derived from human periodontal ligament cells: a pre-clinical study. Cell and tissue research 2010;341:397-404.

[39] Hasegawa M, Yamato M, Kikuchi A, Okano T, Ishikawa I. Human periodontal ligament cell sheets can regenerate periodontal ligament tissue in an athymic rat model. Tissue engineering 2005;11:469-478.

[40] Iwata T, Yamato M, Tsuchioka H, Takagi R, Mukobata S, Washio K et al. Periodontal regeneration with multi-layered periodontal ligament-derived cell sheets in a canine model. Biomaterials 2009;30:2716-2723.

[41] Akizuki T, Oda S, Komaki M, Tsuchioka H, Kawakatsu N, Kikuchi A et al. Application of periodontal ligament cell sheet for periodontal regeneration: a pilot study in beagle dogs. Journal of periodontal research 2005;40:245-251.

[42] Hacking S a, Khademhosseini a. Applications of microscale technologies for regenerative dentistry. *J Dent Res* 2009;88:409–21.

[43] Stevens MM, George JH. Exploring and engineering the cell surface interface. *Science* 2005;310:1135–8.

[44] Holthaus MG, Stolle J, Treccani L, Rezwan K. Orientation of human osteoblasts on hydroxyapatite-based microchannels. *Acta Biomater* 2012;8:394–403.

[45] Chen CS, Mrksich M, Huang S, Whitesides GM, Ingber DE. Micropatterned surfaces for control of cell shape, position, and function. *Biotechnol Prog* 1998;14:356–63.

[46] Jamal M, Bassik N, Cho J, Randall C, Gracias D. Directed growth of fibroblasts into three dimensional micropatterned geometries via self-assembling scaffolds. *Biomaterials* 2010;31:1–14.

[47] Den Braber ET, de Ruijter JE, Smits HT, Ginsel L a, von Recum a F, Jansen J a. Quantitative analysis of cell proliferation and orientation on substrata with uniform parallel surface micro-grooves. *Biomaterials* 1996;17:1093–9.

[48] Leclerc A, Tremblay D, Hadjiantoniou S, Bukoreshtliev N V, Rogowski JL, Godin M, Pelling AE. Three dimensional spatial separation of cells in response to microtopography. *Biomaterials* 2013;34:8097–104.

[49] Watari S, Hayashi K, Wood JA, Russell P, Nealey PF, Murphy CJ, Genetos DC. Modulation of osteogenic differentiation in hMSCs cells by submicron topographically-patterned ridges and grooves. *Biomaterials* 2012;33:128–36.

[50] Yu N, Prodanov L, Riet J Te, Yang F, Walboomers XF, Jansen J a. Regulation of Periodontal Ligament Cell Behaviour by Cyclic Mechanical Loading and Substrate Nanotexture. *J Periodontol* 2012;1–17.doi:10.1902/jop.2012.120513.

[51] Nikkhah M, Edalat F, Manoucheri S, Khademhosseini A. Engineering microscale topographies to control the cell-substrate interface. *Biomaterials* 2012;33:5230–46.

[52] McMahon RE, Wang L, Skoracki R, Mathur AB. Development of nanomaterials for bone repair and regeneration. *J Biomed Mater Res B Appl Biomater* 2013;101:387–97.

[53] Woodruff MA, Hutmacher DW. The return of a forgotten polymer—Polycaprolactone in the 21st century. *Prog Polym Sci* 2010;35:1217–1256.

[54] Lahann J. Vapor-based polymer coatings for potential biomedical applications. *Polym Int* 2006;1370:1361–1370.

[55] Lahann J, Klee D, Hocker H. Chemical vapour deposition polymerization of substituted [2.2]paracyclophanes. *Macromol Rapid Commun* 1998;441444:441–444.

[56] Hu W-W, Elkasabi Y, Chen H-Y, Zhang Y, Lahann J, Hollister SJ, Krebsbach PH. The use of reactive polymer coatings to facilitate gene delivery from poly (epsilon-caprolactone) scaffolds. *Biomaterials* 2009;30:5785–92.

[57] Elkasabi YM, Lahann J, Krebsbach PH. Cellular transduction gradients via vapor-deposited polymer coatings. *Biomaterials* 2011;32:1809–15.

[58] Zhang Y, Deng X, Scheller EL, Kwon T-G, Lahann J, Franceschi RT, Krebsbach PH. The effects of Runx2 immobilization on poly (epsilon-caprolactone) on osteoblast differentiation of bone marrow stromal cells in vitro. *Biomaterials* 2010;31:3231–6.

16

CHAPTER 2

CURRENT AND PROSPECTIVE CLINICAL TECHNIQUES FOR TISSUE ENGINEERING TO PROMOTE BONE AND PERIODONTAL REGENERATION IN THE ORAL CAVITY

Originally published as a review article in *Dental Materials.* Additional description of scaffolds for periodontal ligament-specific regeneration are derived from sections written as a contribution to a book chapter entitled "Bioengineering of the Periodontal Ligament":

Pilipchuk SP, Plonka AB, Monje A, Taut AD, Lanis A, Kang B, Giannobile WV. Tissue engineering for bone regeneration and osseointegration in the oral cavity. *Dent Mater.* 2015;31(4):317-338.

Decker AM, **Pilipchuk SP**, Araujo-Pires AC, Giannobile WV. Bioengineering of the periodontal ligament. In: Kapila SD, Goonewardene M, eds. *Interdisciplinary Therapy: Using Contemporary Approaches for Complex Cases.* Monograph 52, Craniofacial Growth Series, Center for Human Growth and Development, The University of Michigan, Ann Arbor, 2016:195-242.

2.1   Introduction

The alveolar processes of the mandible and maxilla line the alveolus and provide structural support and maintenance for teeth as part of the periodontium, consisting of the periodontal ligament (PDL), cementum, connective tissue, and gingiva. Alveolar bone is especially susceptible to inflammation-induced bone resorption due to high rates of progressive periodontitis—a leading chronic oral inflammatory disease estimated to affect 47.2% of adults in the United States, with a prevalence of 70% for adults aged 65 years and older [1]. Advanced periodontal disease alters alveolar bone morphology and destroys surrounding tooth-supporting tissues, thereby necessitating tooth extraction. Since the existence of alveolar bone is mutually connected to the dentition and other periodontal tissues, the alveolar ridge continues to resorb following tooth

removal even if a dental implant is placed into a fresh extraction socket. Physiologically, this is caused by continuous bone remodeling in response to mechanical loading changes that occur with alterations in the applied force and strain distribution to the osseous tissue during mastication, as stipulated by Wolff's Law [2]. Ridge or socket preservation and augmentation using bone grafting materials is a clinically viable approach to maintain any remaining bone following tooth extraction and further condition it in preparation for dental implant placement. Sufficient bone volume, height, and width are necessary to ensure implant stability and osseointegration that can sustain optimal bone-implant contact biomechanical loading. Other dental procedures that involve grafting include maxillary sinus floor augmentation, which is employed for patients with bone loss in the posterior maxilla that houses premolar and molar teeth [3]. Bone defects in the oral cavity resulting from trauma, chronic infection, congenital defects, or surgical resection require clinical intervention, most frequently using autologous bone grafting techniques. However, critical limitations of this approach include donor site morbidity and inadequate supply of graft tissue. Tissue engineering approaches using scaffolds alone or in combination with growth factor, cell and/or gene delivery have the potential to address existing challenges in managing bone loss and increase clinical options for controllable regeneration of intraoral osseous tissues.

2.2   Scaffolds

2.2.1   *Intraoral bone grafts*

An autologous bone graft is considered the gold standard due to low risk of immunogenicity or disease transmission that could be associated with an allograft (genetically different donor from the same species) or xenograft (donor from another species). Most importantly, bone transplanted from the patient is native to its host environment and readily associates with the remnant tissue, providing a pre-established population of viable cells and growth factors necessary for osteogenesis. Local sites such as the maxillary tuberosity or mandibular symphysis can be used for harvesting of small autologous grafts [4]. Nevertheless, there are several key reasons for a critical need of alternative grafts capable of substituting the autograft: limited availability of autologous tissue for larger bone defects, donor site morbidity and potential wound-based infections, as well as prolonged operative times [5]. Although lacking in osteogenicity, allografts and xenografts can be prepared to have osteoconductive and osteoinductive properties. Bone allografts are available as fresh/fresh-frozen, freeze-dried, or

demineralized and freeze-dried. The mechanical properties of allografts derived from a living donor or cadaveric tissue are changed substantially during extensive tissue processing involving decellularization, sterilization, and preservation for clinical use [6]. Such tissue treatment removes viable cells that are osteogenic and osteoinductive in nature, leaving behind a structurally supportive framework primarily composed of minerals and proteins—termed the extracellular matrix (ECM). The allograft ECM serves as a scaffold for osteoblasts originating from the bone defect into which the graft is placed to facilitate new bone formation. Depending on the method of processing, an allograft can also be osteoinductive if it retains the biological properties necessary to recruit mesenchymal stem cells to the site and stimulate their differentiation into osteoprogenitor cells. One example is demineralized bone matrix (DMB), which has reduced levels of calcium and phosphorus and is primarily type I collagen, but can be considered osteoinductive if it retains factors such as bone morphogenetic proteins (BMPs) and transforming growth factor-β (TGF-β) [7]. As expected, DMB shows an increased rate of resorption relative to a mineralized bone graft during tissue remodeling *in vivo*. In addition, derivation of DBM involves grinding of bone to obtain particulates as opposed to processing the allograft in its native structural form, making it useful for small to moderate defects [8].

Xenografts offer another alternative for bone replacement in dental regeneration, with most products derived from coral, porcine, or bovine sources. A recent study comparing implant placement into sinus floors augmented with an autologous mandibular bone graft versus a commercially-available bovine xenograft found equivalent implant survival rates over an observational period of 5 years [9]. However, implant survivability depends on many factors, including patient demographics and surgical technique, thereby warranting longer-term evaluations and more comprehensive consideration of factors that may influence the clinical outcome. Extensive meta-analysis of histomorphometric and bone graft healing time results for sinus floor augmentation described in the literature over a period of 16 years concluded that autologous bone grafts result in higher total bone volume levels compared to other bone grafting materials [10]. Another comprehensive systematic review of treatment modalities used to evaluate dental implant survival rates in maxillary sinus grafts employed statistically robust methodology to correct for study effects. It concluded that application of grafting membranes for guided bone regeneration supplementary to a bone graft was more important for implant survival rate over factors such as which bone substitute material was selected for the surgery [11]. These results

indicate the difficulty of identifying specific factors that influence final clinical outcomes and underline the fact that there is no unified consensus on whether non-patient derived grafts can perform at the same level as autografts for not only bone regeneration but also implant performance at augmented bone sites. Each case is patient-specific and requires thorough consideration of all contributing factors, including the health of the patient's native bone and its suitability for grafting procedures.

2.2.2 *Natural and synthetic matrices for bone regeneration*

In addition to standard grafting procedures using bone-derived materials, a number of natural and synthetic materials have become commercially available for use in oral surgery. Scaffolds that are architecturally and/or biologically compatible for bone regeneration are frequently based on one or more of the bone's naturally-occurring proteins or minerals, including organic (predominantly collagen type I) and inorganic (hydroxyapatite, a calcium phosphate mineral) components [12]. Calcium phosphate (CaP) materials are subdivided into ceramics and cements, which vary in their rate of *in vivo* degradation, structure, and mechanical strength. Common synthetic CaP bone substitutes include hydroxyapatite (HA) ceramics, β-tricalcium phosphate (β-TCP) cements, and biphasic calcium phosphates (BCPs) [13, 14]. Fragility and poor fatigue resistance of these ceramics and cements requires their use at non-load bearing bone replacement sites or as coatings on load-bearing metal implants for increased bone-to-implant contact. Coating a dental implant surface (i.e., titanium, stainless steel, or an cobalt-chrome alloy) with CaP-derivatives has been extensively investigated using various surface coating deposition techniques to improve implant stability and rate of osseointegration [15, 16]. In addition to containing minerals native to osseous tissue, these biomaterials retain an interconnected porous architecture--allowing adequate space through increased surface area for bone ingrowth via cell infiltration, blood vessel formation, nutrient/oxygen transport, and waste elimination. Ongoing studies are being performed to determine the optimum porosity for bone ingrowth and corresponding bone substitute resorption rate, since an ideal regenerative scenario would consist of a biomaterial resorption rate timed with new osseous tissue ingrowth [17]. Likewise, there are ongoing investigations to confirm the utility of using CaP bone substitutes for implant coating. For example, recent studies of hydroxyapatite coatings on titanium cups for orthopaedic-based

implants such as femoral stems did not show significant differences between HA-coated and non-coated stems and may not constitute a clinical advantage [18].

Bioactive glass (BG), a silicon oxide with substituted calcium first developed in the 1960s by Professor Larry Hench, is a biocompatible glass-ceramic material approved by the US Food and Drug Administration (FDA) for use as a synthetic intraoral bone graft (termed 45S5 Bioglass®). Upon exposure to aqueous solutions the highly reactive surface converts to a gel layer that mineralizes to form a osteoconductive hydroxycarbonate apatite layer that chemically binds with osseous tissues [19]. Bioglass® also has a reported reduced modulus of 35 GPa that is similar to that of cortical bone ($E_{longitudinal}$ = ~14-20 GPa) [20, 21]. Comparatively, the elastic moduli of HA single crystals and β-TCP are in the range of 54-79 GPa and 120-162 GPa, respectively [22, 23]. This makes BG an attractive option for metal implant coating, reducing the potential for stress shielding and subsequent bone resorption which occurs with decreased bone loading [24]. To date, studies using dental implants coated with BGs have not conclusively shown significant increases in osseointegration relative to other coatings such as HA [25]. However, novel exploratory combinations for dental implant coatings using BG are promising: one example is the incorporation of BGs with HA and the polymer poly(lactide-*co*-glycolide) (PLGA), which indicates rapid bone-like apatite formation in vitro, with potential antimicrobial activity on oral bacteria [26].

Polymeric materials that have been commercialized or are currently under investigation for intraoral bone regeneration are either naturally- or synthetically-derived. Natural materials that consist of polymeric networks (i.e., collagen, alginate) have been extensively investigated as composite materials with other bone replacement grafts, including β-TCP and HA [27]. Major advantages of a tissue-sourced polymer such as collagen include its biocompatibility, biodegradability, and ability to readily bind growth factors critical for osteoinduction, including BMPs. Currently, collagen is the most commercially-available natural polymer on the market for use in periodontal bone regeneration as a sponge, membrane, or in particulate form combined with other bone grafts [28]. It is expected that future research will continue to focus on the development of a more diverse array of naturally-derived, fully-resorbable polymeric bone grafts combined with non-immunogenic materials such as alginate and chitosan that can be engineered for growth factor, cell, and/or gene delivery. Such delivery devices may also include synthetically-derived resorbable materials whose physical, mechanical, and degradation properties can be more easily controlled

via polymer chemical composition and molecular weight. Historically, oral surgery has utilized non-resorbable synthetic membranes as cell-occlusive barriers for guided bone regeneration, among which the most broadly used material has been expanded polytetrafluoroethylene (ePTFE) [29]. Unnecessary patient discomfort and added cost of a follow-up visit to remove the membrane has increased demand for resorbable alternatives. Examples of widely-investigated resorbable polymers for applications in bone regeneration include poly-α-hydroxy esters such as polyglycolic acid (PGA), polylactic acid (PLA), and PLGA. The ease of processing synthetic materials enables their fabrication into a variety of structurally-diverse forms, including thin films, meshes, fibers, and porous foams. An existing disadvantage of these materials is their bulk erosion *in vivo* due to hydrolysis that can induce foreign body reactions to acidic polymer degradation products, increasing the potential for fibrous tissue encapsulation during wound healing. Although studies of PLGA utility for guided bone regeneration are still limited, there is evidence that its use as a barrier membrane results in alveolar bone regeneration that is on par with that observed using a collagen-based membrane [30]. Other copolymer combinations that yield useful properties for osseous tissue regeneration include PLGA with poly(ethylene glycol) (PEG), a widely used biocompatible hydrophilic drug delivery carrier. PEG-PLGA thermo-sensitive copolymers can be encapsulated with osteoinductive factors and polymerized into a gel-like structure for delivery into an osseous defect, possibly in combination with other mechanically durable bone grafts [31]. PCL is another biodegradable polymer with significant research indicating its suitability for bone regeneration. An inert material, it shows increased osteoblast adhesion, spreading, and proliferation when coated with CaP or HA [32], and multiple studies have indicated PCL's potential to promote alveolar bone formation in periodontal defects [33, 34]. With greater emphasis placed on materials that can be used for exogenous factor delivery to accelerate and improve existing periodontal tissue defect treatments, polymers such as PCL and PEG which are already FDA-approved as drug delivery devices are expected to be more extensively investigated in pre-clinical models of intraoral bone regeneration in the coming years.

2.2.2 *Natural and synthetic matrices for periodontal ligament regeneration*

The presence of antimicrobial properties and anti-inflammatory effects of naturally-occurring materials such as chitosan also make them applicable matrices and periodontal ligament (PDL) cell-carriers for periodontal tissue regeneration [35]. Composite collage/chitosan scaffolds

can be formed for mechanical reinforcement, and have shown increased human PDL cell adhesion and growth compared to collagen or chitosan alone. Composite scaffolds increased the retention of water, contributing to an increase in pore size and thereby the total internal surface area available for PDL cell invasion [36]. To prolong the residence time of scaffolds in vivo for complete tissue growth and remodeling, increased stiffness and a decreased rate of degradation of natural matrices is preferable, and can be accomplished through their integration with synthetic polymers.

Synthetic biodegradable polymers such as PLGA and PCL are used clinically in drug delivery systems, surgical sutures, and orthopedic fixation devices. These hydrolytically degradable materials undergo cleavage of polymer chains to oligomers and monomers, producing lower molecular weight molecules in the process [37]. As with naturally-derived matrices, these polymers are most applicable for periodontal regeneration when used in combination with cell and growth factor delivery [38, 39], as the material itself has little biological functionality, although it can be improved with the application of protein coatings. However, one of the key advantages of synthetic polymers includes their ability to be formed and processed in a variety of ways to yield highly aligned structures that can be achieved using electrospinning--a technology allows for the formation of long, thin fibers on the nano and micron scale. This technique offers potential for controlled fiber orientation that can be used to influence cell behavior through structural and physical cues that mimic ECM architecture, and allows control over a variety of parameters that determine fiber dimension, density, and porosity [40]. Chen et al used electrospun PLGA/gelatin sheets that were applied at tooth extraction sites in combination with dentin matrix, resulting in the formation of PDL-like tissues [41].

Typically, poly-α-hydroxy acids such as PLGA result in an inflammatory reaction involving multinucleated cells. Rates of degradation vary depending on the molecular weight and copolymer ratios of PLGA, allowing it to be more easily tailored to the expected rate of tissue re-growth at the defect site. After treatment of critical-size supra-alveolar periodontal defects in dogs with rhGDF-5-coated β-TCP/PLGA scaffolds, Kwon et al observed limited residual rhGDF-5/β-TCP/PLGA in two of five sites at 8 weeks, with higher residual amounts present in four of five sites with β-TCP/PLGA only [42]. Given that residual material may obstruct periodontal tissue regeneration, it has been noted with synthetic materials as much as with natural materials that incorporation of growth factors increases the rate of carrier remodeling. In fact, Koo et al also noted this using a ceramic-based calcium carbonate carrier with TGF-β in a critical-size, supra-

alveolar periodontal defect: the growth factor was found to accelerate the degradation of the carrier relative to calcium carbonate without TGF-β [43].

2.3 Engineering Scaffolds for Intraoral Bone Regeneration

The development of scaffolds that are optimal for regeneration of osseous tissues requires a design strategy which adheres to established knowledge of the mechanical, chemical, structural, and biological properties of natural bone that make it a functional entity. Therefore, key considerations in such scaffold design include: (1) biocompatibility/non-toxic degradation; (2) bioactivity, enabling cell interaction with material surface; (3) maintenance of a 3-D shape after implantation; (4) adequate porosity and pore diameter/distribution/orientation; (5) mechanical properties similar to tissue targeted for regeneration (i.e., Young's modulus); (6) degradation mechanics (i.e., bulk erosion, surface erosion); (7) degradation rate, ideally matching the rate of tissue regeneration; and (8) osteoconductive/inductive and angiogenic factors to influence infiltrating cell populations and promote blood vessel invasion [44, 45].

While a broad range of instructive carrier materials in various forms have been investigated for bone regeneration, the addition of cells and application of growth factor delivery strategies can significantly influence the regenerative outcome by engineering the environment that closely matches that of the target tissue in its native state (see **Figure 1**). Current strategies include the use of bone-marrow stromal cells and stem cell varieties including mesenchymal (MSCs), adipose-derived (ADSCs) and induced pluripotent (iPSCs). Analyses of cell-specific markers and transcription factors such as Runx2, alkaline phosphatase (ALP), osteocalcin, osteopontin, and osteonectin allow for the determination of osteogenicity during stem cell differentiation into bone-derived cells [46]. Clinically-applicable cell therapy is focused on the use of patient-derived stem cells that are undifferentiated, given that terminally-differentiated cells are difficult to expand *ex vivo* relative to more highly proliferative stem/progenitor cells. Likewise, the use of stem cells allows for a more completely physiological repair process that involves the differentiation of MSCs or iPSCs not only into bone-derived cells but also cell types involved in neovascularization, such as endothelial cells. However, despite significant progress and tremendous potential in cell therapy, critical challenges remain in transitioning the use of iPSCs into clinically-applicable approaches. Since the creation of iPSCs involves the reprogramming of somatic cells via transcription factors to produce cells with embryonic stem cell-like properties, there is risk of

epigenetic and genetic defect accumulations, immunogenic responses, or tumor formations. While the immunogenic response can be mediated through use of a patient's native somatic cells, overexpression of transcription factors or presence of partially-reprogrammed iPSCs are known to cause teratoma formation, requiring significant efforts to address these safety concerns prior to the consideration of iPSCs for patient-based treatments [47].
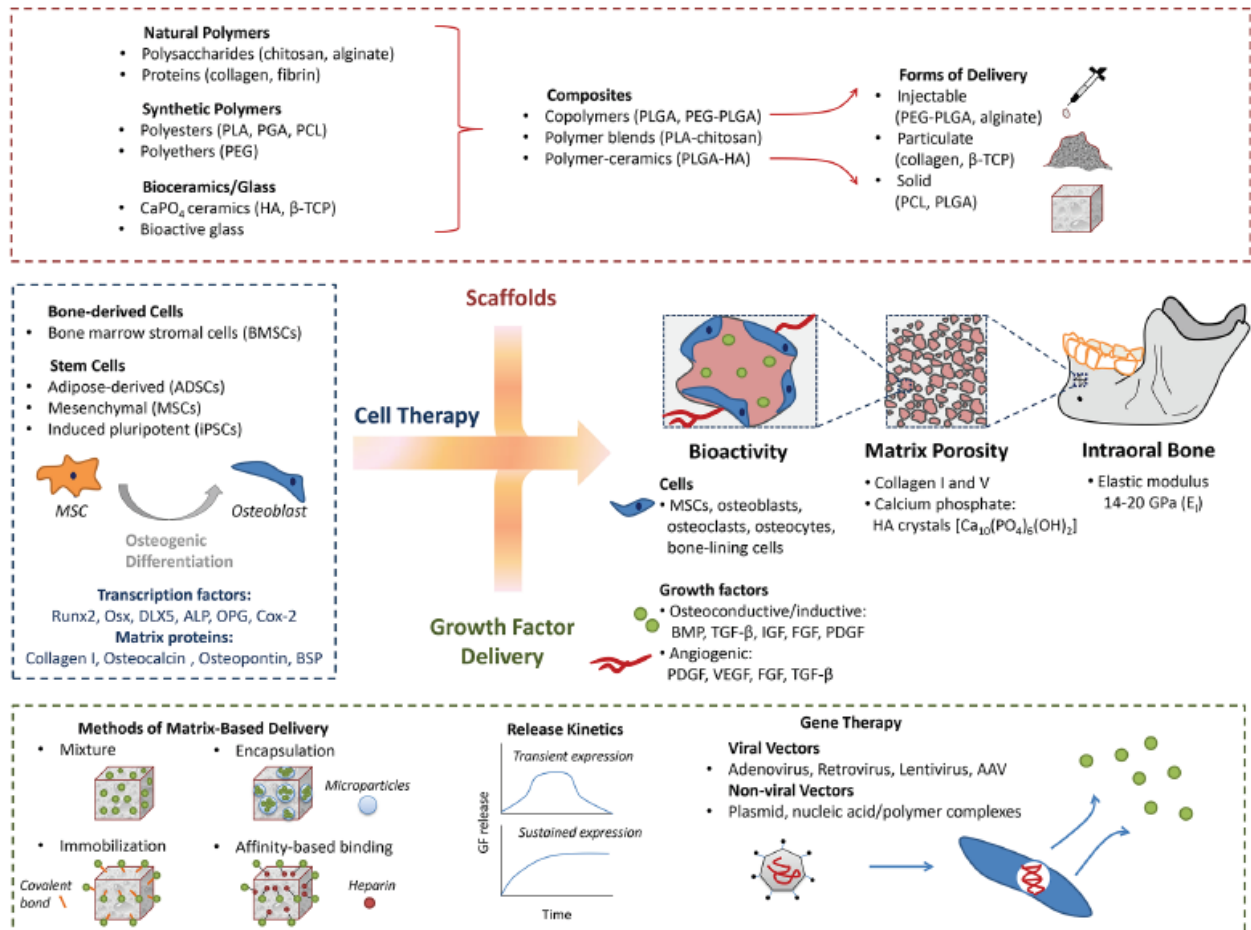
Figure 2.1 Scaffold Material Selection, Cell Therapy, And Growth Factor Delivery
A combination of various approaches in scaffold material selection, cell therapy, and growth factor delivery is required to achieve optimal tissue regeneration that mimics the mechanical, chemical, structural, and biological properties of natural bone that make it a physiologically functional entity. Abbreviations: [*Scaffolds*] Polyglycolic acid (PGA), polylactic acid (PLA), poly(lactic-co-glycolic acid) (PLGA), poly(ethylene glycol) (PEG), hydroxyapatite (HA), β-tricalcium phosphate (β-TCP); [*Cell Therapy*] Osterix (Osx), alkaline phosphatase (ALP), osteoprotegerin (OPG), bone sialoprotein (BSP); [*Growth Factors*] bone morphogenetic protein (BMP), transforming growth factor-beta (TGF-β), insulin-like growth factor (IGF), fibroblast growth factor (FGF), platelet-derived growth factor (PDGF), vascular endothelial growth factor (VEGF).

With advancements in cell therapy, there has been a simultaneous increase in novel scaffold fabrication techniques that emphasize greater control over surface topography, internal microstructure, and pore interconnectivity. Traditionally, porous scaffolds have been widely explored as bone graft substitutes for cell attachment given the importance of allowing adequate room for tissue ingrowth and vascularization (i.e., pore size of 150-500 µm) [48]. While natural materials retain their bioactivity, synthetic non-immunogenic materials have several advantages for development of clinically-translatable scaffolds, including added flexibility in manufacturing, reproducibility, sterilization, and storage times. Electrospinning and solid freeform fabrication (SFF) are two scaffold fabrication techniques which allow increased control over scaffold morphology: Electrospinning is a polymer-processing technique used for creating polymer fibers on the nano and micron scale to influence cell behavior through structural and physical cues that mimic ECM architecture. In addition to allowing control over a variety of parameters that determine fiber dimension, density, and porosity, electrospinning can readily be used for mass production of fiber-based scaffolds [49]. More recently, 3-D printing technology has been adapted for use in bone tissue engineering via solid freeform fabrication (SFF), a rapid prototyping technique. This process consists of developing a computer-aided design (CAD) file that specifies the exact dimensional features of the desired scaffold which is then transferred to a 3-D printer that reproduces the file to yield a printed version of the design with structural integrity. Selective laser sintering (SLS) is an example of a process that creates objects layer-by-layer using polymeric, ceramic, or metal powders that the machine sinters. During sintering, the powder is heated below the melting point, causing its particle boundaries to fuse together at locations dictated by the CAD-based file. When creating a porous material, the sizes and characteristics of the individual pores within the material are limited by the machine's resolution and ability to support a specific printing material [50]. Studies using SLS for bone regeneration have focused on PCL-based printed scaffolds, showing that these are mechanically-appropriate to support bone tissue formation and can be used as BMP-7 and BMP-2 growth factor carriers following biofunctionalization [51, 52]. This technology is especially applicable for clinically-based studies given that patient-specific anatomical bone defects can be obtained using computed tomography (CT) scans and reproduced to yield a scaffold with appropriate structural dimensions. A recent publication by Park et al proposes a potential future application of image-based PCL SFF-based scaffolds for clinical

periodontal regeneration (see **Figure 2**), indicating that further pre-clinical investigation and verification of these technologies will bring them closer to translation into clinical practice [53].
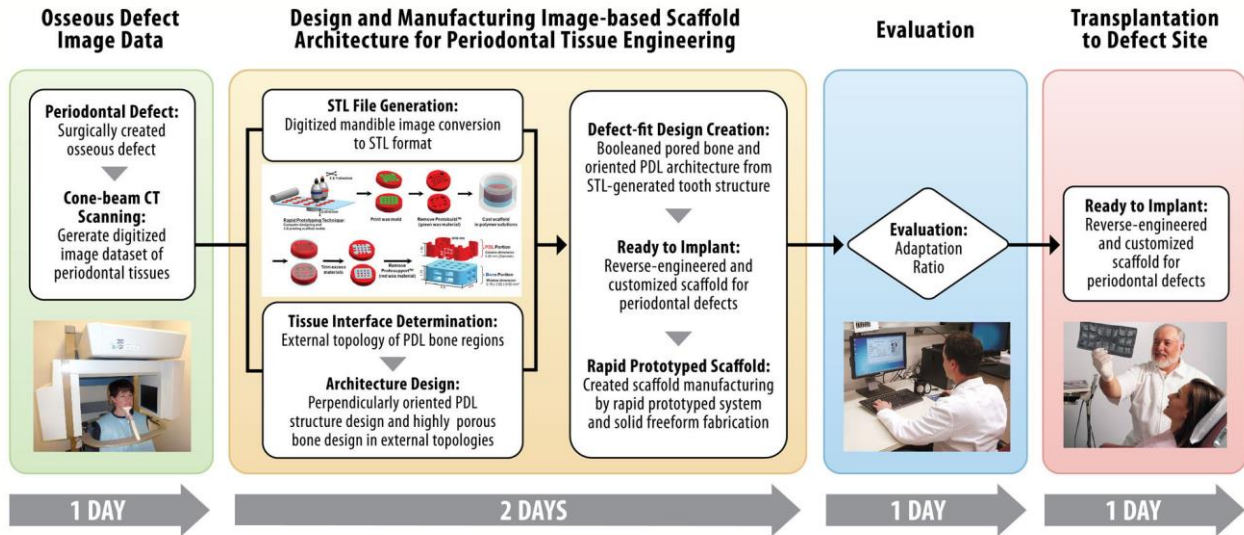
Figure 2.2 Formation of SFF-based Scaffolds for Clinical Application
Solid free-form fabrication (SFF), or rapid prototyping, is emerging as a clinically-viable approach for tissue engineering of anatomically precise scaffolds for periodontal, including intraoral bone, regeneration. This method is based on obtaining a CT scan of the patient-specific defect, generating a CAD-based file of a scaffold with an appropriate fit to the defect, and 3-D printing the final version to obtain a polymer-based scaffold with structural integrity that can be used as a cell therapy and growth factor delivery platform to enhance the regenerative process. Reproduced with permission from Park CH et al [52].

While novel methods of scaffold development and cell therapy are being explored for bone regeneration, there is already an established array of clinically-applicable therapeutic factors and delivery strategies. In order to better understand existing clinical applications and the nature of ongoing pre-clinical studies, the remainder of this review focuses on the areas of growth factor delivery for oral bone regeneration and highlights some of the key studies that have moved previously experimental therapies into today's mainstream clinical applications in periodontal regeneration.

2.4   Growth Factors and Protein Delivery

Growth factor delivery (GFD) is of critical importance in mediating the scaffold environment and subsequent cellular response. Growth factors are soluble polypeptides that bind

to cell membrane receptors and influence cellular function, and the inclusion of osteoinductive/conductive factors (BMP, TGF-β, IGF, FGF-2, PDGF) guides the cell differentiation and tissue formation process in bone regenerative therapies. Likewise, vascularization is vital for the sustainability of newly-formed tissue, and necessitates the inclusion of GFs with angiogenic properties (PDGF, VEGF, FGF-2, and TGF-β). Scaffold-based GFD as opposed to bolus injection of the therapeutic factors into the defect site has several advantages, including the potential for improved control over GF release kinetics and localization. A major challenge in GFD involves the need for release profiles that mimic those present during natural tissue repair or morphogenesis. Sequential or simultaneous spatiotemporal delivery of multiple GFs can be achieved using scaffolds based on the therapeutic time window during which GF delivery is optimal for tissue regeneration, and can involve the combination of factors involved in both tissue formation and angiogenesis. For example, sequential delivery of GF combinations consisting of BMP-2 and TGF-β or VEGF and BMP showed increased bone formation when compared to single GFD [54, 55]. GF rate of release is governed by how it is bound to the scaffold, which can involve (1) mixing the GF with scaffold particles, (2) physical encapsulation within the scaffold, (3) chemical immobilization, and (4) affinity-based binding. Current clinical application of GFs for bone regeneration typically involves the use of biomaterial carriers, yet the factor is usually mixed in and physically adsorbed onto the graft particles and lacks more sophisticated modes of delivery that would enable spatiotemporal control over release kinetics or dual GFD. Other modes of delivery currently investigated in pre-clinical studies are promising: Physical encapsulation of GFs within the scaffold, for example, can be achieved using polymeric microparticles (1-100µm) with varying surface areas through which the encapsulated GF diffuses at a rate that is dependent on carrier particle size, with a larger size leading to slower diffusion. GFs can also be conjugated on the scaffold surface via covalent immobilization, while heparin-binding GFs such as BMP-2 can be presented using affinity-based binding by conjugating heparin to biomaterials [56, 57]. These modes of GFD have potential for future applications in clinical studies, allowing for a broad range of release profiles and controlled spatiotemporal presentation of multiple GFs using carriers that serve as temporary support structures for osseous tissue engineering strategies.

Growth factors and proteins act locally on the activity of periodontal cell populations to modulate bone formation and enhance the regenerative response (see *Table A1.1* in Appendix). A

diverse range of bone matrix-based proteins have been isolated and are delivered alone or in combination with a synthetically- or naturally-derived bone graft. An overview of some of the factors and proteins that are featured most prominently in oral-based surgery or currently being investigated in pre-clinical (see *Table A1.2* in Appendix) and clinical studies (see *Table A1.3* in Appendix) is presented.

2.5   Pre-clinical Studies using Growth Factor and Protein Delivery

2.5.1   *Platelet-derived growth factor (PDGF)*

PDGF's primary role is the promotion of soft-tissue healing. It was introduced to improve healing of diabetic ulcers, and was later approved for periodontal regeneration [58, 59]. *In vitro* studies show that PDGF stimulates cell populations key for periodontal regeneration, increasing cementoblast DNA synthesis and regulating osteopontin expression [60]. PDGF stimulates PDL cell chemotaxis and mitosis, and has synergistic proliferative effects when combined with allografts [61, 62]. PDL cells may modulate bone formation by increasing osteoblast proliferation and blocking osteoblast differentiation and expression of the mineralized tissue markers osteopontin and osteonectin [63-65]. In canine and primate models, application of PDGF, often combined with insulin-like growth factor (IGF), to periodontal defects resulted in increased bone, cementum, and PDL formation [66-72]. In a canine class III furcation defect model, guided tissue regeneration (GTR) with PDGF-BB and ePTFE membranes stimulated PDL formation in early stages followed by total periodontal regeneration [73]. PDGF/IGF-1 for guided bone regeneration (GBR) at implants placed into extraction sockets showed increased early (3-week) histologic and clinical bone formation [66, 74, 75]. When combined with xenograft, PDGF at immediate implants in canines resulted in enhanced radiographic bone gain when used without a collagen membrane [76]. PDGF also enhanced lateral GBR in dogs when used with a collagen membrane and xenograft or alloplastic graft material. In another canine model testing for vertical ridge augmentation, PDGF in a xenogeneic block graft showed increased histologic bone gain when used without a collagen membrane [77, 78].

2.5.2   *Bone morphogenetic proteins*

BMPs are members of the transforming growth factor-beta (TGF-β) superfamily and have strong osteoinductive properties, especially BMP-2, -4, -6, -7, and -9 [79, 80]. BMP-2 and BMP-

7 stimulate PDL cell differentiation into osteoblasts and increase expression of mineralized tissue markers when combined with PDL cells or osteoblasts *in vitro*, although doses greater than 10 ng/mL may be toxic to cells [81-85]. BMPs have also been shown to down-regulate proliferation and mineralization of cementoblasts and gingival fibroblasts. They are used primarily to enhance bone formation for implant site development. When applied to periodontal intrabony defects, BMPs showed enhanced speed and quantity of bone formation but limited cementogenesis, complicated by ankylosis and root resorption [86-92]. Commercially, rhBMP-2 is approved for extraction socket and sinus augmentation. In rat extraction sockets, BMP-2 was shown to increase the speed and quantity of bone formation via its osteoinductive effects [93]. In sinus augmentation models in various species, BMP-2 consistently improved histologic and radiographic bone gain [94-98] and there are indications that it may provide significant vertical and horizontal ridge augmentation. Delivery of BMP-2 via grafting materials may modulate its effects on bone formation, contour, and quality [99-103]. Possible complications of BMP-2 delivery shown in canine ridge augmentation models include increased incidence of seromas and wound failure [100]. When compared to BMP-2, BMP-4 has been shown to have comparable effects on bone gain and improved bone quality in a rat ridge augmentation model [99]. BMP-7, also known as osteogenic protein-1 (OP-1), has similar applications as BMP-2 [104-110]. BMPs may be suitable for periodontal regeneration as demonstrated in canine class III furcations and its modulatory effects on cementoblast mineralization *in vitro* [104, 111].

2.5.3   *Fibroblast growth factor-2*

FGF-2 was initially found to stimulate proliferation of bovine fibroblasts. It has effects in soft tissues by inducing proliferation of gingival epithelial cells, gingival and connective tissue fibroblasts, and PDL cells [112-116]. Interestingly, FGF-2 inhibits mineralization and ALP expression by PDL cells but allows them to maintain their differentiation potential and express bone regulatory compound osteopontin [113, 117]. These features, coupled with its strong angiogenic potential, may allow FGF-2 to promote an environment favoring periodontal regeneration [113, 118]. FGF-2 applied topically has been studied in primate and canine class II furcation defect models, where it significantly increased regeneration of PDL, cementum, and bone without adverse effects [115, 119]. GTR with FGF-2 and a collagen membrane resulted in more defect fill in dog class III furcations versus control groups [120].

2.5.4 Growth/differentiation factor-5

Like BMPs, GDF-5 is another member of the TFG-β superfamily and shares a similar structure [121]. It stimulates PDL cell proliferation, early osteoblast differentiation, and extracellular matrix synthesis by both cell types [122, 123]. It has been shown to significantly increase periodontal regeneration in canines and primates with a β-TCP carrier [124, 125]. Various other carriers tested in dog periodontal regeneration showed a primarily positive effect [126, 127]. In implants, GBR with GDF-5/β-TCP carrier showed increased peri-implant bone, while GDF-5 coated implants had increased stability determined by pull-out test in rabbits [128]. GDF-5 has also been used in mini-pig sinus augmentation, where it enhanced bone formation with a β-TCP carrier [129, 130]. In lateral ridge augmentation with a coated Bio-Oss® block, GDF-5 resulted in increased mineralized tissue formation [131].

2.5.5 Teriparatide

The osteoporosis medication teriparatide consists of parathyroid hormone's first 34 amino acids. In vitro and depending on cell state, teriparatide influences PDL cell survival and causes osteoblast-like behavior with increased osteoprotegerin expression [132, 133]. It has been tested in rats with induced osteoporosis, where it caused increased bone mineralization and formation in extraction sockets and prevented periodontal bone loss [134, 135]. In canine GBR, teriparatide improved bone formation around implants [136, 137].

2.6 Clinical Applications of Growth Factor and Protein Delivery

Periodontal regenerative therapies focus on bone regeneration to provide implant site development. Guided bone/tissue regeneration is the most well-documented technique for targeted bone regeneration and is designed to exclude undesired cells using barrier membranes [138] . Under certain circumstances (i.e., defect shape and size) both procedures have shown high predictability; nonetheless, due to the non-osteogenic characteristics of available biomaterials (xeno-/allo-geneic), some shortcomings have arisen for challenging situations (i.e., vertical bone augmentation). The application of growth factor and protein delivery might overcome these limitations by inducing the proliferation of MSCs to achieve bone formation [139, 140]. Indeed, this approach has shown very promising results from countless pre-clinical studies [141, 142] (see *Table A1.3* in Appendix), which has aroused enthusiasm among clinicians.

Within osseous regeneration, PDGF-BB has been tested for infrabony defects and alveolar bone regeneration. Recently, a multicenter randomized double-masked clinical trial aimed to evaluate the long-term stability of periodontal defects in patients with localized severe periodontitis filled with rhPDGF-BB in a β-TCP scaffold vs. scaffold alone. Results from this study showed that the use of PDGF-BB (0.3 mg/mL) after a 36-month follow-up achieved 87% of bone gain compared to the control group (53.8%). It was also found that, albeit not reaching statistical difference, the steady increase of clinical attachment level and linear bone gain suggest the long-term stability when using this growth factor [143]. These findings were in agreement with results obtained by Jayakumar et al. in a shorter follow-up clinical trial [144]. These demonstrated that after 6 months, a significant increase in bone fill (65.6%) was achieved when using 0.3 mg/mL of PDGF-BB vs. β- TCP alone (47.5%) [59]. Nevins et al. also reported that the use of PDGF-BB in combination with demineralized freeze-dried allogeneic bone graft is capable of attaining complete regeneration of the attachment apparatus for infrabony and Class II furcation defects [145]. Therefore, PDGF-BB seems to promote periodontal regeneration in a safe and effective manner. However, the available data is still limited to draw clear conclusions about its potential. Likewise, PDGF-BB has also been recently used for increasing the predictability of alveolar bone regeneration. Nevins et al. evaluated the effect of PDGF-BB compared with enamel matrix derivative (EMD) and two other grafting materials upon newly formed bone in socket regeneration [146]. Due to the small sample size and weak defect standardization it was not possible to draw a clear line between groups; nevertheless, ridge morphology for implant placement was more convenient for the PDGF-BB group. More recently, the same group [147] studied in a case-series the effect of PDGF-BB in combination with equine/bovine grafting materials on bone regeneration of large extraction site defects. Histologic results revealed new bone formation in association with remaining graft particles and no evidence of inflammatory cell infiltration. Accordingly, horizontal/vertical alveolar bone augmentation might become a more predictable technique with the use of PDGF-BB.

In 2007, rhBMP-2 was approved by FDA as an alternative to autologous bone grafting in alveolar ridge augmentation and sinus elevation procedures [148] due to its osteoinductive potential [149]. Results obtained for sinus augmentation indicate that when compared to autogenous bone, no differences can be observed by means of vertical bone gain and density [150]. Nonetheless, if rhBMP-2 is grafted with autologous bone it seems to increase cell activity, osteoid

lines and vascular supply [151,153]. Contrasting these findings, Kao et al. showed that when rhBMP-2 was blended with bovine-derived xenogeneic graft, less bone formation was found. Authors claimed that this may be due to the enhancement of osteoclast differentiation by the adjustment of RANKL, a protein involved in bone remodeling and regeneration [154]. Additionally, the safety of the growth factor was demonstrated by lack of an immune response in any of the studies [150-152]. Therefore, agreement was found between human clinical trials and preclinical studies [153]. However, more clinical studies need to be conducted focusing on the effect of the carrier and dose-dependent responses [154]. Other findings indicate that rhBMP-2 preserves alveolar ridge heights while also increasing their horizontal dimensions [155-157]. Fiorellini et al. noted the dose-dependence of the protein, showing that a 1.5 mg/mL dose was more optimal than 0.75 mg/mL. Nevertheless, it is worthy to note that although overall safety of rhBMP-2 was demonstrated, moderate signs of local inflammation were present, which may be a trigger for an impaired healing process.

BMP-7 has been predominantly studied for sinus augmentation. Using a small sample size case study, Corinaldesi et al. compared the use of rhBMP-7 with deproteinized bone (0.5g) vs. deproteinized bone alone (2g). Although there were no observed differences by means of bone gain, newly formed bone was statistically greater for the control group (19.9% vs. 6.6%) 4 months after grafting [158].

Another recently studied growth factor is GDF-5, which has been used for periodontal regeneration, alveolar bone and sinus augmentation procedures. A pilot randomized clinical trial was conducted to study the effect of GDF-5 embedded in β-TCP for infrabony periodontal defects of chronic periodontitis patients. Six months after therapy the clinical attachment gain for the test group was almost double compared to the level gained in the control group (3.4mm vs. 1.7mm), although this was not statistically significant [159]. To date, only one study has appraised the use of rhGDF-5 for sinus augmentation: Koch et al. found that at 4 months GDF-5 behaved similarly to an autologous graft in terms of bone formation (28% vs. 32%) [160]. Notably, larger bone augmentation occurred in the composite group of GDF-5 combined with β-TCP regardless of the time point assessed.

After being evaluated in pre-clinical model and showing its effectiveness in regenerating periodontal defects, FGF-2 has also been tested for human use due to its robust angiogenic and mitogeneic potential [119]. Kitamura et al. showed in a Phase 2B multicenter randomized clinical

trial that at 36 weeks after periodontal surgical therapy, bone fill was 35% greater when used with 0.3% FGF-2 compared to the carrier alone [161]. An insignificant increase occurred from 36 up to 72 weeks, which may be explained by different patterns of healing (regeneration vs. long-junctional epithelium).

Currently, teriparatide is being investigated for craniofacial regeneration [161]. One clinical trial assessing its effect on periodontal regeneration in moderate to severe chronic periodontitis patients showed that the adjuvant of teriparatide administration combined with vitamin D daily with periodontal surgery had a favorable influence on attachment levels and bone repair. In addition, it is worthy to mention that improvements were correlated with baseline levels of 1.25 dihydroxyvitamin D3 (better results with baseline levels >20ng/dL) [163]. The use of teriparatide might increase the reliability in cases of poor bone density. Kuchler et al. conducted a randomized controlled feasibility study to appraise the effect of 20 μg of teriparatide daily during 28 days on mandibular dental implants, finding that after a healing period of 9 weeks, new bone-volume-per-tissue-volume for the teriparatide group was 17.6% and 15.4% for the control group. In addition, it was shown that bone-to-implant contact was shown to be higher in the periosteal and medullary compartment for the test group, but not for the cortical compartment (5% vs. 4.4%, respectively) [164]. Based on these findings, the safety and efficacy of several growth factors have been documented, but more clinical trials are necessary to validate these preliminary studies.

2.7   Cell and Gene Delivery

To enhance the therapeutic potential of growth factor delivery, gene therapy has emerged as a method of establishing sustained growth factor expression through the transduction of cell populations via viral and non-viral delivery mechanisms that alter gene expression. Currently investigated methods of vector delivery for intraoral bone regeneration and existing pre-clinical studies of their success are addressed below:

2.7.1   Methods of Gene Delivery

2.7.1.1 Therapeutic viral gene delivery

Targeted gene delivery can be achieved using viral vectors engineered to infect cells with genetic material that will compensate for defective gene(s) or produce a beneficial protein product, without causing disease.   This highly effective cellular uptake and favorable intracellular

trafficking abilities make recombinant viral vectors suitable for both *in vivo* and *ex vivo* application. Gene expression following transfection is generally efficacious and long-lasting, ranging from several weeks to months depending on the vector type and target tissue [165]. Furthermore, the genetic material can either be integrated into the host chromosome or transported into the nuclei of infected cells without chromosomal integration.

Recombinant viral vectors include adenovirus, adeno-associated virus (AAV), and retrovirus, among others. Adenoviruses are large, double-stranded DNA viruses that infect non-dividing cells without integrating into the host chromosome, resulting in relatively short-term gene expression. AAVs are ssDNA viruses with a similar biological profile as adenoviruses, but with the primary added benefit of integration competence. Although AAVs have a broad tropism, they require adenovirus co-infection for replication cycle completion. In contrast, lentiviruses – part of the retrovirus family – will infect both dividing and non-diving cells to provide stable gene expression by integrating into the host genome.

Each of the recombinant viral vectors has its advantages and disadvantages (see *Table 4*). Risks for potential immunogenicity and insertional mutagenesis continue to raise safety concerns with some recombinant viral vectors, which will be circumvented through an improved understanding of our immune response and the viruses themselves.

2.7.1.2   Therapeutic non-viral gene delivery

Non-viral methods rely on the combination of nucleic acids with synthetic or natural vectors, as well as physical forces to deliver genetic information to a target cell population [166]. In general, non-viral gene delivery can be utilized to introduce new genetic material or down-regulate the expression of abnormal genes at the mRNA level. Compounds such as cationic lipids and polymers form condensed complexes with negatively charged nucleic acids to protect and facilitate their cellular uptake and intracellular transport. Additionally, physical forces, including but not limited to electroporation, form transient defects in the plasma and nuclear membranes to further facilitate the transport of genes into the nucleus. Major advantages of non-viral gene delivery include delivery of significantly larger fragments of genetic information and lack of a risk for immunogenicity and infection [167-169]. Further research is required to improve the variability of gene expression and specificity of the cell types being transfected using non-viral methods for gene delivery.

Table 2.1 Viral and non-viral vectors utilized in tissue engineering [168].

Vector	Type	Advantages	Disadvantages	Pre Clinical Studies
Adenovirus	viral	High transduction rate; transfection of wide range of cell types	High immunogenic potential; transient gene expression [168, 203, 204]	Chang et al.[169]; Jin et al. [171]
Lentivirus	viral	Non-immunogenic; sustained gene expression	Risk for insertional mutagenesis; transduction limited to dividing cells [168, 203, 204]	Xiang et al. [174], Logan et al.[175]
Adeno-associated virus	viral	Little/no immunogenicity; transduction in both dividing and non-dividing cells; sustained gene expression	Accommodates only very small size transgenes; production of high titers is difficult [168, 203, 204]	Cirelli et al. [172]; Warrington et al.[173]
Plasmid	non-viral	Non-immunogenic; transfection of wide range of cell types; localized gene expression	Very low transfection efficiency; transient gene expression [168, 204]	Liu et al. [205]; Huang et al. [176]
Nucleic acid/polymer complexes	non-viral	Targeted down regulation of gene expression	Low transfection efficiency; very transient effects on gene expression; potential for immunogenicity [166, 206]	Iwanaga et al. [207]; Kotopoulis et al.[208]

2.8 Safety and Regulatory Considerations of Cell and Gene Therapy

The translation of cell- and gene-based therapies to the clinic is intrinsically linked with reducing or eliminating significant risks associated with the treatment to the patient and improving the clinical outcome. Regulatory policies established by the FDA stipulate that the safety and efficacy of a given treatment must be verified prior to its approval for clinical use. In addition to the safety issues associated with processing cells *ex vivo*, other considerations involve the selected cell source, handling and expansion protocols, including best practices for maintaining cells during transportation, scaffold seeding, and transplantation [170]. While the current safety profile of iPSCs still presents significant barriers to clinical translation, cell-based therapy using MSCs has successfully been applied for treatment of degenerative diseases and investigated as a potential

clinically-viable approach for dental-based tissue engineering strategies. For example, human dental pulp-derived mesenchymal stem cells (DPSC) can be processed using current good tissue practices (cGTP) within a 5 day period post-isolation from an extracted tooth, banked via cryopreservation, and recovered prior to treatment [171]. In the presence of a scaffold that serves as a carrier for cell delivery, additional considerations for safe application to the clinic include adherence to good manufacturing practices (cGMP) for scaffold fabrication and sterilization [172]. Additional steps involving scaffold cell-seeding, maintenance, and transfer to the clinic require stringent quality control measures and comprehensive protocols to ensure safety and efficacy. To minimize the associated treatment costs and improve practicality of cell-based therapy in the clinic with or without scaffold carriers, these processes must be streamlined and simplified to avoid unnecessary complications and reduce regulatory burdens.

Clinically-applicable procedures for the regeneration of oral and craniofacial bone using gene therapy are highly dependent on the selection of vectors with appropriate safety profiles. Primary concerns with viral vectors include their potential to illicit an immune response, exhibit insertional mutagenesis, and activate oncogenes, as has been observed with lentiviruses and retroviruses. Safer alternatives are adeno-associated vectors (AAVs) and adenoviruses: AAVs are non-pathogenic, while adenoviruses do not integrate into the cell genome and thereby are not replicated during cell division [173]. While these vectors are currently being tested in FDA-approved human clinical trials for rare disorders, the development of more efficient non-viral gene therapy methods involving DNA, mRNA, or siRNA delivery can be more promising from a regulatory approval perspective for regeneration of common tissue defects [174].

2.9   Pre-clinical Studies for Regeneration of Oral Tissues using Gene Therapy

Adenoviruses have been used experimentally for tissue engineering of tooth-supported bony defects. One example is the use of an adenovirus encoding the PDGF-B gene (Ad-PDGF-B) on a collagen matrix to treat periodontal lesions *in vivo*. Clinical, hematological and blood chemical tests were done without any significant histopathological changes when Ad-PDGF-B was used [175, 176]. Jin et al. demonstrated Ad-BMP7 induced rapid chondrogenesis, osteogenesis and cementogenesis in bridging periodontal alveolar bone defects without significant inflammatory responses [177]. This is an example of the potential that gene therapy-based vectors such as adenoviral BMP have for successfully engineering bone in a preclinical model (see **Figure**

3) when combined with a transduced cell carrier such as gelatin that provides three-dimensional support for tissue growth during the regenerative process.
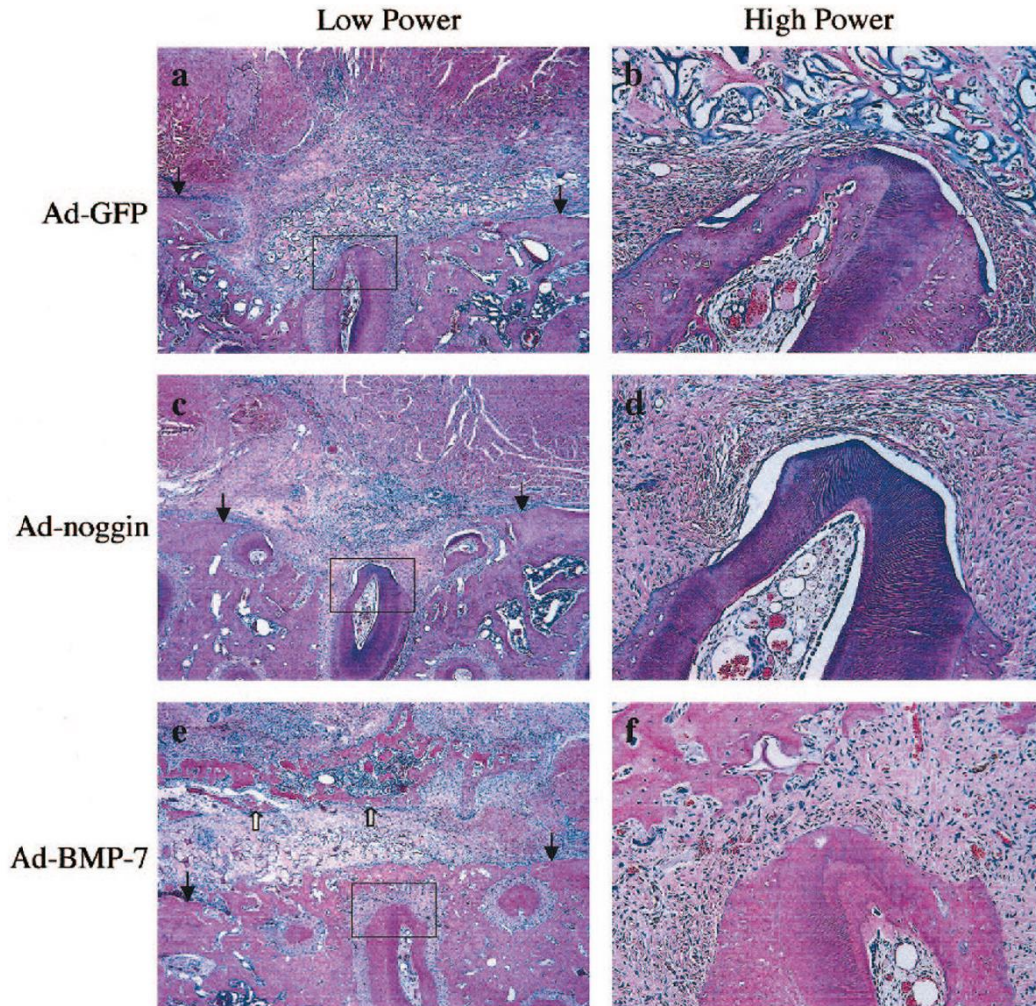
Figure 2.3 Regeneration of Periodontal Tissue using Gene Therapy Vectors
Successful regeneration of alveolar bone and surrounding periodontal tissues using gene therapy vectors such as adenoviral BMP-7 (Ad-BMP-7) has been achieved in animal models. Bone regeneration and bridging was observed with the use of ex vivo BMP-7 gene transfer using a gelatin-based cell carrier in a rat wound model consisting of a large mandibular alveolar bone defect. Comparatively, transduction of syngeneic dermal fibroblasts using green fluorescent protein (Ad-GFP) or noggin (Ad-noggin) did not result in ectopic bone formation (*left panel*). Mature cartilage and newly-formed bone was observed at Day 21 using Ad-BMP-7 gene transfer (*right panel*). Reproduced with permission from Jin Q-M et al [177].

AAVs have been used to prevent periodontal disease progression in rats. Cirelli et al., demonstrated the use of pseudotyped adeno-associated virus vector based on serotype 1 (AAV2/1) to deliver TNF receptor-immunoglobulin Fc (TNFR:Fc) to rats subjected to *Porphyromonas gingivalis* (Pg) lipopolysaccharide (LPS)[178]. Animals treated with AAV2/1-TNFR:Fc showed sustained levels of serum TNFR protein and sustained levels of Pg-LPS-mediated bone loss. AAVs have also been successfully used for the treatment of neurological, cardiovascular and autoimmune diseases [179].

Lentiviral transfection was used to investigate follicular dendritic cell secreted protein (FDC-SP) on the inhibition of osteogenic differentiation of human PDL cells. Xiang et al. used FDC-SP transfection on hPDL cell proliferation, osteogenic and fibrogenic phenotypes [180]. Cell proliferation and cell cycle tests indicated that transfection with FDC-SP did not affect hPDLC proliferation. Moreover, expression levels of type 1 collagen were up-regulated while osteocalcin, osteopontin and bone sialoprotein were down-regulated in the transfected cells. Lentiviral vectors are considered excellent genetic vector systems by being both efficient and stable in gene delivery and therapy [181].

With regard to the application of non-viral vectors for growth factor delivery, plasmids have been used successfully to enhance cell survival and engraftment with IGF-1 in smooth muscle cells. Huang et al. used plasmid DNA encoded BMP-4 in critical-sized cranial defects in rats and demonstrated bone regeneration significantly increased both on the edges and center of the defects as compared to the control group of the scaffold only [182].

2.10   Clinical Applications of Cell Delivery

Cell and gene therapy have the potential to greatly improve current methods of bone regeneration through increased bioactivity of scaffolds and localized growth factor delivery. This concept is being comprehensively studied to provide a more predictable armamentarium of available treatment options for local alveolar bone loss. Reviewed here are documented clinical studies using cell-based therapy to the craniofacial complex. Cell-based therapy pre-clinical studies are in the process of being transitioned into clinically-applicable approaches that are safe and effective in regenerating periodontal tissues.

2.10.1 Alveolar bone augmentation/preservation

Existing studies have investigated the safety of cell-based therapy for alveolar bone augmentation: Filho-Cerruti et al. studied the association of platelet-rich plasma (PRP) and mononuclear cells from bone marrow aspirate and bone scaffold for bone augmentation in the maxillae [183]. An overall graft success rate of 94.7% was reported with enough ridge dimension obtained for proper dental implant placement. Documented graft failures were due to infection of the maxillary sinus and lack of integration into the host cortical bone. Bone formation with the presence of osteoblasts scattered throughout the trabeculae were noted histologically, with minimal marginal bone loss noticed during the 4-year study follow-up. Subsequently, Pelegrine et al. evaluated in a case series study the clinical and histomorphometric behavior of upper anterior extraction sockets treated with an autologous bone marrow graft versus no graft material in the control group [184]. Clinical results showed that the use of bone marrow stem cells (BMSCs) minimized alveolar bone loss after tooth extraction compared to control. Nevertheless, 6 months after grafting, similar outcomes were found by means of mineralized bone. More recently, Kaigler et al. conducted a randomized controlled feasibility trial to compare the use of tissue repair cells (BMSCs) with conventional GBR (membrane only with gelatin carrier) for alveolar bone preservation. At the time of implant placement, a second need of grafting was more frequent (6-fold greater implant exposure) for sockets treated with GBR. Additionally, it is also important to note that the regenerated bone in the test group exhibited greater density and higher vascularization with significant acceleration of osteogenesis at 6 weeks.

2.10.2 Sinus augmentation

Vertical bone augmentation in the sinus antrum is oftentimes an imperative to achieve implant stability due to progressive alveolar bone resorption. The use of stem cell therapy as a complement to conventional graft and scaffold materials could improve bone formation and accelerate regeneration. In a histomorphometric study, Gonshor et al. compared bone formation following sinus augmentation procedures using either an allograft cellular bone matrix containing native mesenchymal stem cells or a conventional allograft. Results of the test group revealed a mean of 32.5% and 4.9% for vital bone and remaining graft material, respectively, over a follow up healing period of 3.7 months. Contrastingly, for the control group, only 18.3% of vital bone content was found while an increase of up to 25.8% was noticed of remaining graft [185]. These

results were consistent with the results obtained by Rickert et al., who aimed to compare bovine-derived mineral bone seeded with mononuclear stem cells with bovine-derived mineral bone mixed with autogenous bone. Significantly greater bone formation was observed in the test (17.7%) when compared with the control group (12.0%) at 14 weeks [186].

Overall, stem cells seeded in allograft or xenograft scaffold particles are capable of inducing sufficient new bone volume formation to achieve primary implant stability. Within these limitations, the high percentage of vital bone content after a relatively short healing period might encourage clinicians to consider implant therapy at an earlier stage post-grafting [187]. However, the clinical significance in small defects is very finite and therefore, the use of this approach should be further studied in more challenging scenarios with standardized randomized clinical trials.

2.11   Existing Limitations

Major advances have been made in the reconstruction of intraoral bone defects as a result of improvements in scaffolding matrices and application of bioactive factors that enhance the regenerative response. However, there are existing limitations in the development of optimized scaffolding matrices that meet all the necessary criteria for the regeneration of structurally and physiologically functional osseous tissues. As described in this review, current technologies such as 3-D printing are being adapted for use in the design and development of natural and synthetic matrices that are architecturally similar to bone that allow for controllable features such as chemical composition, porosity, and rate of degradation. Likewise, the selection of materials in scaffold development for intraoral bone regeneration is limited by the attempt to match the properties and rate of regrowth of the developing tissues to the degradation properties of the supporting biomaterial. It remains a challenge to balance the preference for FDA-approved materials that have been more thoroughly investigated for use in humans with materials that may be more mechanically-appropriate for bone regeneration but have been biologically/chemically modified or release degradation products which may hinder the regenerative process *in situ*. This further relates to the established regulatory requirements for translating novel treatments to the clinic, with more complex strategies involving combinations of materials with cell, growth factor, or gene delivery yielding a biologic-device combination product that is more difficult to evaluate as opposed to a stand-alone biologic or device product. While current clinical applications of growth factors in combination with commercialized material carriers are showing significant

improvements in clinical treatment, further optimization of delivery systems in necessary to ensure that time-dependent biofactor dose and release kinetics are appropriate for the regenerative repair process. Gene therapy is promising in this area of research and is in need of further evaluation to determine the most appropriate vectors for growth factor gene delivery that is safe and clinically acceptable for further implementation in patient-based studies.

2.12   Future Directions

There are many exciting opportunities that lie ahead for the reconstruction of craniofacial deficiencies including periodontal, alveolar ridge and large mandibular/maxillary discontinuity defects. The innovations that are ongoing in materials science and in biology have offered many potential avenues in the laboratory and clinic to extend the field of tissue engineering of oral structures such as alveolar bone and soft tissues of the teeth and dental implants. In particular, recent advances in biomaterial design, drug delivery and biologic agents offer less invasive technologies to accelerate and more predictably promote tissue repair and regeneration. The ability of rapid prototyping, three-dimensional printing, electrospinning, and enhanced drug delivery strategies to personalize patient therapies is allowing a more customized approach for oral tissue engineering to benefit both clinicians and patients. Development of scaffolds that act as delivery vehicles for drugs that can be controllably released to counter bone degenerative processes is an example of a future focus for intraoral tissue engineering strategies, as recently evidenced in a study by Ji et al [188] that focused on the incorporation of hydrophilic naringin into elecrospun amphiphilic copolymer nanofibers for bone resorption treatment. Further improvements to existing materials with a history of use in dental and craniofacial applications, such as calcium phosphate-based cements, are a promising venue for addressing their existing limitations through the improvement of mechanical integrity and incorporation of growth factor delivery vehicles. Lee et al [189] present such an approach through the reinforcement of macroporous calcium phosphate cement (CPC) with absorbable fibers and simultaneous delivery of rhBMP2 in the CPC matrix with VEGF or TGF-β1 in alginate hydrogel microbeads within the matrix. Such combinational approaches to address the need for controlled delivery of growth factors at critical stages of the regenerative process are important in advancing our ability to predictably regrow lost or damaged tissue. Further improvement and streamlining of existing processes and technologies for

addressing these tissue engineering strategies will enable their continued entrance into the clinical arena to provide more predictable regenerative medicine therapeutics for enhanced patient care.

2.13   References

[1]   Eke PI, Dye BA, Wei L, Thornton-Evans GO, Genco RJ. Prevalence of periodontitis in adults in the United States: 2009 and 2010. J Dent Res. 2012;91:914-20.

[2]   Hansson S, Halldin A. Alveolar ridge resorption after tooth extraction: A consequence of a fundamental principle of bone physiology. J Dent Biomech. 2012;3:1758736012456543.

[3]   Reynolds MA, Aichelmann-Reidy ME, Branch-Mays GL. Regeneration of periodontal tissue: bone replacement grafts. Dent Clin North Am. 2010;54:55-71.

[4]   Chen FM, Jin Y. Periodontal tissue engineering and regeneration: current approaches and expanding opportunities. Tissue Eng Part B Rev. 2010;16:219-55.

[5]   Silva FM, Cortez AL, Moreira RW, Mazzonetto R. Complications of intraoral donor site for bone grafting prior to implant placement. Implant Dent. 2006;15:420-6.

[6]   Holtzclaw D, Toscano N, Eisenlohr L, Callan D. The safety of bone allografts used in dentistry: a review. J Am Dent Assoc. 2008;139:1192-9.

[7]   Delloye C, Cornu O, Druez V, Barbier O. Bone allografts: What they can offer and what they cannot. J Bone Joint Surg Br. 2007;89:574-9.

[8]   Louis PJ. Bone grafting the mandible. Oral Maxillofac Surg Clin North Am. 2011;23:209-27.

[9]   Lutz R, Berger-Fink S, Stockmann P, Neukam FW, Schlegel KA. Sinus floor augmentation with autogenous bone vs. a bovine-derived xenograft – a 5-year retrospective study. Clinical Oral Implants Research. 2014:n/a-n/a.

[10]   Klijn RJ, Meijer GJ, Bronkhorst EM, Jansen JA. A meta-analysis of histomorphometric results and graft healing time of various biomaterials compared to autologous bone used as sinus floor augmentation material in humans. Tissue Eng Part B Rev. 2010;16:493-507.

[11]   Duttenhoefer F, Souren C, Menne D, Emmerich D, Schon R, Sauerbier S. Long-term survival of dental implants placed in the grafted maxillary sinus: systematic review and meta-analysis of treatment modalities. PLoS One. 2013;8:e75357.

[12]   McMahon RE, Wang L, Skoracki R, Mathur AB. Development of nanomaterials for bone repair and regeneration. J Biomed Mater Res B Appl Biomater. 2013;101:387-97.

[13]   Dorozhkin SV. Bioceramics of calcium orthophosphates. Biomaterials. 2010;31:1465-85.

[14]   Vlad MD, Gomez S, Barraco M, Lopez J, Fernandez E. Effect of the calcium to phosphorus ratio on the setting properties of calcium phosphate bone cements. J Mater Sci Mater Med. 2012;23:2081-90.

[15]   Alghamdi HS, Cuijpers VM, Wolke JG, van den Beucken JJ, Jansen JA. Calcium-phosphate-coated oral implants promote osseointegration in osteoporosis. J Dent Res. 2013;92:982-8.

[16]   Lin A, Wang CJ, Kelly J, Gubbi P, Nishimura I. The role of titanium implant surface modification with hydroxyapatite nanoparticles in progressive early bone-implant fixation in vivo. Int J Oral Maxillofac Implants. 2009;24:808-16.

[17]   Bashoor-Zadeh M, Baroud G, Bohner M. Simulation of the in vivo resorption rate of beta-tricalcium phosphate bone graft substitutes implanted in a sheep model. Biomaterials. 2011;32:6362-73.

[18]   Camazzola D, Hammond T, Gandhi R, Davey JR. A Randomized Trial of Hydroxyapatite-Coated Femoral Stems in Total Hip Arthroplasty. The Journal of Arthroplasty.24:33-7.

[19]   Hench LL. The story of Bioglass. J Mater Sci Mater Med. 2006;17:967-78.

[20]   Gerhardt L-C, Boccaccini AR. Bioactive Glass and Glass-Ceramic Scaffolds for Bone Tissue Engineering. Materials. 2010;3:3867-910.

[21]   Novitskaya E CP-Y, Hamed E, Jun L, Lubarda V, Jasiuk I, McKittrick J. Recent advances on the measurement and calculation of the elastic moduli of cortical and trabecular bone: a review. Theoret Appl Mech. 2011;38:209-97.

[22]   Teraoka K, Ito A, Maekawa K, Onuma K, Tateishi T, Tsutsumi S. Mechanical properties of hydroxyapatite and OH-carbonated hydroxyapatite single crystals. J Dent Res. 1998;77:1560-8.

[23]   Viswanath B, Raghavan R, Gurao NP, Ramamurty U, Ravishankar N. Mechanical properties of tricalcium phosphate single crystals grown by molten salt synthesis. Acta Biomaterialia. 2008;4:1448-54.

[24]   Yu L, Li Y, Zhao K, Tang Y, Cheng Z, Chen J, et al. A novel injectable calcium phosphate cement-bioactive glass composite for bone regeneration. PLoS One. 2013;8:e62570.

[25]   van Oirschot BA, Alghamdi HS, Narhi TO, Anil S, Al Farraj Aldosari A, van den Beucken JJ, et al. In vivo evaluation of bioactive glass-based coatings on dental implants in a dog implantation model. Clin Oral Implants Res. 2014;25:21-8.

[26]   Mehdikhani-Nahrkhalaji M, Fathi MH, Mortazavi V, Mousavi SB, Hashemi-Beni B, Razavi SM. Novel nanocomposite coating for dental implant applications in vitro and in vivo evaluation. J Mater Sci Mater Med. 2012;23:485-95.

[27]   Bongio M, van den Beucken JJJP, Leeuwenburgh SCG, Jansen JA. Development of bone substitute materials: from 'biocompatible' to 'instructive'. Journal of Materials Chemistry. 2010;20:8747-59.

[28]   Ramseier CA, Rasperini G, Batia S, Giannobile WV. Advanced reconstructive technologies for periodontal tissue repair. Periodontol 2000. 2012;59:185-202.

[29]   Bashutski JD, Wang HL. Periodontal and endodontic regeneration. J Endod. 2009;35:321-8.

[30]   Hua N, Ti VL, Xu Y. Biodegradable Effect of PLGA Membrane in Alveolar Bone Regeneration on Beagle Dog. Cell Biochem Biophys. 2014.

[31]   Dreifke MB, Ebraheim NA, Jayasuriya AC. Investigation of potential injectable polymeric biomaterials for bone regeneration. J Biomed Mater Res A. 2013;101:2436-47.

[32]   Li X, Xie J, Yuan X, Xia Y. Coating electrospun poly(epsilon-caprolactone) fibers with gelatin and calcium phosphate and their use as biomimetic scaffolds for bone tissue engineering. Langmuir. 2008;24:14145-50.

[33]   Lee CH, Hajibandeh J, Suzuki T, Fan A, Shang P, Mao JJ. Three-dimensional printed multiphase scaffolds for regeneration of periodontium complex. Tissue Eng Part A. 2014;20:1342-51.

[34]   Costa PF, Vaquette C, Zhang Q, Reis RL, Ivanovski S, Hutmacher DW. Advanced tissue engineering scaffold design for regeneration of the complex hierarchical periodontal structure. J Clin Periodontol. 2014;41:283-94.

[35]   Yan X-Z, van den Beucken JJ, Cai X, Yu N, Jansen JA, Yang F. Periodontal Tissue Regeneration Using Enzymatically Solidified Chitosan Hydrogels With or Without Cell Loading. Tissue Engineering Part A 2014.

[36]   Peng L, Cheng XR, Wang JW, Xu DX, Wang G. Preparation and evaluation of porous chitosan/collagen scaffolds for periodontal tissue engineering. Journal of bioactive and compatible polymers 2006;21:207-220.

[37]   Yildirimer L, Seifalian AM. Three-dimensional biomaterial degradation—Material choice, design and extrinsic factor considerations. Biotechnology advances 2014;32:984-999.

[38]   Park CH, Rios HF, Jin Q, Sugai JV, Padial-Molina M, Taut AD et al. Tissue engineering bone-ligament complexes using fiber-guiding scaffolds. Biomaterials 2012;33:137-145.

[39]   Akita D, Morokuma M, Saito Y, Yamanaka K, Akiyama Y, Sato M et al. Periodontal tissue regeneration by transplantation of rat adipose-derived stromal cells in combination with PLGA-based solid scaffolds. Biomed Res 2014;35:91-103.

[40]   Agarwal S, Wendorff JH, Greiner A. Use of electrospinning technique for biomedical

[41]   Chen G, Chen J, Yang B, Li L, Luo X, Zhang X et al. Combination of aligned PLGA/Gelatin electrospun sheets, native dental pulp extracellular matrix and treated dentin matrix as substrates for tooth root regeneration. Biomaterials 2015;52:56-70.

[42]   Kwon DH, Bisch FC, Herold RW, Pompe C, Bastone P, Rodriguez NA et al. Periodontal wound healing/regeneration following the application of rhGDF-5 in a β-TCP/PLGA carrier in critical-size supra-alveolar periodontal defects in dogs. Journal of clinical periodontology 2010;37:667-674.

[43]   Koo K-T, Susin C, Wikesjö UM, Choi S-H, Kim C-K. Transforming Growth Factor-β1 Accelerates Resorption of a Calcium Carbonate Biomaterial in Periodontal Defects. Journal of periodontology 2007;78:723-729.

[44]   Amini AR, Laurencin CT, Nukavarapu SP. Bone tissue engineering: recent advances and challenges. Crit Rev Biomed Eng. 2012;40:363-408.

[45]   Hollister SJ. Porous scaffold design for tissue engineering. Nat Mater. 2005;4:518-24.

[46]   Fisher S, Franz-Odendaal T. Evolution of the bone gene regulatory network. Curr Opin Genet Dev. 2012;22:390-7.

[47]   Hong SG, Winkler T, Wu C, Guo V, Pittaluga S, Nicolae A, et al. Path to the clinic: Assessment of iPSC-based cell therapies in vivo in a non-human primate model. Cell reports. 2014;7:1298-309.

[48]   Scaglione S, Giannoni P, Bianchini P, Sandri M, Marotta R, Firpo G, et al. Order versus Disorder: in vivo bone formation within osteoconductive scaffolds. Sci Rep. 2012;2.

[49]   Ho ST, Hutmacher DW, Ekaputra AK, Hitendra D, Hui JH. The evaluation of a biphasic osteochondral implant coupled with an electrospun membrane in a large animal model. Tissue Eng Part A. 2010;16:1123-41.

[50]   Mazzoli A. Selective laser sintering in biomedical engineering. Med Biol Eng Comput. 2013;51:245-56.

[51]   Xia Y, Zhou P, Cheng X, Xie Y, Liang C, Li C, et al. Selective laser sintering fabrication of nano-hydroxyapatite/poly-epsilon-caprolactone scaffolds for bone tissue engineering applications. Int J Nanomedicine. 2013;8:4197-213.

[52]   Williams JM, Adewunmi A, Schek RM, Flanagan CL, Krebsbach PH, Feinberg SE, et al. Bone tissue engineering using polycaprolactone scaffolds fabricated via selective laser sintering. Biomaterials. 2005;26:4817-27.

[53]   Park CH, Rios HF, Taut AD, Padial-Molina M, Flanagan CL, Pilipchuk SP, et al. Image-based, fiber guiding scaffolds: a platform for regenerating tissue interfaces. Tissue Eng Part C Methods. 2014;20:533-42.

[54]   Cui Q, Dighe AS, Irvine JN, Jr. Combined angiogenic and osteogenic factor delivery for bone regenerative engineering. Curr Pharm Des. 2013;19:3374-83.

[55]   Bai Y, Yin G, Huang Z, Liao X, Chen X, Yao Y, et al. Localized delivery of growth factors for angiogenesis and bone formation in tissue engineering. Int Immunopharmacol. 2013;16:214-23.

[56]   Romagnoli C, D'Asta F, Brandi ML. Drug delivery using composite scaffolds in the context of bone tissue engineering. Clin Cases Miner Bone Metab. 2013;10:155-61.

[57]   Lee SH, Shin H. Matrices and scaffolds for delivery of bioactive molecules in bone and cartilage tissue engineering. Adv Drug Deliv Rev. 2007;59:339-59.

[58]   Wieman TJ, Smiell JM, Su Y. Efficacy and safety of a topical gel formulation of recombinant human platelet-derived growth factor-BB (becaplermin) in patients with chronic neuropathic diabetic ulcers. A phase III randomized placebo-controlled double-blind study. Diabetes Care. 1998;21:822-7.

[59]   Nevins M, Giannobile WV, McGuire MK, Kao RT, Mellonig JT, Hinrichs JE, et al. Platelet-derived growth factor stimulates bone fill and rate of attachment level gain: results of a large multicenter randomized controlled trial. J Periodontol. 2005;76:2205-15.

[50]   Saygin NE, Tokiyasu Y, Giannobile WV, Somerman MJ. Growth factors regulate expression of mineral associated genes in cementoblasts. J Periodontol. 2000;71:1591-600.

[51]   Bartold PM, Raben A. Growth factor modulation of fibroblasts in simulated wound healing. J Periodontal Res. 1996;31:205-16.

[62]   Sant'Ana AC, Marques MM, Barroso TE, Passanezi E, de Rezende ML. Effects of TGF-beta1, PDGF-BB, and IGF-1 on the rate of proliferation and adhesion of a periodontal ligament cell lineage in vitro. J Periodontol. 2007;78:2007-17.

[63]   Franchimont N, Durant D, Rydziel S, Canalis E. Platelet-derived growth factor induces interleukin-6 transcription in osteoblasts through the activator protein-1 complex and activating transcription factor-2. J Biol Chem. 1999;274:6783-9.

[64]   Strayhorn CL, Garrett JS, Dunn RL, Benedict JJ, Somerman MJ. Growth factors regulate expression of osteoblast-associated genes. J Periodontol. 1999;70:1345-54.

[65]   Yu X, Hsieh SC, Bao W, Graves DT. Temporal expression of PDGF receptors and PDGF regulatory effects on osteoblastic cells in mineralizing cultures. Am J Physiol. 1997;272:C1709-16.

[66]   Lynch SE, Buser D, Hernandez RA, Weber HP, Stich H, Fox CH, et al. Effects of the platelet-derived growth factor/insulin-like growth factor-I combination on bone regeneration around titanium dental implants. Results of a pilot study in beagle dogs. J Periodontol. 1991;62:710-6.

[67]   Lynch SE, Williams RC, Polson AM, Howell TH, Reddy MS, Zappa UE, et al. A combination of platelet-derived and insulin-like growth factors enhances periodontal regeneration. J Clin Periodontol. 1989;16:545-8.

[68]   Park JB, Matsuura M, Han KY, Norderyd O, Lin WL, Genco RJ, et al. Periodontal regeneration in class III furcation defects of beagle dogs using guided tissue regenerative therapy with platelet-derived growth factor. J Periodontol. 1995;66:462-77.

[69]   Sigurdsson TJ, Nygaard L, Tatakis DN, Fu E, Turek TJ, Jin L, et al. Periodontal repair in dogs: evaluation of rhBMP-2 carriers. Int J Periodontics Restorative Dent. 1996;16:524-37.

[70]   Giannobile WV, Hernandez RA, Finkelman RD, Ryan S, Kiritsy CP, D'Andrea M, et al. Comparative effects of platelet-derived growth factor-BB and insulin-like growth factor-I, individually and in combination, on periodontal regeneration in Macaca fascicularis. J Periodontal Res. 1996;31:301-12.

[71]   Rutherford RB, Niekrash CE, Kennedy JE, Charette MF. Platelet-derived and insulin-like growth factors stimulate regeneration of periodontal attachment in monkeys. J Periodontal Res. 1992;27:285-90.

[72]   Sigurdsson TJ, Tatakis DN, Lee MB, Wikesjo UM. Periodontal regenerative potential of space-providing expanded polytetrafluoroethylene membranes and recombinant human bone morphogenetic proteins. J Periodontol. 1995;66:511-21.

[73]   Cho MI, Lin WL, Genco RJ. Platelet-derived growth factor-modulated guided tissue regenerative therapy. J Periodontol. 1995;66:522-30.

[74]   Becker W, Lynch SE, Lekholm U, Becker BE, Caffesse R, Donath K, et al. A comparison of ePTFE membranes alone or in combination with platelet-derived growth factors and insulin-like growth factor-I or demineralized freeze-dried bone in promoting bone formation around immediate extraction socket implants. J Periodontol. 1992;63:929-40.

[75]   Stefani CM, Machado MA, Sallum EA, Sallum AW, Toledo S, Nociti H, Jr. Platelet-derived growth factor/insulin-like growth factor-1 combination and bone regeneration

around implants placed into extraction sockets: a histometric study in dogs. Implant Dent. 2000;9:126-31.

[76] Al-Hazmi BA, Al-Hamdan KS, Al-Rasheed A, Babay N, Wang HL, Al-Hezaimi K. Efficacy of using PDGF and xenograft with or without collagen membrane for bone regeneration around immediate implants with induced dehiscence-type defects: a microcomputed tomographic study in dogs. J Periodontol. 2013;84:371-8.

[77] Schwarz F, Ferrari D, Podolsky L, Mihatovic I, Becker J. Initial pattern of angiogenesis and bone formation following lateral ridge augmentation using rhPDGF and guided bone regeneration: an immunohistochemical study in dogs. Clin Oral Implants Res. 2010;21:90-9.

[78] Simion M, Rocchietta I, Kim D, Nevins M, Fiorellini J. Vertical ridge augmentation by means of deproteinized bovine bone block and recombinant human platelet-derived growth factor-BB: a histologic study in a dog model. Int J Periodontics Restorative Dent. 2006;26:415-23.

[79] Urist MR. Bone: formation by autoinduction. Science. 1965;150:893-9.

[80] Cheng H, Jiang W, Phillips FM, Haydon RC, Peng Y, Zhou L, et al. Osteogenic activity of the fourteen types of human bone morphogenetic proteins (BMPs). J Bone Joint Surg Am. 2003;85-A:1544-52.

[81] Kobayashi M, Takiguchi T, Suzuki R, Yamaguchi A, Deguchi K, Shionome M, et al. Recombinant human bone morphogenetic protein-2 stimulates osteoblastic differentiation in cells isolated from human periodontal ligament. J Dent Res. 1999;78:1624-33.

[82] Marcopoulou CE, Vavouraki HN, Dereka XE, Vrotsos IA. Proliferative effect of growth factors TGF-beta1, PDGF-BB and rhBMP-2 on human gingival fibroblasts and periodontal ligament cells. J Int Acad Periodontol. 2003;5:63-70.

[83] Muthukuru M. Bone morphogenic protein-2 induces apoptosis and cytotoxicity in periodontal ligament cells. J Periodontol. 2013;84:829-38.

[84] Cheifetz S, Li IW, McCulloch CA, Sampath K, Sodek J. Influence of osteogenic protein-1 (OP-1;BMP-7) and transforming growth factor-beta 1 on bone formation in vitro. Connect Tissue Res. 1996;35:71-8.

[85] Sampath TK, Maliakal JC, Hauschka PV, Jones WK, Sasak H, Tucker RF, et al. Recombinant human osteogenic protein-1 (hOP-1) induces new bone formation in vivo with a specific activity comparable with natural bovine osteogenic protein and stimulates osteoblast proliferation and differentiation in vitro. J Biol Chem. 1992;267:20352-62.

[86] Blumenthal NM, Koh-Kunst G, Alves ME, Miranda D, Sorensen RG, Wozney JM, et al. Effect of surgical implantation of recombinant human bone morphogenetic protein-2 in a

bioabsorbable collagen sponge or calcium phosphate putty carrier in intrabony periodontal defects in the baboon. J Periodontol. 2002;73:1494-506.

[87]   Choi SH, Kim CK, Cho KS, Huh JS, Sorensen RG, Wozney JM, et al. Effect of recombinant human bone morphogenetic protein-2/absorbable collagen sponge (rhBMP-2/ACS) on healing in 3-wall intrabony defects in dogs. J Periodontol. 2002;73:63-72.

[88]   Saito A, Saito E, Handa R, Honma Y, Kawanami M. Influence of residual bone on recombinant human bone morphogenetic protein-2-induced periodontal regeneration in experimental periodontitis in dogs. J Periodontol. 2009;80:961-8.

[89]   Selvig KA, Sorensen RG, Wozney JM, Wikesjo UM. Bone repair following recombinant human bone morphogenetic protein-2 stimulated periodontal regeneration. J Periodontol. 2002;73:1020-9.

[90]   Barboza EP, Caula AL, Caula Fde O, de Souza RO, Geolas Neto L, Sorensen RG, et al. Effect of recombinant human bone morphogenetic protein-2 in an absorbable collagen sponge with space-providing biomaterials on the augmentation of chronic alveolar ridge defects. J Periodontol. 2004;75:702-8.

[91]   Wikesjo UM, Guglielmoni P, Promsudthi A, Cho KS, Trombelli L, Selvig KA, et al. Periodontal repair in dogs: effect of rhBMP-2 concentration on regeneration of alveolar bone and periodontal attachment. J Clin Periodontol. 1999;26:392-400.

[92]   Wikesjo UM, Lim WH, Thomson RC, Cook AD, Wozney JM, Hardwick WR. Periodontal repair in dogs: evaluation of a bioabsorbable space-providing macroporous membrane with recombinant human bone morphogenetic protein-2. J Periodontol. 2003;74:635-47.

[93]   Matin K, Nakamura H, Irie K, Ozawa H, Ejiri S. Impact of recombinant human bone morphogenetic protein-2 on residual ridge resorption after tooth extraction: an experimental study in the rat. Int J Oral Maxillofac Implants. 2001;16:400-11.

[94]   Cha JK, Lee JS, Kim MS, Choi SH, Cho KS, Jung UW. Sinus augmentation using BMP-2 in a bovine hydroxyapatite/collagen carrier in dogs. J Clin Periodontol. 2014;41:86-93.

[95]   Choi Y, Lee JS, Kim YJ, Kim MS, Choi SH, Cho KS, et al. Recombinant human bone morphogenetic protein-2 stimulates the osteogenic potential of the Schneiderian membrane: a histometric analysis in rabbits. Tissue Eng Part A. 2013;19:1994-2004.

[96]   Hanisch O, Tatakis DN, Rohrer MD, Wohrle PS, Wozney JM, Wikesjo UM. Bone formation and osseointegration stimulated by rhBMP-2 following subantral augmentation procedures in nonhuman primates. Int J Oral Maxillofac Implants. 1997;12:785-92.

[97]   Liu Y, Enggist L, Kuffer AF, Buser D, Hunziker EB. The influence of BMP-2 and its mode of delivery on the osteoconductivity of implant surfaces during the early phase of osseointegration. Biomaterials. 2007;28:2677-86.

[98]   Nevins M, Kirker-Head C, Nevins M, Wozney JA, Palmer R, Graham D. Bone formation in the goat maxillary sinus induced by absorbable collagen sponge implants impregnated with recombinant human bone morphogenetic protein-2. Int J Periodontics Restorative Dent. 1996;16:8-19.

[99]   Arosarena O, Collins W. Comparison of BMP-2 and -4 for rat mandibular bone regeneration at various doses. Orthod Craniofac Res. 2005;8:267-76.

[100] Jovanovic SA, Hunt DR, Bernard GW, Spiekermann H, Wozney JM, Wikesjo UM. Bone reconstruction following implantation of rhBMP-2 and guided bone regeneration in canine alveolar ridge defects. Clin Oral Implants Res. 2007;18:224-30.

[101] Kawakatsu N, Oda S, Kinoshita A, Kikuchi S, Tsuchioka H, Akizuki T, et al. Effect of rhBMP-2 with PLGA/gelatin sponge type (PGS) carrier on alveolar ridge augmentation in dogs. J Oral Rehabil. 2008;35:647-55.

[102] Linde A, Hedner E. Recombinant bone morphogenetic protein-2 enhances bone healing, guided by osteopromotive e-PTFE membranes: an experimental study in rats. Calcif Tissue Int. 1995;56:549-53.

[103] Shimazu C, Hara T, Kinuta Y, Moriya K, Maruo Y, Hanada S, et al. Enhanced vertical alveolar bone augmentation by recombinant human bone morphogenetic protein-2 with a carrier in rats. J Oral Rehabil. 2006;33:609-18.

[104] Giannobile WV, Ryan S, Shih MS, Su DL, Kaplan PL, Chan TC. Recombinant human osteogenic protein-1 (OP-1) stimulates periodontal wound healing in class III furcation defects. J Periodontol. 1998;69:129-37.

[105] Leknes KN, Yang J, Qahash M, Polimeni G, Susin C, Wikesjo UM. Alveolar ridge augmentation using implants coated with recombinant human bone morphogenetic protein-2: radiographic observations. Clin Oral Implants Res. 2008;19:1027-33.

[106] Liu Y, Han JX, Xiao SQ, Wang SL, Wang M. Study of recombinant human osteogenic protein-1 expressed in prokaryocyte on the repair of extracted socket in rabbits. J Biomed Mater Res A. 2006;77:324-30.

[107] Margolin MD, Cogan AG, Taylor M, Buck D, McAllister TN, Toth C, et al. Maxillary sinus augmentation in the non-human primate: a comparative radiographic and histologic study between recombinant human osteogenic protein-1 and natural bone mineral. J Periodontol. 1998;69:911-9.

[108] Ripamonti U, Heliotis M, Rueger DC, Sampath TK. Induction of cementogenesis by recombinant human osteogenic protein-1 (hop-1/bmp-7) in the baboon (Papio ursinus). Arch Oral Biol. 1996;41:121-26.

[109] Terheyden H, Jepsen S, Moller B, Rueger D. [Sinus floor augmentation with simultaneous implant insertion using recombinant human osteogenic protein-1]. Laryngorhinootologie. 2001;80:47-51.

[110] Terheyden H, Jepsen S, Moller B, Tucker MM, Rueger DC. Sinus floor augmentation with simultaneous placement of dental implants using a combination of deproteinized bone xenografts and recombinant human osteogenic protein-1. A histometric study in miniature pigs. Clin Oral Implants Res. 1999;10:510-21.

[111] Hakki SS, Foster BL, Nagatomo KJ, Bozkurt SB, Hakki EE, Somerman MJ, et al. Bone morphogenetic protein-7 enhances cementoblast function in vitro. J Periodontol. 2010;81:1663-74.

[112] Dereka XE, Markopoulou CE, Mamalis A, Pepelassi E, Vrotsos IA. Time- and dose-dependent mitogenic effect of basic fibroblast growth factor combined with different bone graft materials: an in vitro study. Clin Oral Implants Res. 2006;17:554-9.

[113] Hidaka T, Nagasawa T, Shirai K, Kado T, Furuichi Y. FGF-2 induces proliferation of human periodontal ligament cells and maintains differentiation potentials of STRO-1(+)/CD146(+) periodontal ligament cells. Arch Oral Biol. 2012;57:830-40.

[114] Hughes-Fulford M, Li CF. The role of FGF-2 and BMP-2 in regulation of gene induction, cell proliferation and mineralization. J Orthop Surg Res. 2011;6:8.

[115] Murakami S, Takayama S, Ikezawa K, Shimabukuro Y, Kitamura M, Nozaki T, et al. Regeneration of periodontal tissues by basic fibroblast growth factor. J Periodontal Res. 1999;34:425-30.

[116] Takayama S, Yoshida J, Hirano H, Okada H, Murakami S. Effects of basic fibroblast growth factor on human gingival epithelial cells. J Periodontol. 2002;73:1467-73.

[117] Terashima Y, Shimabukuro Y, Terashima H, Ozasa M, Terakura M, Ikezawa K, et al. Fibroblast growth factor-2 regulates expression of osteopontin in periodontal ligament cells. J Cell Physiol. 2008;216:640-50.

[118] Murakami S. Periodontal tissue regeneration by signaling molecule(s): what role does basic fibroblast growth factor (FGF-2) have in periodontal therapy? Periodontol 2000. 2011;56:188-208.

[119] Murakami S, Takayama S, Kitamura M, Shimabukuro Y, Yanagi K, Ikezawa K, et al. Recombinant human basic fibroblast growth factor (bFGF) stimulates periodontal regeneration in class II furcation defects created in beagle dogs. J Periodontal Res. 2003;38:97-103.

[120] Rossa C, Jr., Marcantonio E, Jr., Cirelli JA, Marcantonio RA, Spolidorio LC, Fogo JC. Regeneration of Class III furcation defects with basic fibroblast growth factor (b-FGF) associated with GTR. A descriptive and histometric study in dogs. J Periodontol. 2000;71:775-84.

[121] Lee J, Wikesjo UM. Growth/differentiation factor-5: pre-clinical and clinical evaluations of periodontal regeneration and alveolar augmentation - review. J Clin Periodontol. 2014.

[122] Nakamura T, Yamamoto M, Tamura M, Izumi Y. Effects of growth/differentiation factor-5 on human periodontal ligament cells. J Periodontal Res. 2003;38:597-605.

[123] Koch FP, Weinbach C, Hustert E, Al-Nawas B, Wagner W. GDF-5 and BMP-2 regulate bone cell differentiation by gene expression of MSX1, MSX2, Dlx5, and Runx2 and influence OCN gene expression in vitro. Int J Periodontics Restorative Dent. 2012;32:285-93.

[124] Emerton KB, Drapeau SJ, Prasad H, Rohrer M, Roffe P, Hopper K, et al. Regeneration of periodontal tissues in non-human primates with rhGDF-5 and beta-tricalcium phosphate. J Dent Res. 2011;90:1416-21.

[125] Lee JS, Wikesjo UM, Jung UW, Choi SH, Pippig S, Siedler M, et al. Periodontal wound healing/regeneration following implantation of recombinant human growth/differentiation factor-5 in a beta-tricalcium phosphate carrier into one-wall intrabony defects in dogs. J Clin Periodontol. 2010;37:382-9.

[126] Kim TG, Wikesjo UM, Cho KS, Chai JK, Pippig SD, Siedler M, et al. Periodontal wound healing/regeneration following implantation of recombinant human growth/differentiation factor-5 (rhGDF-5) in an absorbable collagen sponge carrier into one-wall intrabony defects in dogs: a dose-range study. J Clin Periodontol. 2009;36:589-97.

[127] Kim YT, Wikesjo UM, Jung UW, Lee JS, Kim TG, Kim CK. Comparison between a beta-tricalcium phosphate and an absorbable collagen sponge carrier technology for rhGDF-5-stimulated periodontal wound healing/regeneration. J Periodontol. 2013;84:812-20.

[128] Simank HG, Stuber M, Frahm R, Helbig L, van Lenthe H, Muller R. The influence of surface coatings of dicalcium phosphate (DCPD) and growth and differentiation factor-5 (GDF-5) on the stability of titanium implants in vivo. Biomaterials. 2006;27:3988-94.

[129] Gruber RM, Ludwig A, Merten HA, Achilles M, Poehling S, Schliephake H. Sinus floor augmentation with recombinant human growth and differentiation factor-5 (rhGDF-5): a histological and histomorphometric study in the Goettingen miniature pig. Clin Oral Implants Res. 2008;19:522-9.

[130] Gruber RM, Ludwig A, Merten HA, Pippig S, Kramer FJ, Schliephake H. Sinus floor augmentation with recombinant human growth and differentiation factor-5 (rhGDF-5): a

pilot study in the Goettingen miniature pig comparing autogenous bone and rhGDF-5. Clin Oral Implants Res. 2009;20:175-82.

[131]   Schwarz F, Rothamel D, Herten M, Ferrari D, Sager M, Becker J. Lateral ridge augmentation using particulated or block bone substitutes biocoated with rhGDF-5 and rhBMP-2: an immunohistochemical study in dogs. Clin Oral Implants Res. 2008;19:642-52.

[132]   Kraus D, Jager A, Abuduwali N, Deschner J, Lossdorfer S. Intermittent PTH(1-34) signals through protein kinase A to regulate osteoprotegerin production in human periodontal ligament cells in vitro. Clin Oral Investig. 2012;16:611-8.

[133]   Lossdorfer S, Gotz W, Jager A. Parathyroid hormone modifies human periodontal ligament cell proliferation and survival in vitro. J Periodontal Res. 2006;41:519-26.

[134]   Kawane T, Takahashi S, Saitoh H, Okamoto H, Kubodera N, Horiuchi N. Anabolic effects of recombinant human parathyroid hormone (1 - 84) and synthetic human parathyroid hormone (1 - 34) on the mandibles of osteopenic ovariectomized rats with maxillary molar extraction. Horm Metab Res. 2002;34:293-302.

[135]   Marques MR, da Silva MA, Manzi FR, Cesar-Neto JB, Nociti FH, Jr., Barros SP. Effect of intermittent PTH administration in the periodontitis-associated bone loss in ovariectomized rats. Arch Oral Biol. 2005;50:421-9.

[136]   Jung RE, Cochran DL, Domken O, Seibl R, Jones AA, Buser D, et al. The effect of matrix bound parathyroid hormone on bone regeneration. Clin Oral Implants Res. 2007;18:319-25.

[137]   Valderrama P, Jung RE, Thoma DS, Jones AA, Cochran DL. Evaluation of parathyroid hormone bound to a synthetic matrix for guided bone regeneration around dental implants: a histomorphometric study in dogs. J Periodontol. 2010;81:737-47.

[138]   Hammerle CH, Jung RE. Bone augmentation by means of barrier membranes. Periodontol 2000. 2003;33:36-53.

[139]   Jung RE, Glauser R, Scharer P, Hammerle CH, Sailer HF, Weber FE. Effect of rhBMP-2 on guided bone regeneration in humans. Clin Oral Implants Res. 2003;14:556-68.

[140]   Urist MR, Maeda H, Shamie AN, Teplica D. Endogenous bone morphogenetic protein expression in transplants of urinary bladder. Plast Reconstr Surg. 1998;101:408-15; discussion 16-7.

[141]   Sawada Y, Hokugo A, Nishiura A, Hokugo R, Matsumoto N, Morita S, et al. A trial of alveolar cleft bone regeneration by controlled release of bone morphogenetic protein: an experimental study in rabbits. Oral Surg Oral Med Oral Pathol Oral Radiol Endod. 2009;108:812-20.

[142] Wikesjo UM, Qahash M, Thomson RC, Cook AD, Rohrer MD, Wozney JM, et al. rhBMP-2 significantly enhances guided bone regeneration. Clin Oral Implants Res. 2004;15:194-204.

[143] Nevins M, Kao RT, McGuire MK, McClain PK, Hinrichs JE, McAllister BS, et al. Platelet-derived growth factor promotes periodontal regeneration in localized osseous defects: 36-month extension results from a randomized, controlled, double-masked clinical trial. J Periodontol. 2013;84:456-64.

[144] Jayakumar A, Rajababu P, Rohini S, Butchibabu K, Naveen A, Reddy PK, et al. Multi-centre, randomized clinical trial on the efficacy and safety of recombinant human platelet-derived growth factor with beta-tricalcium phosphate in human intra-osseous periodontal defects. J Clin Periodontol. 2011;38:163-72.

[145] Camelo M, Nevins ML, Schenk RK, Lynch SE, Nevins M. Periodontal regeneration in human Class II furcations using purified recombinant human platelet-derived growth factor-BB (rhPDGF-BB) with bone allograft. Int J Periodontics Restorative Dent. 2003;23:213-25.

[146] Nevins ML, Camelo M, Schupbach P, Nevins M, Kim SW, Kim DM. Human buccal plate extraction socket regeneration with recombinant human platelet-derived growth factor BB or enamel matrix derivative. Int J Periodontics Restorative Dent. 2011;31:481-92.

[147] Nevins ML, Reynolds MA, Camelo M, Schupbach P, Kim DM, Nevins M. Recombinant human platelet-derived growth factor BB for reconstruction of human large extraction site defects. Int J Periodontics Restorative Dent. 2014;34:157-63.

[148] McKay WF, Peckham SM, Badura JM. A comprehensive clinical review of recombinant human bone morphogenetic protein-2 (INFUSE Bone Graft). Int Orthop. 2007;31:729-34.

[149] Urist MR. Bone: formation by autoinduction. 1965. Clin Orthop Relat Res. 2002:4-10.

[150] Boyne PJ, Marx RE, Nevins M, Triplett G, Lazaro E, Lilly LC, et al. A feasibility study evaluating rhBMP-2/absorbable collagen sponge for maxillary sinus floor augmentation. Int J Periodontics Restorative Dent. 1997;17:11-25.

[151] Triplett RG, Nevins M, Marx RE, Spagnoli DB, Oates TW, Moy PK, et al. Pivotal, randomized, parallel evaluation of recombinant human bone morphogenetic protein-2/absorbable collagen sponge and autogenous bone graft for maxillary sinus floor augmentation. J Oral Maxillofac Surg. 2009;67:1947-60.

[152] Kao DW, Kubota A, Nevins M, Fiorellini JP. The negative effect of combining rhBMP-2 and Bio-Oss on bone formation for maxillary sinus augmentation. Int J Periodontics Restorative Dent. 2012;32:61-7.

[153]   Torrecillas-Martinez L, Monje A, Pikos MA, Ortega-Oller I, Suarez F, Galindo-Moreno P, et al. Effect of rhBMP-2 upon maxillary sinus augmentation: a comprehensive review. Implant Dent. 2013;22:232-7.

[154]   de Freitas RM, Spin-Neto R, Junior EM, Pereira LA, Wikesjo UM, Susin C. Alveolar Ridge and Maxillary Sinus Augmentation Using rhBMP-2: A Systematic Review. Clin Implant Dent Relat Res. 2013.

[155]   Howell TH, Fiorellini J, Jones A, Alder M, Nummikoski P, Lazaro M, et al. A feasibility study evaluating rhBMP-2/absorbable collagen sponge device for local alveolar ridge preservation or augmentation. Int J Periodontics Restorative Dent. 1997;17:124-39.

[156]   Cochran DL, Jones AA, Lilly LC, Fiorellini JP, Howell H. Evaluation of recombinant human bone morphogenetic protein-2 in oral applications including the use of endosseous implants: 3-year results of a pilot study in humans. J Periodontol. 2000;71:1241-57.

[157]   Fiorellini JP, Buser D, Riley E, Howell TH. Effect on bone healing of bone morphogenetic protein placed in combination with endosseous implants: a pilot study in beagle dogs. Int J Periodontics Restorative Dent. 2001;21:41-7.

[158]   Corinaldesi G, Piersanti L, Piattelli A, Iezzi G, Pieri F, Marchetti C. Augmentation of the floor of the maxillary sinus with recombinant human bone morphogenetic protein-7: a pilot radiological and histological study in humans. Br J Oral Maxillofac Surg. 2013;51:247-52.

[159]   Windisch P, Stavropoulos A, Molnar B, Szendroi-Kiss D, Szilagyi E, Rosta P, et al. A phase IIa randomized controlled pilot study evaluating the safety and clinical outcomes following the use of rhGDF-5/beta-TCP in regenerative periodontal therapy. Clin Oral Investig. 2012;16:1181-9.

[160]   Koch FP, Becker J, Terheyden H, Capsius B, Wagner W. A prospective, randomized pilot study on the safety and efficacy of recombinant human growth and differentiation factor-5 coated onto beta-tricalcium phosphate for sinus lift augmentation. Clin Oral Implants Res. 2010;21:1301-8.

[161]   Kitamura M, Akamatsu M, Machigashira M, Hara Y, Sakagami R, Hirofuji T, et al. FGF-2 stimulates periodontal regeneration: results of a multi-center randomized clinical trial. J Dent Res. 2011;90:35-40.

[162]   Chan HL, McCauley LK. Parathyroid hormone applications in the craniofacial skeleton. J Dent Res. 2013;92:18-25.

[163]   Bashutski JD, Eber RM, Kinney JS, Benavides E, Maitra S, Braun TM, et al. Teriparatide and osseous regeneration in the oral cavity. N Engl J Med. 2010;363:2396-405.

[164]   Kuchler U, Luvizuto ER, Tangl S, Watzek G, Gruber R. Short-term teriparatide delivery and osseointegration: a clinical feasibility study. J Dent Res. 2011;90:1001-6.

[165]   Walther W, Stein U. Viral vectors for gene transfer: a review of their use in the treatment of human diseases. Drugs. 2000;60:249-71.

[166]   Al-Dosari MS, Gao X. Nonviral gene delivery: principle, limitations, and recent progress. AAPS J. 2009;11:671-81.

[167]   Nelson CE, Gupta MK, Adolph EJ, Guelcher SA, Duvall CL. siRNA Delivery from an Injectable Scaffold for Wound Therapy. Adv Wound Care (New Rochelle). 2013;2:93-9.

[168]   Rios HF, Lin Z, Oh B, Park CH, Giannobile WV. Cell- and gene-based therapeutic strategies for periodontal regenerative medicine. J Periodontol. 2011;82:1223-37.

[169]   Wegman F, Oner FC, Dhert WJ, Alblas J. Non-viral gene therapy for bone tissue engineering. Biotechnol Genet Eng Rev. 2013;29:206-20.

[170]   Jung Y, Bauer G, Nolta JA. Concise Review: Induced Pluripotent Stem Cell-Derived Mesenchymal Stem Cells: Progress Toward Safe Clinical Products. Stem cells (Dayton, Ohio). 2012;30:42-7.

[171]   Perry BC, Zhou D, Wu X, Yang F-C, Byers MA, Chu TMG, et al. Collection, Cryopreservation, and Characterization of Human Dental Pulp–Derived Mesenchymal Stem Cells for Banking and Clinical Use. Tissue Engineering Part C, Methods. 2008;14:149-56.

[172]   Hollister SJ, Murphy WL. Scaffold Translation: Barriers Between Concept and Clinic. Tissue Engineering Part B, Reviews. 2011;17:459-74.

[173]   Bleich NK, Kallai I, Lieberman JR, Schwarz EM, Pelled G, Gazit D. Gene therapy approaches to regenerating bone. Advanced drug delivery reviews. 2012;64:1320-30.

[174]   Yin H, Kanasty RL, Eltoukhy AA, Vegas AJ, Dorkin JR, Anderson DG. Non-viral vectors for gene-based therapy. Nat Rev Genet. 2014;15:541-55.

[175]   Chang PC, Cirelli JA, Jin Q, Seol YJ, Sugai JV, D'Silva NJ, et al. Adenovirus encoding human platelet-derived growth factor-B delivered to alveolar bone defects exhibits safety and biodistribution profiles favorable for clinical use. Hum Gene Ther. 2009;20:486-96.

[176]   Jin Q, Anusaksathien O, Webb SA, Printz MA, Giannobile WV. Engineering of tooth-supporting structures by delivery of PDGF gene therapy vectors. Mol Ther. 2004;9:519-26.

[177]   Jin QM, Anusaksathien O, Webb SA, Rutherford RB, Giannobile WV. Gene therapy of bone morphogenetic protein for periodontal tissue engineering. J Periodontol. 2003;74:202-13.

[178] Cirelli JA, Park CH, MacKool K, Taba M, Jr., Lustig KH, Burstein H, et al. AAV2/1-TNFR:Fc gene delivery prevents periodontal disease progression. Gene Ther. 2009;16:426-36.

[179] Warrington KH, Jr., Herzog RW. Treatment of human disease by adeno-associated viral gene transfer. Hum Genet. 2006;119:571-603.

[180] Xiang L, Ma L, He Y, Wei N, Gong P. Transfection with follicular dendritic cell secreted protein to affect phenotype expression of human periodontal ligament cells. J Cell Biochem. 2014;115:940-8.

[181] Logan AC, Lutzko C, Kohn DB. Advances in lentiviral vector design for gene-modification of hematopoietic stem cells. Curr Opin Biotechnol. 2002;13:429-36.

[182] Huang YC, Simmons C, Kaigler D, Rice KG, Mooney DJ. Bone regeneration in a rat cranial defect with delivery of PEI-condensed plasmid DNA encoding for bone morphogenetic protein-4 (BMP-4). Gene Ther. 2005;12:418-26.

[183] Filho Cerruti H, Kerkis I, Kerkis A, Tatsui NH, da Costa Neves A, Bueno DF, et al. Allogenous bone grafts improved by bone marrow stem cells and platelet growth factors: clinical case reports. Artif Organs. 2007;31:268-73.

[184] Pelegrine AA, da Costa CE, Correa ME, Marques JF, Jr. Clinical and histomorphometric evaluation of extraction sockets treated with an autologous bone marrow graft. Clin Oral Implants Res. 2010;21:535-42.

[185] Gonshor A, McAllister BS, Wallace SS, Prasad H. Histologic and histomorphometric evaluation of an allograft stem cell-based matrix sinus augmentation procedure. Int J Oral Maxillofac Implants. 2011;26:123-31.

[186] Rickert D, Sauerbier S, Nagursky H, Menne D, Vissink A, Raghoebar GM. Maxillary sinus floor elevation with bovine bone mineral combined with either autogenous bone or autogenous stem cells: a prospective randomized clinical trial. Clin Oral Implants Res. 2011;22:251-8.

[187] Schmelzeisen R, Gutwald R, Oshima T, Nagursky H, Vogeler M, Sauerbier S. Making bone II: maxillary sinus augmentation with mononuclear cells--case report with a new clinical method. Br J Oral Maxillofac Surg. 2011;49:480-2.

[188] Ji Y, Wang L, Watts DC, Qiu H, You T, Deng F, et al. Controlled-release naringin nanoscaffold for osteoporotic bone healing. Dent Mater. 2014;30:1263-73.

[189] Lee K, Weir MD, Lippens E, Mehta M, Wang P, Duda GN, et al. Bone regeneration via novel macroporous CPC scaffolds in critical-sized cranial defects in rats. Dent Mater. 2014;30:e199-207.

[190]   Bsoul S, Terezhalmy G, Abboud H, Woodruff K, Abboud SL. PDGF BB and bFGF stimulate DNA synthesis and upregulate CSF-1 and MCP-1 gene expression in dental follicle cells. Arch Oral Biol. 2003;48:459-65.

[191]   Mumford JH, Carnes DL, Cochran DL, Oates TW. The effects of platelet-derived growth factor-BB on periodontal cells in an in vitro wound model. J Periodontol. 2001;72:331-40.

[192]   Zhao M, Berry JE, Somerman MJ. Bone morphogenetic protein-2 inhibits differentiation and mineralization of cementoblasts in vitro. J Dent Res. 2003;82:23-7.

[193]   Kemoun P, Laurencin-Dalicieux S, Rue J, Farges JC, Gennero I, Conte-Auriol F, et al. Human dental follicle cells acquire cementoblast features under stimulation by BMP-2/-7 and enamel matrix derivatives (EMD) in vitro. Cell Tissue Res. 2007;329:283-94.

[194]   Zhao M, Xiao G, Berry JE, Franceschi RT, Reddi A, Somerman MJ. Bone morphogenetic protein 2 induces dental follicle cells to differentiate toward a cementoblast/osteoblast phenotype. J Bone Miner Res. 2002;17:1441-51.

[195]   Murphy MG, Mailhot J, Borke J, Wataha J, Sharawy M, Smith A. The effects of rhBMP-2 on human osteosarcoma cells and human gingival fibroblasts in vitro. J Oral Implantol. 2001;27:16-24.

[196]   Laflamme C, Curt S, Rouabhia M. Epidermal growth factor and bone morphogenetic proteins upregulate osteoblast proliferation and osteoblastic markers and inhibit bone nodule formation. Arch Oral Biol. 2010;55:689-701.

[197]   Lallier TE, Spencer A. Use of microarrays to find novel regulators of periodontal ligament fibroblast differentiation. Cell Tissue Res. 2007;327:93-109.

[198]   Hakki SS, Nohutcu RM, Hakki EE, Berry JE, Akkaya MS, Somerman MJ. Dexamethasone and basic-fibroblast growth factor regulate markers of mineralization in cementoblasts in vitro. J Periodontol. 2005;76:1550-8.

[199]   Fujisawa K, Miyamoto Y, Nagayama M. Basic fibroblast growth factor and epidermal growth factor reverse impaired ulcer healing of the rabbit oral mucosa. J Oral Pathol Med. 2003;32:358-66.

[200]   Reyes-Botella C, Vallecillo-Capilla MF, Ruiz C. Effect of different growth factors on human cultured osteoblast-like cells. Cell Physiol Biochem. 2002;12:353-8.

[201]   Yoshimoto T, Yamamoto M, Kadomatsu H, Sakoda K, Yonamine Y, Izumi Y. Recombinant human growth/differentiation factor-5 (rhGDF-5) induced bone formation in murine calvariae. J Periodontal Res. 2006;41:140-7.

[202] Sumita Y, Honda MJ, Ueda M, Asahina I, Kagami H. Differential effects of growth differentiation factor-5 on porcine dental papilla- and follicle-derived cells. Growth Factors. 2010;28:56-65.

[203] Takahashi D, Odajima T, Morita M, Kawanami M, Kato H. Formation and resolution of ankylosis under application of recombinant human bone morphogenetic protein-2 (rhBMP-2) to class III furcation defects in cats. J Periodontal Res. 2005;40:299-305.

[204] Sigurdsson TJ, Fu E, Tatakis DN, Rohrer MD, Wikesjo UM. Bone morphogenetic protein-2 for peri-implant bone regeneration and osseointegration. Clin Oral Implants Res. 1997;8:367-74.

[205] Miranda DA, Blumenthal NM, Sorensen RG, Wozney JM, Wikesjo UM. Evaluation of recombinant human bone morphogenetic protein-2 on the repair of alveolar ridge defects in baboons. J Periodontol. 2005;76:210-20.

[206] Terheyden H, Jepsen S, Vogeler S, Tucker M, Rueger DC. Recombinant human osteogenic protein 1 in the rat mandibular augmentation model: differences in morphology of the newly formed bone are dependent on the type of carrier. Mund Kiefer Gesichtschir. 1997;1:272-5.

[207] McAllister BS, Margolin MD, Cogan AG, Taylor M, Wollins J. Residual lateral wall defects following sinus grafting with recombinant human osteogenic protein-1 or Bio-Oss in the chimpanzee. Int J Periodontics Restorative Dent. 1998;18:227-39.

[208] Weng D, Poehling S, Pippig S, Bell M, Richter EJ, Zuhr O, et al. The effects of recombinant human growth/differentiation factor-5 (rhGDF-5) on bone regeneration around titanium dental implants in barrier membrane-protected defects: a pilot study in the mandible of beagle dogs. Int J Oral Maxillofac Implants. 2009;24:31-7.

[209] Leknes KN, Yang J, Qahash M, Polimeni G, Susin C, Wikesjo UM. Alveolar ridge augmentation using implants coated with recombinant human growth/differentiation factor -5 (rhGDF-5). Radiographic observations. Clin Oral Implants Res. 2012.

[210] Kwon DH, Bennett W, Herberg S, Bastone P, Pippig S, Rodriguez NA, et al. Evaluation of an injectable rhGDF-5/PLGA construct for minimally invasive periodontal regenerative procedures: a histological study in the dog. J Clin Periodontol. 2010;37:390-7.

[211] Fischer J, Kolk A, Wolfart S, Pautke C, Warnke PH, Plank C, et al. Future of local bone regeneration - Protein versus gene therapy. J Craniomaxillofac Surg. 2011;39:54-64.

[212] Gower RM, Shea LD. Biomaterial Scaffolds for Controlled, Localized Gene Delivery of Regenerative Factors. Adv Wound Care (New Rochelle). 2013;2:100-6.

[213] Liu TB, Fedak PW, Weisel RD, Yasuda T, Kiani G, Mickle DA, et al. Enhanced IGF-1 expression improves smooth muscle cell engraftment after cell transplantation. Am J Physiol Heart Circ Physiol. 2004;287:H2840-9.

[214]   Cam C, Segura T. Matrix-based gene delivery for tissue repair. Curr Opin Biotechnol. 2013;24:855-63.

[215] Iwanaga K, Tominaga K, Yamamoto K, Habu M, Maeda H, Akifusa S, et al. Local delivery system of cytotoxic agents to tumors by focused sonoporation. Cancer Gene Ther. 2007;14:354-63.

[216] Kotopoulis S, Dimcevski G, Gilja OH, Hoem D, Postema M. Treatment of human pancreatic cancer using combined ultrasound, microbubbles, and gemcitabine: a clinical case study. Med Phys. 2013;40:072902.

CHAPTER 3

SINGLE PATIENT CASE STUDY USING A 3D-PRINTED BIORESORBABLE SCAFFOLD FOR PERIODONTAL REPAIR

Based on a case report published in *Journal of Dental Research* and sections written as a contribution to a book chapter entitled "Bioengineering of the Periodontal Ligament":

Rasperini G, **Pilipchuk SP**, Flanagan CL, Park CH, Pagni G, Hollister SJ, Giannobile WV. 3D-printed bioresorbable scaffold for periodontal repair, *J Dent Res.* 2015;94(9 Suppl):153S-7S

Decker AM, **Pilipchuk SP**, Araujo-Pires AC, Giannobile WV. Bioengineering of the periodontal ligament. In: Kapila SD, Goonewardene M, eds. *Interdisciplinary Therapy: Using Contemporary Approaches for Complex Cases.* Monograph 52, Craniofacial Growth Series, Center for Human Growth and Development, The University of Michigan, Ann Arbor, 2016:195-242.

3.1 Introduction

Tissue engineered constructs have potential to induce bone-ligament complex regeneration to treat disease- or trauma-induced damage to periodontia [1]. Multiphasic designs incorporating several biomaterial layers that serve as regenerating platforms for each region of the periodontum (i.e., PDL, alveolar bone) are increasingly being investigated in combination with the delivery of cells and other biologic factors. These include the layer by layer deposition of a polymer that allows for controlled pore size formation depending on printer resolution, or the printing of a mold that can be cast to produce the final scaffold shape. Lee et al demonstrated the use of PCL-HA layer deposition with microchannels ranging from 100um-600um for the PDL, bone, and cementum/dentin regions of a hierarchical scaffold which incorporated the spatiotemporal delivery of amelogenin, connective tissue growth factor, and BMP-2 within each of the phases, respectively. Seeding of the constructs with dental pulp stem/progenitor cells and subcutaneous implantation in immunodeficient mice resulted in aligned PDL-like collagen fiber formation

connected to bone tissue that was sialoprotein-positive [2]. Biphasic scaffold designs have also been explored combining fabrication technologies such as 3-D printing and electrospinning with cell sheet engineering. Vaquette et al developed a construct of PCL with β-TCP for the bone region,

and an electrospun PCL membrane for the PDL region with placement of several PDL cell sheets which improved attachment to the dentin surface relative to constructs that did not incorporate the sheets [3]. Hybrid PCL/PLGA and fiber-guiding PCL scaffolds with perpendicularly-oriented microchannels were developed by Park et al utilizing computational design and solid-free form fabrication for the direct guidance of PDL fibers in vivo, resulting in more predictable formation of organized periostin-positive ligamentous structures [4, 5]. Findings from these studies indicate that bone-ligament complex regeneration in the clinic has the potential to be guided via 3-D printed, hybrid scaffolds with a multi-compartmental architecture designed based on patient defect CT scans [6]. The anatomical complexity of PDL tissue makes combinatorial approaches and advanced multiphasic scaffold designs appealing for improving its structural and functional regeneration.

Herein we provide the first reported human case of treatment of a large periodontal osseous defect with a 3D printed bioresorbable patient-specific polymer scaffold and signaling growth factor. Specifically, 3-D printing technology was used to generate a scaffold which conformed to defect site parameters obtained via cone beam computed tomography (CBCT) scans. The treated site remained intact for 12 months following therapy. This report suggests that 3D printed, image-based scaffolds offer potential for periodontal reconstruction. Limitations gleaned from this case and opportunities for treatment of other bony defects are discussed.

3.2   Methods and Materials

3.2.1   *Case Presentation*

A healthy, 53-year old Caucasian male, diagnosed with generalized aggressive periodontitis presented for treatment to preserve his dentition. The patient received full-mouth scaling/root planing and 2 years later still showed signs of periodontal stability, but with a resulting large labial soft and osseous defect associated with the mandibular cuspid, tooth #22 (**Figure 3.1**, top panels). The patient consented to treatment of the deficiency by a bioengineering approach described below. The study protocol was approved by the University of Milan Institutional Review Board, Milan Italy.

3.2.2   3D Printed scaffold fabrication

An .STL format was used as an input data file for the manufacturing process and to determine a best fit based on a CT scan of the patient's defect (400um slice thickness, 400x400um voxel size). Magics 15 (Materialise Inc, Leuven, Belgium) was used to subtract STL-generated defect from designed scaffold to generate a 3-D design, then further modified using NX 7.5 (Siemens PLM software, Plano, TX) and Mimics (Materialise Inc; **Figure 3.1**, middle panels). The design consisted of perforations for fixation, an internal port for delivery of recombinant human platelet-derived growth factor (rhPDGF-BB), and pegs oriented perpendicularly to the root for periodontal ligament formation (PDL) guidance as previously described using PCL scaffolds in a rat periodontal fenestration defect model (**Figure 3.1**, bottom). Selective laser sintering (SLS) allows for fabrication of precise scaffold features that can be designed to support structural and functional tissue regeneration in vivo. SLS (Formiga P100 system; EOS e-Manufacturing Solutions) was used to 3-D print the scaffold with polycaprolactone (PCL) powder (Polysciences Inc, Warrington, PA; milled at Jet Pulverizer, Moorestown, NJ) containing 4% hydroxyapatite. PCL is a Food and Drug Administration (FDA)-approved, hydrolytically-degradable polymer. Geometric interface adaption of the scaffold to the defect was assessed using a patient-specific 3D printed prototype model (University of Michigan Medical Innovation Center). Micro-computed tomography (eXplore Locus SP, GE Healthcare, London, ON, Canada) scans of prototyped mandible with scaffold were used to determine the adaptation ratio based on the methodology for periodontal fiber guidance. Measurements of gap distance between scaffold PDL region and modeled tooth root were repeated (n=3) to determine mean adaptation for eventual in vivo placement (**Figure 3.1** lower middle panels; **Figure 3.3**). The scaffold was sterilized using ethylene oxide (Nelson Laboratories, Salt Lake City, UT). University of Michigan Institutional Review Board granted exemption status for evaluation of the scaffold material.

3.2.3   Surgical Procedure and Scaffold Delivery

The patient was prepared with local infiltration anesthesia (**Figure 3.2**). A trapezoidal full-thickness labial flap was elevated encompassing the adjacent teeth. Vertical incisions were extended beyond the mucogingival junction to allow relaxation of the flap and ease scaffold placement. The tooth root surface was mechanically instrumented and EDTA (Straumann® PrefGel®, Institut Straumann AG, Basel, Switzerland) was used as a root modification agent. The

scaffold was immersed in 0.5mL rhPDGF-BB (0.3mg/mL) (Gem 21S, Osteohealth, Shirley, NY, USA) for 15 min, filled with autologous blood from the defect site, and stabilized over the defect with ultrasound-activated resorbable poly-D and L-lactic acid (PDLLA) pins (SonicWeld, KLS Martin Group, Tuttlingen Germany). Remaining PDGF-BB solution was applied at the defect site prior to scaffold stabilization. The flap was released to allow tension-free primary closure with non-resorbable sutures. The patient refrained from mechanical oral hygiene procedures using 0.12% chlorhexidine rinses for 3 weeks. The patient was prescribed Amoxicillin 875mg + clavulanic acid 125mg BID for 6d and Ibuprofen 600 mg as needed for pain post-operatively. Sutures were removed 7d following surgery.

3.3   Results

The scaffold design incorporated pegs 160–380um in length consistent with human PDL, the superior PDL region being shorter to accommodate to root proximity. Mean strut length was 600um for support of extensions in the PDL region, while channel width for growth factor delivery was ~500um (**Figure 3.1**). The interface was determined to have an adaptation ratio of 0.82 ± 0.07, which characterizes gap width distribution between scaffold and tissue (**Figure 3.3**). In vitro release kinetics demonstrated an overall burst release of rhPDGF-BB from the scaffold matrix over a 3h period (**Figure 3.4**).

The scaffold remained covered for 12m, demonstrating 3mm gain of clinical attachment and partial root coverage (*Table 3.1*). The implanted 3-D scaffold served to fill the human periodontal osseous defect without signs of chronic inflammation or dehiscence (**Figure 3.5**). However, at 13m, the scaffold became exposed requiring removal. The biopsy specimen was fixed in formalin, evaluated histologically and for scaffold molecular weight. Based on gel permeation chromatography, 75.9% of the scaffold molecular weight remained after 13m (*Table 3.2*) with minimal evidence of bone repair as evidenced by histological analysis (**Figure 3.5**).
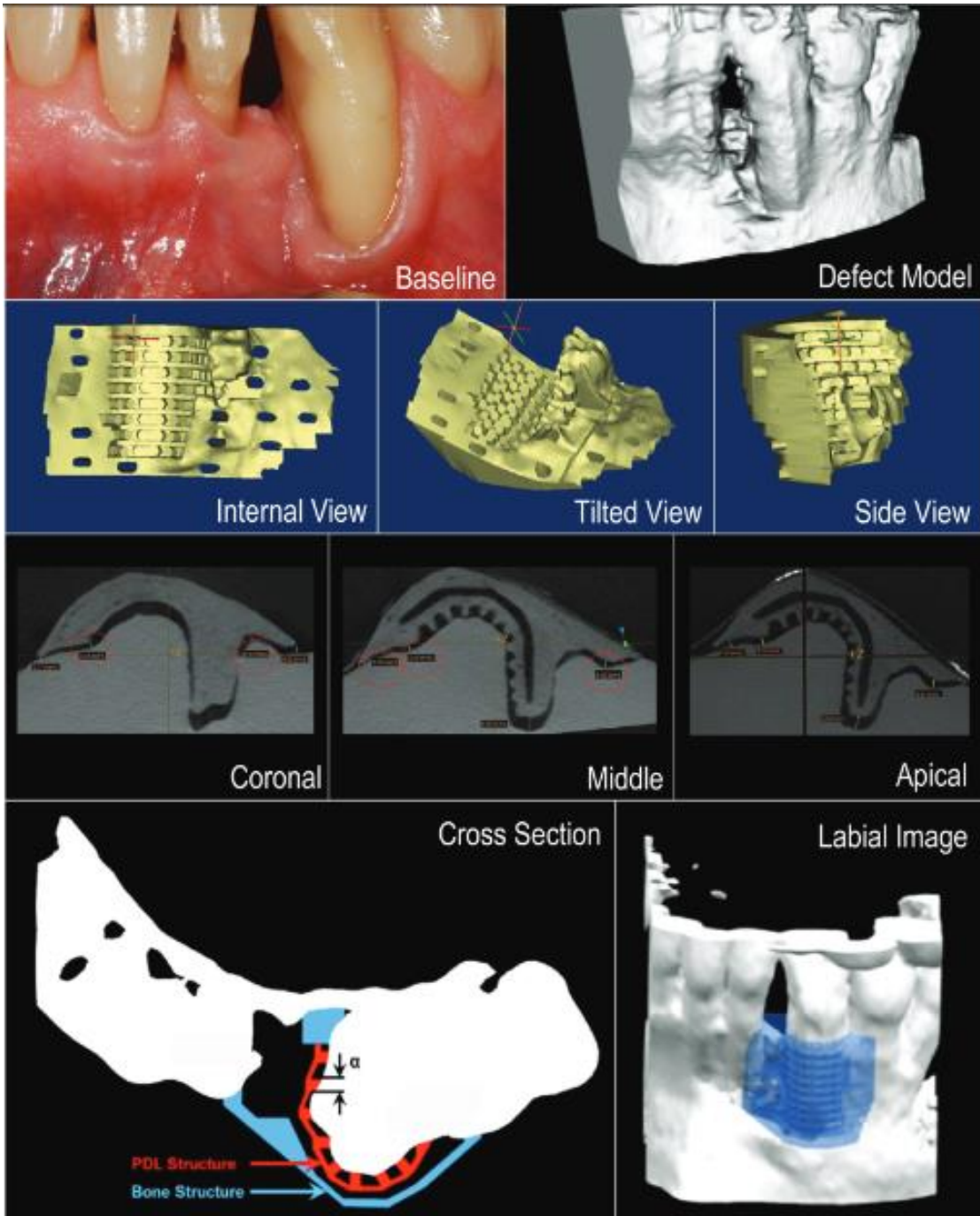
Figure 3.1 Customized Scaffold for Peri-osseous Defect
A customized scaffold was 3-D printed using medical grade polycaprolactone (PCL) to fit the periosseous defect using a prototyped model of the defect from the patient's CBCT scan. The scaffold's internal region consisted of extended pegs for the support and guidance of periodontal ligament formation, perforations for fixation, and an internal compartment for rhPDGF-BB delivery, as shown in the cross-sectional view. Micro-computed tomography scans of the PCL scaffold fitted into the prototyped defect model (*see* coronal, middle, apical views) were used to determine the topographical adaptation of the scaffold to the root surface.

Figure 3.2 Clinical Outcome of Scaffold Implantation
Clinical attachment loss and alveolar ridge resorption characterized the patient periosseous defect involving tooth #22. A trapezoidal full thickness flap was elevated to expose the defect, the root surface mechanically instrumented, and EDTA solution applied during root preparation. Prior to implantation, the scaffold matrix was immersed in 0.3mg/mL rhPDGF-BB solution for 15 min at RT. During placement, the scaffold was filled with autologous blood, positioned over the exposed tooth root, and stabilized using PDLLA pins. Tension-free primary intention method was employed during wound closure. The implanted 3-D scaffold filled the periodontal osseous defect without clinical signs of chronic inflammation or rejection of the PCL-based material during the first year.

Adaptation Ratio of 3-D Scaffold

Mean ± s.d. = **0.82 ± 0.07**
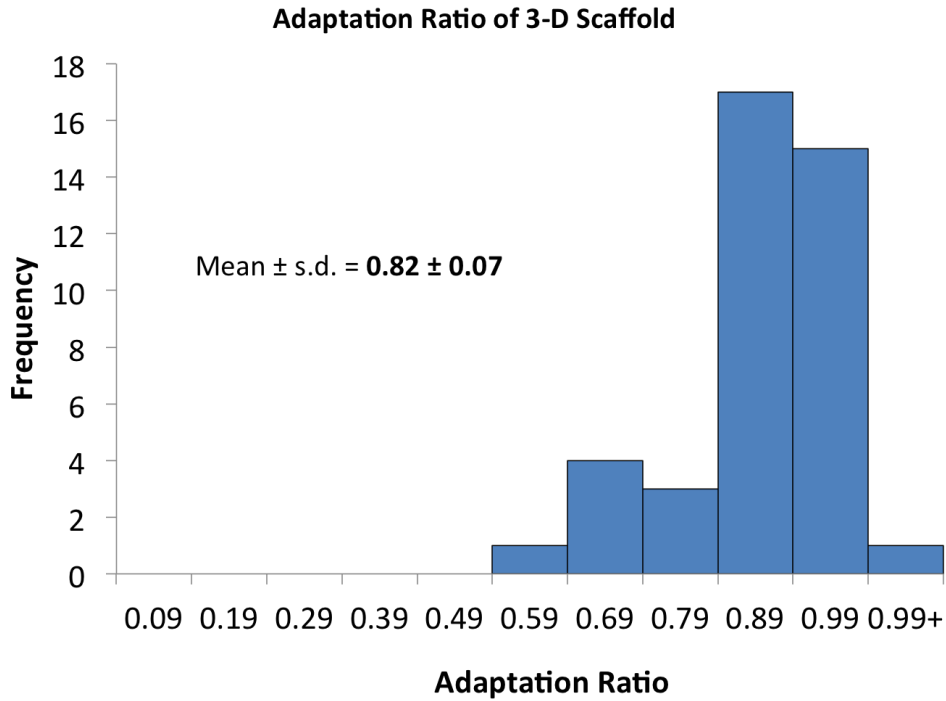
Figure 3.3 Adaptation of 3D-Printed Scaffold

Adaptation ratio of polycaprolactone scaffold fitted into a prototyped model of the periosseous defect was determined as an assessment of the topographic adaptation of the scaffold to the root surface. A 100% (ratio of 0.1) adaptable scaffold would indicate a perfect fit. The final design of the polycaprolactone scaffold was adaptable to the periosseous defect by 82% ± 7% (mean ± SD).
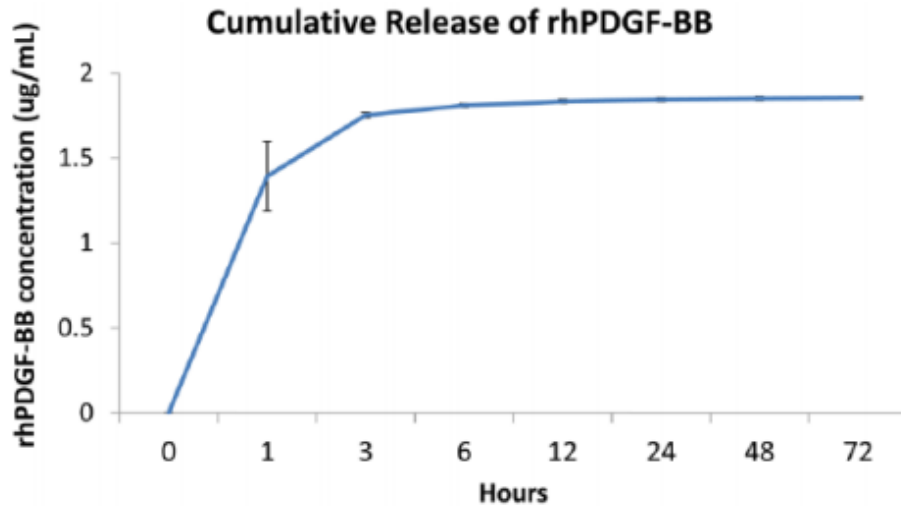
Figure 3.4 Release Kinetics of rhPDGF-BB from PCL Scaffold

In vitro release kinetics of recombinant human platelet-derived growth factor BB (rhPDGF-BB) from polycaprolactone scaffolds (155.6 ± 0.9 mg) into phosphate-buffered saline from a rhPDGF-BB loading of 48.2 μg per scaffold for 20 min at room temperature. Each data point represents mean ± SD (n= 3).

68
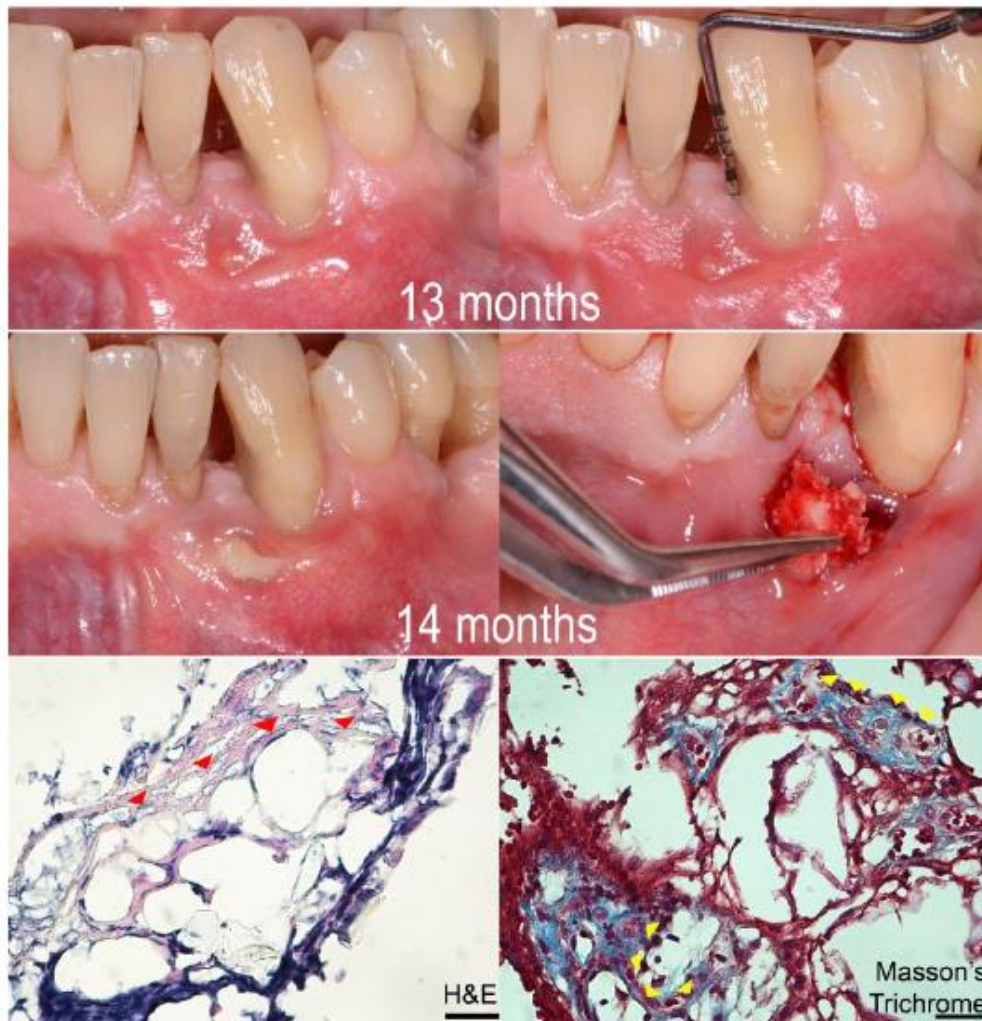
Figure 3.5 Post-operative Exposure and Retrieved Scaffold Matrix
Postoperative exposure and retrieved scaffold matrix. The top panel shows the initial soft tissue dehiscence over the scaffold at 13 mo. The middle panel shows the more extensive exposure and wound failure of the scaffold matrix, necessitating removal at 14 mo (middle panels). The bottom panel shows histologic analysis of the retrieved scaffold matrix, which was performed with hematoxylin and eosin (H&E) and Masson's trichrome staining. Frozen sectioning of the decalcified tissue stained with H&E shows tissue attachment to scaffold remnants (red arrowheads). Masson's trichrome paraffin-embedded sections indicate small islands of new bone formation within a milieu of primarily granulomatous tissue (yellow arrowheads). Scale bar = 50 μm.

Table 3.1 Clinical Parameters

Parameter	Baseline	2 mo	6 mo	12 mo	13 mo
Probing pocket depth, mm[a]	2	N/A	N/A	5	2
Recession, mm[a]	9	2	2	3	7
Clinical attachment level, mm[a]	11	N/A	N/A	8	9
Plaque[a]	No	No	No	No	No
Bleeding on probing[a]	No	No	No	No	No
Full-mouth plaque score, %	<10	<10	<10	<10	<10
Full-mouth bleeding score, %	<10	<10	<10	<10	<10

[a]Mesiobuccal.

Table 3.2 Gel Permeation Chromatography: Analysis of Changes in Mean Molecular Mass of Polycaprolactone Scaffold Matrix

Scaffold	Mean Molecular Mass, kDa
Nonimplanted polycaprolactone scaffold	89.8
Patient scaffold after 14 mo in situ	68.2
Total change in mean	21.6 (24.1%)

3.4   Discussion

When applying tissue engineering approaches to the reconstruction of complex tissue structures such as the periodontium, biomaterials serve as 3-D templates and synthetic extracellular-matrix (ECM) environments for the regenerative process [7]. Printed biomaterials represent promising tools, allowing customization to the desired size, configuration and architecture of a given defect. Their efficacy in the regeneration of complex structures such as new PDL has been shown pre-clinically [5]. Successful use of a 3-D printed PCL splint for the treatment of tracheobronchomalacia has been recently reported using a similar approach [8]. We believe a limitation of this study was use of the PCL biomaterial that may not be ideal for periodontal applications. It appears that a more rapidly resorbing matrix with a healing window of <1 year combined with a less bulky design would be better suited to avoid wound dehiscence, exposure and subsequent microbial contamination in a peri-mucosal environment around teeth. Histological analysis indicating minimal collagenous tissue ingrowth into the scaffold (**Figure 3.5**) supports the need for a more interconnected internal structure with greater surface area. Selection of a biomaterial with a faster rate of resorption (i.e., polylactic-co-glycolic acid (PLGA)) combined with a highly porous structure would contribute to greater tissue ingrowth and vascularization. As evidenced by gel permeation chromatography results (*Table 3.2*) which indicate a PCL degradation of only 24.1%, improvements in the resorptive properties of the scaffold are intrinsic to improved bony infill, which is difficult to achieve with a slowly-degrading polymer. Compartmentalized delivery of PDGF-BB to the PDL-forming region of the scaffold and BMP-2 to the bone region may further facilitate tissue growth and remodeling. Although PDGF-BB has previously been shown to bind and release from a PCL-based scaffold in a biological manner [9], optimization of the growth factor release kinetics may further increase PDGF bioactivity *in situ*. A hybrid PLGA-PCL scaffold design may also provide optimal mechanical and resorptive properties for engineering a PDL-bone interphase. Further studies would focus on the analysis of scaffold stiffness to reduce risk of tissue dehiscence.

3.5   Conclusions

This case represents the first application of a personalized, 3-D bioprinted scaffold to treat a periodontal defect. Although this case was not successful long term, we believe the approach warrants further study for more personalized oral regenerative medicine clinical applications.

71

3.6   References

[1]   Ivanovski S, Vaquette C, Gronthos S, Hutmacher DW, Bartold PM. 2014. Multiphasic Scaffolds for Periodontal Tissue Engineering. J Dent Res 93:1212-21.

[2]   Lee CH, Hajibandeh J, Suzuki T, Fan A, Shang P, Mao JJ. Three-dimensional printed multiphase scaffolds for regeneration of periodontium complex. Tissue Engineering Part A 2014;20:1342-1351.

[3]   Vaquette C, Fan W, Xiao Y, Hamlet S, Hutmacher DW, Ivanovski S. A biphasic scaffold design combined with cell sheet technology for simultaneous regeneration of alveolar bone/periodontal ligament complex. Biomaterials 2012;33:5560-5573.

[4]   Park CH, Rios HF, Jin Q, Sugai JV, Padial-Molina M, Taut AD, et al. 2012. Tissue engineering bone-ligament complexes using fiber-guiding scaffolds. Biomaterials; 33:137-45.

[5]   Park CH, Rios HF, Taut AD, Padial-Molina M, Flanagan CL, Pilipchuk SP, Hollister SJ, Giannobile WV. 2014. Image-based, fiber guiding scaffolds: a platform for regenerating tissue interfaces. Tissue Eng Part C Methods;20(7):533-42.

[6]   Park CH, Rios HF, Jin Q, Bland ME, Flanagan CL, Hollister SJ et al. Biomimetic hybrid scaffolds for engineering human tooth-ligament interfaces. Biomaterials 2010;31:5945-5952.

[7]   R. Tevlin, A. McArdle, D. Atashroo, G.G. Walmsley, K. Senarath-Yapa, E.R. Zielins, K.J. Paik, M.T. Longaker, and D.C. Wan. 2014. Biomaterials for craniofacial bone engineering. J Dent Res 93:1187-1195.

[8]   Zopf DA, Hollister SJ, Nelson ME, Ohye RG, Green GE. 2013. Bioresorbable airway splint created with a three-dimensional printer. N Engl J Med; 368:2043-5.

[9]   Phipps MC, Xu Y, Bellis SL. Delivery of platelet-derived growth factor as a chemotactic factor for stem cells by bone-mimetic electrospun scaffolds. 2012. PLoS One; 7(7): e40831.

CHAPTER 4

INTEGRATION OF 3D PRINTED AND MICROPATTERNED POLYCAPROLACTONE SCAFFOLDS FOR GUIDANCE OF ORIENTED COLLAGENOUS TISSUE FORMATION *IN VIVO*

4.1   Abstract

Scaffold design incorporating multi-scale cues for clinically-relevant, aligned tissue regeneration has potential to improve structural and functional integrity of multi-tissue interfaces. The objective of this pre-clinical study was to develop poly(ε-caprolactone) (PCL) scaffolds with mesoscale and microscale architectural cues specific to human ligament progenitor cells and assess their ability to form aligned bone-ligament-cementum complexes *in vivo*. PCL scaffolds were designed to integrate a 3D printed bone region with a micropatterned PCL thin film consisting of grooved pillars. The patterned film region was seeded with human ligament cells, fibroblasts transduced with BMP-7 genes seeded within the bone region, and a tooth dentin segment positioned on the ligament region prior to subcutaneous implantation into a murine model. Results indicated increased tissue alignment *in vivo* using micropatterned PCL films, compared to random-porous PCL. At 6 weeks, 30um groove depth significantly enhanced oriented collagen fiber thickness, overall cell alignment, and nuclear elongation relative to 10um groove depth. This study demonstrates for the first time that scaffolds with combined hierarchical mesoscale and microscale features can align cells *in vivo* for oral tissue repair with potential for improving the regenerative response of other bone-ligament complexes.

4.2   Introduction

Formation of tissues with structural and functional integrity is reliant upon cellular alignment and organization that in turn is influenced by nano- and micro-scale environmental cues [1-3]. Soft collagenous tissues such as tendon and ligament require aligned collagen fiber formation to maintain resistance to mechanical loading. Similarly, the periodontal ligament (PDL) is a structure in the oral cavity composed primarily of collagen type III which anchors alveolar bone to the tooth root and resists compressive loading--allowing for tooth movement. Periodontitis is a chronic oral inflammatory disease associated with damage to the tooth-supporting apparatus and subsequent osseous tissue resorption. It is the primary cause of permanent tooth loss estimated to affect 47.2% of adults in the United States, with a prevalence of 70% for adults aged 65 years and older [4]. Tissue engineering strategies have shown potential to address existing deficiencies in clinically-induced periodontal regeneration through combinational approaches using biomaterials, growth factors, and cell-based therapy [5, 6]. Existing studies have focused on whether precise topographical mesoscale features can influence structural and functional properties of PDL-like tissue through contact guidance *in vitro* [7, 8]. However, their further translation and performance *in vivo* has not yet been described, yet is needed to optimize scaffold constructs for oriented, multi-tissue interface regeneration.

The complex hierarchical organization of periodontal tissues requires multi-phasic biomaterial constructs that can recapitulate the structural integrity of the bone-ligament interface [9]. Microscale technologies have been used in fabricating scaffolds that facilitate control of multiple tissue organization and positioning, as required for the regeneration of a bone-ligament interface [10, 11]. Surface topography on the micro- and nano-scale profoundly affects cell behavior, including adhesion, migration, alignment, intracellular signaling pathways, and ultimately tissue formation in combination with biochemical cues. As such, there is a growing emphasis being placed on a multiscale approach to scaffold development that should incorporate strategically-positioned, biologically-relevant design features ranging from the nano- to the macro-scale [12]. Fabricating scaffolds sufficient for clinical application remains a challenge for tissue engineering of multi-phase, oriented tissue interfaces.

Polycaprolactone (PCL)—a hydrolytically-biodegradable polyester approved by the FDA for some clinical indications—is easily manufactured into a variety of shapes and porosities with variable mechanical properties and has been the material of choice in multi-phasic scaffolds for

regeneration of periodontia. Park et al. used 3-D printed wax-based molds to cast PCL for a "bone compartment" of an image-based, bi-phasic scaffold "periodontal complex" [13, 14]. Costa et al. and Vaquette et al. employed PCL for the bone compartment and electrospun PCL for the PDL region, [15, 16] while Lee et al. used a layered 3-D printed scaffold with three PCL interphases for the cementum, PDL, and alveolar bone [17]. However, the precise effect of topography on the guidance of PDL-like tissue formation *in vivo* has not been thoroughly explored to understand how micro-scale patterning affects the regenerative outcome.

The objective of this study was to develop a scaffold with micro- and macro-scale cues for guided formation of aligned tissue that would meet design criteria for periodontal ligament-like architecture. Given PCL's malleability and ability to be formed into polymeric matrices of various physical and mechanical properties, 2D PCL films were micropatterned and assessed *in vitro* to determine optimal parameters for PDL cell alignment. This informed the design of a 3D PCL film having 250um high pillars to replicate the average thickness of PDL tissue, with grooves embedded into the pillars at widths of 15-60um and depths of 10-30um. Films were incorporated into a 3D printed PCL region to create a macro-scale bone-ligament interphase reminiscent of the alveolar bone-PDL complex in the oral cavity. We integrated 3D printed and micropatterned regions to develop a multi-tissue interphase with macro- and micro-specific features of the scaffold. We then examined the potential of the designed scaffold construct for guidance of mineralized (bone, cementum) and collagenous (PDL-like) tissue formation using subcutaneous implantation in an ex vivo model. Our findings identify the importance of grooved features and the influence of their depths on cellular alignment, elongation, and oriented collagenous tissue formation *in vivo*.

4.3 Methods and Materials

4.3.1   Preparation and imaging of patterned 2D and 3D films

Polycaprolactone films (2D) were prepared by dissolving PCL (MW: 43-50 kDA) in chloroform (Sigma) (10% w/v) and spin coating the solution (1st coat at 100 rpm for 8 sec, 2nd coat at 800 rpm for 20 sec) onto polydimethylsiloxane (PDMS) (Sylgard 184; Dow Corning) designed via established soft lithography techniques with grooves ranging from 10-50um in width, 10 um in depth [32]. Briefly, a CAD-based program (LEdit) was used to design micropatterns and define the silicon and SU-8 master molds with standard photolithography. All steps for mold fabrication were performed at Lurie Nanofabrication Facility (University of Michigan, Ann Arbor, MI). To

transfer the pattern of SU-8 molds onto a flexible polymer, PDMS was mixed in a ratio of 10:1 v/v of base to curing agent, degassed under vacuum, poured onto molds, and cured (65°C). PDMS was then peeled from SU-8 mold and used as a mold to pattern PCL. Control films were made by spin coating PCL onto non-patterned PDMS stamps. Similarly, 3D micropatterned PCL films were prepared by casting PCL solution onto PDMS molds with grouped arrays of five different designs: (1) 400x400μm non-grooved square pillars 250um in height spaced 400um apart, (2) same pillars with 10um deep, 60um wide grooves on the perimeter, (3) pillars with 10um deep, 15um wide grooves, (4) pillars with 30um deep, 60um wide grooves, and (5) pillars with 30um deep, 15um wide grooves. SEM was performed at the Microscopy and Image Analysis Laboratory (University of Michigan) using an Amray FE 1900 SEM to image patterned 3D films which were gold sputter coated and observed at an acceleration voltage of 5kV.

4.3.2   Surface treatment and MTS assay

Amination of films was performed using 10% (w/v) 1,6-hexanediamine for 1hr at 37°C. Hydrolysis was achieved using 1M sodium hydroxide solution (4 hours at room temperature). Fibronectin treatment consisted of incubating films overnight in phosphate buffered saline (1X PBS), exposed to bovine-derived fibronectin solution (10ug/mL, Sigma) for 30min at 37°C, with washes in PBS. All non-patterned films were sterilized in 70% ethanol for 30 min and washed in sterile dH_20 prior to treatment, and again washed in sterile dH_2O post-treatment with amination or hydrolysis.   Prior to cell seeding, all films were incubated for 30 min in cell culture media consisting of Dulbecco's Modified Eagle Medium with glutamine (DMEM), 10% fetal bovine serum (FBS), and antibiotics (100 units/ml penicillin and 100 mg/ml streptomycin). Human PDL cells (passages 4-6) were seeded at a density of $1.5x10^4$ cells/film on non-treated and surface-treated PCL films (n=3). Cell adhesion and proliferation was assessed at days 1 and 5 post-seeding by adding MTS solution (CellTiter 96® Aqueous One Solution, Promega Corp, Madison, WI) to films washed three times in PBS, and reading triplicates at 490 nm after 2 hr incubation (37°C).

4.3.3   In vitro cell culture and alignment analysis on 2D patterned films

To assess PDL cell alignment on patterned 2D substrates, films were seeded with hPDL cells (passages 4-6, $1.2x10^4$ cells/film) stained with DilC(12)3 (10ug/mL, BD Biosciences, Bedford, MA, USA). Prior to cell seeding, films were surface treated with hydrolysis and

fibronectin as described previously. At 24hrs post-seeding, films were washed three times in PBS and imaged using fluorescence microscopy (Nikon Eclipse 50i, Nikon Instruments Inc). ImageJ (NIH) was used to evaluate cell orientation angle (OA) between 0° and 90° via a virtual axis placed in each cell, with the angle between the axis of the cell and direction of the pattern (corresponding to 0°) measured for all films (n=4). Results from OA analysis were used to inform the design of 3D pillared PCL films.

4.3.4   *Preparation of biphasic integrated scaffold with 3D-printed and 3D patterned PCL regions*

To model the interphase between alveolar bone and periodontal ligament, a biphasic scaffold based on a previous design was fabricated with individual compartments for bone and PDL growth using 3-D printed PCL structures for a bone compartment combined the aforementioned 3D micropatterned films for a PDL interface, respectively [13]. PCL scaffold geometry for 3-D printing was designed using CAD-based software (NX 7.5, Siemens PLM Software), with base dimensions of 5.1 x 4.1 x 2.1 mm, a 1.1 mm high enclosure to contain the PCL film, and pore openings of 0.7 x 0.7mm. Selective laser sintering (SLS) was used to fabricate the bone compartment using PCL powder (43-50kDa; Polysciences, Warrington, PA) and 4 wt% hydroxyapatite (Plasma Biotal Limited) [34, 45, 46]. To assemble the biphasic scaffold, a micropatterned 3D PCL film (3.6 x 2.8 mm) containing an array of 20 square pillars and 400um circular pores was directly fitted onto the 3D printed PCL bone region. The four corners of the upper bone scaffold region (Figure 3B) anchor, stabilize, and integrate the PCL film in place.

4.3.5   *In vivo implantation and specimens harvest*

One day prior to implantation, PCL films was treated with fibronectin and seeded with hPDL cells as previously described using *in vitro* cell culture to allow for cell attachment and alignment. The day of surgery, two surgical pockets were made on the dorsa of immunodeficient 6 week-old NIH III nude mice (20-25g; Charles River Laboratories, Wilmington MA) for subcutaneous scaffold implantation (n=6 per time point) under isofluorane anesthesia. The bone region was seeded with Ad-BMP7 (MOI=500) expressing hGFs (2.5×10^5 cells in 8uL fibrinogen mixed with 2ul thrombin) and the PDL region seeded with hPDLs (1.5×10^5 cells in 15mL fibrinogen mixed with 3uL thrombin). A human-derived dentin segment surface-treated with 37% orthophosphoric acid and trimmed to scaffold size was press-fit onto 3D patterned PCL film to

ensure contact between pillars and dentin surface. Dentin segments derived from healthy human teeth were obtained in accordance with a University of Michigan-Institutional Review Board (IRB) approved protocol, and animal studies were performed with approval from University of Michigan-University Committee on Use and Care of Animals (UM-UCUCA) according to ARRIVE guidelines for preclinical studies. Samples were harvested at 3 and 6 weeks and fixed in 10% buffered formalin phosphate solution for 2 days before being transferred into 70% ethanol.

4.3.6 *Micro-computed tomography (Micro-CT), histomorphometry, immunofluorescence, and immunohistochemistry*

Tissue-fixed specimens were embedded in alginate, scanned using micro-CT (Scanco Medical) at a resolution of 12um, at 70kV energy and 114uA intensity, and calibrated to Hounsfield units (HU). Bone volume (BV) and tissue mineral density (TMD) were determined for internal and external regions of the bone compartment using Microview software (Parallax Innovations) with a threshold of HU=1050 for bone. After scanning, samples were decalcified in 10% EDTA, embedded in paraffin, and cut into 5um sections for histological analysis using hematoxylin and eosin (H&E) and Masson's trichrome staining to evaluate fibrous tissue orientation and collagen formation, respectively. Immunofluorescence staining was performed using 4',6-diamidino-2-phenylindole (Prolong Gold Antifade Reagent with DAPI; Life Technologies) to label cell nuclei and anti-tubulin antibody with AlexaFluor488 (1:100 dilution, Abcam Inc, Cambridge MA) to label microtubules. Stained slides were imaged using fluorescence microscopy (Nikon Eclipse 50i) to capture cell nuclear alignment for all groups using a specified ROI (150um x 250um). ImageJ was used to quantify percentage of cells aligned perpendicular to the dentin segment, with cells considered aligned at an angle of $\pm 20°$ from the perpendicular at $90°$ (i.e., $70° \leq x \leq 110°$, where x is the alignment angle). Nuclear shape index was used to assess cell nuclear elongation. ImageJ was used to threshold the images and run an analysis of elongation based on a measure of circularity (C=4*π*area/perimeter^2, where C=1 indicates a circle) [19]. Masson's trichrome images were further used to assess thickness of collagen bundles oriented perpendicular to dentin segment at sites bordering the grooved and non-grooved pillars for samples obtained at 6 weeks.

Formation of cementum-like tissue was quantified using H&E sections and further assessed via immunohistochemical analysis of bone sialoprotein (BSP) positive staining using

deparaffinized sections. Before immunostaining, rehydrated sections were treated with 3% hydrogen peroxide and blocked in bovine serum albumin to reduce non-specific binding. Sections were exposed to primary antibody (1:200, Anti-bone sialoprotein antibody, Abcam, Cambridge, MA) for 24 hours at 4°C, washed in PBS with 0.2% Triton-X, and exposed to secondary antibody for 1hr (Goat Anti-rabbit IgG H&L (HRP), Abcam). After washes in PBS with Triton-X, sections were briefly exposed to a chromogen/substrate solution (DAB substrate kit, Abcam) and counter-stained (Hematoxylin, Sigma-Aldrich).

4.3.7 *Statistical analysis*

Data were expressed as mean ± standard deviation of the mean. One-way analysis of variance (ANOVA) with post hoc Tukey's multiple comparison method was used to perform comparative analysis, with a p-value <0.05 ($\alpha<0.05$) considered significant.

4.4 Results

4.4.1 *PCL surface treatment and ligament cell alignment on 2D grooved PCL films*

Four different surface treatments of non-patterned PCL films were performed prior to cell seeding to assess periodontal ligament (PDL) cell adhesion and proliferation relative to non-treated films: (1) amination to generate a PCL-NH$_2$ surface chemistry, (2) hydrolysis to reduce surface hydrophobicity, (3) fibronectin, and (4) hydrolysis pre-treatment prior to fibronectin coating. Significantly higher mean hPDL cell adhesion percentage of the initial cell seeding density was shown using treatment of PCL with fibronectin alone and a combined treatment of hydrolysis and fibronectin at day 1 post-seeding, relative to a non-treated PCL film. At day 5, the total percentage of adhered cells was significantly higher on hydrolysis, fibronectin, and combined hydrolysis and fibronectin treatment of PCL surfaces relative to amination and no treatment (**Figure 4.1**). Based on these results, all PCL patterned and control films were hydrolyzed the day before and fibronectin-coated the day of hPDL cell seeding to increase cell attachment to the inert PCL surface.

To create a 3D micropattern design for the PDL region of the scaffold, a 2D pattern was first generated to study the parameters that assisted in periodontal progenitor cell alignment. Three different molds were fabricated using three groove widths ranging from 10-50um, with a depth of 10um (**Figure 4.2**A). PCL was readily patterned, replicating mold features and creating a film that

79

can be easily handled without distorting the features (Figure 2B). Human PDL cells seeded onto the surface treated, patterned films showed elongation of filopodia within the grooves, whereas cells on a non-patterned PCL surface were randomly oriented (Figure 2C). Quantitative analysis of average orientation angle (OA) demonstrated significant differences between the non-patterned and patterned groups and significantly higher OA on 50um grooved PCL relative to 25um and 10um grooved films. No significant differences in OA were observed between the 25 and 10um patterned films (Figure 2D). An analysis of the distribution of aligned cells in specific ranges (5° to 15° degree ranges) indicated a higher percentage of cells with the lowest OA (0-5°) on the 10um (86.9%) grooved surface, followed by 25um (79.8%), 50um (32.3%), and control (6.1%) films (Figure 2E). Our results show that cell alignment was highly associated with groove width on 2D PCL films.
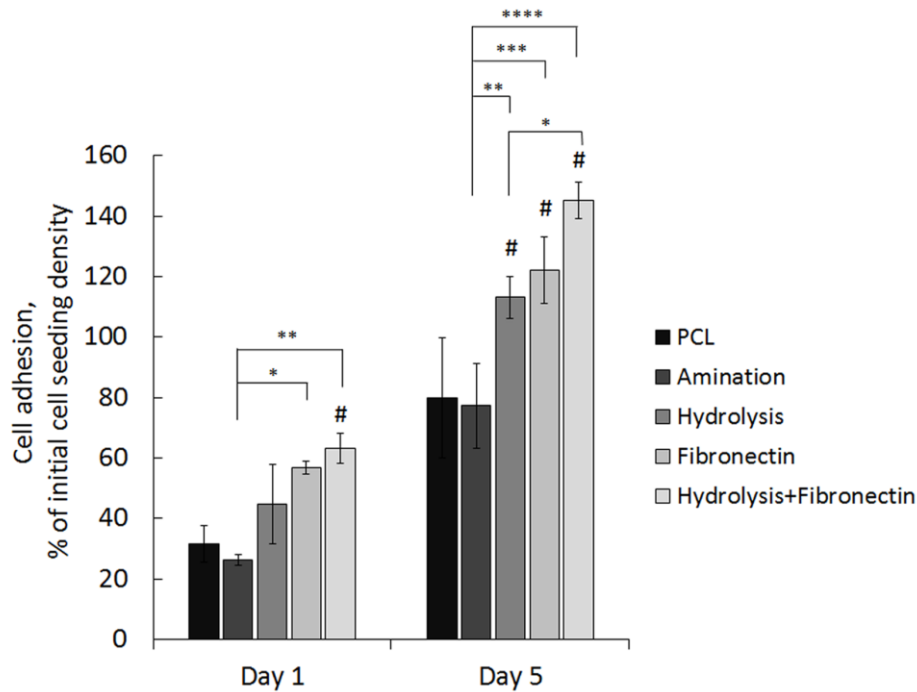
Figure 4.1 PCL Scaffold Surface Modification
Surface treatment of PCL films using aminolysis, hydrolysis, fibronectin coating, and combined treatment of hydrolysis and fibronectin assessed to determine conditions for increased hPDL cell attachment. Data shows mean percentage of ligament progenitor cells adhered to non-treated PCL films *in vitro* versus surface-treated PCL at 1 and 5 days post-seeding. (Error bars: ± SD; ** $p<0.01$; *** $p<0.001$, **** $p<0.0001$; # indicates $p<0.05$ relative to non-treated PCL film at each timepoint; n=3).

a.
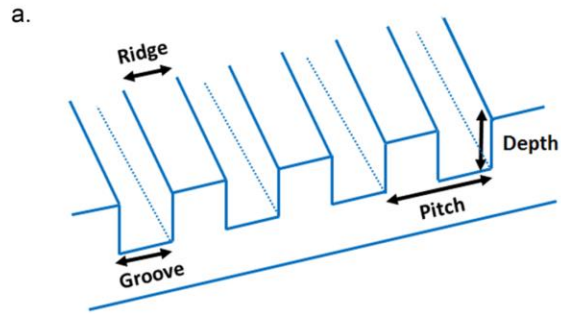
Mold #	Growth width	Groove depth	Pitch
1	10 um	10 um	20 um
2	25 um	10 um	50 um
3	50 um	10 um	100 um

b. **2D Patterned PCL Film**

Scale bar = 100um

c. Control – non-patterned | 50 um grooves

25 um grooves | 10 um grooves

d.

e.
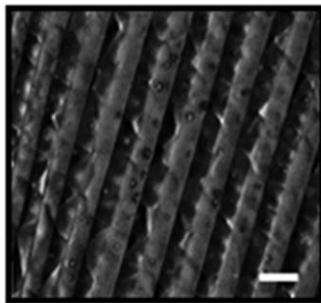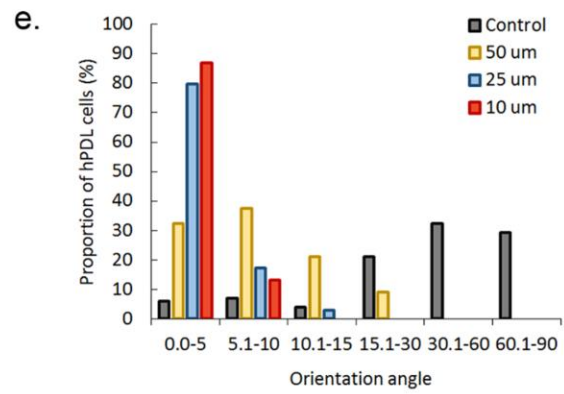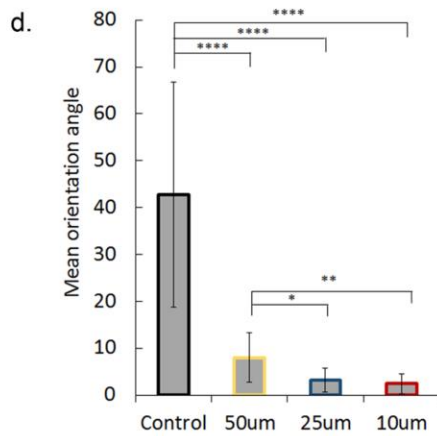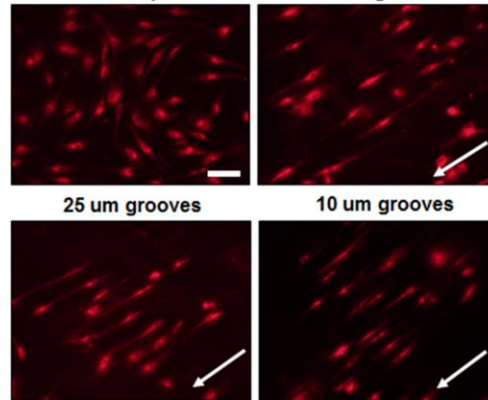
Figure 4.2 2D-Micropatterned Film Design and Cell Seeding Assessment
Micropatterned 2D PCL film design was used to determine effects of groove width on hPDL cell alignment *in vitro*. Films were patterned using three different molds (**a**) to embed grooved features onto the polymer surface (**b**, surface with 50um wide grooves, Nikon SMZ18 stereo microscope). DilC(12)-3 stained hPDL cells seeded on hydrolyzed and fibronectin treated PCL films with non-grooved (control) and grooved surfaces (**c**). White arrows indicate direction of grooves (scale bar=50um). Average orientation of hPDL cells on control (non-patterned), 50 um, 25 um, and 10 um grooved PCL films, where 0° indicates complete alignment with pattern and 90° indicates a cell that is perpendicular to a groove (**d**). Proportion of hPDL cells within a specific orientation angle for all PCL film groups, with 0-5° groups indicating highest alignment of cells within grooved microfeatures (**e**). (Error bars: ± SD; * $p < 0.05$; ** $p < 0.01$; **** $p < 0.0001$).

4.4.2 *Design of PCL scaffolds with 3D patterned film and 3D printed base*

The tooth root is covered with a layer of calcified tissue known as cementum, into which PDL collagen fiber bundles are inserted and further anchored into the alveolar bone. To mimic the known anatomical features of the bone-PDL interphase bordering a tooth root, a scaffold containing compartments for bone and periodontal ligament tissue formation was designed (**Figure 4.3**A). In detail, the bone region of the scaffold was adapted for selective laser sintering based on previous parameters established in our laboratory by Park et al [13]. This region was designed to be 5.1x4.1mm with a height of 3.2mm, where the first 2.1mm are part of the base and the remaining 1.1mm on the four corners form an enclosure to contain the film and dentin segment (Figure 3B). Pore sizes were restricted to a minimum of 700um x 700um given the 3D-printer resolution, with composition of the scaffold consisting of PCL mixed with 5% hydroxyapatite (HA) to mimic the mineral-based content of natural bone. The PDL region of the scaffold was designed to provide architectural guidance for cell alignment and subsequent collagen fiber formation using pillars that would act as supportive structures for PDL-like tissue formation between calcified tissues (i.e., bone and dentin). Pillar height was 250um to mimic the average thickness of human PDL tissue. Based on results of cell alignment on 2D-grooved PCL films, pillars were formed with grooves of 60um or 15um and depth of 10 or 30um to investigate effects of groove width and depth on PDL-like tissue formation. A porous salt-leached PCL sponge was included as a negative control, in addition to non-grooved pillars to assess effect of pillars alone on cell and tissue alignment. SEM images indicate the random nature of the porous PCL sponge relative to grooved pillars that present clear boundaries for groove width and depth corresponding to mold design and overall stability of the 250um high features (Figure 3C).

a.

Main Regions of Scaffold Design

Cementum
Calcified tissue

Periodontal Ligament (PDL)
- *Aligned collagen fibers anchored to bone and cementum*
- *Average thickness: 250um*

Tooth Root
Dentin
Calcified tissue

Alveolar Bone

b.

CAD Model of 3D-printed "Bone" Region

3.2mm
0.7x0.7mm
5.1mm
4.1mm

Biomaterial: Polycaprolactone
5% Hydroxyapatite

Schematic of Micropatterned "Ligament" Region

5 pillar designs

0.4mm
0.4mm
2.8mm
3.6mm

Non-grooved
400um x 400um, 250um height

Wide grooves with deep depth
60um width, 30um depth

Wide grooves with shallow depth
60um width, 10um depth

Narrow grooves with deep depth
15um width, 30um depth

Narrow grooves with shallow depth
15um width, 10um depth

Biomaterial: Polycaprolactone
400um wide pores

Ex Vivo "Periodontal Complex"

Dentin Segment

Assembled Scaffold

c.

TOP view

100µm

400um
250um

90.5X
5.0KV   22.1mm   0.0 Spot

PCL sponge   3D patterned film

W: 60um
D: 30um

W: 60um
D: 10um

W: 15um
D: 30um

W: 15um
D: 10um

d.

"Periodontal Complex"
Scaffold SIDE VIEW   H&E

Dentin chip
Ligament region: Patterned PCL with hPDL cells
Bone region:
3D-printed PCL with AdBMP7 transduced
hGF cells

Figure 4.3 3D-Micropatterned Film Design and Ectopic Murine Model
Schematic design of the scaffold intergrating 3D printed and micropatterned regions for the bone-ligament oral complex. Anatomical features of the alveolar bone-periodontal ligament interphase present innately at the tooth root surface **(a)** were used to design a scaffold combining a 3D printed PCL region and a 3D patterned PCL film for the bone and PDL regions, respectively **(b)**. A total of six groups **(c)** were tested *in vivo* by varying the geometry (width, W and depth, D of the grooves) of the PCL in the PDL region of the scaffold: (1) random-porous, salt-leached PCL sponge, (2) 400x400 um square pillars 250um in height, (3) square pillars with 60um wide and 30um deep grooves, (4) pillars with 60um wide and10um deep grooves, (5) pillars with 15um wide, 30um deep and 15um wide, 10um deep (6) grooves. **(d)** An ex vivo murine model was used to subcutaneously implant the combined scaffold to promote bone (B) and periodontal ligament formation, with a dentin segment (D) press-fit on top of the combined scaffold after cell-seeding the PDL region prior to implantation.

Cementum covers the dentin surface of the tooth root, but this layer was removed from human-derived roots to obtain dentin segments that were cut down to dimensions of the scaffold and positioned over 3D micropatterned film regions (Figure 3D). *In vivo* assessment of tissue alignment within the PDL region was performed using a previously established murine model utilizing human gingival fibroblast (hGF) cells transduced with adenoviral (Ad) bone morphogenetic protein (BMP)-7 to generate bone formation [13, 18].

4.4.3   Mineralized tissue formation in 3-D printed scaffold region in vivo

Analysis of bone volume (BV) in samples at 3 and 6 weeks shows a significant difference (p<0.0001) in the volume measured encompassing the 3-D printed region of the scaffold versus the volume identified within the entire scaffold region. As evidenced by uCT scans of a scaffold at 6 weeks (**Figure 4.4**A) the majority of bone was formed encompassing the scaffold along the 3D-printed PCL walls. However, no significant differences in BV were observed between weeks 3 and 6 for both regions. Tissue mineral density (TMD) indicating maturity of bone showed no differences between regions when comparing both time points, but TMD increased significantly for both the bone region (p<0.0001) and entire scaffold (p<0.001) from week 3 to week 6 (Figure 4B).
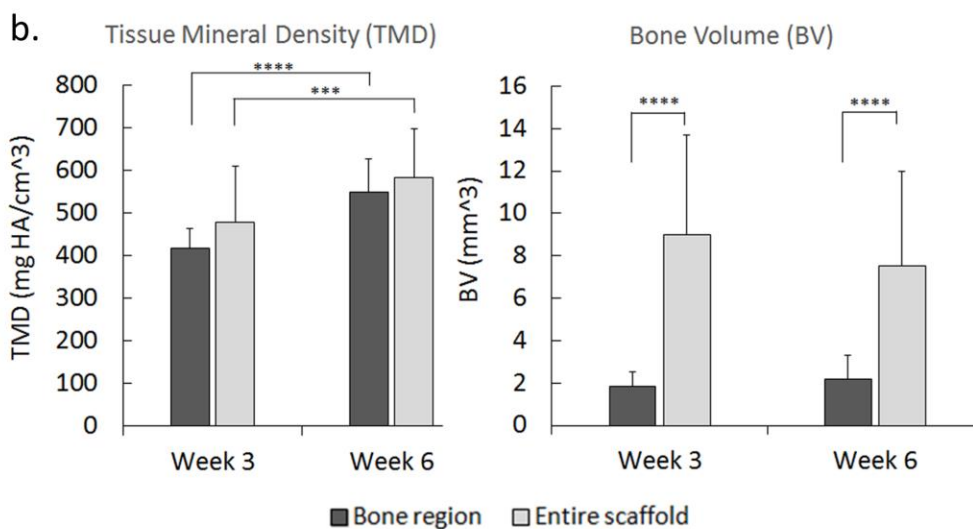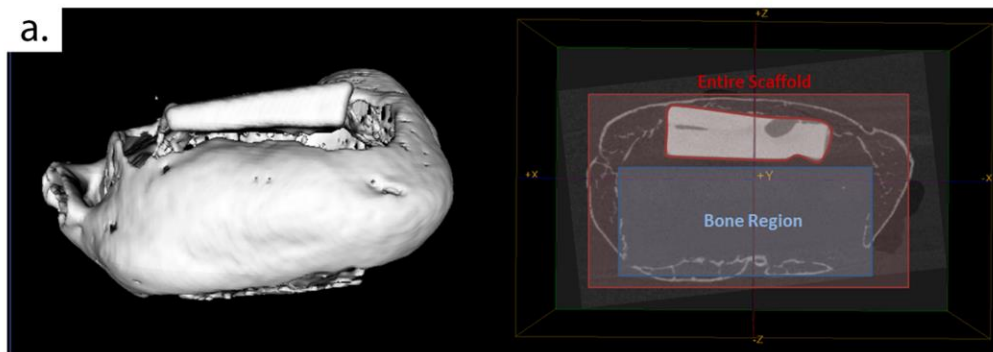
Figure 4.4   Bone Volume and Tissue Mineral Density
Formation of bone in the 3D printed scaffold region seeded with adenoviral BMP7 transduced gingival fibroblasts. Micro-computed tomography (uCT) of implanted scaffolds was used for bone volume (BV) and tissue mineral density (TMD) analysis of osseous tissue growth in vivo in the bone region of the scaffold **(a)** compared to the formation of tissue in the entire scaffold external to bone region at 3 and 6 weeks post-harvesting **(b)**. (Error bars: ± SD; *** p<0.001, **** p<0.0001; n=5-6).

4.4.4   Histomorphology of soft, mineralized, and cementum-like tissue formation in vivo

To delineate the histomorphology of soft and mineralized tissue formation *in vivo*, we performed studies using several staining methods. Hematoxylin and Eosin stains at 3 weeks (data not shown) and 6 weeks indicated soft tissue formation in the region of 3D patterned film, as well as in most of the 3D printed scaffold where bone had not invaded further into the scaffold interior. Trichrome staining of PDL regions revealed randomly-oriented collagenous tissue formation in groups with porous PCL, while pillared PCL films showed fibrous collagen formation with increased directionality towards the dentin segment at 6 weeks (**Figure 4.5**A). Staining using DAPI and tubulin-based markers showed high cell density and extracellular matrix formation in the PDL region of the scaffold confined to areas within the inter-pillar distance. Indication of early-stage formation of an immature cementum-like tissue at 6 weeks on the dentin below the PDL region was identified descriptively and also using bone sialoprotein (BSP)-positive staining. The amount of new tissue formation that had cementogenesis-like indicators was minimal overall, with an average length of 337±66um when averaged for all patterned groups, compared to the 2.7mm approximate length of dentin segments.

4.4.5   Effect of 3D patterned design on cell alignment in vivo

Cell alignment *in vivo* was evaluated using nuclear alignment and shape index following immunofluorescence staining of tissue sections. Our data revealed an increasing tendency of cells along the pillar edge to align perpendicular to the dentin surface with increasing groove depth (**Figure 4.6**A), particularly with more cells shown to be aligning further away from the pillar wall. At 3 weeks, all groups had a significantly higher percentage of aligned cells compared to porous PCL, with the same observation present at 6 weeks, except for non-grooved pillars which were not significantly different from the porous sponge. Relative to non-grooved pillars, both of the deeper-grooved groups (60W, 30D and15W, 30D) exhibited significantly higher alignment at 3 weeks ($p<0.001$ and $p<0.01$, respectively). At 6 weeks, the differences in alignment were more apparent, with all grooved pillars irrespective of groove depth (60W, 10D; 15W, 10D; 60W, 30D; and 15W, 30D) showing significantly higher cellular alignment ($p<0.001$ and $p<0.0001$) relative to non-grooved pillars. Likewise, grooved pillars with a depth of 30um also had significantly higher alignment ($p<0.001$) relative to pillars with shallower grooves (**Figure 6**B).

a.

	SEM Image (90X)	H&E (4X)	Masson's Trichrome (20X)	DAPI and Tubulin (40X)
Porous PCL				
W: 0um D: 0um				
W: 60um D: 10um				
W: 15um D: 10um				
W: 60um D: 30um				
W: 15um D: 30um				

b.

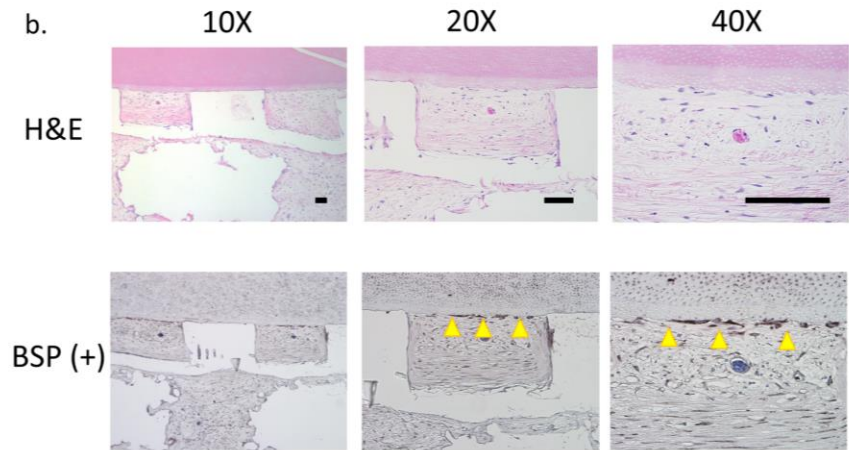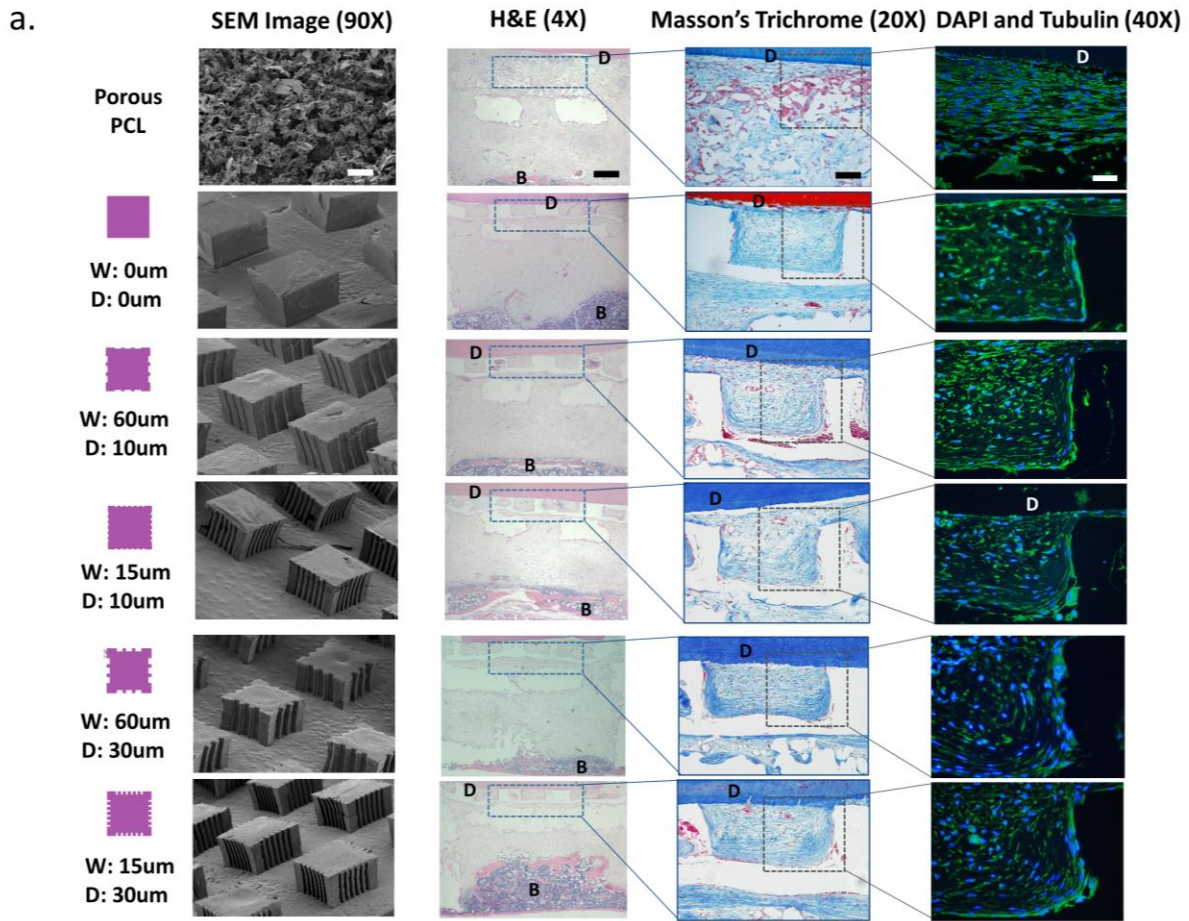|	10X	20X	40X
H&E			
BSP (+)			

Figure 4.5 Histomorphological Assessment of Soft and Mineralized Tissue Formation
Histomorphological assessment of soft and mineralized tissue formation in the micropatterned PDL and 3D printed bone scaffold compartments, respectively. **(a)** H&E, Masson's trichrome, and DAPI (blue)/tubulin(green) staining was performed to assess bone (B) and tissue formation, collagen alignment, and cellular alignment in the region of the PCL film or sponge at 3 and 6 weeks (images shown are at 6 week timepoint only). Note the formation of fibers approaching the dentin surface and bone more distant in the bone region of the scaffold (near bottom of the H&E sections). **(b)** Formation of cementum-like tissue newly-deposited at the dentin (D) surface was observed on week 6 samples using H&E staining and immunohistochemical analysis for bone sialoprotein (BSP) positive expression. Scale bar = 100um.

Nuclear shape index was used to assess nuclear elongation as a complement to the cellular alignment data, with values closer to 1 indicating increased nuclear circularity (Figure 6C) [19]. At 3 weeks, only deeper grooved pillars had significantly higher elongation values compared to both PCL sponge and non-grooved pillars, with the 60W, 30D pillars having more elongated cells relative to non-grooved ($p<0.0001$) and 15W, 30D pillars ($p<0.05$). Only 60W, 30D pillars had significantly higher elongation relative to both of the shallow-grooved pillars at 3 weeks ($p<0.01$). At 6 weeks, all groups had significantly higher elongation relative to cells on the PCL sponge, while all grooved pillars ($p<0.01$-0.0001) also had a significantly lower shape index relative to non-grooved designs. However, no significant differences were noted among the grooved pillar groups, irrespective of groove depth.

Overall, these results demonstrate increased cell alignment further from the pillar boundary in films with grooves compared to non-grooved pillars, with increased alignment in deeper-grooved (30um) pillars compared to shallow-grooved (15um) pillars. This can be attributed to soft tissue maturation and alignment which correspond to a significant increase in overall cell elongation from week 3 to 6, albeit not necessarily perpendicular to the dentin since this quantification considers only cell morphology independent of orientation.

4.4.6   Effect of 3D patterned design on oriented collagen thickness in vivo

The extracellular component of PDL consists of collagen fiber bundles which assist with allowing the tooth to withstand substantial compressive forces. We therefore analyzed collagen thickness oriented along the pillar wall creating a bundle-like structure perpendicular to the dentin segment. Our data showed that collagen thickness at 6 weeks is significantly greater in both deeper-

grooved pillar groups with grooves of 60um and 15um compared to non-grooved pillars (p<0.0001) (**Figure 4.7**). Only one shallow-grooved group (60W, 10D) showed greater thickness relative to 0W, 0D (p<0.001). The 60W, 30W group had a total collagen thickness that was significantly higher than other groups, except for its deep-grooved counterpart with narrower grooves of 15um (15W, 30D). These results further reinforce the findings shown with cell alignment at 6 weeks, indicating that groove depth is a more critical parameter than width for encouraging formation of cell alignment and subsequent increase in oriented collagen fiber density at sites of increased cellular orientation.
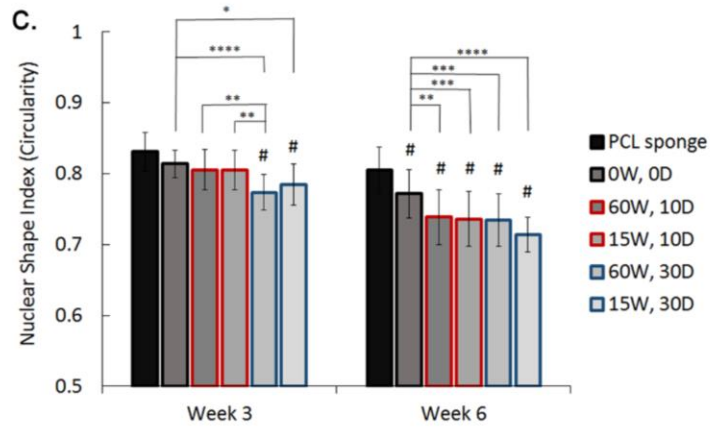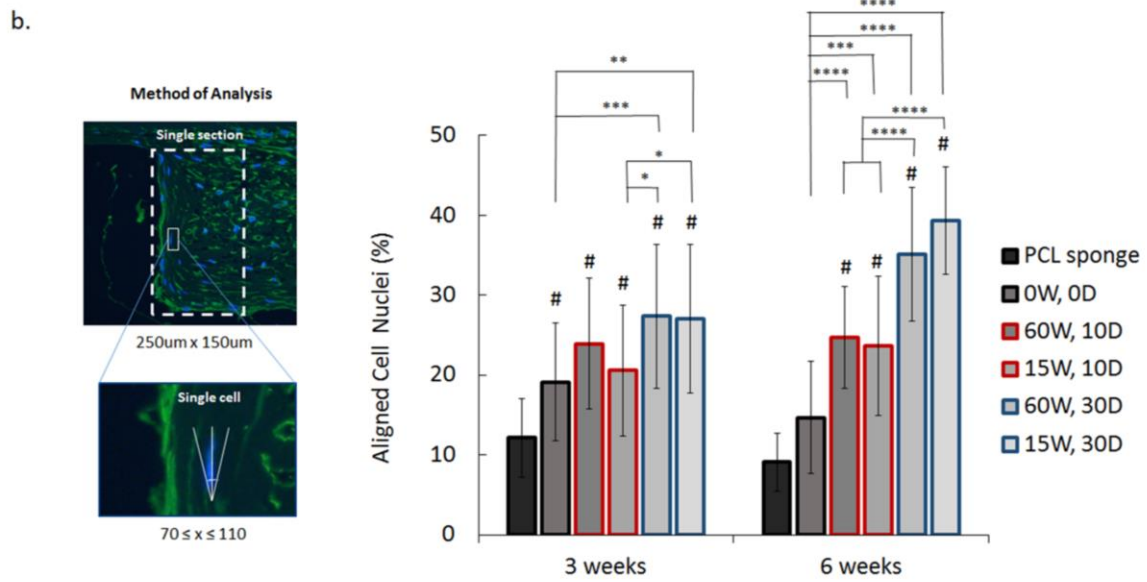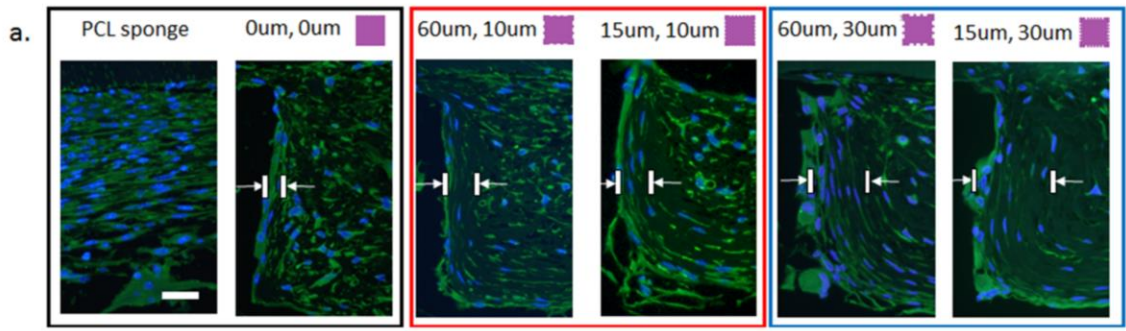
Figure 4.6 Immunofluorescence: Cell Alignment and Nuclear Shape Index
Cell alignment and nuclear shape index assessed using immnufluorescence staining at 6 weeks. **(a)** DAPI (blue) and tubulin (green) shows increased cell alignment further from the pillar boundary in films with grooves compared to non-grooved pillars, and in films with deep grooves (30um) compared to more shallow grooves (10um). Scale bar = 50um. **(b)** Mean percentage of aligned cell nuclei (within 20° of preferred perpendicular orientation: $70° \leq x \leq 110°$) in vivo on PCL sponge, non-grooved pillars (0W, 0D), and grooved pillars (60 um and 15um wide (W) grooves) with varying groove depths (D) (10 um—red outline, and 30um—blue outline). **(c)** Mean nuclear shape index analysis indicating cellular elongation in vivo on all groups based on measure of nuclear circularity ($C=4*\pi*area/perimeter^2$). (Error bars: ± SD; ** $p<0.01$; *** $p<0.001$, **** $p<0.0001$; # indicates $p<0.05$ relative to PCL sponge at each timepoint; n=5 in each group).
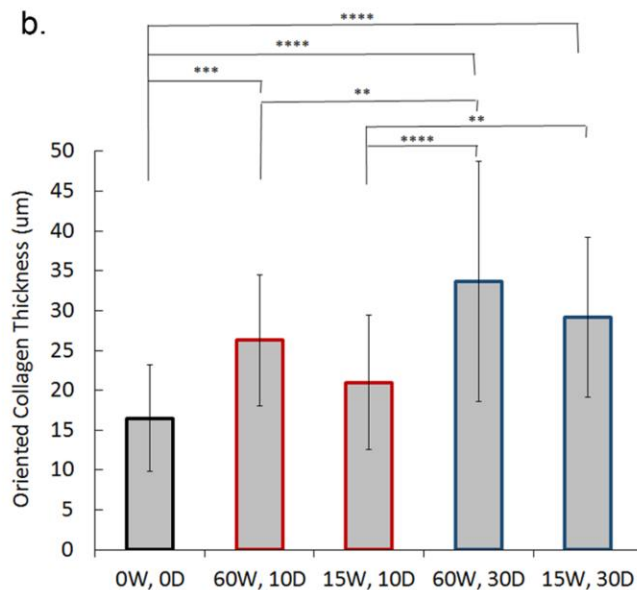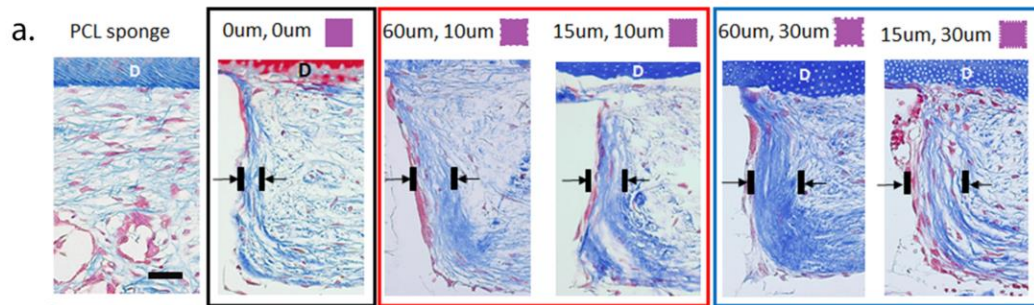
Figure 4.7 Collagenous Tissue Alignment using Micropatterned Films
Collagen thickness at inter-pillar distances bordering grooved or non-grooved features used to determine oriented tissue formation at 6 weeks *in vivo*. **(a)** Masson's Trichrome stining of samples indicates increased collagen orientation perpendicular to dentin (D) segment at the pillar boundary in the presence of grooves (scale bar = 100um). **(b)** Mean thickness (um) of oriented collagen bundles in vivo at non-grooved (0W, 0D) and grooved (15-60um wide, 10-30um deep) pillar borders at 6 weeks based on Masson's Trichrome staining. (Error bars: ± SD; ** $p<0.01$; *** $p<0.001$, **** $p<0.0001$; n=5).

4.5 Discussion

Promoting orientation of cells in a specific and structurally-relevant direction via substrate guidance has been shown to stimulate cell behavior and create organized tissues *in vitro* that mimic their native form and function, including cardiac and nerve tissues [20]. Overall, micro- and meso-scale cues have been strongly implicated in aligned cellular and fibrillary collagen formation *in vitro*. Gilchrist et al found that a width of 500um was the maximum *in vitro* meso-scale boundary for guidance of neo-tissue alignment using mesenchymal stem cells [21]. Likewise, highly aligned tissue formation consisting of fibrillary collagen was observed when cells were arranged longitudinally end-to-end. This *in vitro* finding is consistent with our observations *in vivo* of highly aligned cell formation on pillar walls which appears to correspond to increased collagen fiber formation seen with Trichrome staining at sites of increased cell alignment. In fact, our study identified a strong positive correlation (r=0.863, data not shown) between cell alignment and collagen thickness based on values obtained from these measurements (Figure 6-7).

Cellular morphology assessed using both cellular alignment angle and nuclear elongation suggests significant (p<0.0001) and overriding effects of groove depth over width. Our results indicate increased preferential alignment of cells *in vivo* on grooved substrates over a non-grooved surface. Nano- and micro-structured groove widths and depths have been extensively investigated using a variety of cells to determine optimum parameters for cell alignment using *in vitro* models [22]. While results can be cell-specific, fibroblasts in particular have been shown to have a nano- and micro-limit of alignment ranging from 50-100nm to 500um [23-25]. Likewise, several studies have reported increased cell alignment with increasing groove depth, both on nano- and micro-levels [26-28]. There are strong indications that in particular cases the depth can reinforce, if not override, cellular guidance via groove width. Increase in cell alignment and collagen fiber alignment may also be a factor of the cell's innate ability to align *in vitro* and *in vivo*. Aubin et al showed cells with intrinsic ability to form aligned tissue *in vivo* are more likely to organize into oriented tissue *in vitro* in presence of guidance-based microarchitecture [29].

Previous studies successful in achieving aligned collagenous tissue formation using substrates with cell-guiding cues have utilized electrospun fibers composed of naturally- and synthetically-derived polymers. Jiang et al reported increased PDL-like tissue formation with mature collagen fibers using aligned PCL-polyethylene glycol (PEG) nanofibers embedded into porous chitosan scaffolds and seeded with bone marrow mesenchymal stem cells [30]. Similar

93

findings have been observed in applications for neural and cardiac tissue regeneration: Koepsell et al noted increased cellular orientation of intervertebral disc-derived cells on increasingly aligned electrospun PCL fibers resulted in higher ECM production, including collagen and glycosaminoglycans, while Ifkovits et al found enhanced collagen alignment on oriented poly(glycerol sebacate) fibers when seeded with cardiocytes and implanted subcutaneously [31, 32]. However, it remains difficult to create three-dimensional scaffolds using these techniques without the presence of a more complex and customizable system such as a 3-D printer that could position fibers in directions relevant to the anatomical structure of tissue we attempt to model, thereby recapitulating its unique geometric complexity. Additive manufacturing has been used extensively for guided tissue regeneration of PDL-like structures, but micro-level control over scaffold structure is constrained by limited resolution and material selection [14, 17]. To address these limitations, our approach focuses on using a combination of 3-D printing and micropatterning to create a scaffold with the dual function of presenting features on the macro and micro-level for guidance of bulk and oriented tissue formation (i.e., mineralized and soft tissue). To our knowledge, this is the first reported attempt to quantify cell alignment on a micropatterned polymeric construct implanted *in vivo*. While numerous aforementioned publications have signaled the importance and potential of guiding aligned tissue formation using this approach, existing studies have focused on *in vitro* assessment of cellular alignment, without further translation into *in vivo* models.

The development of a 3-D pattern consistent with known geometric parameters of the human periodontal ligament (i.e., 250um average thickness), including presence of collagen I and III fiber bundles that orient perpendicular to the alveolar bone and tooth root (Figure 3), was executed to assess the role of groove width and depth using an *in vivo* model. The 3-D printed bone region and PDL film consisted of defined openings to create porosity within the bulk structure, promoting nutrient exchange and cellular migration between the regions. Seeding of AdBMP-7 expressing hPDL cells in the bone region resulted in bone formation that was mostly external to the interior region of the 3-D printed scaffold as shown using histology and micro-CT analysis (Figures 4 and 5A, respectively), a limitation of the model inherent in the non-localized expression of the growth factor that likely resulted in its diffusion to the exterior regions of the scaffold, as has been observed in other studies [33, 34]. The use of a non-loading model may have contributed to lack of significant increase in bone volume between weeks 3 and 6, although

94

existing bone was found to mature over time, as evidenced by increase in tissue mineral density. Likewise, due to limited bone growth below the PDL region of the scaffold, no integration between the bone and PDL regions was observed. This is an important indicator of bone-ligament complex regeneration and requires future improvements in the design of the bone compartment and localization of bone-stimulating growth factor delivery. Specifically, native bone-PDL integration consists of Sharpey's fiber insertions into osseous tissue that stabilize and connect the soft tissue. A bone region which promotes formation of such attachments below the PDL compartment through incorporation of increased and possibly directional porosity would improve regeneration of this multiphasic tissue complex. To fully and successfully realize periodontal tissue regeneration using a multiphasic scaffold, cementum must be formed along the dentin surface. While our data does not show definitive mature cementum, BSP-positive staining (Figure 5B) does suggest early-stage mineralized, cementum-like tissue formation localized at the boundary between the dentin segment and inter-pillar areas filled with collagenous soft-tissue.

Our results detailing cellular alignment and collagen formation are indicative of the need for guidance of cellular alignment to promote oriented collagen formation *in vivo*. In fact, Wang et al had previously shown that grooved substrates resulted in alignment of synthetized collagen matrix *in vitro* parallel to the grooves, preceded by the alignment of cells [35]. In this study, we show that this holds true using a micropatterned substrate under *in vivo* conditions, albeit with the added factor of groove depth as an important precursor to the percentage of aligned cells (Figure 6) and resultant thickness of oriented collagenous tissue (Figure 7). It is important to note that while cellular alignment and increased collagen thickness is seen at pillar boundaries, the existing space of 400um between the pillars does not currently allow for aligned tissue formation in that area within a period of 6 weeks. There is likewise the potential of tissue formed between pillars to lose orientation given large inter-pillar distances. Therefore, an improvement to the current patterned film design to better replicate periodontal ligament fiber architecture and increase fiber density would consist of reducing this distance to 100-150um, given that the average thickest formation of oriented collagenous tissue at 6 weeks was ~35um for one side of the 30um-deep grooved pillars. Another area of further study may include an analysis of whether there is a limit to the aligned tissue formation boundary layer away from the pillar surface, since the given results are an indication of the capacity for aligned tissue formation at only 6 weeks *in vivo*.

Future improvements in addition to scaffold morphology would involve introduction of other factors that play a crucial role in formation of functional periodontal ligament, including growth factors such as platelet derived growth factor (PDGF) and mechanical stimulation at physiological levels, which has been show to modulate PDL cell gene activity [8, 36]. Increased control and localization of bone-stimulatory growth factor protein release such as BMP would further benefit osseous tissue formation within the bone compartment. While the use of gene therapy significantly increases sustained growth factor release and stability *in vivo*, further improvements in minimizing growth factor diffusion from the target site would greatly improve its application in scaffold-based therapies [37]. Such strategies could include the direct adsorption or chemical conjugation of BMPs onto the scaffold surface, or tethering of viral vectors expressing BMP genes to PCL surfaces using chemical vapor deposition [38-41].

In attempting to transition scaffold-based designs from the bench-top to clinical applications that can benefit patients, use of 3D printing has become a promising strategy for creating customized implants with potential to mimic patient-based bulk defects, even for cases of periodontal therapy [42, 43]. In guided regeneration of ligamentous structures, the combination of 3D printed and micropatterned regions into one construct is an innovative approach that can provide a means of re-establishing the interfacial integrity of aligned tissue formation in bone-ligament complexes. Although the scaffold design used in this study was simplistic relative to a true periodontal defect involving bone resorption, it can be easily adapted to more complex defects using patient-based computed tomography scans to design the 3D printed region, and create an overlay of a micropatterned film in the region of missing PDL. The results of our study indicating the importance of groove depth over width for aligned tissue formation *in vivo* can play a vital role in the establishment of a design that can incorporate this cell-guiding parameter into future grafts meant for the purpose of inducing structurally-relevant alignment of PDL tissue. Future translation of micropatterned constructs into the clinic may provide greater opportunities for more controlled tissue regeneration using not only ridge-groove structures, but also other relevant designs that can help orient tissue based on incorporated material boundaries. The combination of a custom-designed 3-D printed scaffold and a micropatterned region fit to control the structural integrity of new tissue growth is a clinically-relevant approach that holds significant potential for regeneration of collagenous tissue not only in periodontal and orthopaedic applications, but other areas of tissue

engineering with a strong focus on improving collagen fiber orientation as it relates to tissue structure and function.

4.6   Conclusion

In summary, the findings from this preclinical study indicate that groove micro-depth has a significant effect on guiding cellular alignment and collagenous tissue orientation *in vivo*, overriding the effects of groove micro-width. The 3-D patterned scaffold conceived and designed in this study further presents a novel and unique combination of 3-D printing and micropatterning to enhance the micro- and macro-level design of scaffolds with the aim of regenerating multiple tissues and their interfaces. Using a combination of gene therapy and topographical guidance cues to achieve osseous tissue formation and oriented collagen fibers has potential for bone-ligament regeneration for treatment of periodontal osseous defects. Overall, these findings are supportive of the advantageous effects of using 3-D printed, micropatterned substrates as architectural templates for guided regeneration of oriented collagenous tissues. This approach may have significant potential for clinical applications in the development of bone-ligament constructs for dental and orthopaedic clinical scenarios.

4.7   References

[1]   Bettinger CJ, Langer R, Borenstein JT. Engineering substrate topography at the micro- and nanoscale to control cell function. *Angew. Chem. Int. Ed. Engl.* 2009; 48, 5406.

[2]   Hui EE, Bhatia SN. Micromechanical control of cell-cell interactions. *Proc. Natl. Acad. Sci. USA* 2007; 104, 5722.

[3]   Hoehme S., Brulport M, Bauer A, Bedawy E, Schormann W, Hermes M, Puppe V, Gebhardt R, Zellmer S, Schwarz M, Bockamp E, Timmel T, Hengstler JG, Drasdo D. Prediction and validation of cell alignment along microvessels as order principle to restore tissue architecture in liver regeneration. *Proc. Natl. Acad. Sci. USA* 2010; 107, 10371.

[4]   Eke PI, Dye BA, Wei L, Thornton-Evans GO, Genco RJ. Prevalence of periodontitis in adults in the United States: 2009 and 2010. *J. Dent. Res.* 2012; 91, 914.

[5]   Kaigler D, Cirelli JA, Giannobile WV. Growth factor delivery for oral and periodontal tissue engineering. *Expert Opin. Drug. Deliv.* 2006; 3, 647.

[6]   Rios HF, Lin Z, Oh B, Park CH, Giannobile WV. Cell- and gene-based therapeutic strategies for periodontal regenerative medicine. *J. Periodontol.* 2011; 82, 1223.

[7]   Hamilton DW, Oates CJ, Hasanzadeh A, Mittler S. Migration of periodontal ligament fibroblasts on nanometric topographical patterns: influence of filopodia and focal adhesions on contact guidance. *PLoS One* 2010; 5, e15129.

[8]   Yu N, Prodanov L, te Riet J, Yang F, Walboomers XF, Jansen JA. Regulation of periodontal ligament cell behavior by cyclic mechanical loading and substrate nanotexture. *J. Periodontol.* 2013; 84, 1504.

[9]   Ivanovski S, Vaquette C, Gronthos S, Hutmacher DW, Bartold PM. Multiphasic scaffolds for periodontal tissue engineering, *J. Dent. Res.* 2014; 93, 1212.

[10]   Hacking S, Khademhosseini A. Applications of microscale technologies for regenerative dentistry. *J. Dent. Res.* 2009; 88, 409

[11]   Stevens MM, George JH. Exploring and engineering the cell surface interface. *Science* 2005; 310, 1135.

[12]   Wegst UG, Bai H, Saiz E, Tomsia AP, Ritchie RO. Bioinspired structural materials. *Nat. Mater.* 2015; 14, 23.

[13]   Park CH, Rios HF, Jin Q, Bland ME, Flanagan CL, Hollister SJ, Giannobile WV. Biomimetic hybrid scaffolds for engineering human tooth-ligament interfaces. *Biomaterials* 2010; 31, 5945.

[14]   Park CH, Rios HF, Jin Q, Sugai JV, Padial-Molina M, Taut AD, Flanagan CL, Hollister SJ, Giannobile WV. Tissue engineering bone-ligament complexes using fiber-guiding scaffold. *Biomaterials* 2012; *33*, 137.

[15]   Costa PF, Vaquette C, Zhang Q, Reis RL, Ivanovski S, Hutmacher DW. Advanced tissue engineering scaffold design for regeneration of the complex hierarchical periodontal structure. *J. Clin. Periodontol.* 2014; *41*, 283

[16]   Vaquette C, Fan W, Xiao Y, Hamlet S, Hutmacher DW, Ivanovski S. A biphasic scaffold design combined with cell sheet technology for simultaneous regeneration of alveolar bone/periodontal ligament complex. *Biomaterials* 2012; *33*, 5560.

[17]   Lee CH, Hajibandeh J, Suzuki T, Fan A, Shang P, Mao JJ. Three-dimensional printed multiphase scaffolds for regeneration of periodontium complex. *Tissue Eng Part A* 2014; *20*, 1342.

[18] Jin Q, Anusaksathien O, Webb SA, Rutherford RB, Giannobile WV. Gene therapy of bone morphogenetic protein for periodontal tissue engineering. *J. Periodontol.* 2003, *74*, 202.

[19] Versaevel M, Grevesse MT, Gabriele S. Spatial coordination between cell and nuclear shape within micropatterned endothelial cells. *Nat. Commun.* 2012, *3*, 671.

[20] Nikkhah M, Edalat E, Manoucheri S, Khademhosseini A. Engineering microscale topographies to control the cell-substrate interface. *Biomaterials* 2012, *33*, 5230.

[21] Gilchrist CL, Ruch DS, Little D, Guilak F. Micro-scale and meso-scale architecture cues cooperate and compete to direct aligned tissue formation. *Biomaterials* 2014, *35*, 10015.

[22] Flemming RG, Murphy CJ, Abrams GA, Goodman SL, Nealey PF. Effects of synthetic micro- and nano-structure surfaces on cell behavior. *Biomaterials* 1999, *20*, 573.

[23] Biela SA, Su Y, Spatz JP, Kemkemer R. Different sensitivity of human endothelial cells, smooth muscle cells and fibroblasts to topography in the nano-micro range. *Acta. Biomater.* 2009, *5*, 2460.

[24] Leclerc A, Tremblay D, Hadjiantoniou S, Bukoreshtliev NV, Rogowski JL, Godin M, Pelling AE. Three dimensional spatial separation of cells in response to microtopography. *Biomaterials* 2013, *34*, 8097.

[25] Loesberg WA, te Riet J, van Delft FC, Schon P, Figdor CG, Speller S, van Loon JJ, Walboomers XF, Jansen JA. The threshold at which substrate nanogroove dimensions may influence fibroblast alignment and adhesion. *Biomaterials* 2007, *28*, 3944.

[26] Clark P, Connolly P, Curtis AS, Dow JA, Wilkinson CD. Cell guidance by ultrafine topography in vitro. *J. Cell Sci.* 1991, *99* (Pt 1), 73.

[27] Fraser SA, Ting YH, Mallon KS, Wendt AE, Murphy CJ, Nealey PF. Sub-micron and nanoscale feature depth modulates alignment of stromal fibroblasts and corneal epithelial cells in serum0rich and serum-free media. *J. Biomed. Mater. Res. A* 2008, *86*, 725.

[28] Teixeira AI, Abrams GA, Bertics PJ, Murphy CJ, Nealey PF. Epithelial contact guidance on well-defined micro- and nanostructured substrates. *J. Cell Sci.* 2003, *116*, 1881.

[29] Aubin H, Nichol JW, Hutson CB, Bae H, Sieminski AL, Cropek DM, Akhyari P, Khademhosseini A. Directed 3D cell alignment and elongation in microengineered hydrogels. *Biomaterials* 2010, *31*, 6941.

[30] Jiang W, Li L, Zhang D, Huang S, Jing Z, Wu Y, Zhao Z, Zhao L, Zhou S. Incorporation of aligned PCL-PEG nanofibers into porous chitosan scaffolds improved the orientation of collagen fibers in regenerated periodontium. *Acta Biomater.* 2015, *25*, 240.

[31]   Koepsell L, Remund T, Bao J, Neufeld D, Fong H, Deng Y. Tissue engineering of annulus fibrosus using electrospun fibrous scaffolds with aligned polycaprolactone fibers. *J. Biomed. Mater. Res. A* 2011, *99*, 564.

[32]   Ifkovits JL, Wu K, Mauck RL, Burdick JA. The influence of fibrous elastomer structure and porosity on matrix organization. *PLoS One* 2010, *5*, e15717.

[33]   Saito E, Suarez-Gonzalez D, Murphy WL, Hollister SJ. Biomineral coating increases bone formation by ex vivo BMP-7 gene therapy in rapid prototyped poly-L-lactic acid) (PLLA) and poly(e-caprolactone) (PCL) porous scaffolds. *Adv. Healthc. Mater.* 2015, *4*, 621.

[34]   Williams JW, Adewunmi A, Schek RM, Flanagan CL, Krebsbach PH, Feinberg SE, Hollister SJ, Das S. Bone tissue engineering using polycaprolactone scaffolds fabricated via selective laser sintering. *Biomaterials* 2005, *26*, 4817.

[35]   Wang JH, Jia F, Gilbert TW, Woo SL. Cell orientation determines the alignment of cell-produced collagenous matrix. *J. Biomech.* 2003, *36*, 97.

[36]   Kim SG, Kim SG, Viechnicki B, Kim S, Nah HD. Engineering of a periodontal ligament construct: cell and fibre alignment induced by shear stress. *J. Clin. Periodontol.* 2011, *38*, 1130.

[37]   Pilipchuk SP, Plonka AB, Monje A, Taut AD, Lanis A, Kang B, Giannobile WV. Tissue engineering for bone regeneration and osseointegration in the oral cavity. *Dent. Mater.* 2015, *31*, 317.

[38]   Patel JJ, Flanagan CL, Hollister SJ. Bone morphogenetic protein-2 adsorption onto polycaprolactone better preserves bioactivity in vitro and produces more bone in vivo than conjugation under clinically relevant loading scenarios. *Tissue Eng. Part C Methods.* 2015, *21*, 489.

[39]   Patel JJ, Modes JE, Flanagan CL, Krebsbach PH, Edwards SP, Hollister SJ. Dual delivery of EPO and BMP2 from a novel modular polycaprolactone construct to increase the bone formation in prefabricated bone flaps. *Tissue Eng. Part C Methods.* 2015, *21*, 889.

[40]   Zhang H, Migneco F, Lin CY, Hollister SJ. Chemically-conjugated bone morphogenetic protein-2 on three-dimensional PCL scaffolds stimulates osteogenic activity in bone marrow stromal cells. *Tissue Eng. Part A*. 2010, *16*, 3441.

[41]   Hu WW, Elkasabi Y, Chen HY, Zhang Y, Lahann J, Hollister SJ, Krebsbach PH. The use of reactive polymer coatings to facilitate gene delivery from PCL scaffolds. *Biomaterials* 2009, *30*, 5785.

[42]   Park CH, Rios HF, Taut AD, Padial-Molina M, Flanagan CL, Pilipchuk SP, Hollister SJ, Giannobile WV. Image-based, fiber guiding scaffolds: a platform for regenerating tissue interfaces. *Tissue Eng. Part C Methods.* 2014, *20*, 533.

[43]   Rasperini G, Pilipchuk SP, Flanagan CL, Park CH, Pagni G, Hollister SJ, Giannobile WV. 3D-printed bioresorbable scaffold for periodontal repair. *J. Dent. Res.* 2015, *94(9 Suppl)*:153S.

[44]   Qin D, Xia Y, Whitesides GM. Sot lithography for micro- and nanoscale patterning. *Nat. Protoc.* 2010, *5*, 491.

[45]   Partee B, Hollister SJ, Das S. Selective laser sintering process optimization for layered manufacturing of CAPA 6501 PCL bone tissue engineering scaffolds. *Journal of Manufacturing Science and Engineering* 2006, *128*, 531.

[46]   Zopf DA, Hollister SJ, Nelson ME, Ohye RG, Green GE. Bioresorbable airway splint created with a three-dimensional printer. *N. Engl. J. Med.* 2013, *368*, 2043.

CHAPTER 5

IN VIVO ASSESSMENT OF PERIODONTAL REGENERATION VIA IMMOBILIZATION OF GENE THERAPY VECTORS ON 3D-PRINTED, MICROPATTERED SCAFFOLDS – A PILOT STUDY

Contributions to the data collection/analysis that are part of this chapter were made by: Drs. Jie Hao and Ning Yu (*Periodontics and Oral Medicine, University of Michigan*).

5.1   Introduction

Current clinical therapies cannot predictably regenerate bone-ligament interfaces in tooth-supporting tissues damaged by trauma or disease. We previously developed a scaffold with 3D-printed, micropatterned features for guidance of osseous and soft tissue formation *in vivo* [1]. However, bone formation within the scaffold resulted from *in vitro* transduction of cells with adenoviral (Ad) vectors expressing bone morphogenetic protein (BMP-7) prior to implantation. This study investigates a more clinically-relevant gene delivery approach by localized immobilization of AdBMP7 and platelet-derived growth factor (AdPDGF) onto scaffold 'bone' and 'PDL' regions, respectively, for evaluation in a subcutaneous murine extra-orthotopic model. While growth factors have been delivered via physical absorption onto scaffolds, this method lacks the ability to control the spatiotemporal release of the GF and specifically target the GF for immobilization.

Chemical vapor deposition (CVD) is a technique that allows for the functionalization of complex 3D scaffold architectures: the surface is made to present a variety of functional groups (i.e., amine, carboxylic acid, ketones, aldehyde) depending on the chemical composition of the binding biomolecules**.** CVD-based polymer coatings have been shown to be biocompatible and approved by the FDA for use in certain applications. Improved growth factor binding to material surfaces treated with CVD-based polymer coatings have been shown, as in the formation of

oxygen-terminal groups on nano-crystalline diamond surfaces to allow for interaction with recombinant human (rh) bone morphogenetic protein-2 (rhBMP-2) through an affinity that resembles that of specific receptor-ligand interactions. Several studies have explored the idea of using such polymer coating for localized gene delivery through the use of gene vectors that can be immobilized to the material surface so as to enable the infection of implanted or endogenous cells, with the added benefit of reducing the risk of virus dispersion while also reducing the necessary administration dose and increasing transduction efficiency. Zhang et al showed that adenovirus expressing runt-related transcription factor 2 (AdRunx2) can be immobilized onto polycaprolactone (PCL) through the deposition of amine-reactive active ester groups, such that an anti-adenovirus antibody could be conjugated to the material surface via an amide chemical bond, followed by AdRunx2 attachment to the PCL surface via antibody-antigen interaction. The treated PCL surface with AdRunx2 was incubated in the presence of bone marrow stromal cells (BMSCs), resulting in high alkaline phosphate (ALP) activity and subsequent matrix mineralization [3-5].

Most recently, Hao et al adopted this technique to investigate adenoviral vector conjugation to a variety of materials, including polylactic-co-glycolic acid (PLGA) and titanium, as well as PCL [1] (**Figure 5.1**). Immobilization of AdPDGF-BB and AdBMP7 resulted in transduction of seeded human periodontal ligament (hPDL) cells, resulting in the production of both PDGF-BB and BMP7. Enzyme-linked immunosorbent assay (ELISA) was used to determine the production of Collagen types I, III, and V as well as osteopontin, ALP, and osteocalcin, all of which allowed for an examination of whether hPDL cells were differentiating. Additionally, a scaffold with 3D geometry was used for combinational gene delivery, such that one compartment of the scaffold was immobilized with AdBMP7, and the other with AdPDGF-BB. Interestingly, while PDGF expression was not significantly reduced by the presence of BMP7 expression in the nearby compartment of the scaffold when compared to its expression in a control experiment which used Ad-empty vector in place of AdBMP7, the expression of BMP7 was significant reduced in the presence of concurrent PDGF-BB expression. A previous study investigating the repair of periodontal defects in beagle dogs using BioGlass/silk scaffolds with AdPDGF-B and AdBMP7 showed that AdPDGF recruited PDL cells more effectively (by 6-fold) compared to AdBMP7, while AdBMP7 itself promoted PDL cell differentiation to osteoblasts. The combined use of both adenoviral growth factors resulted in increased PDL, alveolar bone, and cementum regeneration compared to groups that delivered each adenovirus separately without combining with the other,

thereby having a synergistic effect on wound healing [6].

The primary goal of this study is to expand upon the Hao et al work showing the potential of gene therapy vector delivery and apply it to a second-generation, improved 3D-printed, micropatterned scaffold (described in Chapter 4), in order to investigate the best methodology of obtaining periodontal regeneration using an ectopic model initially, then progressing to the rat fenestration defect. This is the first known investigation of CVD-coated materials for the purpose of delivering gene therapy vectors to stimulate regeneration in vivo. In addition, this study also focuses on determining the optimal scaffold design for use in a rat fenestration defect model based on previously observed limitations of the existing scaffold design described in Chapter 4.
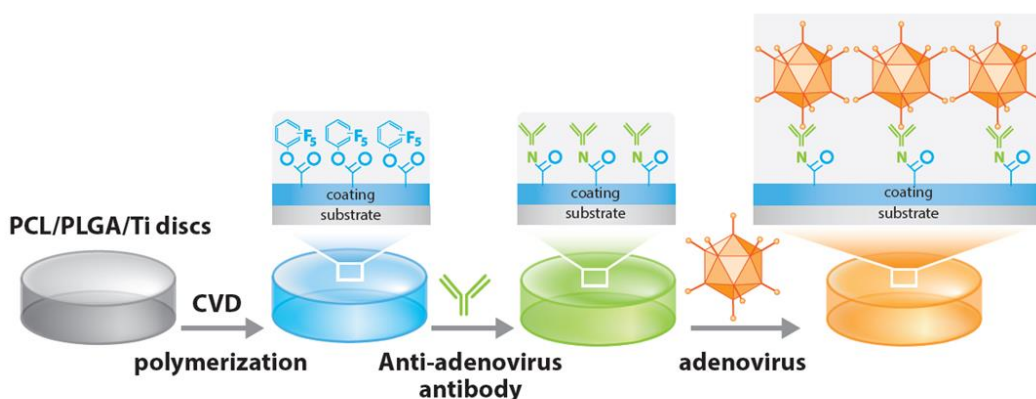
Figure 5.1 Immobilization of Gene Therapy Vectors on Biomaterial Surfaces
The immobilization of biomolecules (i.e., adenoviral vectors) on a polymer surface (i.e., PCL, PLGA) can be achieved using chemical vapor deposition (CVD) polymerization of substituted paracyclophanes. This consists of (1) coating the material with a layer of pentafluorophenol (PFP)-ester groups using CVD polymerization, (2) immobilizing an anti-adenovirus antibody onto the surface, and (3) further immobilization of the adenovirus (i.e., AdBMP, AdPDGF) through antigen-antibody interaction. This surface modification technique can be used on 2D and 3D surfaces without compromising biocompatibility (i.e., introducing components which would be cytotoxic). This method is versatile, such that a surface can be made to present a variety of functional groups (i.e., amine, carboxylic acid, ketones, aldehyde) depending on the chemical composition of the binding biomolecules. *Figure used with permission from* [2].

5.2   Materials and Methods

5.2.1   *Preparation of scaffolds for ectopic murine model*

The 3D-printed region of the scaffold was designed and fabricated as previously described [1]. Briefly, the design was performed using CAD-based software (NX 7.5, Siemens PLM

Software) such that the base had dimensions of 5.1 x 4.1 x 2.1 mm, a 1.1 mm high enclosure to contain the PCL film, and 0.7 mm wide pores. The scaffold was 3D printed using PCL powder (43-50kDa; Polysciences, Warrington, PA) and 4 wt% hydroxyapatite (Plasma Biotal Limited) via selective laser sintering (Formiga P100 system; EOS e-Manufacturing Solutions). The micropatterned region of the scaffold was altered from the previous design such as to: (1) decrease the inter-pillar distance from 400um to 150um, while retaining the same height (250um), (2) reduce the pillar length x width measurement from 400um x 400um to 300um x 300um, (3) increase the base porosity using water-based leaching of sugar particles (diameter = 125um), and (4) increase biomaterial degradation rate by forming the patterned film using PLGA. The pillar groove design consisting of 15um wide, 30um deep grooves was selected among the previous designs described [1] due to the previous results showing that groove depth (i.e., 10um vs. 30um) was a determining factor in the amount (i.e., width at pillar boundary) of aligned tissue formation.

As previously reported, a CAD-based program (LEdit) was used to design the new micropatterns and define the silicon and SU-8 master molds with standard photolithography, with mold fabrication performed at Lurie Nanofabrication Facility (University of Michigan, Ann Arbor, MI). Polydimethylsiloxane (PDMS, Sylgard 184; Dow Corning) was mixed in a ratio of 10:1 v/v of base to curing agent, degassed under vacuum, poured onto SU-8 master molds, cured (65°C), and peeled to reveal the pattern. The pillars were formed via casting of 2.5% PLGA (75:25, 137kDa, Evonik Industries) onto the PDMS mold until they were filled. A solution of 10% PCL containing sieved sugar particles (125um diameter) was then cast onto the pillars in order to form a layer approximately 250um thick. The films were dried under vacuum for a period of 24 hours before placement in deionized water to dissolve away the sugar particles.

5.2.2   *Preparation of scaffolds for rat fenestration defect*

Preparation of the micropatterned film was undertaken as described in Section 5.2.1, except that a solution of PLGA-PCL (50/50) was used instead of PLGA alone, based on results from the pilot study using this formulation in the ectopic murine model. Additionally, instead of the 3D-printed scaffold region created using SLS, the "bone" region of the scaffold was formed by mixing sugar particles (ranging from 100-400um in diameter) with 10% PCL solution and casting into a glass dish to produce a 250um thick base that was dried overnight under vacuum before being placed in deionized water to allow for sugar particle leaching out of the film.

105

5.2.3 Chemical vapor deposition (CVD) and gene therapy vector immobilization

Scaffolds (i.e., 3D-printed region and micropatterned film, or amorphous region and micropatterned film) were coated with a layer of amine-reactive polymer using a custom-built CVD system, as previously reported (Hao et al). Briefly, the coating process consisted of fixing the scaffolds inside the deposition chamber at 15°C, with the starting material sublimated at 120°C, followed by pyrolyzation at 540°C to form into a stream of reactive di-radical vapor which deposited and polymerized on the scaffold surface (pressure of 0.1 mbar, argon as carrier gas). The scaffolds were turned to the other side and the process repeated to ensure that the coating deposited on all sides. After this process, scaffolds either stored under vacuum until further use of sterilized in 70% ethanol (1hr) to prepare for virus immobilization and subsequent cell seeding, as needed.

The experimental groups consisted of immobilizing adenovirus encoding BMP7 for the "bone" region of the scaffold (i.e., 3D printed scaffold or amorphous PCL film) and adenovirus encoding PDGF-BB on the "PDL" region of the scaffold (i.e., porous micropatterned film). Control groups consisted of immobilization with adenovirus without any growth factor gene (i.e., empty adenovirus, or Ad-empty). After sterilization, scaffolds were treated with 10 μg/mL solution of goat anti-adenovirus (AbD Serotec; 0151- 9004) polyclonal antibody in phosphate-buffered saline (PBS), determined based on a previously established saturation point. The scaffolds were incubated in solution overnight (4°C), rinsed 5 times (5 minutes each) with PBS, followed by incubation in 12 mL cold adenovirus solution (4 hrs at 4°C), then rinsed in PBS (5 times, 5 minutes each). The adenovirus solution (10^{12} particle number) contained either vectors not expressing any gene (Ad-empty), or vectors expressing PDGF-BB or BMP7 genes (prepared by University of Michigan Vector Core), depending on which scaffold region was being treated. After the final PBS wash, the scaffolds were ready for cell seeding (i.e., human periodontal ligament (hPDL) cells in the "PDL" region of the scaffold or human gingival fibroblasts (hGFs) in the "bone" region of the scaffold).

5.2.4 Scanning electron microscopy (SEM), immunofluorescence, and enzyme-linked immunosorbent assay (ELISA)

Scanning electron microscopy (SEM) was performed at Microscopy and Image Analysis Laboratory (University of Michigan) using an Amray FE 1900 SEM to image patterned 3D films

with Ad-empty, or patterned 3D films after hPDL cell seeding (passages 4-6, 1.2×10^4 cells/film) to observe cell behavior on the re-designed films, as well as to confirm micropattern parameters (i.e., height, inter-pillar distance, porosity). Prior to imaging, the films were gold sputter-coated and observed at an acceleration voltage of 5kV. To further examine cell behavior on the re-designed micropatterned films, immunofluorescence staining was performed using 4',6-diamidino-2-phenylindole (Prolong Gold Antifade Reagent with DAPI; Life Technologies) to label cell nuclei and anti-tubulin antibody with AlexaFluor488 (1:100 dilution, Abcam Inc, Cambridge MA) to label microtubules. Stained scaffolds were imaged using fluorescence microscopy (Nikon Eclipse 50i) to examine cell orientation within grooves and on pillar sides. Additionally, to confirm the transduction of seeded hPDL and hGF cells and verify bioactivity of the growth factors (BMP7, PDGF-BB), an ELISA assay (R&D Systems, Minneapolis, MN, USA) was performed to quantify the release of each growth factor at 1 and 3 days post-seeding in the respective scaffold region (n=3).

5.2.5   *In vivo implantation: Ectopic murine model and rat fenestration defect*

The first pilot study (n=12, detailed in **Figure 5.6**) consisted of repeating the same implantation of the 3D-printed, micropatterned scaffold using an ectopic murine model, as described in Chapter 4. However, as described in the above methodology, the scaffolds were immobilized with AdBMP7 in the 3D-printed base region or with AdPDGF-BB in the micropatterned film region prior to cell seeding with hGF cells (2.5×10^5 cells in 8uL fibrinogen mixed with 2ul thrombin) or hPDL cells (1.5×10^5 cells in 15mL fibrinogen mixed with 3uL thrombin), respectively, one day prior to implantation. The control group (n=6) consisted of all scaffold regions being immobilized with Ad-PDGF or AdBMP7 but with no prior to cell seeding. The day of surgery, a human-derived dentin segment (surface-treated with 37% orthophosphoric acid and trimmed to scaffold size) was press-fit onto the patterned film. Two surgical pockets were made on the dorsa of immunodeficient 6 week-old NIH III nude mice (20-25g; Charles River Laboratories, Wilmington MA) for subcutaneous scaffold implantation under isofluorane anesthesia. Unlike in the previous study reported in Chapter 4, there was no additional cell seeding the day of the surgery. Samples were harvested at 6 weeks and fixed in 10% buffered formalin phosphate solution for 2 days before being transferred into 70% ethanol for micro-CT scanning,

followed by decalcification. Dentin segments derived from healthy human teeth were obtained in accordance with a University of Michigan-Institutional Review Board (IRB) exempt protocol.

The second pilot study (detailed in **Figure 5.10**) consisted of implanting the scaffold described in Section 5.2.2 in a rat fenestration defect, using the following groups: Experimental group (n=5) consisting of AdBMP7 and AdPDGF-BB immobilization with hGF and hPDL cell seeding, and control group (n=5) without any cell seeding to examine if tissue regeneration would occur without pre-seeding the scaffold. Athymic rats (250g, Charles River Laboratories Inc., Wilmington) were ordered, general anesthesia performed under isofluorane during periodontal defect creation, with a single fenestration defect (3 x 2mm^2) created for each animal on the buccal side of the right mandible such that the distal root of the first molar tooth was exposed. The cementum layer was also carefully removed to expose the dentin surface, after which the patterned film (with AdDGF-hPDL) was positioned with the pillars against the dentin, followed by the amorphous PCL film (with AdBMP7-hGF) directly above. The site was sutured and closed with surgical staples, with administration of analgesic subcutaneously at 24 hrs post-surgery. After 3 weeks, specimen were harvested and fixed in 10% buffered formalin phosphate solution for 2 days before being transferred into 70% ethanol for micro-CT scanning, followed by decalcification. All animal studies were performed with approval from University of Michigan-University Committee on Use and Care of Animals (UM-UCUCA) according to ARRIVE guidelines for preclinical studies.

5.2.6 *Micro-computed tomography (micro-CT) and histomorphometry*

Micro-CT was used to determine the adaptation ratio of 20% barium-sulfate coated patterned films to the rat fenestration defect site. The ratio was calculated by determining how closely the pillars were to the tooth root, with measurements taken at each column and row of the patterned film (1.3mm x 1.65mm), calculating the distance from the two edges and the center of each pillar to the tooth root. Micro-CT was also used for purposes of evaluating bone regeneration post-implantation: Tissue-fixed specimens were embedded in alginate, scanned using micro-CT (Scanco Medical) at a resolution of 12um, at 70kV energy and 114uA intensity, and calibrated to Hounsfield units (HU). Bone volume (BV) and tissue mineral density (TMD) were determined for internal and external regions of the bone compartment using Microview software (Parallax Innovations) with a threshold of HU=1050 for bone. After scanning, samples were decalcified in

108

10% EDTA, embedded in paraffin, and cut into 5um sections for histological analysis using hematoxylin and eosin (H&E).

5.2.7 Statistical analysis

Data were expressed as mean ± standard deviation of the mean. One-way analysis of variance (ANOVA) with post hoc Tukey's multiple comparison method was used to perform comparative analysis, with a p-value <0.05 ($\alpha < 0.05$) considered significant.

5.3 Results

Design changes to the original micropatterned film were implemented in order to address limitations previously encountered, including inter-pillar spacing being too wide, slow degradation rate of polycaprolactone (PCL) used to form the film, and need for increased porosity of the film. The interpillar distance was reduced to 150um, with pillar dimensions decreased to 300um, and a base porosity of approximately 60% achieved using sugar-leaching. SEM images of the new pattern design that was covered with CVD-based polymer coating and subsequently had Ad-empty immobilized via antibody-antigen interaction confirms the presence of adenovirus particles at a magnification of 10,000X (**Figure 5.2A**). In fact, the virus was observed not only on top of the pillars, but also on pillar sides (image not shown), indicating that the polymer coating extends well into 3D patterned (i.e., grooves).

Additionally, given that both sides of the film were coated with polymer during treatment, presence of virus particles was also confirmed at the base of the patterned film (**Figure 5.2B**). To further investigate cell behavior (i.e., induced alignment) on the new patterned films, hPDL cells seeded on the films were fixed and imaged using SEM, revealing induced cell alignment at the inter-pillar spaces as well as along the pillar grooves (**Figure 5.3**). Single cells were observed aligning along grooves, with an entire sheet of cells covering the tops of the pillars such that they were undistinguishable from a top-down view. Additional assessment to examine the orientation of cell nuclei along the patterned films was made by labeling the cells with DAPI and tubulin, with the result showing the congregation of cells within pillar grooves (**Figure 5.4A**). There is overall a tendency of the cells to align parallel to the pillar grooves, both within the film region and on the edges (**Figure 5.4B**).
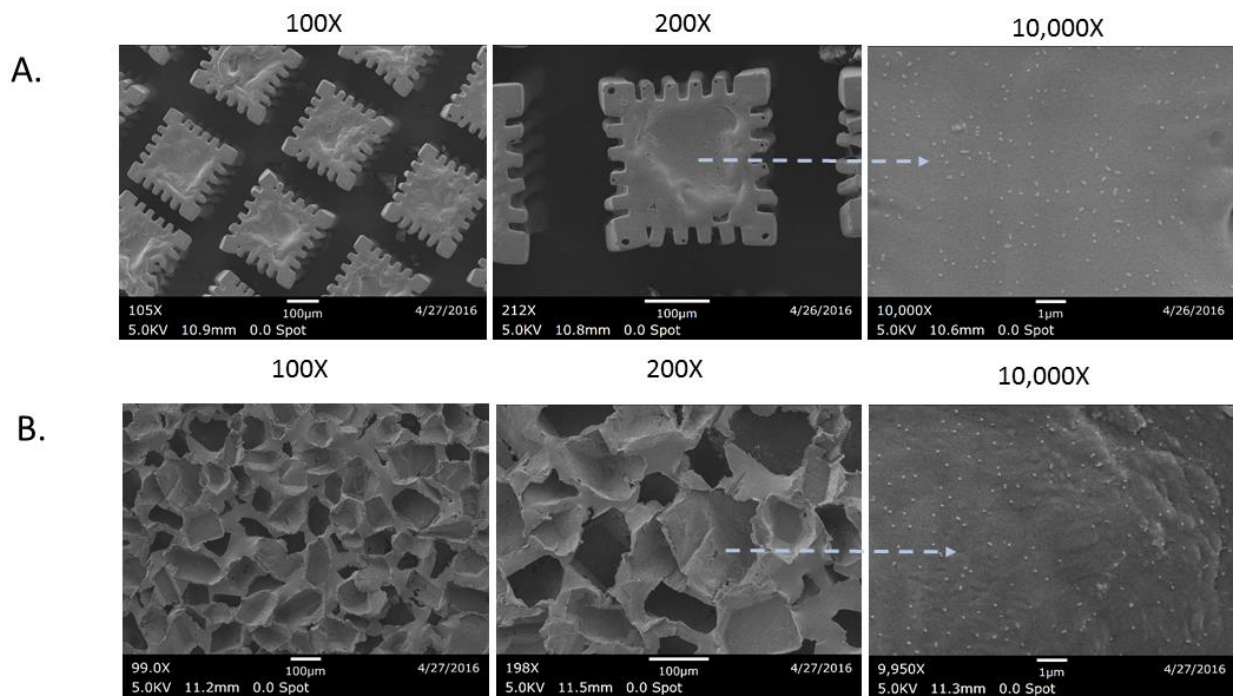
Figure 5.2 Scanning Electron Microscopy of Micropatterned Films with Adenovirus
Scanning electron microscopy (SEM) images of micropatterned film consisting of 250um high pillars (A), confirming the presence of attached adenovirus (Ad-empty) (at 10,000X). The base of the micropatterned film (B), formed with polycaprolactone (PCL) using salt-leaching, is also confirmed to have immobilized adenovirus, even within the pores of the film.
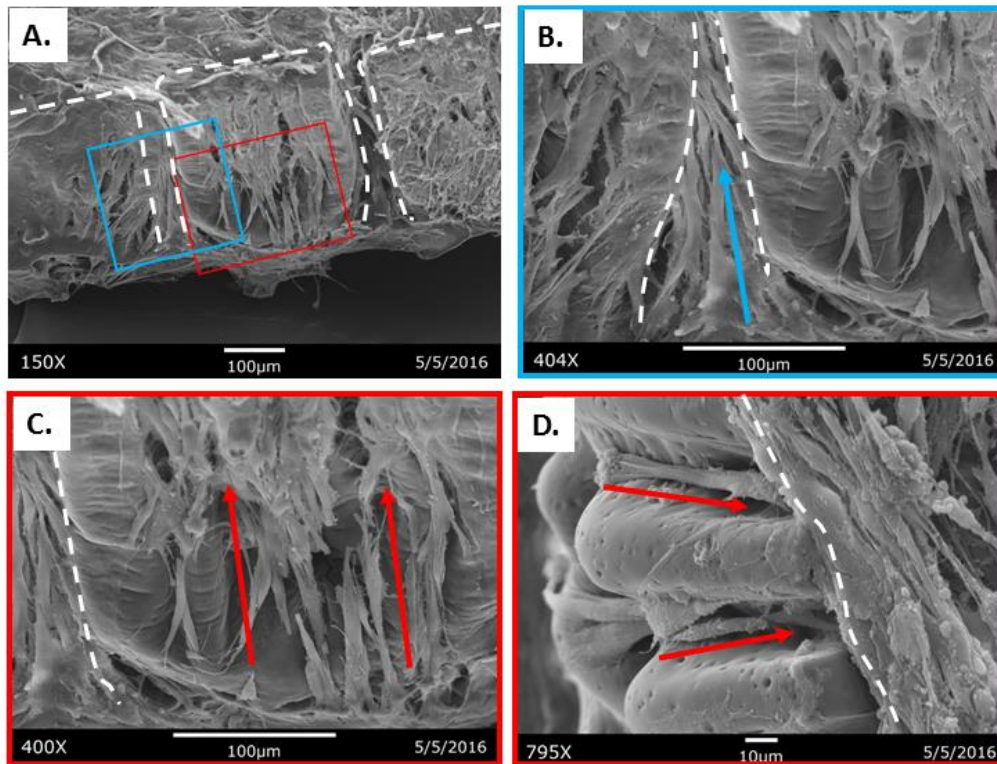
Figure 5.3 Alignment of Periodontal Ligament Cells on Micropatterned Films
Alignment of seeded human periodontal ligament cells (hPDLs) 3 days post-seeding on micropatterned films was confirmed using SEM: (A) denotes the region of interest—two areas where cell alignment in observed, at the pillar grooves (red square, magnified in C and D) and the inter-pillar region (blue square, magnified in B). White dotted lines denote the pillars of the film. Arrows indicate direction of cellular alignment between pillars (blue) and along grooves (red).

Figure 5.4 Immunofluorescence Staining of Aligned Cells on Micropatterned Films
Immunofluorescence staining of hPDL cells on micropatterned film to observe cell behavior
(i.e., alignment, denoted by arrows). (A) DAPI (blue) and tubulin (green) shows increased
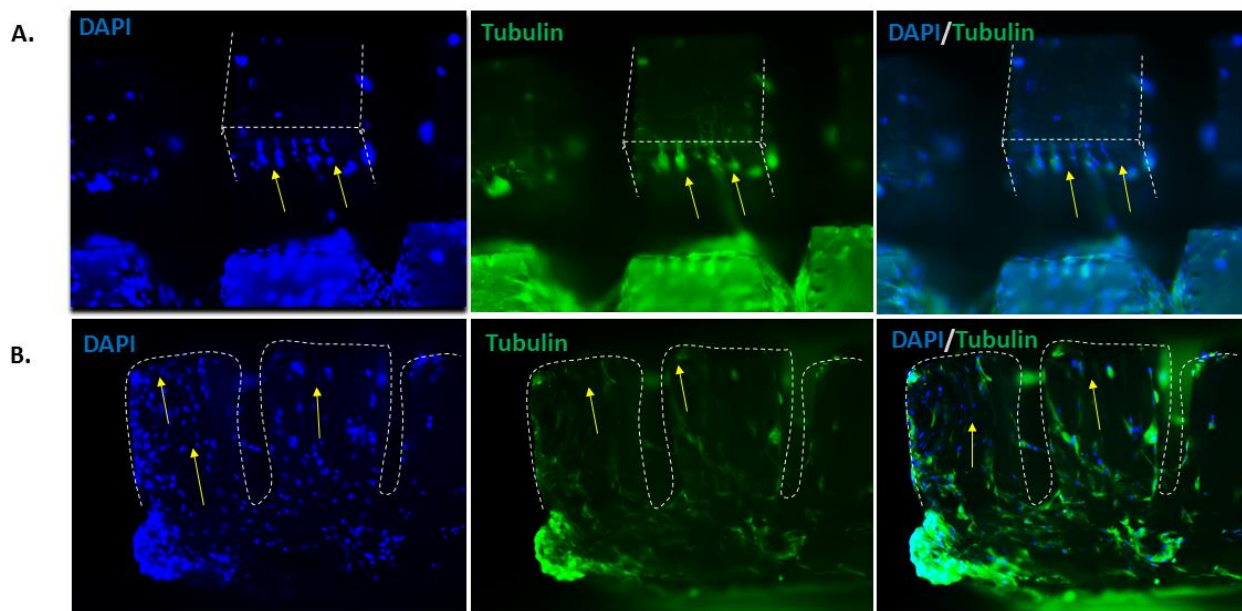density of cells within pillar grooves (15um wide, 30um deep), with aligned cell nuclei (DAPI)
along the micropillar grooves as seen on the side of the patterned film (B). White dashed lines
designate pillar regions.

Once virus immobilization to the scaffold was confirmed using Ad-empty, an ELISA assay
was performed to ensure growth factor bioactivity following transduction of hGF and hPDL cells
with AdBMP7 and AdPDGF at the 3D printed and micropatterned regions of the scaffold,
respectively. The two regions of the scaffold were treated and analyzed separately rather than as
an assembled unit. Results (**Figure 5.5**) showed significant (p<0.05) increase in both the BMP and
PDGF growth factor production when comparing Day 1 and Day 3 growth factor levels. At Day
1, PDGF production was 58.1±13.9 ng/mL compared to 220±78.7 ng/mL at Day 3. BMP7
production was only 3.8±2.4 ng/mL at Day 1 compared to 132.9±43.8 ng/mL at Day 3. These data
confirmed that cells were transduced post-seeding onto scaffold regions immobilized with each
respective adenovirus encoding BMP7 or PDGF-BB. Compared to values reported for 2D PCL by
Hao et al, both PDGF and BMP7 production, particularly by day 3, was higher using the same 10^{12}
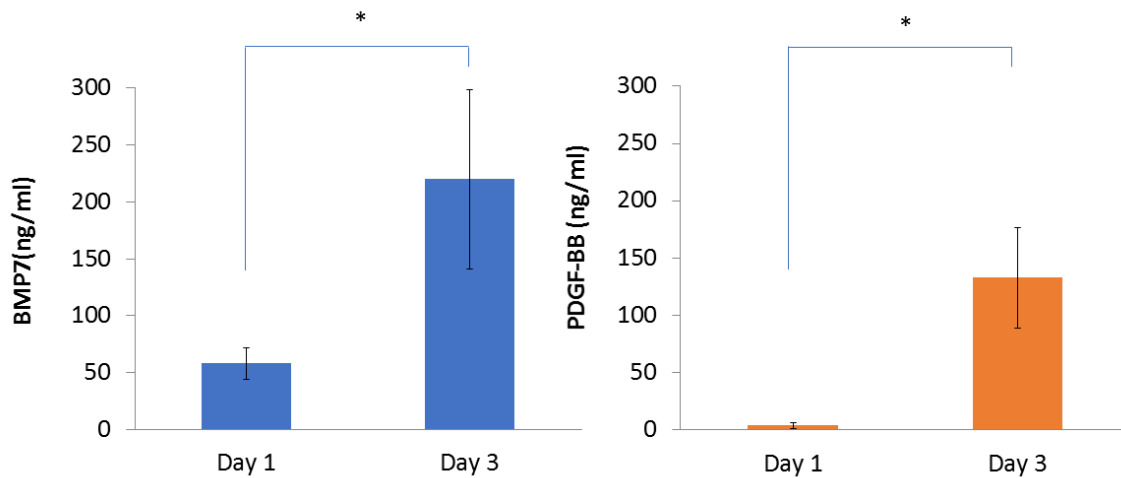particle number.

Figure 5.5   PDGF-BB and BMP7 Production by Transduced hPDL Cells *In Vitro*
Production of BMP7 and PDGF-BB proteins was confirmed using an ELISA assay to verify that
human periodontal ligament (hPDL) and human gingival fibroblast (hGF) cells were transduced
with AdPDGF-BB (immobilized on patterned film) and AdBMP7 (immobilized on 3D printed
base), respectively, after 1 and 3 days post-cell seeding.

In order to investigate whether localized transduction of cells (i.e., only cells that come in
contact with specific scaffold region) in turn improves the spatiotemporal availability of growth
factors, particularly resulting in bone formation localized to the 3D-printed region, the scaffold
complex was tested in a pilot study using the same ectopic murine model from which results of
cell alignment and bone formation were assessed in Chapter 4. Here, the focus was to examine
how cells transduced with AdBMP7 and AdPDGF-BB regenerated tissue compared to cells that
were exposed to Ad-empty (**Figure 5.6**). After implantation, tissue samples were harvested at 6
weeks. **Figure 5.7** shows the resulting micro-CT images of all samples from the experimental
(n=6) group that included dual growth factor delivery—no bone was formed in the control groups
(Ad-empty), as indicated by bone volume measurements in (A). There is noticeable variation in
bone formation within the 3D-printed region, with some bone tissue invasion seen occurring into
the micropatterned film region (directly below the dentin segment). However, there are no
significant differences between total bone volume and the volume of osseous tissue found to be
localized to the 3D printed region. Overall, bone volume and tissue mineral density measurements
show significant ($p<0.05$) increases in bone formed in the experimental group compared to control
group. These results were further confirmed using hematoxylin and eosin staining (**Figure 5.8**)

which shows bone formation within the 3D printed region, but also its invasion into the micropatterned film region, such that the inter-pillar space shows immature bone formation in place of PDL-like (soft) tissue. There appears to be an improved integration of tissue between the 3D printed and patterned regions of the scaffold as a result of improved patterned film base porosity, as opposed to the distinct separation of tissue between the "bone" and "PDL" regions of the scaffold that was observed in results reported in Chapter 4. One additional observation is that the presence of bone tissue in the patterned film region stabilized the film such that the pillars did not change in size (i.e., expanded) as much as in the absence of bone formation (see **Figure 5.9**).
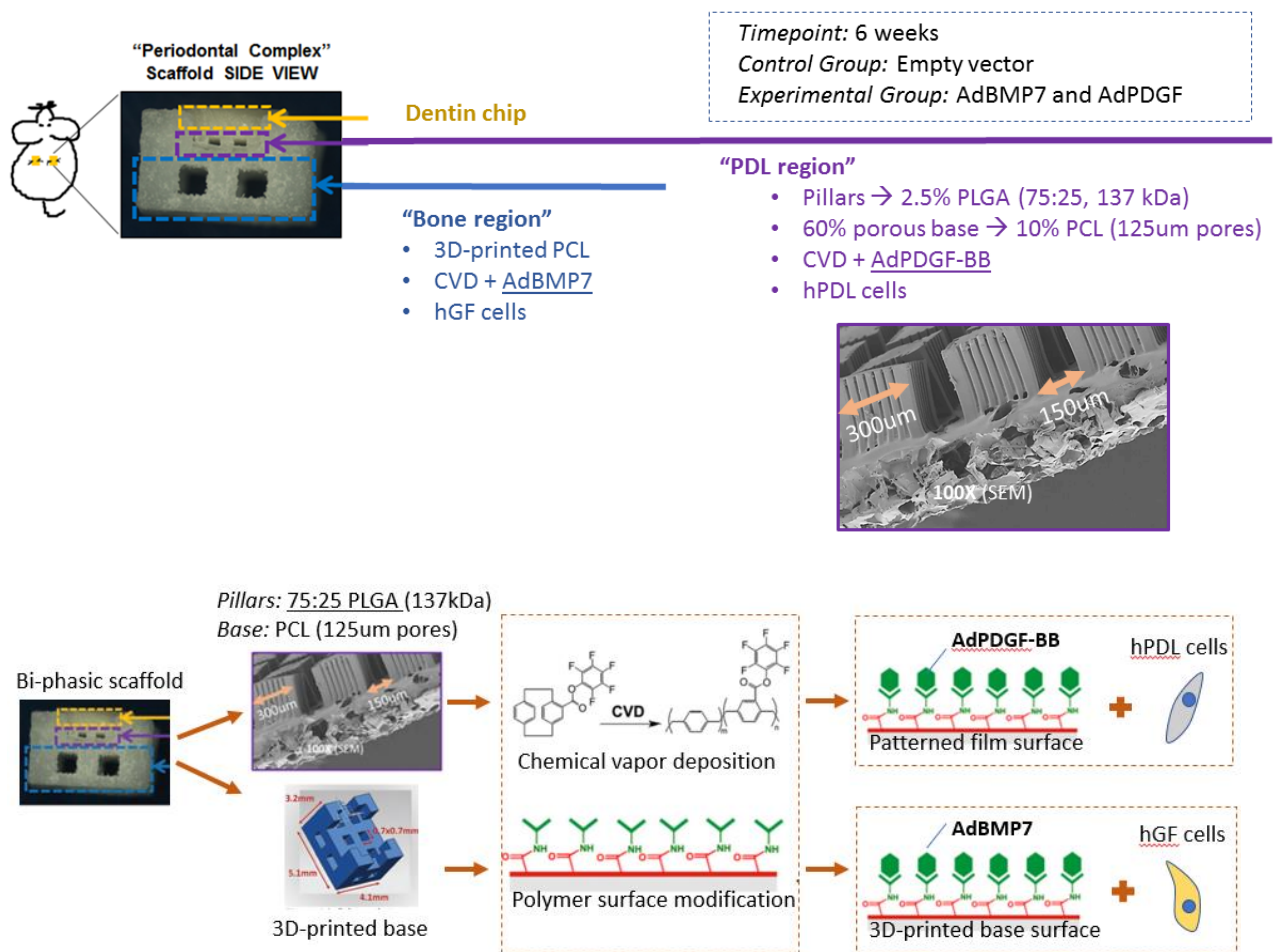
Figure 5.6 Ectopic Murine Model using CVD-Coated Scaffolds

The ectopic murine model shown here was used to implant scaffolds for a period of 6 weeks. The scaffolds were designed to have the following regions: (1) A 3D-printed polycaprolactone (PCL) base for the regeneration of alveolar bone that serves as a region for the covalent attachment of adenoviral BMP7 (AdBMP7) via chemical vapor deposition (CVD)-based polymerization, with further transduction of the human gingival fibroblast (hGF) cells that are seeded on its surface prior to implantation; (2) A micropatterned film consisting of 250um high, 300um wide pillars with 15um wide, 30um deep grooves. The pillars (formed via casting of 2.5% PLGA (75:25, 137kDa) onto a silicone mold) are spaced 150um apart and attached to a base with 60% porosity formed via casting of a 10% PCL solution containing sugar particles (125um diameter) that are dissolved in water after the films are dried. The films allow for immobilization of AdPDGF-BB via CVD-based coating, followed by seeding with human-derived periodontal ligament (PDL) cells. The control group (n=6) differed from experimental group (n=6) in that the CVD-coated regions of the scaffold were incubated with empty adenovirus vector (Ad-empty). *Schematic of functional groups shown on sample CVD-coated polymer surface modified from [5].*

D = dentin chip

A. Volume of Formed Bone

B. Tissue Mineral Density of Formed Bone
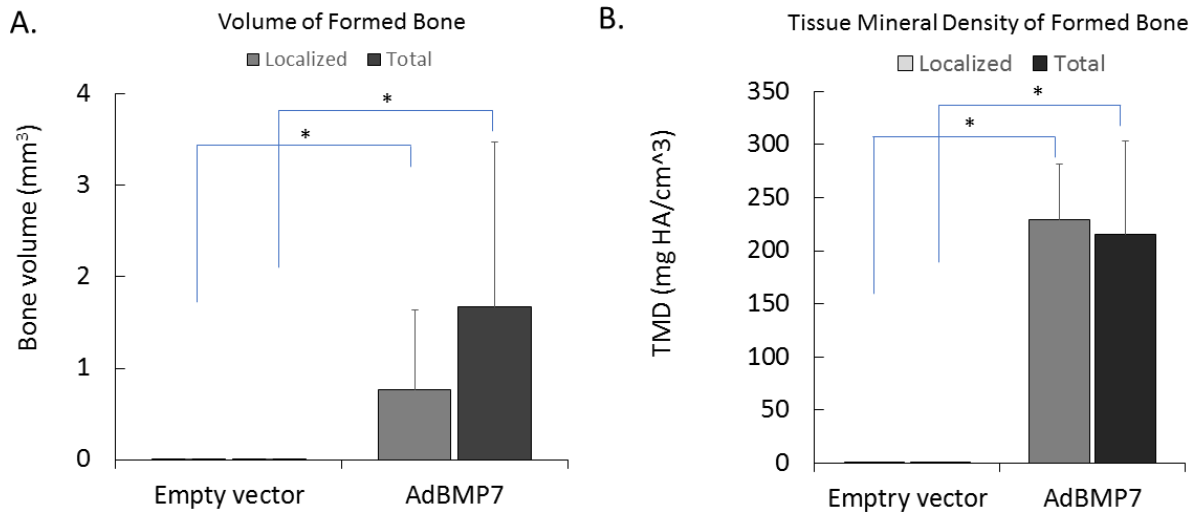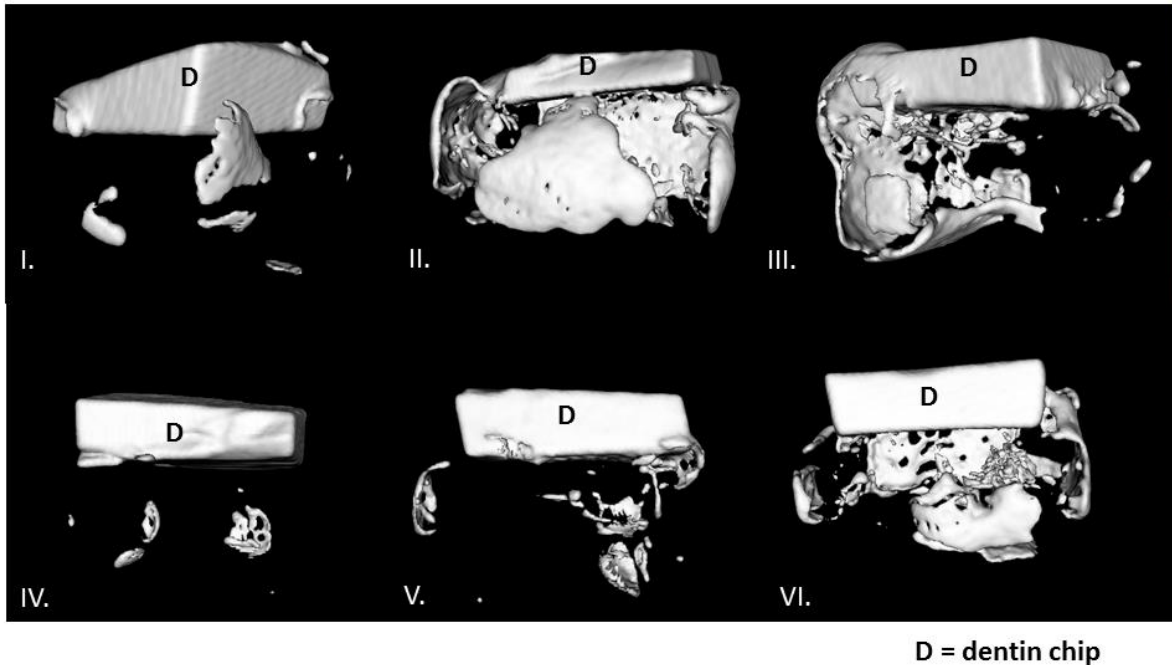
Figure 5.7 Bone Volume and Tissue Mineral Density using Ectopic Murine Model
Micro-CT images (I-VI, top panel) at 6 weeks post-implantation of 3D-printed, micropatterned scaffolds (n=6) using an ectopic murine model, showing formation of bone in the 3D-printed scaffold region immobilized with AdBMP7 and seeded with human gingival fibroblasts prior to implantation. There is a variation in bone formation through the 6 experimental samples (I-VI), with noticeable infiltration into the patterned film "PDL region" of the scaffold in some of the samples (III, VI). Samples in control group (with Ad-empty vector) not shown given lack of any bone formation. The bone volume (BV) (shown in A.) and tissue mineral density (TMD) (shown in B.) analysis of osseous tissue growth in vivo in the bone region of the scaffold compares the

total volume of bone formed to the volume specifically localized to the 3D-printed region of the scaffold (*p<0.05).

Additionally, as noted in the Methods section, this study differed from the previous ectopic murine model study (Chapter 4) in that there was no additional cell pre-seeding on the day of implantation; instead, all cells were encapsulated in the fibrin/thrombin gel prior to seeding onto the patterned film and bone region in order to reduce the step of additional cell seeding the day of surgery. However, in the pilot study, it was noticed that this use of a gel in place of direct cell-seeding seemed to inhibit cellular alignment at the pillar sites. As a result, a single animal was used (n=1) as a means of testing whether direct cell seeding on the PLGA pillars day prior to surgery (without growth factor delivery), allowed for cellular orientation (**Figure 5.9**). The results confirmed that direct cell seeding was essential in order to ensure cell alignment within the grooves, which might otherwise be blocked by the use of a hydrogel as a cell delivery vehicle. This is significant given that oriented tissue formation (at a scale that would allow for generation of quantifiable data) was not observed in most of the experimental and control groups.
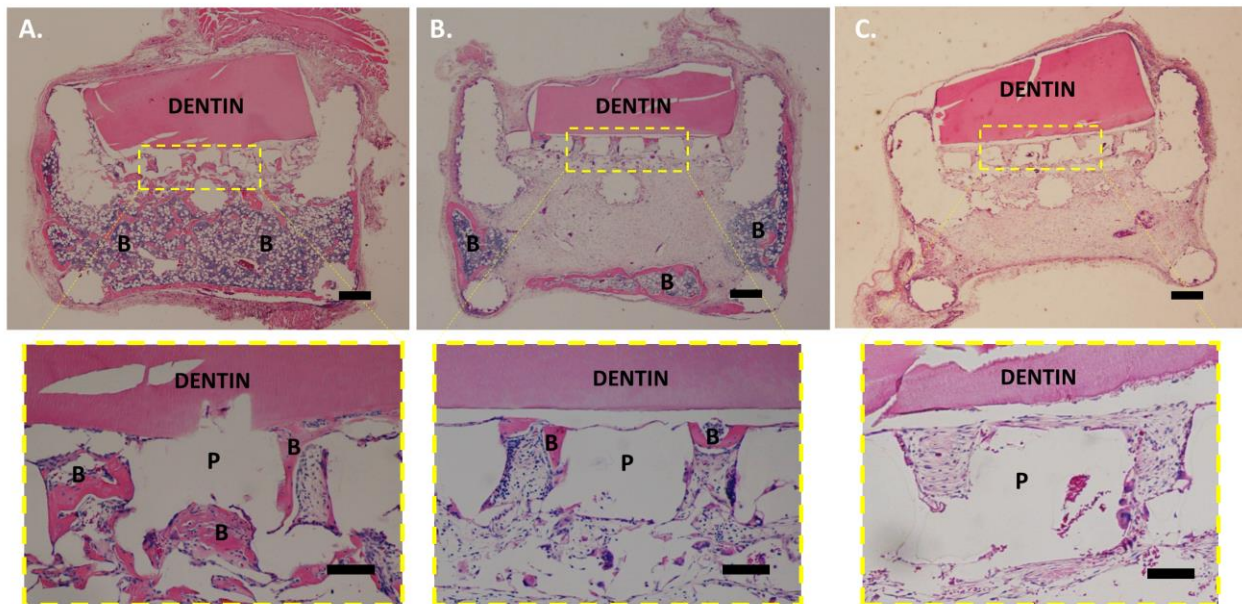
Figure 5.8 Hematoxylin and Eosin (H&E) Staining of Scaffolds after 6 Weeks *In Vivo*
Hematoxylin and eosin (H&E) images of scaffolds harvested at 6 weeks post-implantation. Bone formation with varying volume is seen in the 3D printed region of the scaffolds with AdBMP7-hGF (A and B, at 2X). Likewise, infiltration of the bone into the patterned film (with AdPDGF-hPDL) region is noticeable in the magnified images (10X) in the lower panel. The control group

(C) shows no bone formation, as expected given the use of Ad-empty. Scale bar corresponds to 150um (top panel) and 500um (bottom panel). B = bone, P = pillar.
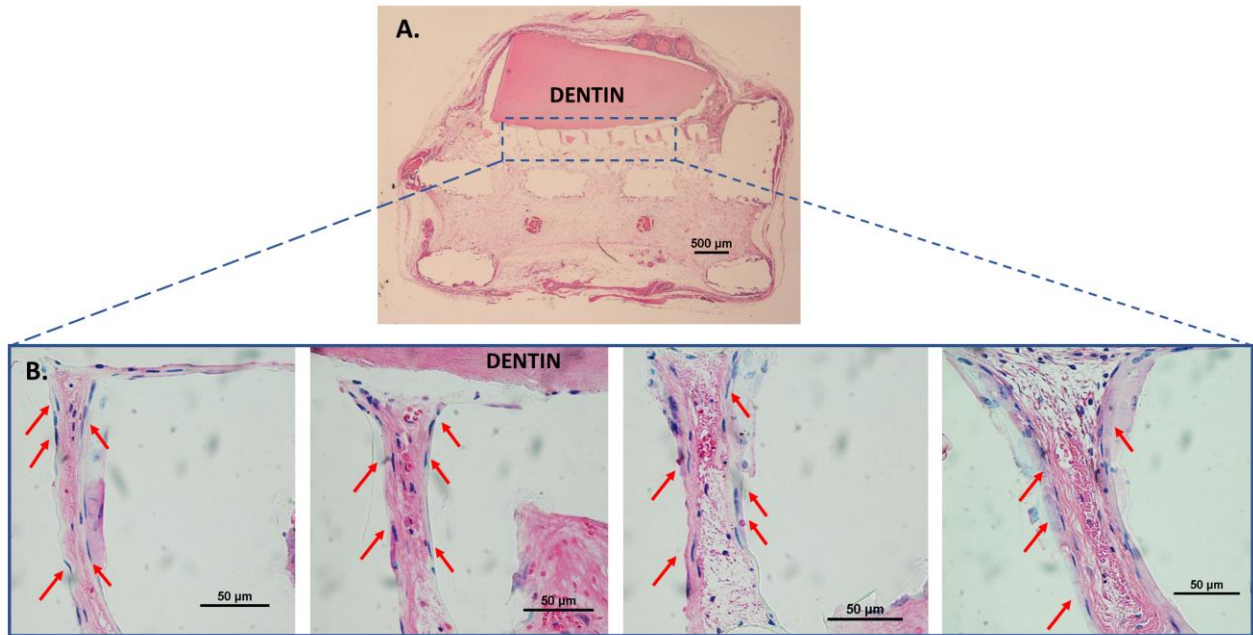

Figure 5.9 Tissue Alignment in Scaffolds Seeded with hPDL Cells
Hematoxylin and eosin (H&E) images of scaffold with patterned film that show guidance of tissue alignment at inter-pillar regions. Noticeable reduction in inter-pillar space is observed due to hydrolysis of PLGA over 6 week period in vivo. Arrows correspond to cell nuclei shown to be perpendicular to the dentin segment.

Based on the results reported from the ectopic murine model pilot study, an additional pilot study was performed, this time with the implantation of CVD-treated scaffolds with AdBMP7 and AdPDGF in a rat fenestration defect (**Figure 5.10**). Here, as described in the Methods section, the 3D printed "bone" region was substituted with an amorphous film with porosity achieved using sugar-leaching. As with the patterned films, the amorphous film was verified to have immobilized gene therapy vectors on the surface using SEM imaging, in addition to observing hGF cell attachment and response **(Figure 5.11)**. Additionally, based on previously-noted limitations, the following improvements were made: (1) micropatterned film was formed using PCL-PLGA (50/50) to decrease the observed "swelling" of the pillars as a result of increased rate of hydrolysis seen with PLGA *in vivo*, (2) direct, one-time delivery of cells onto the patterned film and amorphous bone regions the day prior to surgery. The groups tested in the study consisted of (1) AdBMP7-hGF and AdPDGF-hPDL on the amorphous PCL "bone" region and patterned PCL-PLGA "PDL" region, respectively and (2) AdBMP7 and AdPDGF immobilization on the

respective regions of the scaffold, <u>without</u> cell seeding (i.e., no hPDL or hGF pre-seeding the day before surgery). The aim was to determine whether bone regeneration in particular could be induced without the need to cell seed prior to implantation, which would enable the elimination of an additional step in the scaffold preparation process prior to surgical use.
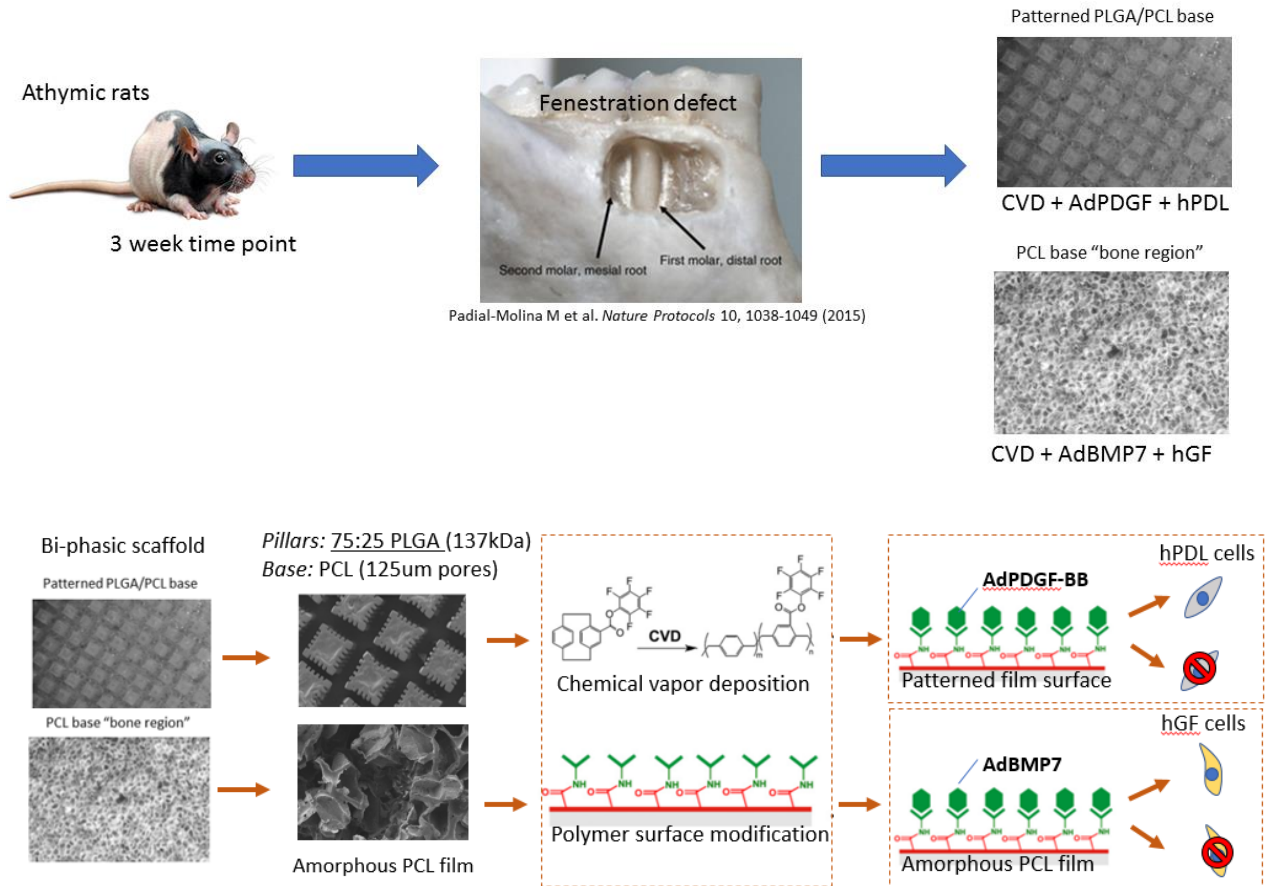
Figure 5.10 Rat Fenestration Defect Model using CVD-Coated, Micropatterned Films
Rat fenestration defect created in athymic rats exposing the distal root of the first molar to allow for implantation of a scaffold consisting of (1) patterned PLGA/PCL region for delivery of AdPDGF-hPDL and (2) amorphous PCL region for delivery of AdBMP7-hGF. Scaffolds (n=5) were implanted and remained at the site for 3 weeks prior to harvesting. Control group (n=5) consisted of the same scaffold regions, with Ad-PDGF-no cells in the patterned film and Ad-BMP7-no cells in the amorphous film regions. *Schematic of functional groups shown on sample CVD-coated polymer surface modified from [5].*

Prior to implantation, in order to verify the scaffold fit within the fenestration defect, micropatterned films and the amorphous "bone" region were coated with 20% barium sulfate and micro-CT scanned at the defect site (**Figure 5.12**). The calculated adaptation ratio revealed that the pillars were fit well against the tooth root, with minimal spacing in between (adaptation ratio = 90% $\pm$1%). After 3 weeks in the rat fenestration defect, rat mandibles were harvested, fixed, and imaged using micro-CT. The results reveal lack of noticeable bone formation within the defect site (confirmed using bone volume fraction (BVF) calculations) in the control group (without cell seeding), compared to robust bone formation in the experimental group (**Figure 5.13**). However, while there is significant presence of bone in this group, it is mostly confined to spaces outside of the defect. Measurements of the bone fill within the defect site only for the exprimental group reveals an average BVF of 14.2%, with the highest fill at 36.2% and the lowest at 6.2%. Further assessment using histology (H&E) showed increased PDL-like tissue formation in the experimental group, with limited orientation in the control group (**Figure 5.14**). Likewise, there were clear differences in the tissue morphology at the amorphous PCL film site *in vivo* when comparing the experimental and control groups, with bone islands only visible in sections derived from groups that included hGF cell transduction with AdBMP7 prior to implantation.
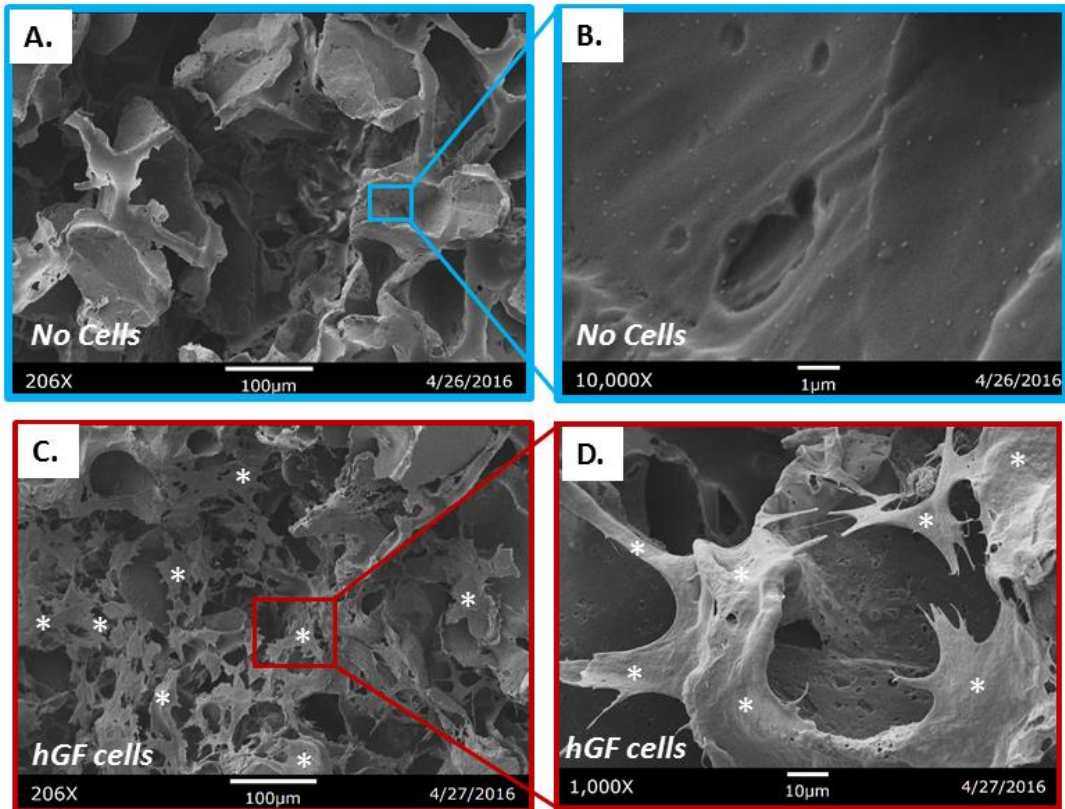
Figure 5.11 AdBMP7-Immobilized Amorphous PCL Films with and without Cell Seeding
Amorphous PCL film for the "bone" region of the scaffold complex used in the rat fenestration defect with immobilization of AdBMP7 and with/without cell seeding. The porous, amorphous surface without cells is seen is (A) at 206X, with (B) showing a region at 10,000X in order to identify presence of adenovirus vector. Image (C) shows the film seeded with hGF cells at the same magnification as (A), and (D) showing more precise features of the cell spreading and adhesion on the film surface with a magnified view (1000X). * denotes areas of cell presence on the amorphous film.
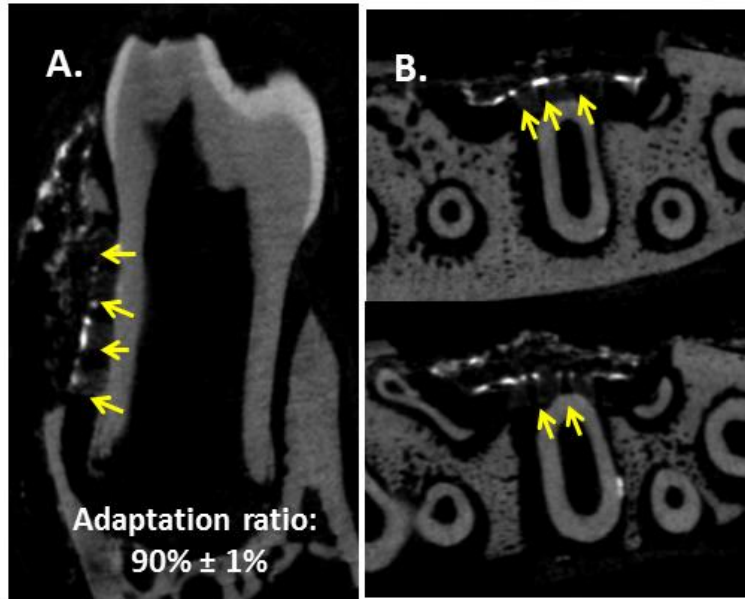
Figure 5.12 Adaptation of Micropatterned Films at Rat Fenestration Defect Site
Positioning of scaffolds along tooth root surface in vivo. The adaptation ratio of the patterned film to the rat fenestration defect site was calculated based on micro-CT images of 20% barium-sulfate coated scaffolds. The ratio was calculated by determining how closely the pillars (indicated by yellow arrows) were to the tooth root, with measurements taken at each column (A) and row (B) of the patterned film, calculating the distance from the two edges and the center of each pillar to the tooth root.

Figure 5.13   Bone Regeneration: CVD-Coated Scaffolds with and without Cell Seeding
Micro-CT images of control (A) and experimental (B) groups showing lack of bone formation at the rat fenestration defect site 3 week post implantation or significant bone formation, respectively. Panel B indicates robust bone formation located mostly outside of the defect site (shown by arrows and outlined using dashed orange line). Measurements showed an average defect fill (bone volume fraction) of 14.2% , with the highest fill at 36.2% and the lowest at 6.2%.

Figure 5.14 **Hematoxylin and Eosin (H&E) Staining of Scaffolds after 3 Weeks *in Vivo***
Hematoxylin and eosin (H&E) images of defect site at 3 weeks post-implantation of a micropatterned film and amorphous film to promote PDL and bone regeneration, respectively.

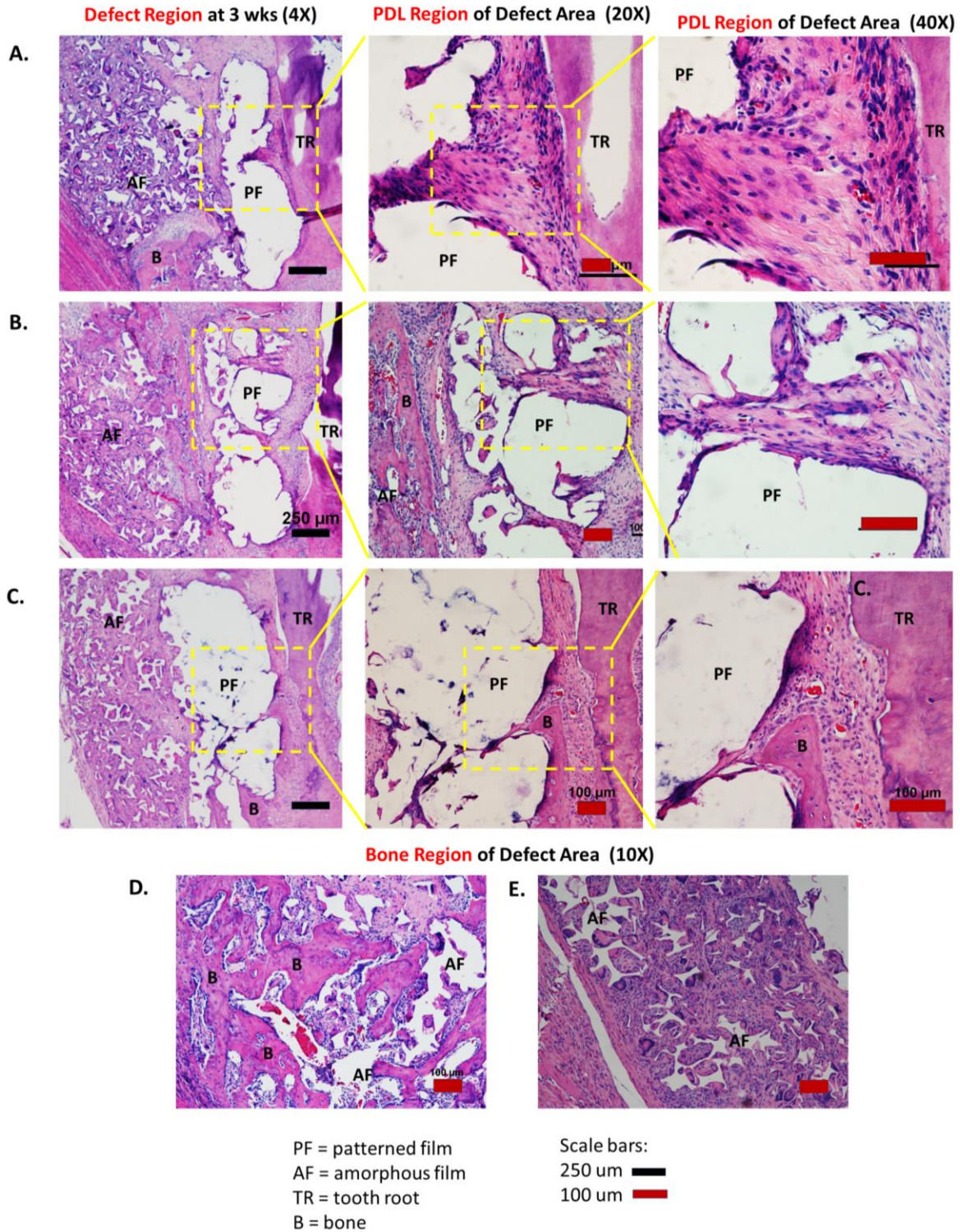Images in (A) and (B) correspond to experimental groups with AdPDGF-hPDL cells and AdBMP7-hGF cells, and images in (C) show tissue regeneration in control group (Ad-empty-hPDL and Ad-empty-hGF, in the patterned film and amorphous film regions, respectively). PDL-like tissue formed in region with micropatterned pillars is seen at 20X and 40X, with distinct perpendicularity to the tooth root, which is lacking in the control group. Images (D., experimental) and (E., control) compare the regions where the amorphous film was positioned, showing distinct bone islands in the experimental group (with AdBMP7-hGF cells).

5.4 Discussion

The results of this study indicate the potential to use CVD-based polymer coating for immobilization of AdBMP7 and AdPDGF for the purposes of transducing cells locally in specific scaffold regions prior to implantation. Immobilization of the vectors allows for reduced risk of virus dispersion (i.e., systemic effects) and transduction of surrounding tissue compared to ex vivo transduction of cells that are not necessarily contained to the defect site post-implantation. Specifically, this surface modification technique immobilizes the virus onto the material surface via antigen-antibody interaction, such that the virus is released from the PCL/PLGA surface only when it comes in contact with and binds to protein receptors on the target cell's membrane, followed by its entry into the cell thorough the cell's phospholipid bilayer. The virus particle number (PN) selected for immobilization onto the scaffold surface was based on previous verification of total virus attachment on the surface, which indicates that use of a PN of 10^{12} resulted in higher virus attachment density on PLGA (~90 PN/ROI using PN=10^{12} compared to ~20 PN/ROI using PN=10^{11}) with no significant differences observed on PCL PLGA (~250 PN/ROI using PN=10^{12} compared to ~190 PN/ROI using PN=10^{11}) with an ROI of 101.4 μm^2. Multiplicity of infection (MOI), which corresponds to the number of virus particles used to target a cell (i.e., MOI=300 where the ratio is 300:1) was also determined based on the results from the study by Hao et al, where a range of 50-400 MOI was tested, with MOI=300 being optimal. Given that the total amount of virus attached to the scaffold surface increased using a higher PN, SEM images as well as the total number of cell transduced was shown to increase correspondingly, thereby confirming that the virus stays on the polymer surface [2]. The primary use of SEM imaging of the virus particles on the surface in this study was not only to confirm its presence, but also ascertain that the complex 3D morphology of the scaffold allowed for equal distribution of viral particle attachment throughout the scaffold.

Likewise, the use of cell transduction in order to stimulate growth factor expression in place of direct growth factor delivery has advantages such as extending the otherwise transient GF bioactivity, as well as avoiding short half lives and dissolution rates that are too fast. Gene therapy has been investigated widely as an alternative to direct growth factor delivery, specifically with the use of adenoviruses, which show high transduction efficiency *in vivo* [7]. The selection of PDGF-BB and BMP7 for this study stems from the fact that recombinant PDGF and BMPs (i.e., rhBMP2) are already FDA-approved for clinical use in periodontal and oral surgery (i.e., alveolar ridge augmentation, sinus elevation). Both growth factors are known as stimulators of mesenchymal progenitor cell recruitment, with BMP having osteo-inductive properties [8]. In this study, we show that CVD-based immobilization of growth factors (BMP7 specifically) yields bone *in vivo* while allowing for the local transduction of cells only at designated regions of the scaffold, as opposed to *ex vivo* transduction of cells prior to cell seeding onto a scaffold. In support of other groups who have previously used CVD for the purposes of gene therapy vector delivery [2, 4, 6] this study also confirmed that virus immobilization and subsequent growth factor expression is successful on geometrically complex (i.e., 3D-printed, micropatterned) scaffolds (**Figures 5.2, 5.5**).

Various improvements from the previous study reported in Chapter 4 were made prior to implementing the immobilization of growth factors, including the use of polymer (PCL-PLGA) for the micropatterned film with a faster rate of degradation compared to PCL alone. The use of PLGA alone resulted in deformation to the pillars on the patterned film (as observed in the ectopic murine model pilot study, **Figures 5.8 and 5.9**), despite 75:25 PLGA, which has a slower degradation rate given the higher ratio of lactic acid to glycolic acid. However, due to the faster rate of hydrolysis than PCL, the result is increased deformation that is more prevalent and noticeable with time, especially in the absence of bone tissue which may limit the hydrolysis rate and also stabilize the polymer in place which reduces any noticeable deformation during histological analysis. Overall, the re-designed patterned film was shown to support cellular alignment (**Figures 5.3, 5.4**), given that despite the difference in the polymer, the topographical cues incorporated into the material remained the most important factor in determining cellular behavior. This was not transferred over to *in vivo* cell alignment in the first pilot study (**Figure 5.8**) given that the cells were encapsulated in a thrombin/fibrinogen hydrogel during seeding, which is likely to have prevented cellular contact with grooves in order to allow for contact

guidance in the first 24 hours prior to implantation. This was improved upon in the rat fenestration defect study (as well as a single mouse assessment), resulting in improved tissue alignment observed in sections stained with H&E (**Figures 5.9, 5.14**).

The variation in bone volume among scaffold groups in the experimental group (ectopic murine model) was greater than expected, with approximately half of samples in the experimental group showing osseous tissue infiltration into the patterned "PDL" region. A potential explanation of this is because the 3D printed scaffold region is immobilized with gene therapy vectors on all sides of the scaffold, such that the top region onto which the patterned film is press-fit is also in contact with the transduced hGF cells which can migrate along the porous "PDL" film base into the pillar regions (**Figure 5.7**). When comparing this result to the bone regeneration observed in the rat fenestration defect pilot study, there is a noticeable decrease in the osseous tissue presence in the defect site relative to the areas adjacent to it (**Figure 5.13**). However, due to the thickness of the patterned film (~500um), the amorphous PCL film designated to serve as a vehicle for transduced hGF cells ended up being positioned mostly outside of the defect. In order to better customize the scaffold for use in a rat fenestration defect, the next generation of scaffolds (discussed in Chapter 6) had the following improvements: (1) Decreased pillar height from 250um down to 100um (average thickness of native rat PDL), (2) reduced base thickness of patterned film to 100um, and base thickness of amorphous film to 150um for a total combined scaffold width of 250um, given that the rat fenestration defect depth is on average 500um (250um [amorphous film] + 100um [pillar height] + 150um [patterned film porous base] = 500um total).

Additionally, in the rat fenestration defect pilot study, we failed to observe bone formation in the control groups (i.e., no cell pre-seeding prior to implantation). The option of implanting the prepared scaffold without cell seeding (i.e., allowing for transduction of the endogenous cell population) would be a more clinically-relevant approach that would eliminate an additional step in the preparation process. A potential explanation for why no bone formation was observed is that once the material is implanted (i.e., biomaterial, medical device, prosthesis), there is a foreign body reaction—the material comes in contact with inflammatory cells (i.e., macrophages, foreign body cells) [9-12]. The use of nude mice/athymic rats (i.e., lack of a thymus gland resulting in the absence of T cells) allows for implantation and engraftment of human-derived cells. However, other immune-derived cells are present which interact with the implanted material at the tissue/biomaterial interface: the presence of viral vectors can activate macrophages. Likewise,

127

when the scaffold is exposed to host proteins (i.e., albumin, fibrinogen, fibronectin, and others) that may form a layer on the surface prior to it coming in contact with host cells. As such, this may prevent host cells from being exposed to the immobilized gene therapy vectors (i.e., AdBMP7), thereby resulting in the lack of bone formation observed [10]. Overall, it is possible that the adenovirus may infect macrophages or other inflammatory cells that come in contact with the gene therapy vectors in place of the host cells: a number of studies have verified that macrophages can be infected with adenovirus, in response to which they undergo pro-inflammatory nectoric death in vivo, with a recent study further confirming this through the identification of an adenovirus receptor in mice macrophages [21, 22]. Given this likelihood of infection, the immobilized adenovirus is not able to access the host cell population, thereby requiring a different scaffold design in order to mask it from host proteins and inflammatory cells until later in the wound healing stage when the gene therapy vectors can be made available to transduce the host cell population instead. For example, the scaffold may be designed in layers such that the outer regions are not immobilized with the adenovirus while the inner regions are, allowing the presentation of the gene therapy vectors to the host cell population over a prolonged period of time corresponding to the rate of scaffold degradation. Likewise, it may be possible to mask certain layers of the scaffold during CVD coating using low-melting polyester wax so as to allow spatial control of virus immobilization on dedicated regions of the scaffold [23]. An additional strategy to attract host cells to the scaffold may be to incorporate the initial delivery of BMP7 and PDGF without the use of adenovirus into the scaffold in order to allow these growth factors to recruit cells through their mitogenic/morphogenic and chemotactic properties in the first stages of the wound healing process, followed the exposure of scaffold sites with immobilized adenovirus during scaffold degradation, allowing for the transduction of the host cells and pro-longing growth factor expression.

Other ideas for scaffold design can be based on previous studies that have successfully transduced host cells in vivo as opposed to ex vivo: A previous study by Liao IC et al addressed this limitation through the fabrication of adenovirus-encapsulated fibrous scaffolds via electrospinning (i.e., polyethylene glycol (PEG)-based porogen was incorporated into the fiber shells during the fabrication process, leaving a space inside the fibers on the order of nanometers for the transport of viral particles), showing that viral vector-based macrophage cell activation was reduced due to the encapsulation of the adenovirus within core-shell polycaprolactone (PCL)

128

fibers. Specifically, when macrophages were cultured *in vitro* on virus-encapsulated scaffold, they were shown to produce anti-viral cytokines that are pro-inflammatory at much lower levels than macrophages with direct exposure to adenoviruses. At the same time, virus-encapsulated scaffolds cell seeded with human embryonic kidney (HEK 293) cells showed prolonged transgene expression for a period of more than 1 month [13]. This suggests a potential future direction of investigation, focusing on immobilizing the adenovirus in such a way that it can be encapsulated within the scaffold and transduce the host cells over time as the biomaterial degrades *in vivo.*

5.5 Conclusion

This study supports the potential of polymer-immobilized delivery of gene therapy vectors for *in vivo* tissue regeneration, with ongoing studies investigating use of CVD-coated scaffolds in a cell-free approach. There is clear indication that immobilization of gene therapy vectors onto the scaffold surface has potential to be used clinically where both the periodontal ligament and bone are damaged. In this study, noticeable tissue alignment (guided by scaffold morphology) and significant bone formation (possibly due to transduced hGF cell expression of BMP7 via immobilized gene therapy vector) was observed in a pilot study using a rat fenestration defect. In a potential clinically-relevant scenario, this reduces the additional step of having to transduce patient cells *ex vivo* prior to cell seeding—instead, once the scaffold is fully prepared (including steps involved in surface modification), all that remains is to seed patient-derived cells prior to implantation. Future research will focus on optimizing both the scaffold geometry and gene therapy vector localization in order to make the final regenerative outcome more predictable.

Additionally, this chapter introduces the use of an amorphous PCL film for the "bone" region of the scaffold, eliminating the use of the 3D-printed region for the rat fenestration defect, primarily due to the size constrains of the 3mm x 2mm defect with a depth of approximately 0.5mm. This highlights some of the limitations of using current 3D printing technology, not limited to selective laser sintering, for periodontal tissue engineering given that many printers still have relatively low resolution that does not enable the formation of scaffolds with adequate porosity for smaller defects [14]. Typically, when designing a scaffold for a patient or animal defect, CT imaging data is needed to approximate the defect, as was done here using the rat fenestration defect model. However, technical limitations exist and need to be addressed in the future to better assist the translation of this approach to clinical defects, given the following: (1) potential for errors

associated with the import of CT scan data during image acquisition (i.e., pixel sizes, thickness of slices) that can produce errors during virtual reconstruction, (2) difficulty obtaining high-quality scans that allow for accurate scaffold design approximations especially in the potential presence of human/animal movement, and (3) scaffold manufacturing that can produce so-called "stair-step" artifacts as well as irregular surface features that are not originally present in the design, and may not seem relevant on the macro-scale, but can have significant effects on the micro-scale levels at which cells sense the surface, especially in bone-ligament interfaces that exist in the periodontium where the PDL region may be only 100um (rat) or 250um (human) in width [15-20].

5.6   References

[1]   Pilipchuk SP, Monje A, Jiao Y, Hao J, Kruger L, Flanagan CL, Hollister SJ, Gianobile WV. Integration of 3D printed and micropatterned polycaprolactone scaffolds for guidance of oriented collagenous tissue formation in vivo. *Adv Healthc Mater,* 2016; 5(6): 676-87.

[2]   Hao J, Cheng KC, Kruger LG, Larsson L, Sugai JV, Lahann J, Giannobile WV. *Adv Mater*, 2016; 28(16):3145-51.

[3]   King WJ, Krebsbach PH. Growth factor delivery: how surface interfactions modulate release in vitro and in vivo. *Adv Drug Deliv Rev,* 2012; 62(12): 1239-1256.

[4]   Elkasabi YM, Lahann J, Krebsbach PH. Cellular transduction gradients via vapor-deposited polymer coatings. *Biomaterials*, 2011: 32(7):1809-15.

[5]   Zhang Y, Deng X, Scheller EL, Kwon TG, Lahann J, Franceschi RT, Krebsbach PH. The effect of Runx2 immobilization on PCL on osteoblast differentiation of bone marrow stromal cells in vitro. *Biomaterials*, 2010; 31(120):3231-3236.

[6]   Zhang Y, Miron RJ, Li S, Shi B, Sculean A, Cheng X. Novel mesoporous bioglass/silk scaffold containing adPDGF-B and adBMP7 for the repair of periodontal defects in beagle dogs. *J Clin Periodontol*, 2015;42(3):262-71.

[7]   Ramseier CA, Abramson ZR, Jin Q, Giannobile WV. Gene therapeutics for periodontal regenerative medicine. *Dent Clin North Am*, 2006:50(2):245-63.

[8]   Larsson L, Decker AM, Nibali L, Pilipchuk SP, Berglundh T, Giannobile WV. Regenerative medicine for periodontal and peri-implant diseases. *J Dent Res,* 2016;95(3):255-66.

[9]   Anderson JM, Rodriguez A, Chang DT. Foreign body reaction to biomaterials. *Semin Immunol*, 2007;20(2):86-100.

[10]   Moore LB, Kyriakides TR. Molecular Characterization of Macrophage-Biomaterial Interactions. *Adv Exp Med Biol,* 2015;865:109-122.

[11]   Bryers JD, Giachelli CM, Ratner BD. Engineering biomaterials to integrate and heal: the biocompatibility paradigm shifts. *Biotechnol Bioeng*, 2012: 109(8): 1898-1911.

[12]   Sheikh Z, Brooks PJ, Barzilay O, Fine N, Glogauer M. Macrophages, foreign body giant cells and their response to implantable biomaterials. *Materials (Basel)*, 2015;8(9):5671-5701.

[13]   Liao IC, Chen S, Liu JB, Leong KW. Sustained viral gene delivery through core-shell fibers. *J Control Release*, 2009; 139(1):48-55.

[14]   Hokmabad R, Davaran S, Ramazani A, Salehi R. Design and fabrication of porous biodegradable scaffolds: a strategy for tissue engineering. *J Biomater Sci Polym Ed.* 2017;28(16):1797-1825.

[15]   Kim K, Yeatts A, Dean D, Fisher JP. Stereolithographic bone scaffold design parameters: osteogenic differentiation and signal expression. *Tissue Eng Part B Rev.* 2010; 16(5): 523–539.

[16]   Chia NH, Wu BM. Recent advances in 3D printing of biomaterials. *J Biol Eng.* 2015, 1;9:4.

[17]   Brunello G, Sivolella S, Meneghello R, Ferroni L, Gardin C, Piattelli A, Zavan B, Bressan E. Powder-based 3D printing for bone tissue engineering. *Biotechnol Adv.* 2016;34(5):740-753.

[18]   Gaviria L, Pearson JJ, Montelongo SA, Guda T, Ong JL. Three-dimensional printing for craniomaxillofacial regeneration. J Korean Assoc Oral Maxillofac Surg. 2017;43(5):288-298.

[19]   Lee CH, Hajibandeh J, Suzuki T, Fan A, Shang P, Mao JJ. Three-dimensional printed multiphase scaffolds for regeneration of periodontium complex. Tissue Eng Part A. 2014 Apr;20(7-8):1342-51.

[20]   Roseti L, Parisi V, Petretta M, Cavallo C, Desando G, Bartolotti I, Grigolo B. Scaffolds for bone tissue engineering: state of the art and new perspectives. *Mater Sci Eng C Mater Biol Appl,* 2017;78:1246-1262.

131

[21]   Di Paolo NC, Doronin K, Baldwin LK, Papayannopoulou T, Shayakhmetov DM. The transcription factor IRF3 triggers "defensive suicide" necrosis in response to viral and bacterial pathogens. *Cell Rep*, 2013;3(6):1840-6.

[22]   Maler MD, Nielsen PJ, Stichling N, Cohen I, Ruzsics Z, Wood C, Engelhard P, Suomalainen M, Gyory I, Huber M, Müller-Quernheim J, Schamel WWA, Gordon S, Jakob T, Martin S, Jahnen-Dechent W, Greber UF, Freudenberg MA, Fejer G. Key Role of the Scavenger Receptor MARCO in Mediating Adenovirus Infection and Subsequent Innate Responses of Macrophages. *mBio*, 2017 8(4): e00670-17.

[23]   Hu WW, Elkasabi Y, Chen HY, Zhang Y, Lahann J, Hollister SJ, Krebsbach PH. The use of reactive polymer coatings to facilitate gene delivery from polycaprolactone scaffolds. *Biomaterials.* 2009 Oct; 30(29): 5785–5792.

CHAPTER 6

EFFECT OF IMMOBILIZED ADENOVIRAL PLATELET-DERIVED GROWTH FACTOR (PDGF) AND BONE MORPHOGENETIC PROTEIN (BMP-7) DELIVERY ON PERIODONTAL TISSUE REGENERATION IN VIVO USING MICROPATTERNED SCAFFOLDS

Contributions to the data collection/analysis that are part of this chapter were made by:
Drs. Farah Asa'ad (*Department of Biomedical, Surgical & Dental Sciences, University of Milan, Italy*), Tobias Fretwurst *(Department of Oral- and Craniomaxillofacial Surgery, Center for Dental Medicine, University Medical Center Freiburg, Germany)*, Lena Larsson *(Department of Periodontology, Institute of Odontology, University of Gothenburg, Sweden),* Ning Yu *(Periodontics and Oral Medicine, University of Michigan).*

6.1   Introduction

The development of biomaterial systems intended for the regeneration of specific tissue typically includes the consideration of multiple design criteria, including scaffold material selection, topography, as well as intended inclusion of growth factors and/or cells natively expressed in the tissue. Design for the regeneration of periodontal tissue specifically requires the consideration of its anatomical complexity: the alveolar bone-periodontal ligament (PDL)-cementum complex consists of alveolar bone transitioning into bundle bone that houses Sharpey's fibers which are extending from the PDL, a collagen III-rich collagenous soft tissue that further anchors into the cementum, a mineralized layer that covers the tooth root's dentin surface (**Figure A1.1** in Appendix). Many studies have examined the scaffold design that would allow for multi-tissue regeneration relevant to periodontal tissue engineering [1-5]. Most recently, 3D-printed, micropatterned scaffolds detailed in Chapters 4-5 were developed with emphasis on the use of grooves in the PDL scaffold compartment for promoting cellular alignment and subsequently aligned collagenous tissue formation [6]. Previous studies have established that topography allows for the functional regulation of cells derived from various types of tissues, including myocardium

and nerve [7-10]. To build upon previous findings, this study focused on improving the existing scaffold design for better adaptation to a fenestration defect of a rat model, while also introducing growth factors through adenoviral BMP-7 and PDGF-BB immobilized onto the scaffold surface through chemical vapor deposition (CVD)-based polymer surface modification to improve both the localization and spatio-temporal distribution of gene therapy vectors.

Bone morphogenetic protein (BMP) is a widely known growth and differentiation factor, as well as a chemotactic agent, stimulating cell migration, angiogenesis, and differentiation of MSCs into bone forming cells and cartilage. Platelet derived growth factor (PDGF) has been shown to promote the regeneration of alveolar bone, PDL, and cementum, with PDL and alveolar bone cells showing the presence of PDGF cell surface receptors, thereby effecting their chemotaxis and proliferation. PDGF-BB specifically has been shown as a safe and effective treatment of periodontal osseous defects, with clinical data confirming that it can be used to achieve significant improvements in clinical and radiographic parameters in moderate-to-severe cases of 2 and 3-wall periodontal infrabony defects [11-12]. The selection of PDGF-BB and BMP-7 for this study stems from previous work establishing the optimal methods for transduction of human gingival fibroblast (hGF) cells with Ad-BMP7 and PDL cells with AdPDGF-BB. For example, Jin QM et al previously used Ad-BMP7 ex vivo gene transfer to transduce syngeneic dermal fibroblasts, showing osteogenesis, cementogenesis, and bridging of periodontal bone defects in a rat wound repair model. Likewise, Chang PC et al confirmed that AdPDGF-B delivery via a collagen matrix to rat alveolar bone defects could have clinical applications for treatment of bone in the oral and craniofacial regions [13-15].

Other groups have also pursued this method in combination with biomaterials to serve as scaffolds for tissue regeneration, including the following: Zhang et al recently showed that use of a mesoporous bioglass (MBG)/silk fibrin scaffold in combination with AdBMP7 and AdPDGF in beagle dog periodontal defects promoted periodontal regeneration when both gene therapy vectors were used in unison as opposed to individually [16]; previous to that, Zhang et al had also shown that chitosan/collagen scaffolds combined with AdBMP7 or AdPDGF-B and seeded with hPDL cells did not show cytotoxicity, with AdPDGF-hPDL resulting in higher proliferation rate while scaffolds with AdBMP7-hPDL resulted in hPDL cells having a stronger tendency to differentiate towards a osteoblast phenotype *in vitro*. This study also showed *in vivo* implantation of the scaffolds in beagle dog periodontal defects resulted in significant increases in bone formation using

AdBMP, but the combination of both growth factors produced the highest increase through synergistic effects [17]. However, the main limitation of using adenoviral-based gene therapy vectors has been the potential for virus dispersion and lack of spatio-temporal control of gene expression.

Most recently, Hao J et al used chemical vapor deposition (CVD)-based polymer coatings as surface treatment for 2D and 3D-shaped biomaterials to examine the transduction of hPDL and hGF cells with AdPDGF-BB and AdBMP7, respectively, to examine the production of these growth factors *in vitro* [18]. Based on their findings and methodology, it is possible to have more defined control over cell transduction such that only those cells that are in contact with certain regions of the scaffold can be transduced. Chapter 6 confirmed that this strategy can be applied for the transduction of hPDL cells on patterned regions of the scaffold developed specifically for a rat fenestration defect, with immobilization of either AdBMP7 or AdPDGF-BB. This study further investigates the effects of combined and single growth factor delivery (BMP7, PDGF-BB) on periodontal regeneration in combination with changes in the topography of the PDL region of the scaffold (i.e., patterned versus amorphous), presenting the first known in-depth assessment of scaffolds with immobilized gene therapy vectors applied as an implant *in vivo*, for periodontal tissue engineering or otherwise.

6.2 Materials and Methods

6.2.1 Preparation and surface modification of scaffolds for rat fenestration defect

Preparation of the micropatterned films (for the "PDL" region of the scaffold) and amorphous films (for the "bone" region of the scaffold) was undertaken as described in Chapter 5 (Sections 5.2.1 and 5.2.2), with some modification described here. Briefly, a solution of 5% PLGA-PCL (50/50) ((75:25, 137kDa, Evonik Industries) was used to cast the pillar spaces within a PDMS mold with a design to accommodate the parameters necessary for a rat fenestration defect (Design specifications: 100 um (pillar height), 150 um (inter-pillar distance), 150 um x 150um (pillar length x width), with 15um wide/30um deep grooves). A solution of 10% PCL was cast onto the filled pillars while adding sugar particles (≤75um), in order to create a base of 150um in thickness. After drying overnight under vacuum, the sugar was leached out in deionized water. An amorphous PCL film based was formed in a similar manner, with a final base thickness of 250um, such that the combined scaffold construct could fit within a 0.5mm deep fenestration defect.

Similarly, in order to test the effect of topography on PDL regeneration, an amorphous and porous PCL-PLGA (50/50) film was also formed (total thickness of 250um) using the same technique. Following scaffold fabrication, each of the films was surface treated on each side using chemical vapor deposition (CVD), as previously described. Briefly, the coating process consisted of fixing the scaffolds inside the deposition chamber, the starting material sublimated at 120°C and pyrolyzed 540 °C to allow for deposition and polymerization on scaffold surface. Afterwards, all films were sterilized in 70% ethanol (1hr) to prepare for virus immobilization and subsequent cell seeding.

For gene therapy vector immobilization, scaffolds were treated with 10 μg/mL solution of goat anti-adenovirus (AbD Serotec; 0151- 9004) polyclonal antibody in phosphate-buffered saline (PBS), incubated in solution overnight (4°C), rinsed in PBS (5 times by 5 min), incubated in 12 mL cold adenovirus solution (4 hrs at 4°C), and again rinsed in PBS (5 times by 5 min). The adenovirus solution (10^{12} particle number) either had empty vectors without a transgene (Ad-empty), or vectors expressing PDGF-BB or BMP7 genes (prepared by University of Michigan Vector Core). Human periodontal ligament (hPDL) or human gingival fibroblast (hGF) cells were seeded onto the "PDL" (patterned or amorphous) region and "Bone" (amorphous) region of the scaffold, respectively, with $5.0*10^5$ cells per film (both sides), allowing for the cells to attach before transferring them to a well with fresh medium. Afterwards, all scaffolds with seeded cells were incubated overnight prior to analysis/surgical implantation.

6.2.2   *Scanning electron microscopy (SEM), barium sulfate treatment*

Scanning electron microscopy (SEM) was performed at Microscopy and Image Analysis Laboratory (University of Michigan) using an Amray FE 1900 SEM to image patterned 3D films. Prior to imaging, the films were gold sputter-coated and observed at an acceleration voltage of 5kV. Each scaffold region (i.e., patterned film and amorphous film) was exposed to 20% barium sulfate for 30 minutes prior to being placed into a sample pre-made rat fenestration defect (~3mm x 2mm) on a dried, sterilized mandible for micro-CT scanning to check on the scaffold adaptation.

6.2.3   *In vivo implantation: Rat fenestration defect*

The *in vivo* study design consisted of the following 5 groups (**Figure 6.1**): (1) a negative control with CVD-treated, amorphous ("PDL" region) and amorphous ("bone" region) films with Ad-empty in all regions, (2) a positive control with CVD-treated, patterned film with amorphous

film and AdPDGF-hPDL and AdBMP7-hGF, respectively, (3) a CVD-treated, patterned film and amorphous film with AdBMP7-hGF in both regions, (4) a CVD-treated amorphous films, one with AdPDGF-hPDL and the other with AdBMP7-hGF delivery, and (5) a CVD-treated, patterned film and amorphous film with Ad-empty in all regions. The time points tested specific to tissue regeneration were at 3 and 6 weeks. Two groups (positive and negative controls) were also extended to a 9 week time point (n=6), with the intention of looking at retention of human-based cells at early and late time points, as well as the mechanical properties of regenerated bone and PDL-like tissue both at weeks 3 and 9. As such, groups (1-2) for the 3 week time point had a total number of n=10 for the positive/negative control groups and n = 6 for the remaining groups (3-5), groups (1-5) for the 6 week time point has an n=6, and groups (1-2) for the 9 week time point had a total of n=5.

Athymic rats (250g, Charles River Laboratories Inc., Wilmington) were ordered, general anesthesia performed under isofluorane during periodontal defect creation, with a single fenestration defect (3 x 2mm^2) created for each animal on the buccal side of the right mandible such that the distal root of the first molar tooth was exposed. The cementum layer was also carefully removed to expose the dentin surface, after which the "PDL" region film (i.e., patterned or amorphous) was positioned with the pillars against the dentin, followed by the amorphous PCL film directly above. The site was sutured and closed with surgical staples, with administration of analgesic subcutaneously at 24 hrs post-surgery. After 3, 6 and 9 weeks, specimen were harvested and fixed in 10% buffered formalin phosphate solution for 2 days before being transferred into 70% ethanol for micro-CT scanning, followed by decalcification. All animal studies were performed with approval from University of Michigan-University Committee on Use and Care of Animals (UM-UCUCA) according to ARRIVE guidelines for preclinical studies.

6.2.4 *Micro-computed tomography (micro-CT) and histomorphometry*

Micro-CT was also used for purposes of evaluating bone regeneration post-implantation: Tissue-fixed specimens were embedded in alginate, scanned using micro-CT (Scanco Medical) at a resolution of 12um, at 70kV energy and 114uA intensity, and calibrated to Hounsfield units (HU). Bone volume (BV) and tissue mineral density (TMD) were determined for internal and external regions of the bone compartment using Microview software (Parallax Innovations) with a threshold of HU=1050 for bone. After scanning, samples were decalcified in 10% EDTA,

embedded in paraffin, and cut into 5um sections for histological analysis using hematoxylin and eosin (H&E).

6.2.5 Immunohistochemistry for anti-human nuclear staining

Sections, about 5 μm thick, were de-waxed and incubated in DIVA antigen retrieval solution (Biocare medical, Concord, CA) at 60°C over night. The sections were incubated with 3% bovine serum albumin (BSA) for blocking of unspecific binding followed by incubation overnight at 4°C with primary antibody mouse anti-human nuclei diluted 1:100 (MAB 1281, EMD Millipore Corp, Temecula, CA) over night at 4°C. The sections were then incubated with MACH4 polymer (Biocare medical) for 30 min. Positive cells were detected using DAB substrate (Biocare medical). The sections were counterstained using haematoxylin.

6.2.6 Immunofluorescence, periostin fluorescence intensity profiles

Sections, about 5 μm thick, were de-waxed and incubated in DIVA antigen retrieval solution (Biocare medical, Concord, CA) at 60°C over night. The sections were incubated with 3% bovine serum albumin (BSA) for blocking of unspecific binding followed by incubation overnight at 4°C with the following primary antibodies (Dilution 1:500): anti-periostin (rabbit polyclonal, ab14041, Abcam, USA) and anti-collagen III (mAB ab6310, Abcam, USA), The sections were then incubated with Alexa-conjugated secondary antibodies: Alexa-488 anti-mouse (dilution 1:200) and Alexa-555 anti-rabbit (dilution 1:200) for 2 hours at room temperature. The sections were treated with 4',6-diamidino-2-phenylindole (Prolong Gold Antifade Reagent with DAPI; Life Technologies) to visualize the cell nuclei. Additionally, a separate analysis of periostin-stained slides only were performed for each group. Specifically, in order to compare the mean fluorescence intensity of periostin at sites of regenerated PDL-like tissue to sites directly opposite on the same sample where there is native PDL, a total width of 100um (approximate rat PDL width) was selected in the regenerated and native PDL regions in order to calculate the ratio of periostin intensity for each group (n=6) (i.e., mean periostin intensity at regenerated tissue site/mean expression at native site). In addition to this quantification, an expression profile was generated for samples from each group. Finally, in order to quantify scaffold displacement and total PDL-like tissue width in all groups, toluidine blue staining was performed (n=6) to allow better

distinction between the bone and soft tissue areas. Slides were de-waxed and stained with toluidine blue for approximately 1hr prior to washing in deionized water.

6.2.7 Nanoindentation

Mandibles reserved for nanoindentation were frozen after harvesting at 3 and 9 weeks post-implantation. Sample preparation for mechanical testing consisted of the following: thawing the frozen sample, trimming the mandible to only retain the molars by cutting off the incisors and ramus using a low-speed diamond wheel saw (South Bay Technology Inc, San Clemente, CA), embedding the trimmed sample in epoxy resin (EMBED 812 Embedding Kit, Electron Microscopy Sciences, Hatfield, PA), sectioning using a microtome (Leica Biosystems Inc, Germany), and polishing using silicon carbide abrasive paper (2400 grit) under water irrigation for two minutes followed by cleansing to remove particles using ultrasonication in water for 15 minutes. Prior to nanoindentation using the 950 TI TriboIndenter (Hysitron Incorporated, Minneapolis, MN), the sample was glued to a steel stub (Ted Pella, Inc., CA). Indentation was performed using a standard Berkovich diamond probe with a penetration depth of 500 nm, and 3 seconds for each load, hold, and unload [19, 20-22]. Fused silica was used as the calibration standard. The reduced modulus (E_r) and hardness (H) were calculated using the load-displacement curve based on five indents (each 10um apart, in accordance with ASTM standards) at the following four regions for each sample (i.e., distal root of first molar): (1) regenerated PDL-like tissue at original defect site, (2) regenerated alveolar bone at the original defect site, (3) native alveolar bone, and (4) native PDL at the region directly opposite of the defect site. Specifically, the E_r (GPa) is calculated based on Oliver-Pharr analysis using Equation (1), where S (μN/nm) is the contact stiffness (obtained from the unload curve slope, where P is the indentation force and h is displacement), and A is the projected area (nm^2) of elastic contact:

$$E_r = \frac{\sqrt{\pi}}{2} \frac{S}{\sqrt{A}} \quad \text{, where } S = \frac{dP}{dh}\bigg|_{P_{max}} \tag{1}$$

The hardness, H (MPa), is calculated using Equation (2), where P_{max} is the maximum indentation force (μN), A_C is the projected area (nm^2) of contact:

$$H = \frac{P_{\max}}{Ac} \tag{2}$$

All testing was performed at the Michigan Center for Materials Characterization (MC^2, University of Michigan).

6.2.8   Statistical analysis

Data were expressed as mean ± standard deviation of the mean. One-way analysis of variance (ANOVA) with post hoc Tukey's multiple comparison method was used to perform comparative analysis, with a p-value <0.05 (α<0.05) considered significant.

6.3   Results

The *in vivo* study that is the main focus of this chapter was based on the examination of how scaffold topography (primarily in PDL region of the scaffold) and selection of growth factor delivery (i.e., PDGF-BB vs BMP7) influenced periodontal regeneration. As seen in **Figure 6.**1, the groups were divided primarily based on whether PDL scaffold region was patterned or amorphous, and the type of immobilization (i.e., AdBMP7, Ad PDGF, or Ad-empty). Given that the previous pilot study showed that cells should be included (i.e., seeded prior to implantation) in order to allow time for transduction, all groups included cell seeding. This *in vivo* experiment was used to test growth factor delivery on a scaffold consisting of two layers: an amorphous PCL region for the delivery of AdBMP-7 to promote bone regeneration, and a patterned PLGA/PCL region for the delivery of AdPDGF-BB to promote PDL tissue regeneration. The groups tested included single growth factor delivery (i.e., AdBMP-7 only) to both regions of the scaffold. The negative control consisted of an amorphous film in both regions of the scaffold, with an adenovirus encoding an empty vector (Ad-empty vector). Prior to implantation, the scaffolds fabricated to fit the defect (3mm x 2mm x ~0.5mm) were barium sulfate coated to allow for contrast during micro-CT scanning. **Figure 6.2** shows the scaffold assembly: First, the micropatterned (or amorphous) "PDL" region film (PCL-PLGA) is placed such that the pillars are oriented towards the tooth root. The amorphous film (PCL) designed for the "bone" region of the scaffold is then positioned directly on top such that the entire two films are able to fit within the defect. This adjustment to the scaffold thickness (250um total for each film) was made following the results of the pilot rat fenestration defect study described in Chapter 5.
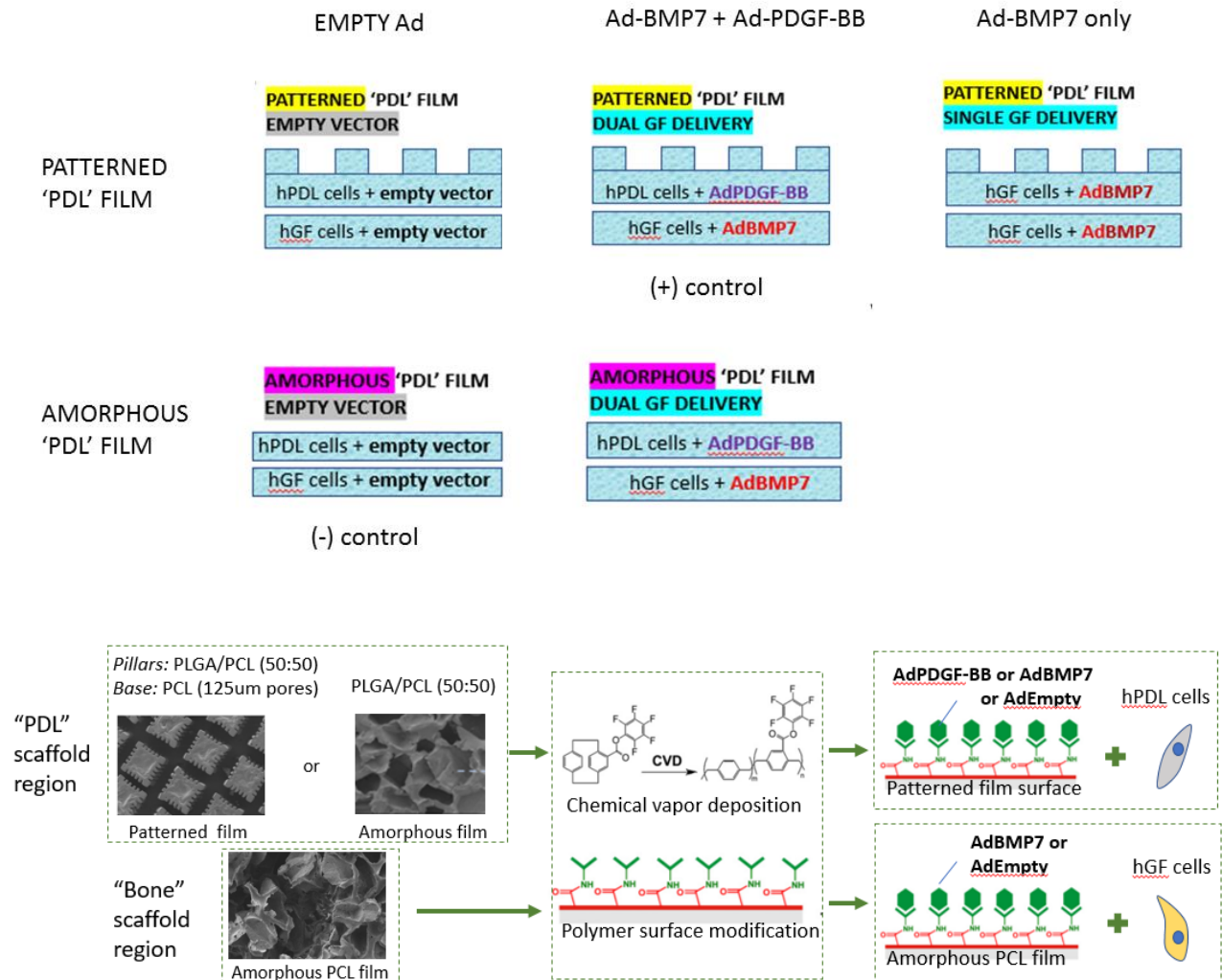
Figure 6.1 Scaffold Groups with/without Growth Factor Delivery in Fenestration Defect
The scaffold design consisted of either a patterned or amorphous PLGA/PCL film for the 'PDL' region, and an amorphous PCL film for the 'bone' region. Adenovirus encoding growth factors were immobilized onto the surface of each scaffold region for dual (i.e., PDGF-BB in the patterned or amorphous 'PDL' region, and BMP7 in the amorphous 'bone' region) or single (BMP7 in the PDL and bone regions) growth factor (GF) delivery. As a control, both regions were also used for delivery of an empty adenoviral vector (Ad), with the scaffolds consisting of an amorphous film for the 'PDL' region serving as the negative (-) control group. All films were seeded with hPDL cells or hGF cells, in the PDL and bone regions of the scaffold, respectively. *Schematic of functional groups shown on sample CVD-coated polymer surface modified from [30].*
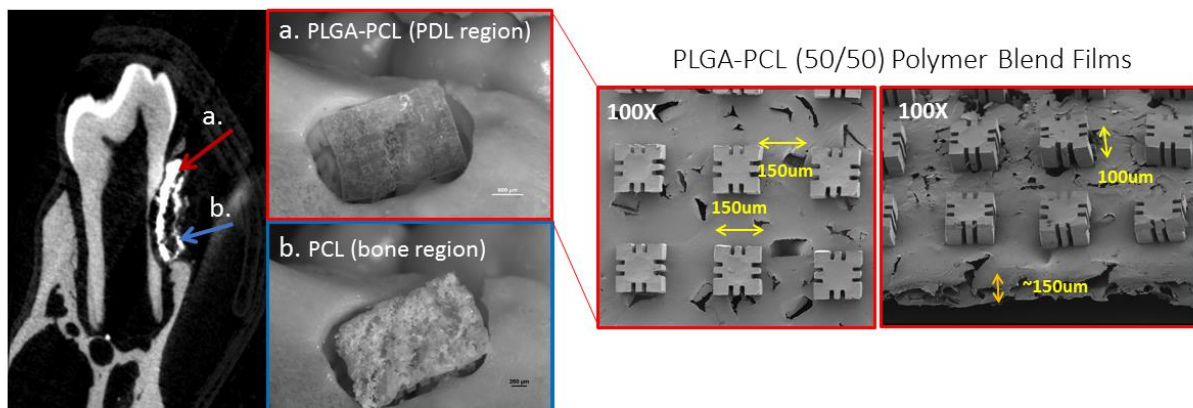
Figure 6.2 Micropatterned Scaffold Design and Adaptation at Rat Fenestration Defect
Barium sulfate-coated regions of the scaffold (micropatterned film in a, amorphous film in b) are shown on a micro-CT scan of a rat fenestration defect to confirm that the scaffold total thickness (500um) conforms to the defect area without over-filling it. SEM images of the PLGA-PCL patterned films (100X) are shown with corresponding measurements of pillar height (100um), inter-pillar distance (150um), and thickness of the porous film base (150um).

After the mandibulae were harvested at weeks 3-9 post-implantation, micro-CT scans were performed for groups at 3 and 6 weeks, revealing that at 3 weeks, limited bone formation was visible in the groups with Ad-empty, compared to groups involving any form of growth factor delivery. By week 6, all groups had almost completely covered tooth roots (including patterned + Ad-empty), except for the negative control (**Figure 6.3**). Analysis of total bone volume at the defect site only (**Figure 6.4**) confirmed significant ($p<0.05$) increases in bone formation in all groups that had growth factor delivery compared to groups with Ad-empty, with lesser differences noted at 6 weeks; tissue mineral density did not show a very noticeable variation among groups at 3 or 6 weeks, except for higher values for TMD for groups with dual GF delivery compared to BMP7 delivery only (**Figure 6.5**). This was further confirmed using an examination of the percentage of bone fill within the original defect site, showing significantly higher ($p<0.05$) bone fill in all groups with growth factor expression compared to the negative control at both 3 and 6 weeks. At 3 weeks, the positive control group bone fill was not significantly different from the empty vector group with a patterned film, and by 6 weeks, all of the groups with growth factor expression did not different in the % of bone fill compared to the empty vector group with patterned film. When comparing changes in bone volume between the 3 and 6 week time points, significant increases were observed in the negative control ($p<0.05$, from 38.2% to 48.1%), empty

vector with patterned film (p<0.05, from 45.6% to 62.7%), and the positive control (p<0.01, from 49.9% to 68.6%). Bone fill in the Ad-BMP7 only group (mean change from 59.3% to 60.3%) and dual growth factor expression using amorphous films group (mean change from 65.8% to 68.0%) did not show any significant changes (**Figure 6.5**).
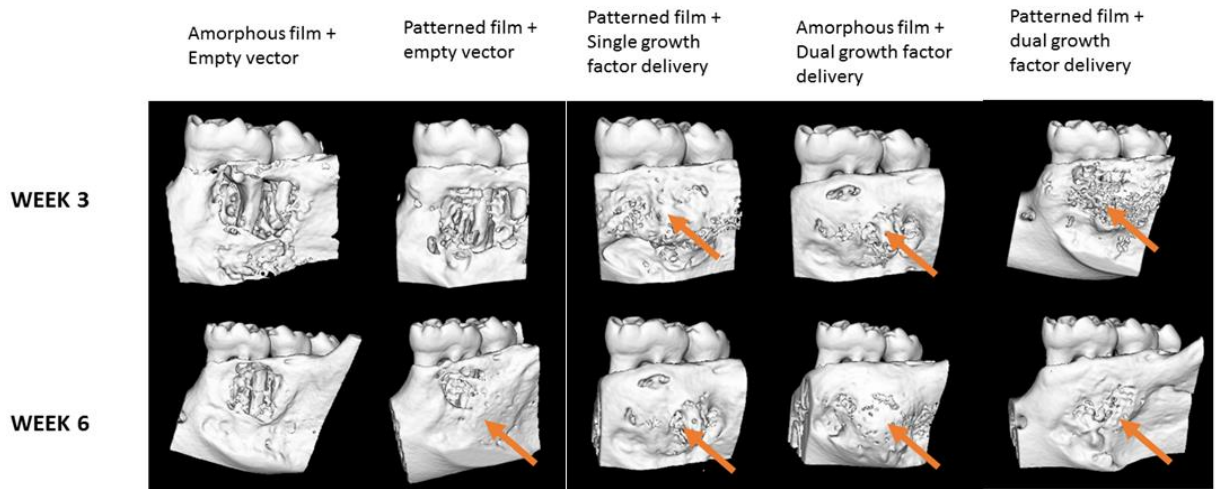

Figure 6.3 Bone Regeneration at 3 and 6 Weeks Post-Implantation
Micro-CT images showing regeneration of bone at 3 and 6 weeks post-implantation of the scaffolds with delivery of adenovirus with empty vector, single growth factor (AdBMP7), or dual growth factor (AdBMP7 and AdPDGF-BB). As indicated by arrows, there is increased coverage of the distal root of the first molar in groups with delivery of AdBMP7 at 3 weeks. By 6 weeks, significant increases in bone regeneration are noted across all groups.
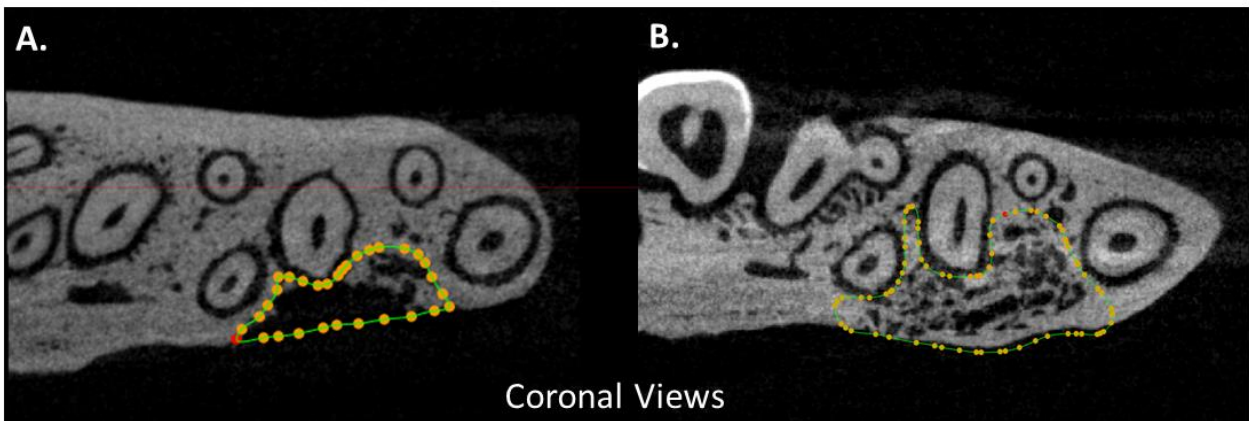

Figure 6.4 Transverse Section View of Bone Regeneration at Defect Site
Micro-CT images showing transverse section of defect site with minimal (A) and maximal (B) bone fill, which is used to determine the total bone volume within the defect at 3 and 6 weeks post-implantation.
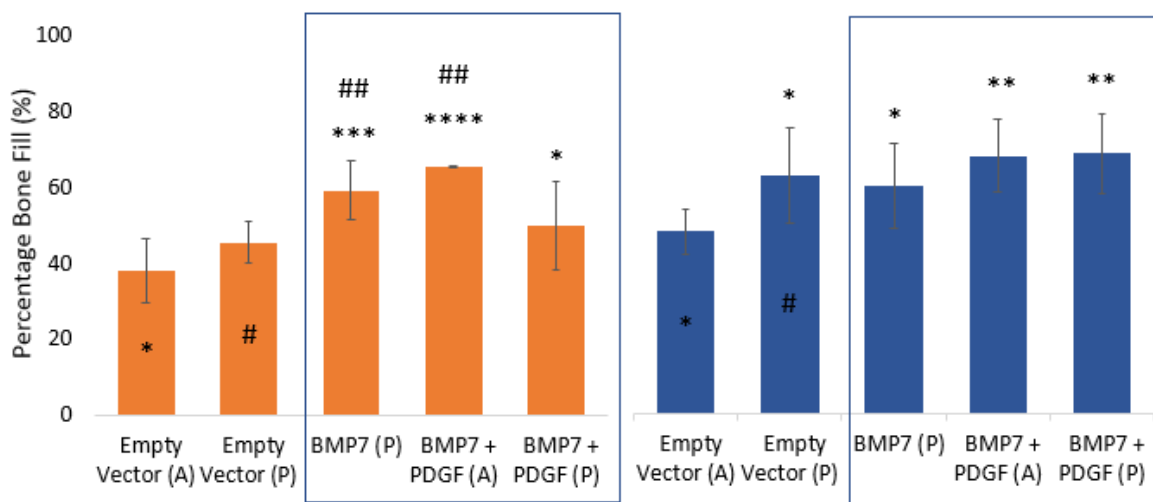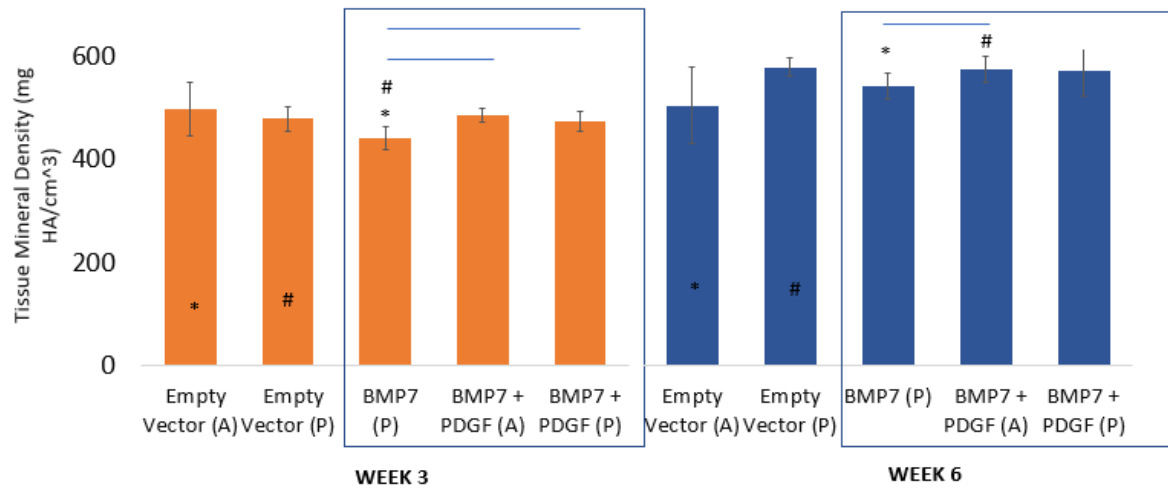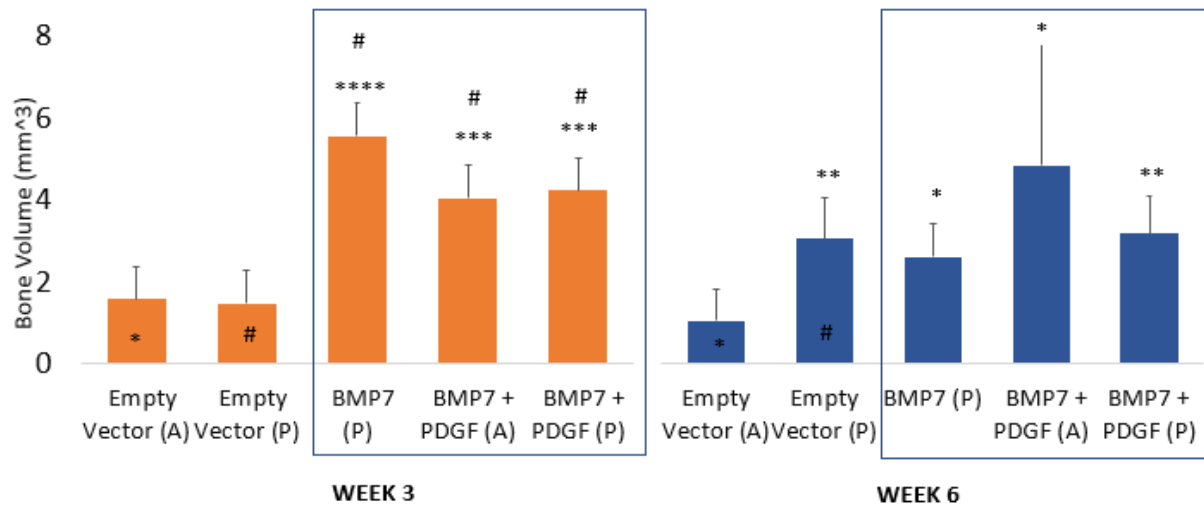
Figure 6.5   Bone Volume, Tissue Mineral Density, and Bone Fill (%) at 3 and 6 Weeks *In Vivo*

Bone volume and tissue mineral density values were obtained based on uCT scans at weeks 3 and 6 post-implantation. The 3 weeks, significant difference (p<0.05) were observed between the patterned 'PDL' film group with single (BMP7) GF expression, and the patterned (P) and amorphous (A) films with dual GF expression for TMD, with differences also observed at 6 weeks between the patterned group with single GF expression and amorphous group with dual GF expression. No significant differences in bone volume were observed among the groups with any form of GF delivery (outlined in blue) at weeks 3 and 6. However, at week 3, all of these groups had significantly higher BV compared to the amorphous group with empty vector (***p<0.001, ****p<0.0001), or patterned group with empty vector (#p<0.05). By week 6, both the patterned group with empty vector and all other groups with any form of GF delivery had significant higher (*p<0.05, **p<0.01) volume of bone formation compared to the negative control (-). Bone fill within the defect site (%) was compared among all groups at weeks 3 and 6, with similar pattern of increased bone formation at defect site observed for groups with growth factor expression and patterned film with empty vector.

Hematoxylin and eosin (H&E) stains at 3 weeks show increased PDL-like tissue present especially in groups with patterned film + AdBMP7-hGF, as well as groups with a patterned film and dual growth factor delivery (**Figure 6.6**). Bone formation is seen at sites close to the PDL-like tissue in all groups, but, interestingly, there is a very clear tendency of the bone to concentrate with the inter-pillar regions, which is observed at all groups with a patterned film. While this may indicate that the patterning may attract osteoblasts due to the difference in material topography, it also explains why there may be bone formation observed quantitatively (as shown in **Figure 6.5**) in the patterned film + AD-empty vector group that is significantly higher compared to the negative control at week 6. However, this also appears to impede the intended orientation of tissue at the pillar grooves so as to form PDL tissue. At the same time, PDL-like tissue does form between the tooth root and regenerated bone, although the patterned film is located behind this initial layer of new bone as opposed to being in front of it, as intended by the design and incorporation of the amorphous region for BMP7-hGF delivery. At week 6, H&E images reveal that more of the tissue bordering the tooth root is becoming increasingly aligned perpendicular to the dentin, as indicated by arrows in **Figure 6.7**, except for the negative control group (amorphous "PDL" film + Ad-empty). Likewise, immunofluorescence images reveal how closely the soft tissue formation is consistent with PDL-like tissue, which also expresses periostin and collagen type III. **Figure 6.8** shows increased collagen III expression specifically in the patterned film + AdBMP7-hGF group as well as the positive control (patterned film + AdPDGF-hPDL). Periostin is more consistently

145

expressed through the PDL-like tissue in groups with dual growth factor delivery only (i.e., with AdPDGF-hPDL in the "PDL" region of the scaffold). By week 6 (**Figure 6.9**), collagen III expression remains consistent with what is observed at week 3, except for an increase in this protein expression in the patterned group with Ad-empty. Overall, groups with patterned films and either single (BMP7) or dual (BMP7 and PDGF) growth factor expression appear to have more PDL-like tissue by week 6, compared to the negative control and amorphous + dual growth factor delivery groups.
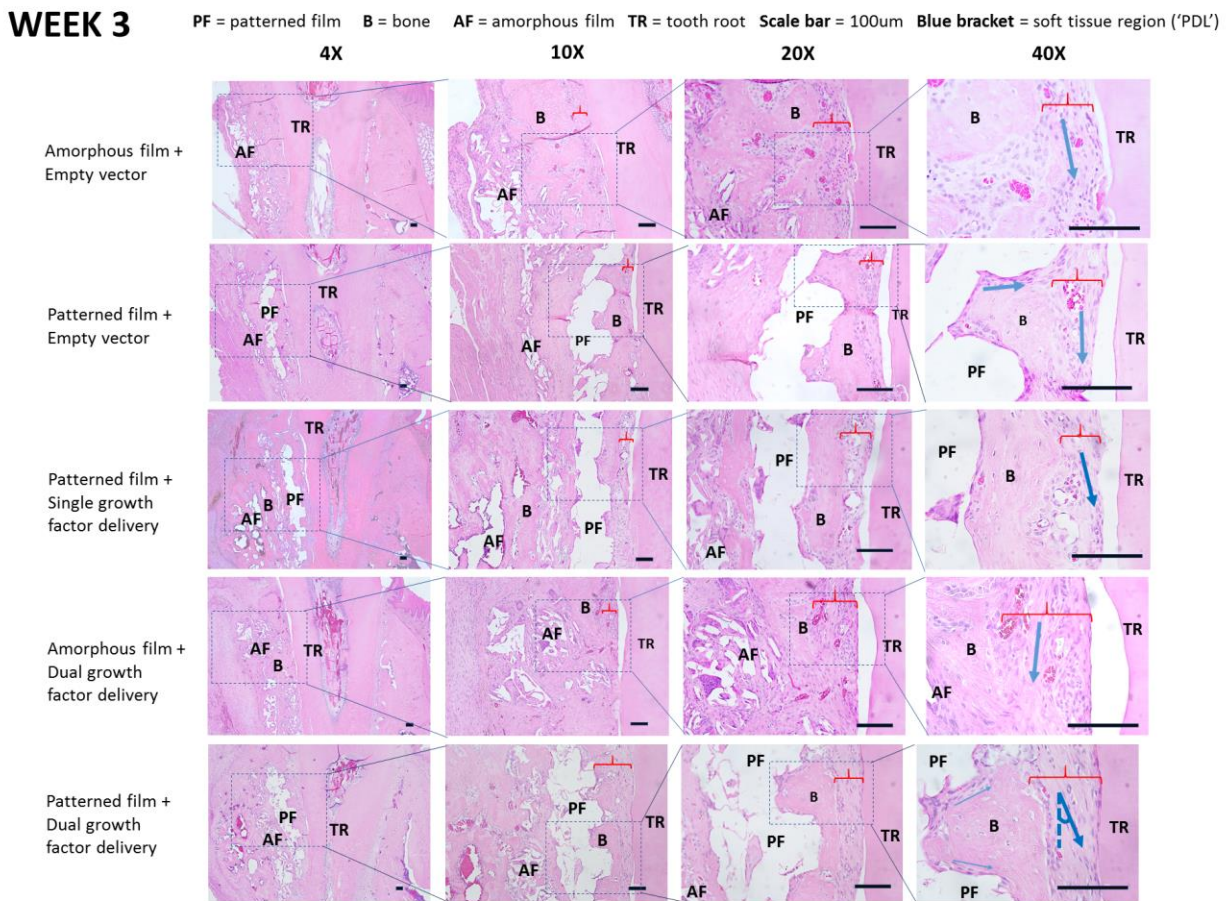

Figure 6.6 Hematoxylin and Eosin (H&E) Staining at 3 Weeks *In Vivo*
Hematoxylin and eosin (H&E) staining to evaluate tissue formation at rat fenestration defect site along patterned films or amorphous films (with dual growth factor delivery (AdPDGF and AdBMP7), single growth factor delivery (AdBMP7), or empty vector) at 3 weeks post implantation in rat fenestration defect. Blue arrows indicate general orientation of cell nuclei relative to the tooth root (TR). Scale bar is 100um for all images. TR = tooth root, AF = amorphous film, PF = patterned film, B = bone.
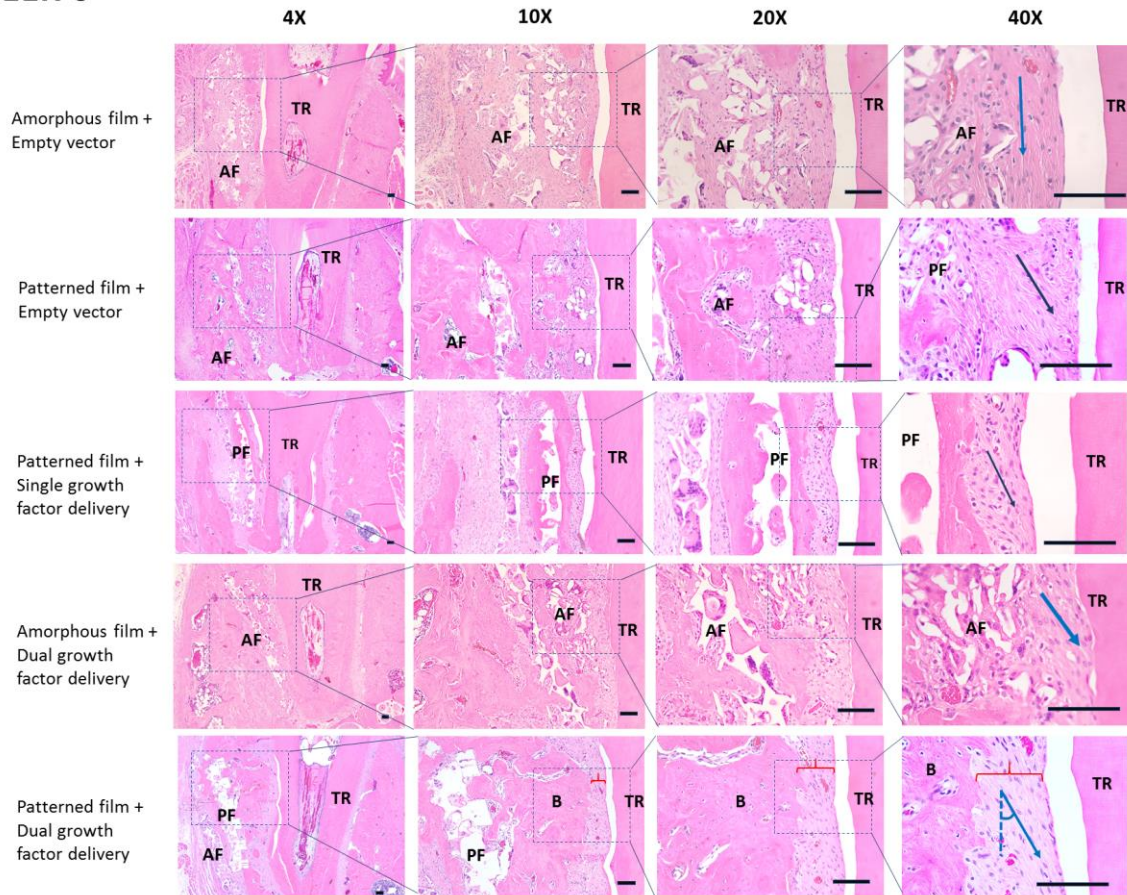
Figure 6.7 Hematoxylin and Eosin (H&E) Staining at 6 Weeks *In Vivo*
Hematoxylin and eosin (H&E) staining to evaluate tissue formation at rat fenestration defect site along patterned films or amorphous films (with dual growth factor delivery (AdPDGF and AdBMP7), single growth factor delivery (AdBMP7), or empty vector) at 6 weeks post implantation in rat fenestration defect. Blue arrows indicate general orientation of cell nuclei relative to the tooth root (TR). Scale bar is 100um for all images. TR = tooth root, AF = amorphous film, PF = patterned film, B = bone.
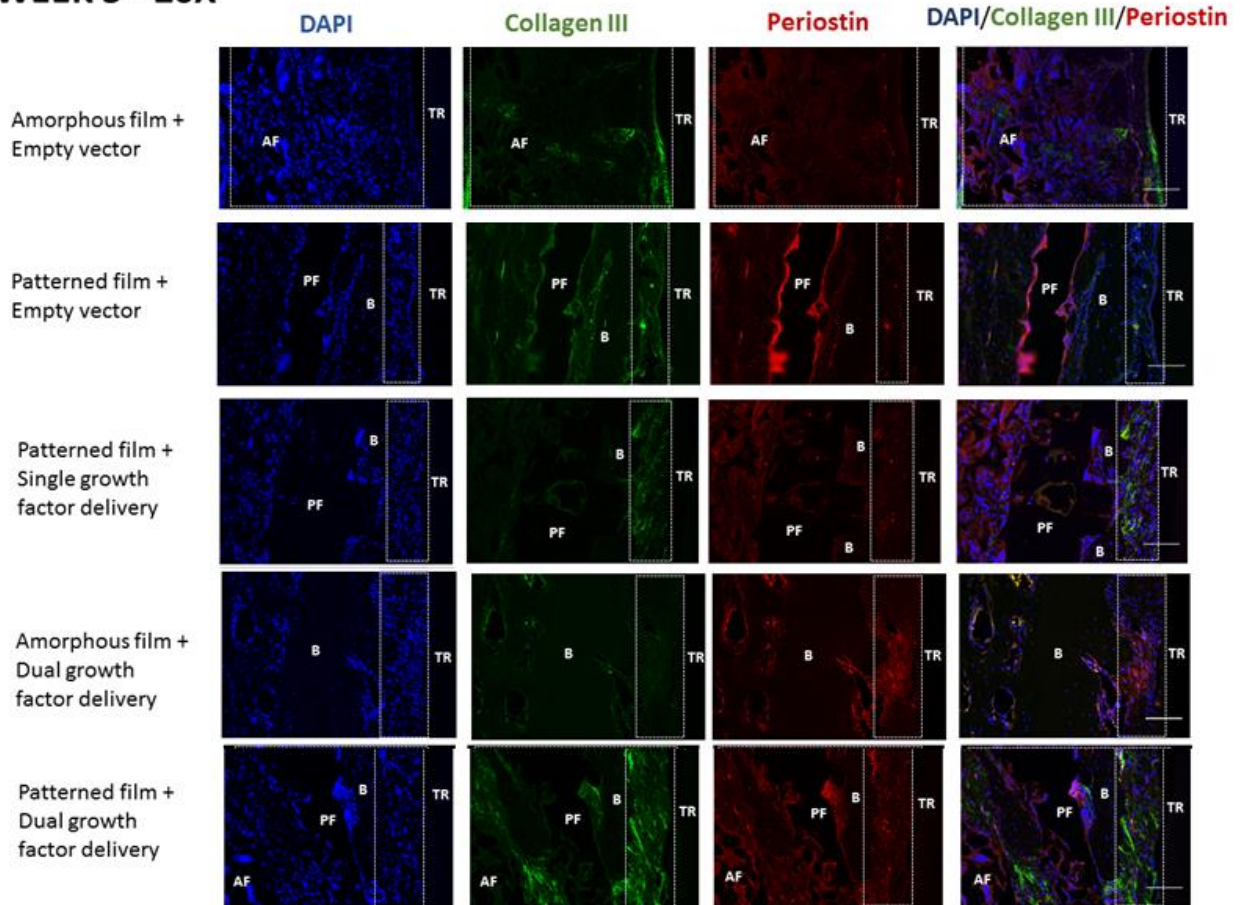
Figure 6.8 Immunofluorescence: PDL-Like Tissue at 3 Weeks *In Vivo*
Immunofluorescence analysis of fibrous connective tissue formation along patterned films or amorphous films (with dual growth factor delivery (AdPDGF and AdBMP7), single growth factor delivery (AdBMP7), or empty vector) at 3 weeks post implantation in rat fenestration defect. Scale bar is 100um for all images. TR = tooth root, AF = amorphous film, PF = patterned film, B = bone. Dashed white lines represent regions of PDL-like soft tissue formation corresponding to areas where periodontal ligament and cementum were removed along the tooth root during formation of the rat fenestration defect.
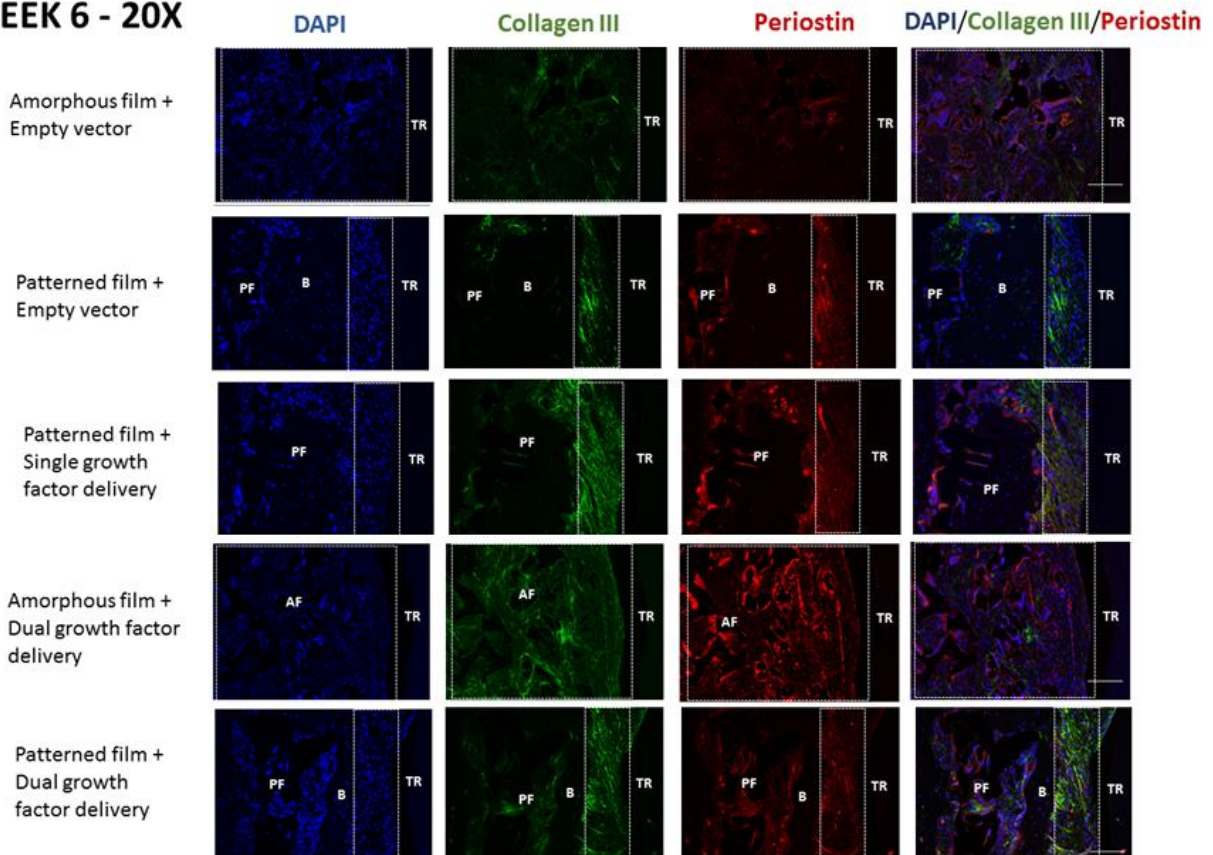
Figure 6.9   Immunofluorescence: PDL-Like Tissue at 6 Weeks *In Vivo*
Immunofluorescence analysis of fibrous connective tissue formation along patterned films or amorphous films (with dual growth factor delivery (AdPDGF and AdBMP7), single growth factor delivery (AdBMP7), or empty vector) at 3 weeks post implantation in rat fenestration defect. Scale bar is 100um for all images. TR = tooth root, AF = amorphous film, PF = patterned film, B = bone. Dashed white lines represent regions of PDL-like soft tissue formation corresponding to areas where periodontal ligament and cementum were removed along the tooth root during formation of the rat fenestration defect.

Further analysis of ratio of mean periostin intensity (PDL-like tissue versus native PDL tissue, **Figure 6.12**), shows significantly higher expression at 3 weeks for the patterned + AdBMP7-hGF group compared to the amorphous + Ad-empty group (negative control). Overall, at 3 weeks the ratios are lower for the Ad-empty groups compared to all groups with growth factor delivery. At 6 weeks, the ratios for the positive control group and single growth factor delivery group are significantly higher ($p<0.05$) compared to the negative control. Individual plots of the intensity profiles (shown in **Figures 6.10 and 6.11**) show that the regenerated tissue areas have periostin intensity profiles are either close to the native PDL tissue or much lower (i.e., observed at week 3 for groups with Ad-empty, and at week 6 for groups with Ad-empty as well as amorphous film with dual growth factor delivery). To complement these findings, additional assessment was performed using toluidine blue-stained sections (**Figure 6.13A**) for all groups (n=6) to determine scaffold displacement from the defect site (given significant amounts of bone observed to have formed in front of the patterned film), as well as the average width of the PDL-like tissue. **Figure 6.13B** shows significantly narrower PDL tissue (i.e., closer to the average rat PDL width of 100um) for groups that have the patterned film included, with much higher widths (~230um for the amorphous group with dual growth factor delivery, and up to 400um in the negative control) for groups with amorphous film for the "PDL" region of the scaffold. This pattern is observed at 6 weeks as well, with the positive control group having a mean thickness of ~100um, while the remaining groups with patterned film showing PDL-like tissue widths slightly greater than 100um. Both of the amorphous film groups have widths that are between 200-400um. Another interesting assessment is the scaffold displacement ("PDL" scaffold region in particular) from the defect site (**Figure 6.13C**). At week 3, significant differences in displacement are noted between the patterned + single growth factor delivery and pattern +dual growth factor delivery groups (with the positive control group showing more displacement relative to the pattern + AdBMP7-HGF group). This is in line with the previous observations of increasing bone formation at inter-pillar spaces, which appear to stabilize the scaffold at the defect site such that the new formed tissue does not push it away as much as seen in other groups. By week 6, significant differences are observed between the patterned film + Ad-empty and the negative control only.
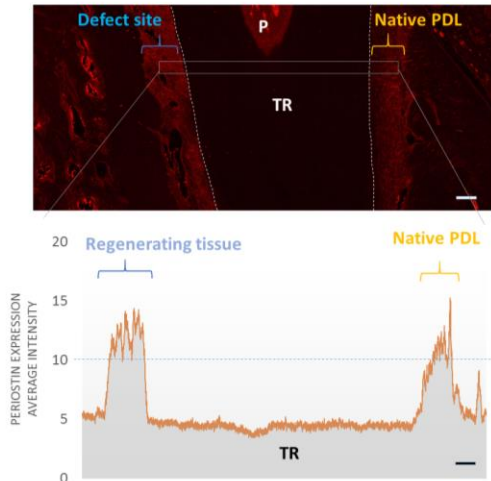
WEEK 3

Patterned film + **Dual growth factor** delivery
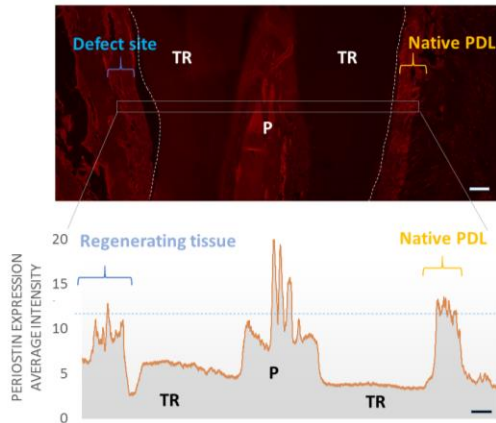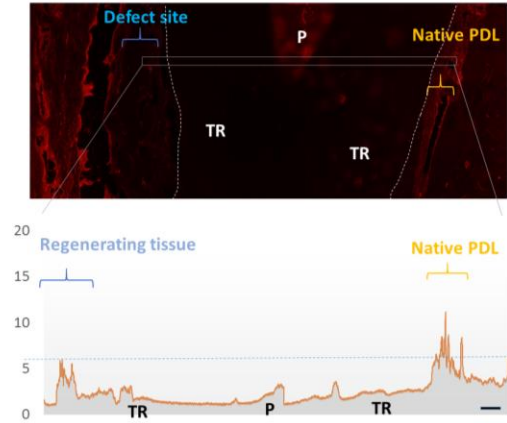
Patterned film + **Empty vector**

Amorphous film + **Dual growth factor** delivery

Amorphous film + **Empty vector**

Patterned film + **Single growth factor** delivery

151

Figure 6.10 Average Intensity Profile: Periostin Expression at 3 Weeks *In Vivo*
Periostin expression average intensity profiles for representative samples from 3 experimental and 2 control groups harvested at 3 weeks post implantation in a rat fenestration defect. Periostin expression is observed at both the original defect site and the native PDL site. The blue line indicates average native PDL intensity values as a comparison to the values observed at regenerated sites with PDL-like tissue. TR = tooth root, P = pulp. Scale bar = 100um.

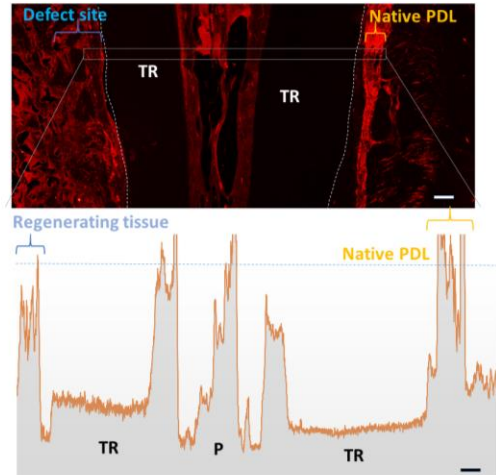**WEEK 6**   Patterned film + **Dual growth factor** delivery   Patterned film + **Empty vector**

Amorphous film + **Dual growth factor** delivery   Amorphous film + **Empty vector**

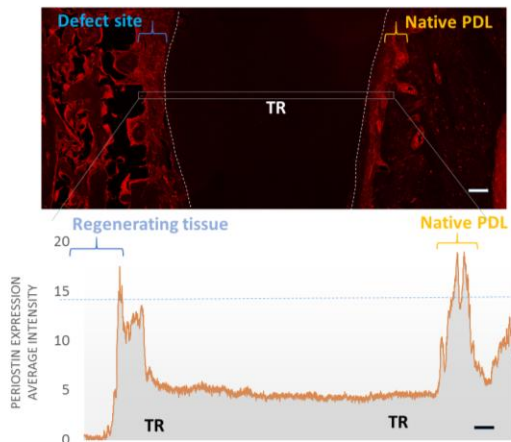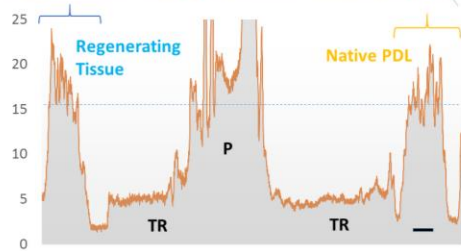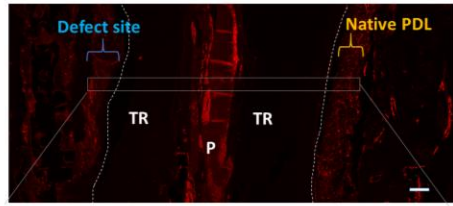Patterned film + **Single growth factor** delivery

153
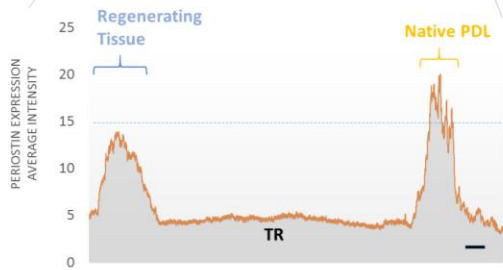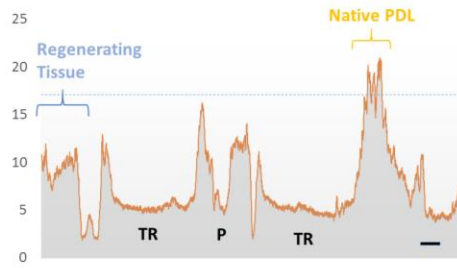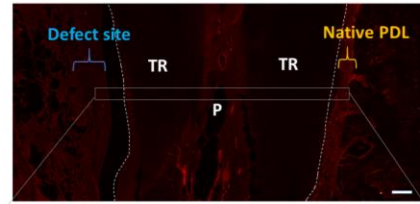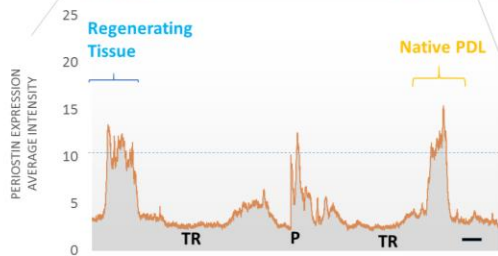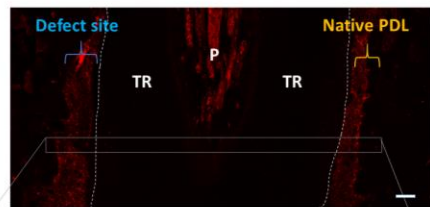
Figure 6.11   Average Intensity Profile: Periostin Expression at 6 Weeks *In Vivo*
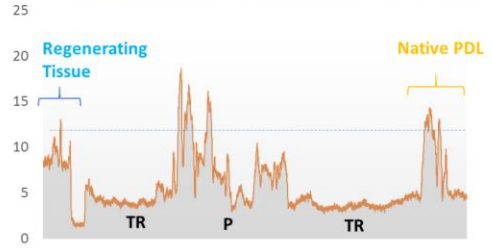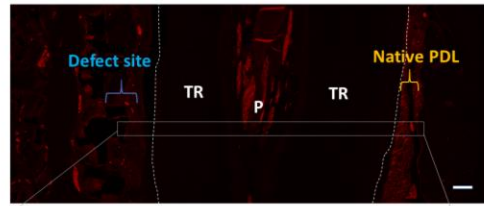Periostin expression average intensity profiles for representative samples from 3 experimental and 2 control groups harvested at 6 weeks post implantation in a rat fenestration defect. Periostin expression is observed at both the original defect site and the native PDL site. The blue line indicates average native PDL intensity values as a comparison to the values observed at regenerated sites with PDL-like tissue. TR = tooth root, P = pulp. Scale bar = 100um.
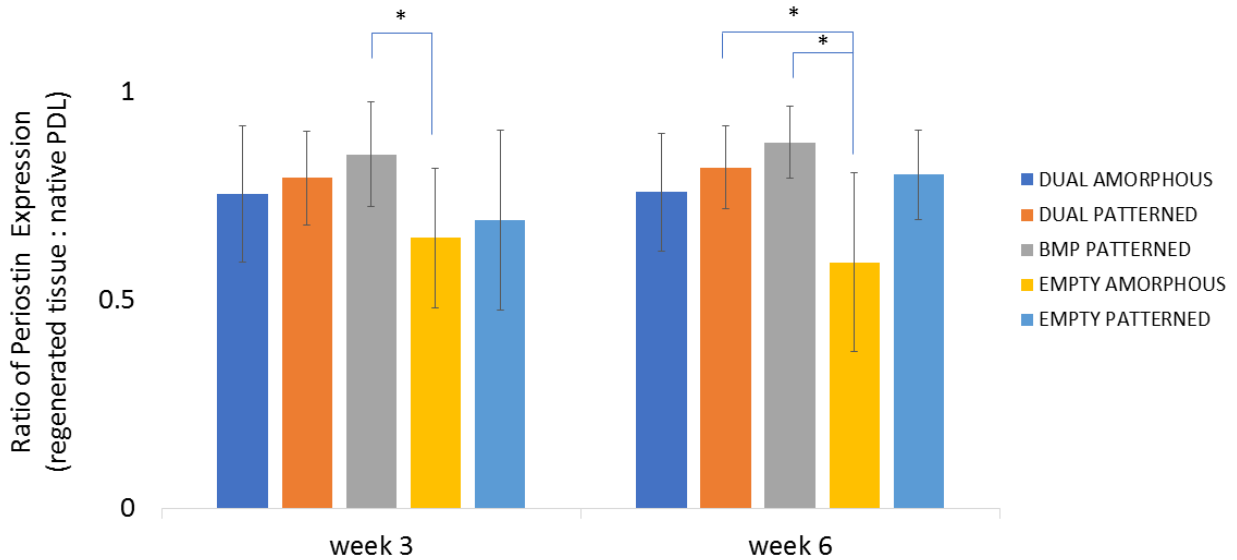
Figure 6.12 Comparison of Periostin Intensity between Native and Regenerated PDL
To compare periostin expression among groups at 3 and 6 weeks, the mean fluorescence intensity was calculated for the PDL-like tissue formation at the defect site (n=6), and compared to the mean periostin fluorescence values obtained at the native PDL site (n=6) for the same sample. Significant (p<0.05) difference were observed at 3 weeks between the group with a patterned film at the 'PDL' region of the scaffold with BMP-7 expression, and the group with an amorphous film at the 'PDL' region with an empty vector. At 6 weeks, the same significant differences were seen between the two groups, as well as between the amorphous film with empty vector group and the patterned film with dual GF delivery group.

154

A.
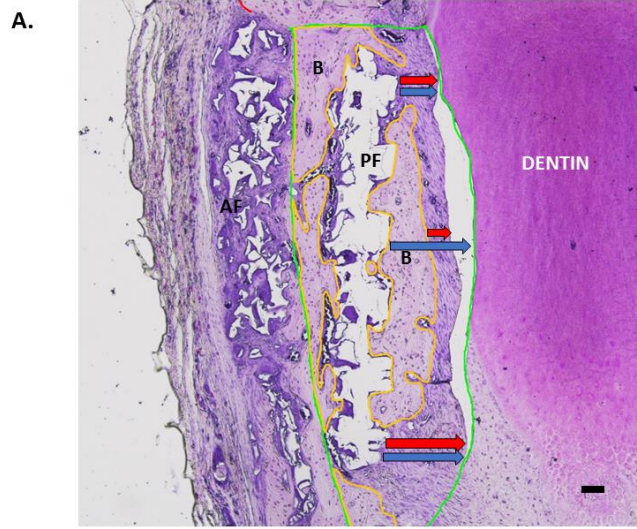
B = bone, **PF** = patterned film, **AF** = amorphous film, scale bar: 100um

B.

Soft Tissue Width (um)

- DUAL AMORPHOUS
- DUAL PATTERNED
- BMP PATTERNED
- EMPTY AMORPHOUS
- EMPTY PATTERNED

3 weeks   6 weeks

C.

Scaffold displacement (um)

- DUAL AMORPHOUS
- DUAL PATTERNED
- BMP PATTERNED
- EMPTY AMORPHOUS
- EMPTY PATTERNED

3 weeks   6 weeks

Figure 6.13   Scaffold Displacement and Total PDL-like Tissue Width at Defect Site
Toluidine blue-stained section (A) of a sample group containing a patterned film with dual growth factor delivery at 6 weeks post-implantation, with improved visibility of the bone (B) formation regions surrounding the patterned (PF) and amorphous (AF) films. Measurements of total PDL-like soft tissue width (red arrows, graph shown in B) and scaffold displacement (blue arrows, graph shown in C) were made to determine variations among groups, focusing on effects of both growth factor delivery and "PDL" scaffold region morphology (i.e., amorphous vs. patterned). Data points specific to patterned films are outlined using dashed black lines. Statistical significance indicated using * ($p < 0.05$).

Finally, another consideration during the analysis of this data was whether the implanted human-derived cells would remain at the defect site or be replaced entirely with the host cells by the specific harvest time points of 3, 6 and 9 weeks. Results from anti-human nuclear staining shown in **Figure 6.14** indicate that, in fact, human-derived cells are not entirely replaced by the host cells, with cells close to the scaffold surface (which retains the dark brown color of the stain). Overall, it appears that there are more human-derived cells in the negative controls (no growth facto delivery) compa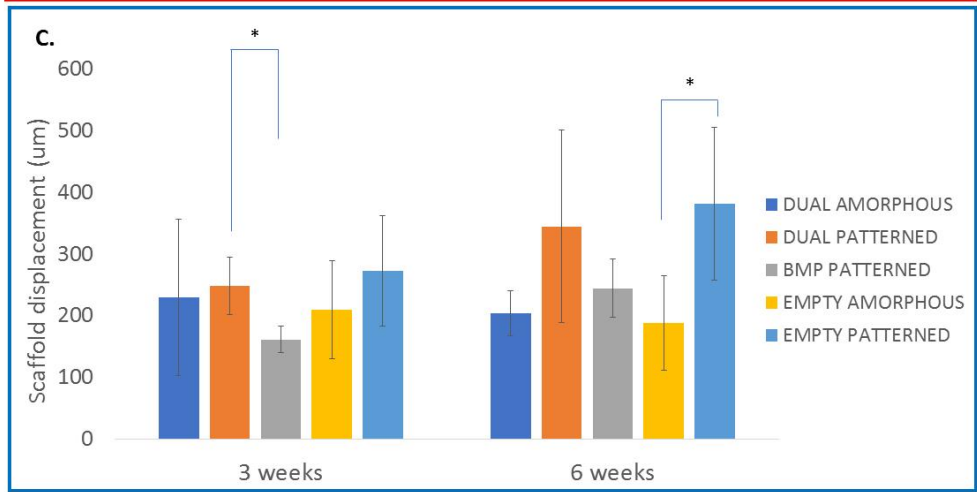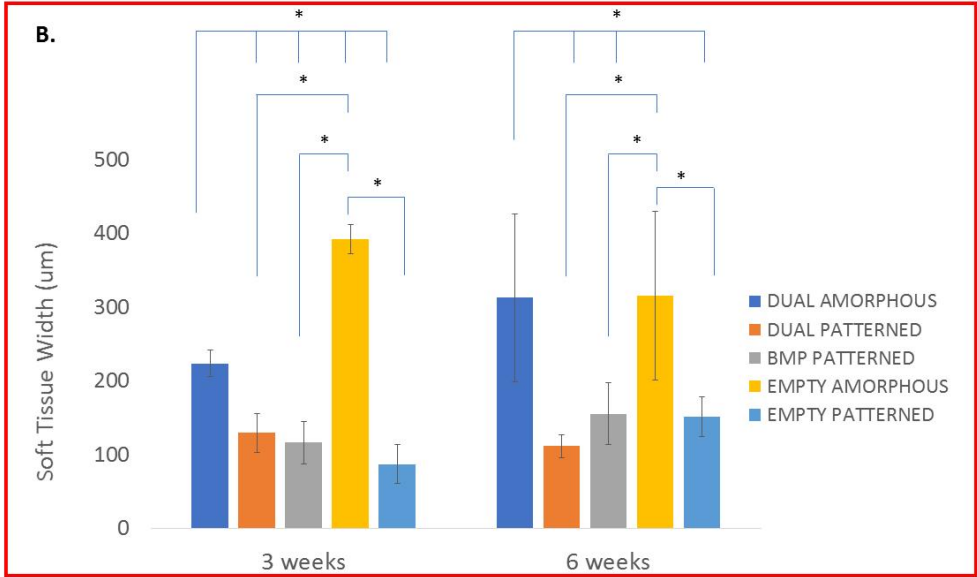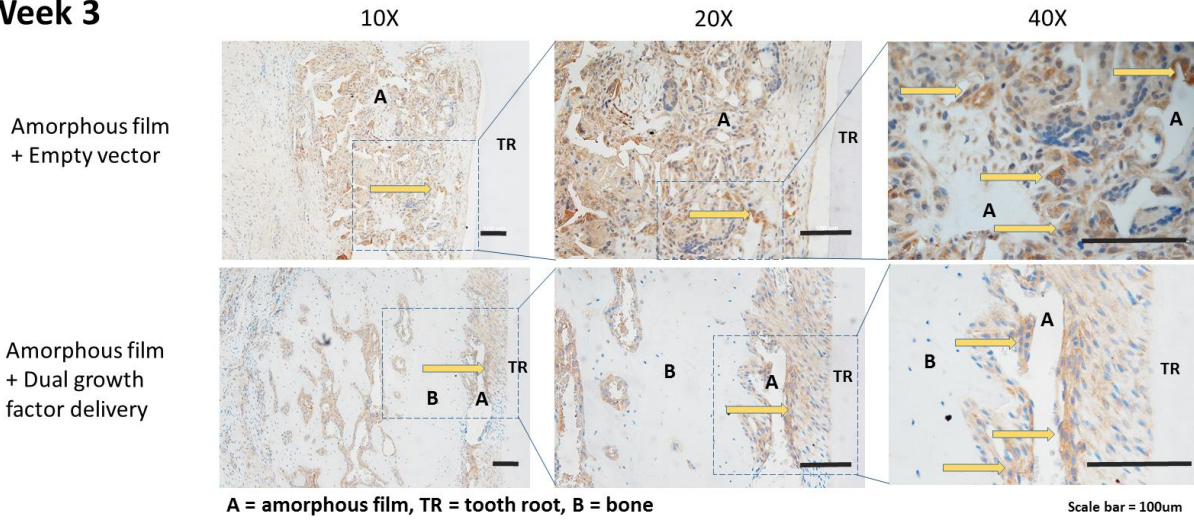red to the positive controls at both weeks 3 and 6. Likewise, the non-specific staining of the scaffold that is specifically striking in the amorphous scaffold groups appears to decrease, potentially as a result of scaffold degradation over time.

As an additional assessment of the tissue regeneration at the interface of the PDL-like tissue and new alveolar bone, nanoindentation was performed on the positive and negative control groups at weeks 3 and 9 (*Table 6.1*). The indentation was performed on both the native bone and PDL tissue and the regenerated bone and PDL-like tissue for each sample (n=3). Values are reported as a range due to heterogenicities in the tissue architecture, as previously done in other studies [20-22]. As expected, at 3 weeks the reduced elastic modulus (i.e., stiffness) range is higher for both the native (1.5-6.9GPa) and regenerated (1.5-4.3 GPa) bone relative to native (0.18-1.7GPa) and regenerated PDL (0.2-1.0 GPa). At 9 weeks, this pattern repeats with native (2.4-10.9GPa) and regenerated (2.4-6.3GPa) bone having a higher stiffness than ranges recorded for native (0.2-2.8GPa) and regenerated (0.1-1.9GPa) PDL, given that bone is known to be much stiffer compared to non-mineralized tissue (i.e., PDL). Hardness values show the same result: at 3 weeks, native (0.03-0.17GPa) and regenerated (0.02-0.15GPa) bone is shown to have higher values than native (0.01-0.04GPa) and regenerated (0.008-0.03GPa) PDL. By week 9, native (0.07-0.15GPa) and regenerated (0.02-0.12GPa) bone is shown to have hardness values higher than those observed in native (0.01-0.07GPa) and regenerated (0.005-0.02GPa) PDL-like tissue. Overall, at week 3 the

156

reduced modulus range for the regenerated PDL measured in positive control samples (0.2-1.0GPa) versus negative control samples (0.2-0.8GPa) fall within the range of values observed in native PDL (0.18-1.7GPa). This is also observed for regenerated bone (1.5-4.3GPa) in the positive and negative (1.7-3.8GPa) controls versus native bone (1.5-6.9GPa). **Figure 6.15** confirms that presence of dual growth factor expression resulted in regenerated bone stiffness matching the stiffness of native bone on the uninjured side, with no significant differences between the two groups at weeks 3 and 9. This was further confirmed at weeks 3 and 9 for PDL-like tissue stiffness in the positive control groups versus native PDL stiffness measured in un-injured regions.

Week 3

	10X	20X	40X

Amorphous film
+ Empty vector

Amorphous film
+ Dual growth
factor delivery

A = amorphous film, TR = tooth root, B = bone

Scale bar = 100um

Week 6

Amorphous film
+ Empty vector

Amorphous film
+ Dual growth
factor delivery

A = amorphous film, TR = tooth root, B = bone

Scale bar = 100um

Week 9

Amorphous film
+ Empty vector

Amorphous film
+ Dual growth
factor delivery
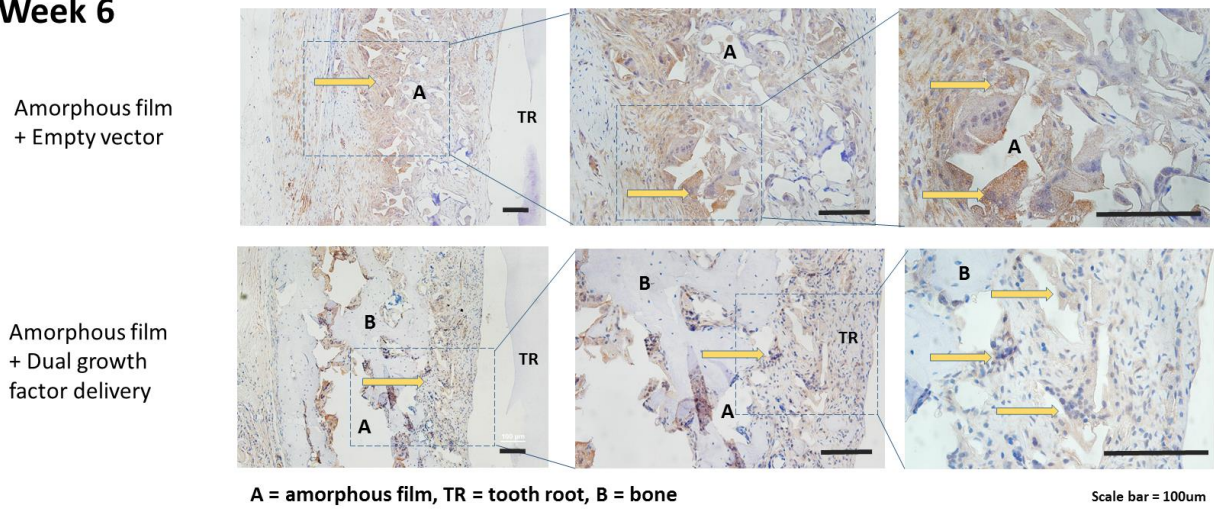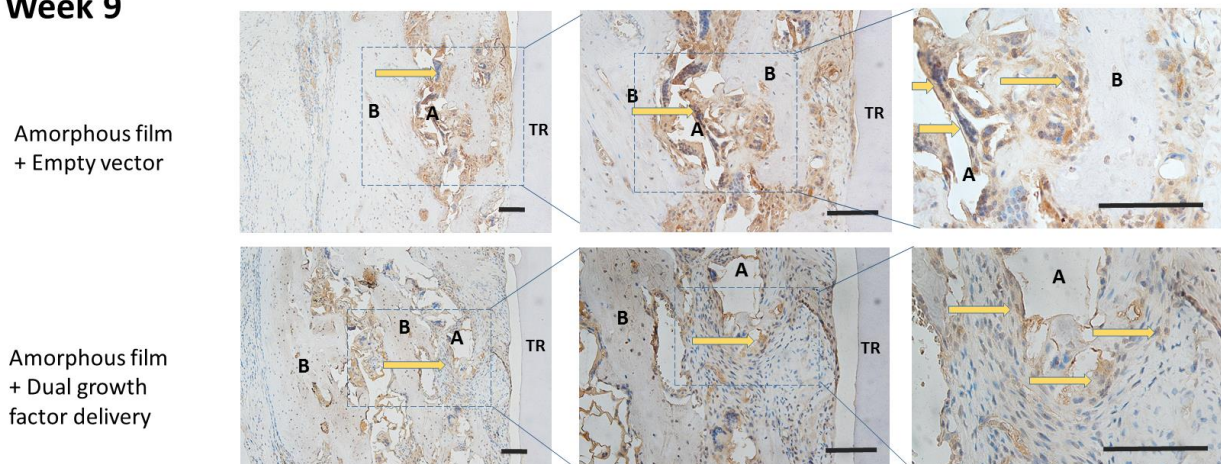
Figure 6.14 Anti-human Nucleus Staining at 3, 6, an d 9 Weeks Post-Implantation

Anti-human nucleus staining was performed on samples harvested at 3, 6 and 9 weeks post-implantation to determine of human-based cells remained present at the defect site or migrated outside of it over the course of the implantation period. A comparison of empty vector and dual growth factor delivery groups is presented, with specific regions of human cells indicated (yellow arrows). The amorphous scaffold remnants result in unspecific brown-colored staining using MACH4, therefore the human nucleus-positive cells are identified using both the background brown stain and blue stain which identifies cell nuclei. A = amorphous film, TR = tooth root, B = bone. Scale bar = 100um.

Table 6.1 Nanoindentation (DRY): Bone-PDL Interface of Regenerated Tissue vs. Native Tissue

Group	Reduced Elastic Modulus 'E$_r$' (GPa)			
Timepoint = 3 weeks	PDL-like Tissue	Regenerated Bone	Native PDL	Native Bone
Amorphous Film (Ad-empty)	**0.2 – 0.8** (0.4 ± 0.1)	**1.7 – 3.8** *## (2.0 ± 0.8)	**0.18 – 1.7** (0.6 ± 0.4)	**1.5 – 6.9** (4.0 ± 1.0)
Patterned Film (AdBMP7 + AdPDGF)	**0.2 – 1.0** # (0.5 ± 0.2)	**1.5 – 4.3** * (3.0 ± 0.8)		
Timepoint = 9 weeks				
Amorphous Film (Ad-empty)	**0.1 – 0.7** ** (0.4 ± 0.2)	**2.5 – 4.0** *## (3.1 ± 0.5)	**0.2 - 2.8** (0.9 ± 0.8)	**2.4 – 10.9** (4.6 ± 2.2)
Patterned Film (AdBMP7 + AdPDGF)	**0.2 - 1.9** **# (0.8 ± 0.5)	**2.4 – 6.3** * (3.9 ± 1.2)		

Group	Hardness 'H' (GPa)			
Timepoint = 3 weeks	PDL-like Tissue	Regenerated Bone	Native PDL	Native Bone
Amorphous Film (Ad-empty)	**0.01 – 0.03** *# (0.02 ± 0.005)	**0.03 - 0.15** * (0.08 ± 0.03)	**0.01 – 0.04** (0.02 ± 0.01)	**0.03-0.17** (0.09 ± 0.05)
Patterned Film (AdBMP7 + AdPDGF)	**0.008 – 0.02** * (0.01 ± 0.003)	**0.02 – 0.11** * (0.05 ± 0.03)		
Timepoint = 9 weeks				
Amorphous Film (Ad-empty)	**0.006 – 0.02** # (0.01 ± 0.005)	**0.07 - 0.09** *** (0.08 ± 0.006)	**0.01 - 0.07** (0.03 ± 0.02)	**0.07-0.15** (0.1 ± 0.03)
Patterned Film (AdBMP7 + AdPDGF)	**0.005 – 0.02** (0.01 ± 0.004)	**0.02 - 0.12** *** (0.05 ± 0.03)		

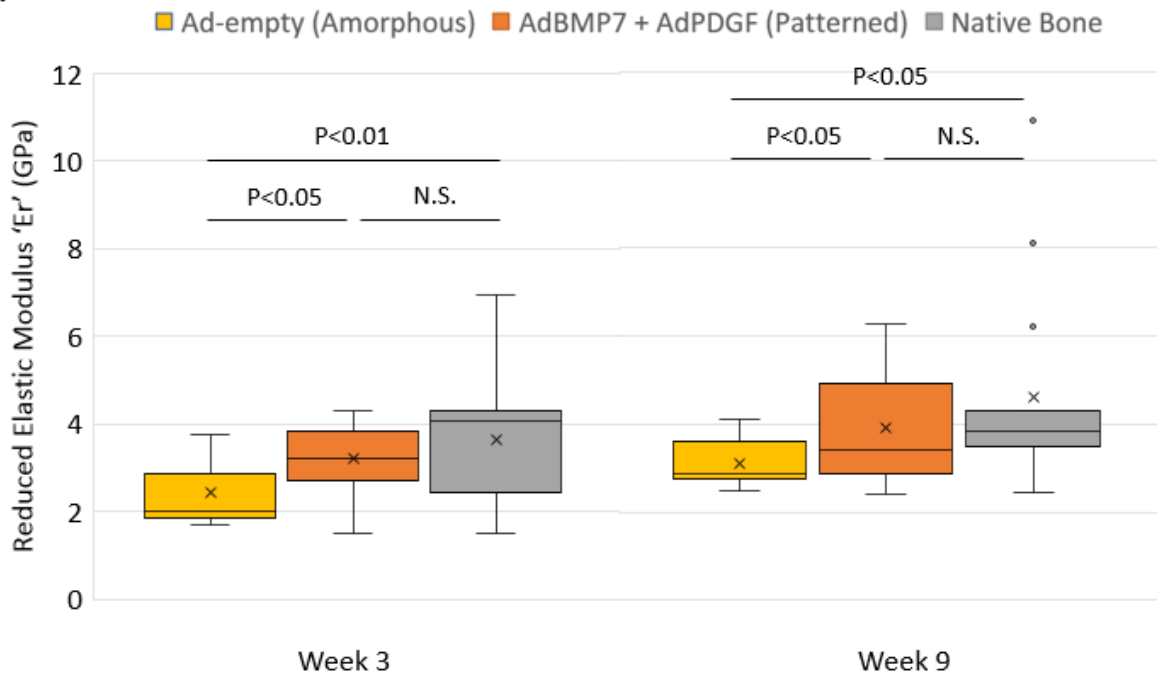*corresponds to sig. diff. between negative and positive control groups at same time point, same tissue (i.e., regenerated bone at 3 or 9 weeks, PDL-like tissue at 3 or 9 weeks)
*$p<0.05$, **$p<0.01$, ***$p<0.001$

corresponds to sig. diff. between negative controls or sig. diff. between positive controls at 3 and 9 weeks (for same tissue type)
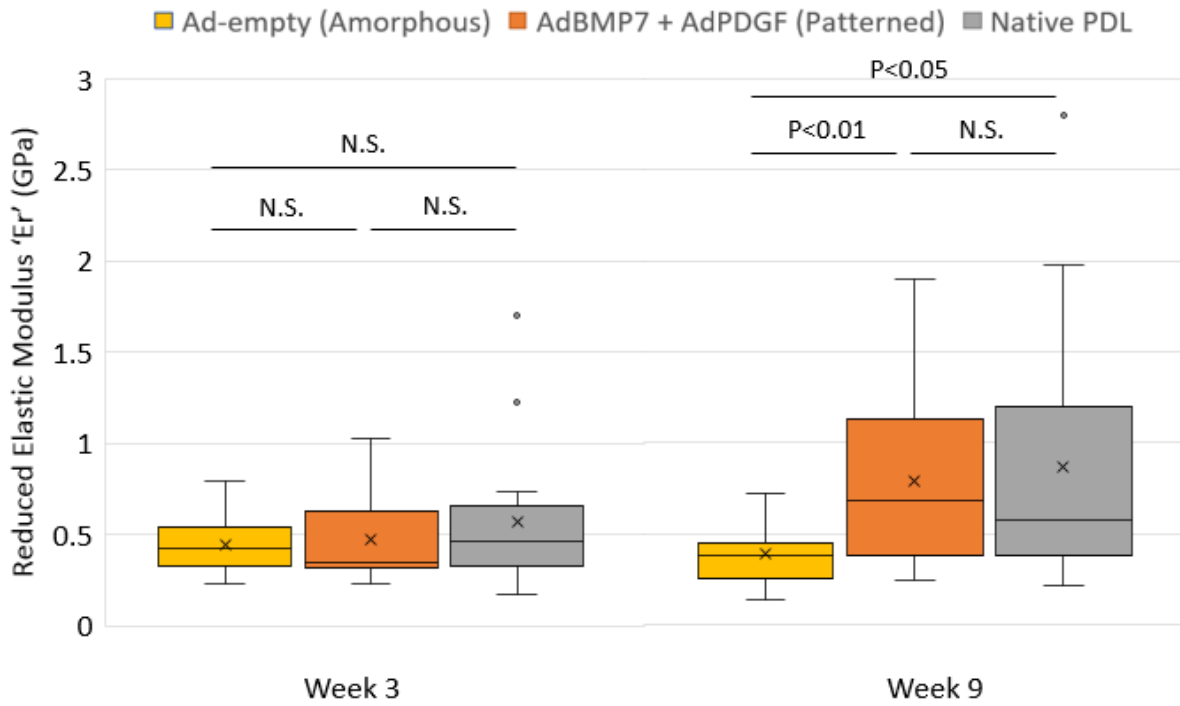#$p<0.05$, ##$p<0.01$, ###$p<0.001$

A.

B.

161

Figure 6.15 Comparison of Elastic Moduli for Regenerated and Native Tissues at 3 Weeks and 9 Weeks Post-Implantation
Box plots showing the reduced elastic modulus values obtained at 3 and 9 weeks post-implantation at sites of the negative control (Ad-empty, amorphous film), positive control (AdBMP7 and AdPDGF, patterned film), and native tissue. In (A), the values represent stiffness of bone in both controls relative to the native bone stiffness measurements at the non-injured site, while in (B) the values represent stiffness of the PDL in both controls relative to the native uninjured PDL. At 3 weeks and 9 weeks, there are no significant differences between the positive control bone and native bone stiffness values. PDL tissue stiffness in negative and positive controls shows no difference from native PDL at week 3, but by week 9 stiffness of negative control PDL is significantly lower compared to the positive and native PDL stiffness, with no differences observed between the positive control and native PDL stiffness values.

6.4   Discussion

This study was designed to examine the effects of scaffold topography (i.e., patterned versus amorphous) coupled with delivery of immobilized gene therapy vectors (i.e., BMP7 and PDGF-BB) for periodontal tissue regeneration. As shown in **Figure 6.1**, the design incorporated a negative control (Ad-empty) and a group with single growth factor delivery (Ad-BMP7 only in both regions of the scaffold). The scaffolds compartments were adjusted to contain films that each separately had a thickness of 250um, for a total combined thickness of 500um, allowing for a calculated fit within the 500um deep fenestration defect (**Figure 6.2**). Implantation of the scaffold *in vivo* showed increased root coverage in groups with BMP7 production, as expected. No significant differences in BV were observed among the groups with BMP7 production at the defect site specifically (**Figure 6.4**), where all regions contained the same amorphous film with AdBMP7-hGF. In accordance with previously reported results using the ectopic murine model (Chapter 6), groups with Ad-empty vector did not show noticeable coverage of the root at 3 weeks (**Figure 6.3**), but by 6 weeks the patterned film group with Ad-empty, as is also confirmed using BV and bone defect fill measurements (**Figure 6.5**), had significantly higher defect fill compared to the negative control. As later observed histologically, there appears to be a potentially osteo-conductive effect of the patterning, with new bone consistently seen to be forming in regions between the pillars (**Figures 6.6-6.7**).

Material surface topography and roughness are important parameters in determining cell response: Fibroblasts have a preference for attaching to smooth surfaces, while bone-derived cells prefer a surface that is rough. This corresponds to the design of the scaffold compartments for bone

162

and PDL regeneration, where the amorphous PCL region has more surface area with greater cell-based perception of roughness compared to the somewhat smoother and more structured morphology of the patterned films (as seen in SEM images, **Figures 5.3** and **5.12**). Nevertheless, the tendency of bone to form at the inter-pillar regions indicate that other factors, such as the presence of patterning on the pillar sides, may override the lack of its porosity relative to the amorphous films. Interestingly, grooves measuring 10um in width have previously been shown to result in significantly increase both adhesion and viability of osteoblastic cells [23, 24]. Here, pillars had grooves with widths of 15um, and depths of 30um, based on previously-established parameters that were shown to promote aligned collagenous tissue formation. In future studies, it would be worthwhile to examine whether increasing groove width (i.e., 30-60um) would decrease the tendency of bone to localize at inter-pillar regions. It is also known that micro-rough surfaces with different topographies show enhanced osseointegation (i.e., functional/structural connection that forms between load-bearing implant surface and existing bone), as evidenced by the use of dental implant design featuring threads that promote implant stability. Depending on the type of implant (i.e., V-shaped, square threads), thread pitches (groove + ridge) can range from 0.8-1.5mm, with thread widths from 0.1-0.6mm. The patterned film pillar pitch (0.3mm) and pillar width (0.15mm) is not far from this range, with recent studies indicating that an even smaller dental implant pitch may benefit osseointegration [25]. It is therefore reasonable to suggest that the patterned film may inadvertently be functioning as a more osteo-conductive surface than the amorphous film, both being comprised of PCL, especially given that bone formation between pillars is observed even in the groups with Ad-empty delivery (i.e., lacking AdBMP7-hGFs) as seen in **Figure 6.6**.

When comparing these results to the rat fenestration defect pilot study described in Chapter 5, there are significant differences histologically (see **Figure 5.14**), given the lack of bone formation between pillar regions. However, the film pattern dimensions are also significantly larger, consisting of 300um x 300um pillars with heights of 250um and 150um inter-pillar spacing. The formed PDL-like tissue is much wider than what would be observed in native rat periodontium, which is addressed in this study by large reductions in pillar height to 100um, resulting in PDL-like tissue width (**Figure 6.13B)** that is within the 100um approximate width in native rat PDL, specifically in groups that contain the patterned film. Groups with the patterned film that tends to have inter-pillar region bone formation integrating with PDL-like tissue provide

163

better control of tissue spacing that is otherwise lost in the groups with amorphous "PDL" films. Another important distinction to note between the earlier pilot study scaffold design and the design presented here is the significantly reduced thickness of the amorphous "bone" film. Previously, the patterned film would cover the defect such that the amorphous film would be positioned directly on top. Here, the film thickness was reduced by ~2X to allow for complete insertion into the region where alveolar bone is removed during formation of the defect. It is likely that this served as a barrier to the migration of hGFs producing BMP7 towards the patterned film and inter-pillar regions. The patterned film porous base was also thinned by ~100um, thereby eliminating an additional barrier that may have reduced infiltration of BMP7-expressing cells or BMP7 itself into the inter-pillar spaces. Additionally, the amorphous film is more porous than the patterned film or its base, such that additional bone (i.e., BMP) can infiltrate into that region, but in the patterned film region it tends to navigate around the patterned film region as that is the easier route with less restriction given the increased polymer density. Anchoring the scaffold in place in order to prevent its displacement from the root would likely stabilize it and possibly limit infiltration of bone at inter-pillar regions.

In order to better understand the sequence of events that results in the observed tissue regeneration seen in this study, it is worthwhile re-visit the wound healing process that sets into action as soon as the fenestration defect is created (**Figure A1.2** in Appendix): Removal of the bone-PDL-cementum complex results in injury to vascularized tissue, forming a provisional matrix that includes fibrin, activated platelets, endothelial cells, and inflammatory cells. Activation of platelets causes the release of PDGF (synthesized and stored in platelet alpha granules), contributing to angiogenesis, which involves vascular endothelial growth factor (VEGF)—a PDGF sub-family of growth factors. Transforming growth factor beta (TGF-β), a platelet-derived cytokine, promotes the chemotaxis and proliferation of osteoprogenitor cells which are recruited by cell signaling through BMPs, with the interaction of progenitor cells with BMPs further resulting in the induction of bone-forming osteoblasts [26]. With regard to PDL regeneration, fibroblasts are the dominant cells of the proliferative stage in wound healing, during which they synthesize collagen in response to platelet-, macrophage-, and mesenchymal cell-specific growth factor release (i.e., PDGF, FGF, IGF, described in more detail in Chapter 2). As a result, even in groups that have only Ad-empty immobilized, there is still observed bone and soft tissue regeneration. However, based on micro-CT, histomorphometric, and immunofluorescence data,

there are visible advantages of incorporating additional (human-derived) cells producing BMP and PDGF (BMP7 and PDGF-BB, specifically), delivered via a scaffold with macro- and micro-topographical cues intended to promote the regeneration of the bone-PDL-cementum complex that is structurally- and functionally-consistent with that of native tissue.

Incubation of hPDL cells on the patterned film with immobilized AdPDGF overnight prior to implantation at the distal root of the first molar ensures that transduction is limited to only those cells that come in direct contact with the film, while also giving the cells adequate time to begin aligning within the pillar grooves such that they will already be positioned perpendicular to the root surface when the film is implanted. Likewise, the amorphous film region is also immobilized with AdBMP7 and seeded with hGFs in order to ensure the localization of BMP-producing cells specifically to the region of the defect where bone is removed. Using adenoviral gene therapy vectors ensures that only the transduced cells produce growth factors—future generations of these human-derived cells would likely be unaffected. However, it appears that human-derived cells continue to remain at the defect site even into week 9 post-implantation, as evidenced using anti-human nuclear staining (**Figure 6.14**) of positive and negative control groups. At 3, 6, and 9 weeks, the Ad-empty (negative control) group appears to have greater presence of human-derived cells compared to the amorphous "PDL" film group with AdBMP7-hGFs and AdPDGF-hPDLs. A potential explanation is that the presence of the growth factors promotes the regenerative process which increases cell turn-over with time. Likewise, the extended expression pattern of BMP and PDGF above what is typically found in the wound environment may cause migration of the elevated growth factor concentrations in the wound site (i.e., BMP) towards other areas of the scaffold besides the "bone" region. Given that PDGF is also known to induce osteoblast chemotaxis, its presence may further favor infiltration of the area with osteoblast progenitor cells. Overall, as has previously been reported by Zhang Y et al using scaffold-based, combined and separate delivery of AdBMP7 and AdPDGF in dog furcation defects, the presence of both growth factors contributed to a more robust regeneration of the periodontium [16]. In this study, bone regeneration is observed to be robust in all groups with either single or dual growth factor expression, while PDL-like tissue is more evident (based on combined collagen III, periostin staining) in groups with a patterned film and single as well as dual growth factor expression at weeks 3 and 6 post-implantation (**Figures 6.8, 6.9**). This is further confirmed when analyzing the mean periostin fluorescence intensity at weeks 3 and 9. Periostin is a mesenchymal stem cell

marker that is found in collagen-rich connective tissues such as tendons and periosteum. PDL-specific periostin has been shown to positively regulate PDL cell mineralization and cytodifferentiation. Due to its importance as an ECM protein involved in maintaining the homeostasis of periodontal tissues, as well as showing strong expression during PDL cell differentiation, a more thorough assessment of its expression in all groups tested was performed. At 3 weeks, higher mean periostin intensity values were observed for all groups involving growth factor expression (highest being in the group with AdBMP7-hGF in both regions). By week 6, the highest values were observed in groups with a patterned film and either dual or single growth factor expression [28, 29].

Interestingly, a very recent study by Sowmya et al consisting of a tri-layered nanocomposite hydrogel scaffold also utilized film-like layers for the delivery of cells and growth factors to rabbit maxillary periodontal defects. The scaffold layers were positioned as follows: chitin-PLGA/nanobioactive glass ceramic (nBGC)/cementum protein 1 (cementum layer), chitin-PLGA/FGF-2 (PDL layer), and chitin/PLGA/nBGC/platelet rich plasma growth factors (alveolar bone). Implantation of the scaffold with the growth factors resulted in complete closure of the defect and healing, with confirmed regeneration of new cementum, fibrous PDL, and alveolar bone compared to a scaffold alone without growth factors, at 1 and 3 months post-implantation [27]. Compared to this study, which did not incorporate a specific layer for cementum regeneration. These results may indicate that in order to observe cementum regeneration, which is lacking in this study, a separate growth factor or scaffold compartment may be needed to ensure the full tri-layer periodontal complex formation.

Nanoindentation was used to further elucidate the functional characteristics of the regenerated bone-PDL complex. Several studies have used micro- and nano-indentation to determine the mechanical properties of the native periodontium in rats. Grandfield et al reported 12.1 ± 3.4 GPa (8.7 - 15.5 GPa range, under wet conditions) in the rat alveolar bone region at the molar PDL-bone interface [19]. It is important to note that in native periodontal tissue, the region of alveolar bone where PDL fiber bundles (i.e., Sharpey's fibers) insert is called the bundle bone, whereas the alveolar bone is the region of bone into which bundle bone (i.e., inner wall of alveolar socket) transitions. While this is anatomically identifiable in native PDL (see Figure A1.1 in **Appendix**), in the samples tested this transition as not as obvious in the regenerated tissue regions. As such, the indentations were performed at the regions of bone closest to the PDL region (the

166

bundle bone region). Ho SP et al previously performed nano-indentation under the same loading conditions, albeit using hydrated human tissue, showing a range of E_r = 2-8GPa for bundle bone, which falls within the range of values reported here (*Table 6.1*). Another study performed to characterize PDL-bone attachment sites in human molars shows an E_r range of 0.01-0.05 GPa for PDL tissue (0.1-1.0 GPa for PDL-AB region) and 0.2 – 9.6 GPa range for bone tissue. Hardness values were reported to range from 0.01-0.15 GPa for bone regions of the periodontium and 0.01-0.03 GPa for the PDL-AB regions, using nanoindentation [20-22]. Although there are no major discrepancies between the presented and reported values, it is important to mention that a variety of factors may affect the stiffness and hardness ranges, including the hydration state (i.e., testing under wet versus dry conditions), probe geometry, and loading conditions.

Having established that the stiffness and hardness of native PDL and bone regions reported here correlate to previously reported values, the main purpose of the presented results is to compare and contrast these same values among the positive (patterned film/amorphous film + AdPDGF-hPDL/AdBMP7-hGF), negative (amorphous film/amorphous film + Ad-empty/Ad-empty) control groups, and determined native PDL and AB stiffness and hardness values. These are load-bearing tissues that integrate over time, making these parameters important in determining whether the regenerated tissue is mechanically similar to its native counterpart. As previously noted, there is heterogeneity in the bone tissue which is specifically identifiable using nanoindentation as opposed to microindentation, given that there are regions of lamellar bone integrating with bundle bone, thereby giving the observed range of values. Overall, the positive and negative control values for bone and PDL fall within the native bone and PDL values, respectively at 3 and 9 weeks. As expected, the largest difference the lowest and highest reported stiffness values is seen in the bone regions (native: Δ5.4GPa, positive control: Δ2.8 GPa, negative control: Δ2.1 GPa), compared to the PDL regions (native: Δ1.5 GPa, positive control: Δ 0.8GPa, negative control: Δ 0.6 GPa). Interestingly, the highest values for both the regenerated bone and PDL tissues relative to the native bone and PDL tissues are observed in the positive control group (patterned film + dual growth factor delivery) (i.e., 1.0 GPa for positive control versus 0.8 GPa for negative control in PDL-like tissue, and 4.3 GPa for positive control versus 3.8 GPa for negative control in bundle bone tissue). This is an indication that the regenerative process may be more complex in the positive control given that involvement of dual growth factor delivery, with increased potential for having more mature tissue relative to the negative control tissue sites at the earlier time point of 3 weeks. At 9

167

weeks, the tissue in both group is expected to be more mature. Here, we observe that again the stiffness values for both positive and negative control regenerated PDL and bone regions falls within the range observed in native bone. Again, the positive controls have a range with highest values (i.e., 1.9 GPa for PDL in positive control versus 0.7 GPa for PDL in negative control, and 2.8 GPa in native PDL; 6.3 GPa for positive control bone versus 4.0GPa for negative control bone, with 10.9GPa in native bone). Comparing week 3 and week 9 values clearly shows an increase in the lowest values reported within the regenerated bone stiffness range for all groups. All of the groups also show an increase in the highest value reported within the stiffness range for bone, although this value increases more prominently in the positive control samples (4.3 GPa at 3 weeks to 6.3 GPa at 9 weeks) compared to the negative control (3.8GPa at 3 weeks to 4.0 GPa at 9 weeks). For the PDL region values, there is also an increase in stiffness range for the positive control (i.e., 1.9 GPa from 1.0GPa) compared to a slight decrease observed in the negative control (i.e., 0.8GPa to 0.7GPa). Statistically, there are significant differences ($p<0.05$) between the E_r (regenerated bone) for the negative and positive controls at both 3 and 9 weeks, as well as the E_r (PDL-like tissue) between the negative and positive controls at 9 weeks ($p<0.01$), such that the values for the patterned film/dual growth factor delivery are higher. Comparing the same groups between 3 and 9 weeks shows significantly higher E_r values for PDL-like tissue ($p<0.05$, in patterned film/dual growth factor delivery group), and higher values for regenerated bone ($p<0.01$, in amorphous film/Ad-empty group), over time.

Figure 6.15 further illustrates the ranges reported in *Table 6.1* with statistical analysis of differences in stiffness between the positive or negative control and native tissue (PDL or bone), with results confirming that positive control group tissue stiffness matched that of native tissue at both time points for PDL and bone., with no significant differences between them. Likewise, positive control values were significantly higher for bone and PDL stiffness when comparing to negative control values at 3 and 9 weeks, except for PDL-like tissue at the 3 week time point being of the same general stiffness for both negative and positive controls. While *Table 6.1* presents the effects of time and growth factor presence/patterning on tissue regeneration, **Figure 6.15** focuses on both the effects of growth factor expression (given statistical comparison between the negative and positive control groups), as well as provides a comparison to native PDL and/or bone tissue values in a box plot that emphasizes the differences in the range of values for all groups evaluated, emphasizing the importance of growth factor expression over time on tissue regeneration.

168

When considering the reported hardness values at weeks 3 and 9, the values for the native bone region (0.03-0.17 GPa and 0.07-0.15 GPa) are typically higher than the native PDL region (0.01-0.04 GPa and 0.01-0.07 GPa), as expected. Once again the negative and positive control values fall within the range reported for native bone at weeks 3 and 9, although the week 9 positive control lowest value is outside the range (0.02GPa), while it also has the highest value (0.12GPa) within the range compared to the negative control group. Interestingly, the PDL-like tissue hardness range for both the positive (0.005-0.02 GPa) and negative (0.06-0.02 GPa) controls is just slightly inside the range of native PDL hardness (0.01-0.07 GPa) at week 9. Overall, the hardness range for PDL is seen to increase for both groups from week 3 to week 9. This may indicate that as the tissue matures, there are increasing heterogeneities in the region given increased collagenous tissue formation that also has a tendency to vary in stiffness and hardness in varying parts of the PDL. Statistically, there are significant differences between both the PDL-like tissue ($p < 0.05$) and regenerated bone ($p < 0.05$) for the negative and positive controls at week 3. At week 9, only the regenerated bone values for both negative and positive controls show significant differences ($p < 0.001$), indicating harder tissue in the patterned film/dual growth factor delivery group. Comparing weeks 3 and 9, only the amorphous film/Ad-empty groups shows a significantly increased ($p < 0.05$) range of values for PDL-like tissue hardness. Based on values extracted from nano-indentation, this data permits the conclusion that, at week 9, the positive control group tissue overall is more mature and closer to native tissue modulus values compared to the negative control. This further supports the previously discussed data that highlights the improved regeneration of the periodontal complex in groups with customized biomaterial micro-architecture and dual growth factor delivery.

6.5   Conclusion

This study explores the effects of surface topography combined with growth factor delivery on periodontal tissue regeneration. There are clear indications that dual growth factor delivery (i.e., combined delivery of PDGF-BB and BMP-7) leads to improved bone formation and regeneration of PDL-like tissue, as evidenced by a thorough assessment of protein expression (i.e., collagen III, periostin), and tissue mechanical properties. While the surface topography does not serve to provide guidance for oriented PDL tissue orientation (as originally intended) due to the

displacement of the scaffold from the defect site and infiltration of the inter-pillar regions with osseous tissue, there is nevertheless important indications that the patterning has effects on the overall integrity of the final bone-PDL interface. Moreover, this study confirms that gene therapy vectors can be immobilized onto the scaffold surface in order to localize the transduction of cells, specifically for subsequent implantation *in vivo*. Future studies can focus on improved scaffold stabilization at the defect site, as well as potential improvement of the scaffold fabrication process to allow encapsulation of gene therapy vectors within the scaffold such that transduction can take place *in vivo* instead of *in vitro* prior to implantation.

6.6　References

[1]　Park CH, Rios HF, Jin Q, Bland ME, Flanagan CL, Hollister SJ, Giannobile W V. Biomimetic hybrid scaffolds for engineering human tooth-ligament interfaces. *Biomaterials* 2010;31:5945–52.

[2]　Park CH, Rios HF, Jin Q, Sugai J V, Padial-Molina M, Taut AD, Flanagan CL, Hollister SJ, Giannobile W V. Tissue engineering bone-ligament complexes using fiber-guiding scaffolds. *Biomaterials* 2012;33:137–45.

[3]　Park CH, Rios HF, Taut AD, Padial-Molina M, Flanagan CL, Pilipchuk SP, Hollister SJ, Giannobile WV. 2014. Image-based, fiber guiding scaffolds: a platform for regenerating tissue interfaces. Tissue Eng Part C Methods;20(7):533-42.

[4]　Ivanovski S, Vaquette C, Gronthos S, Hutmacher DW, Bartold PM. 2014. Multiphasic Scaffolds for Periodontal Tissue Engineering. J Dent Res 93:1212-21.

[5]　Vaquette C, Fan W, Xiao Y, Hamlet S, Hutmacher DW, Ivanovski S. A biphasic scaffold design combined with cell sheet technology for simultaneous regeneration of alveolar bone/periodontal ligament complex. *Biomaterials* 2012;33:5560–73.

[6]　Pilipchuk SP, Monje A, Jiao Y, Hao J, Kruger L, Flanagan CL, Hollister SJ, Gianobile WV. Integration of 3D printed and micropatterned polycaprolactone scaffolds for

guidance of oriented collagenous tissue formation in vivo. *Adv Healthc Mater,* 2016; 5(6): 676-87.

[7]   Lim JY, Donahue HJ. Cell sensing and response to micro- and nanostructured surfaces produced by chemical and topographic patterning. *Tissue Eng*, 2007*;* 13(8):1879-91.

[8]   Chiu LL, Janic K, Radisic M. Engineering of oriented myocardium on three-dimensional micropatterned collagen-chitosan hydrogel. *Int J Artif Organs*, 2012; 35(4):237-50.

[9]   Fozdar DY, Lee JY, Schmidt CE, Chen S. Selective axonal growth of embryonic hippocampal neurons according to topographic features of various sizes and shapes. *Int J nanomedicine*, 2010;6:45-57.

[10]   Recknor JB, Sakaguchi DS, Mallapragada SK. Directed growth and selective differentiation of neural progenitor cells on micropatterned polymer substrates. *Biomaterials*, 2006;27(22):4098-108.

[11]   Nevins M, Kao RT, McGuire MK, McClain PK, Hinrichs JE, McAllister BS, Reddy MS, Nevins ML, Genco RJ, Lynch SE, Giannobile WV. Platelet-derived growth factor promotes periodontal regeneration in localized osseous defects: 36-month extension results from a randomized, controlled, double-masked clinical trial. *J Periodontol*, 2013; 84(4):456-64.

[12]   Kaigler D, Cirelli JA, Giannobile WV. Growth factor delivery for oral and periodontal tissue engineering. *Expert Opin Drug Deliv,* 2006; 3(5):647-62.

[13]   Chang PC, Cirelli JA, Jin QA, Seol YJ, Sugai JV, D'Silva NJ, Danciu TE, Chandler LA, Sosnowski BA, Giannobile WV. Adenovirus encoding human platelet-derived growth factor-B delivered to alveolar bone defects exhibits safety and biodistribution profiles favorable for clinical use. *Hum Gene Ther,* 2009;20(5):486-96.

[14]   Jin QM, Anusaksathien O, Webb SA, Rutherford RB, Giannobile WV. Gene therapy of bone morphogenetic protein for periodontal tissue regeneration. *J Periodontol,* 2003;74(2):202-13.

[15]   Jin Q, Anusaksathien O, Webb S, Printz MA, Giannobile WV. Engineering of tooth-supporting structures by delivery of PDGF growth therapy vectors. *Mol Ther.* 2004;9(4):519-26.

[16]   Zhang Y, Miron RJ, Li S, Shi B, Sculean A, Cheng X. Novel mesoporous bioglass/silk scaffold containing adPDGF-B and adBMP7 for the repair of periodontal defects in beagle dogs. *J Clin Periodontol*, 2015;42(3):262-71.

[17]   Zhang Y, Shi B, Li C, Wang Y, Chen Y, Zhang W, Luo T, Cheng X. The synergetic bone-forming effects of combinations of growth factors expressed by adenovirus vectors on chitosan/collagen scaffolds. *J Control Release*, 2009:136(3):172-8.

[18]   Hao J, Cheng KC, Kruger LG, Larsson L, Sugai JV, Lahann J, Giannobile WV. Multigrowth factor delivery via immobilization of gene therapy vectors. *Adv Mater*, 2016; 28(16):3145-51.

[19]   Grandfield K, Herber RP, Chen L, Djomehri S, Tam C, Lee JH, Brown E, Woolwine WR 3rd, Curtis D, Ryder M, Schuck J, Webb S, Landis W, Ho S. Strain-guided mineralization in the bone-PDL-cementum complex of a rat periodontium. *Bone Rep.* 2015;3:20-31.

[20]   Ho SP, Kurylo MP, Grandfield K, Hurng J, Herber RP, Ryder MI, Altoe V, Aloni S, Feng JQ, Webb S, Marshall GW, Curtis D, Andrews JC, Pianetta P. The plastic nature of the human bone-periodontal ligament-tooth fibrous joint. *Bone*. 2013;57(2):455-67.

[21]   Ho SP, Marshall SJ, Ryder MI, Marshall GW. The tooth attachment mechanism defined by structure, chemical composition and mechanical properties of collagen fibers in the periodontium. *Biomaterials.* 2007;28(35):5238-45.

[22]   Ho SP, Kurylo MP, Fong T, Lee S, Wagner HD, Ryder M, Marshall GW. The biomechanical characteristics of the bone-periodontal ligament-cementum complex. *Biomaterials.* 2010; 31(25): 6635–6646

[23]   Ismail FSM, Rohanizadeh R, Atwa S, Mason RS, Ruys AJ, Martin PJ, Bendavid, A. The influence of surface chemistry and topography on the contact guidance of MG63 osteoblast cells. *J. Mater. Sci., Mater. Med.,* 2007,18, 705–714.

[24]   Chen J, Mwenifumbo S, Langhammer C, McGovern J, Li M, Beye A, Soboyejo WO. Cell/surface interactions and adhesion on Ti-6Al-AV: effects of surface texture. *J. Biomed.Mater. Res. B, Appl. Biomater.*, 2007, 82, 360–373.

[25]   Abuhussein H, Pagni G, Rebaudi A, Wang H-L. The effect of thread pattern upon implant osseointegration. *Clin. Oral Impl. Res*, 21, 2010; 129–136.

[26]   Ghodadra N and Singh K. Recombinant human BMP-2 in the treatment of bone fractures. *Biologics*; 2008, 2(3):345-54.

[27]   Sowmya S, Mony U, Jayachandran P, Reshma S, Arun Kumar R, Arzate H, Nair SV, Jayakumar R. Tri-layered nanocomposite hydrogel scaffold for the concurrent regeneration of cementum, periodontal ligament, and alveolar bone. *Adv Healthcare Mater.* 2017, 6, 1601251.

[28]   Yamada S, Tauchi T, Awata T, Maeda K, Kajikawa T, Yanagita M, Murakami S. Characterization of a novel periodontal ligament-specific periostin isoform. *J Dent Res*, 2014;93(9):891-897.

[29]   Rios HF, Bonewald LF, Conway SJ. Lessons from the Matricellular Factor Periostin. *J Dent Res*, 2014; 93(9):843-845.

[30]   Zhang Y, Deng X, Scheller EL, Kwon T-G, Lahann J, Franceschi RT, Krebsbach PH. The effects of Runx2 immobilization on poly (epsilon-caprolactone) on osteoblast differentiation of bone marrow stromal cells in vitro. *Biomaterials* 2010;31:3231–6.

CHAPTER 7

CONCLUSIONS AND FUTURE DIRECTIONS

The "Future Directions" section of this chapter includes excerpts from sections written as a contribution to the following article: Fretwurst T, Larsson L, Yu SH, **Pilipchuk SP**, Kaigler D, Giannobile WV. "Periodontal Tissue Bioengineering: Is the Future Now?" *Compendium of Continuing Education in Dentistry* (publication pending).

7.1   Conclusions

Novel tissue engineering strategies are required for the regeneration of lost periodontal tissues due to instances where clinically-based periodontal therapy is not predictable or fails to promote the regeneration of the alveolar bone-PDL-cementum complex. While many studies have examined the interplay among different biomaterial scaffolds, growth factors, and cells necessary for predictable tissue regeneration, there is still a lack of specifically-established parameters that are required to obtain tissues that are not only structurally, but also functionally similar to native periodontium that further matches its hierarchical architecture. As described throughout the chapters, this work focuses on the use of specific technologies (3D-printing and micropatterning) that allow for the scaffold to be fabricated with macro- and micro-scale cues that can guide the formation of aligned tissue. There is clear evidence that patterning does in fact promote aligned soft tissue formation, as shown using the ectopic murine model. More specifically, increased groove depth is shown to be a more significant parameter in determining the percentage of aligned tissue relative to groove width. In combination with gene therapy vectors, the 3D-printed, micropatterned scaffold is able to improve the bone-PDL-like regeneration that is needed to recapitulate the structural integrity of the periodontal complex, as described in Chapter 4. However, improved localization of growth factor expression as well as increased rate of degradation to allow more rapid replacement of the biomaterial with native tissue is necessary to further improve upon the existing scaffold design.

Chapter 5 explores the application of a re-designed scaffold incorporating PLGA to promote increased degradation of the "PDL" scaffold region in ectopic murine model and rat fenestration defect model pilot studies. In addition, to allow for more predictable delivery of gene therapy vectors while also localizing the transduction of cells to specific regions of the scaffold (i.e., AdBMP7 transduced cells to the "bone" region and AdPDGF-BB transduced cells to the "PDL" region), a novel surface immobilization technique is explored using chemical vapor deposition (CVD). Based on the results of these findings, immobilization of gene therapy vectors is a potential solution for increased control over transduced cells and limitation of potential adenovirus dispersion that is of greater concern when the virus is not immobilized onto the surface. As discovered in Chapter 6, the architecture and overall dimensions of the scaffold at the defect site are critical parameters in determining the localization of the growth factors, given that a decrease in the amorphous "bone" region film thickness to better fit within the rat fenestration defect allowed for more localized expression of the AdBMP7-transduced cells on the scaffold surface such that the regenerated bone was within the defect site where alveolar bone was removed, as opposed to being mostly ectopic, as originally was found in the fenestration defect pilot study in Chapter 5. A more thorough focus on the selection of growth factors for each region of the scaffold showed that both single (BMP7) and dual (BMP7 and PDGF-BB) delivery promoted the formation of a bone-PDL-like tissue complex most similar to what is natively present *in vivo.* However, this regeneration was observed specifically in regions that included the presence of a patterned film, especially when comparing the results for groups with dual growth factor delivery combined with an amorphous film versus patterned film for the "PDL" region of the scaffold. The primary conclusion from the results observed on Chapter 6 is that the combination of scaffold topography (i.e., patterning, albeit more so for bone anchoring than oriented PDL formation) and growth factor delivery (i.e., BMP7 alone or in combination with PDGF-BB) resulted in improved periodontal tissue regeneration in a mechanically-loaded defect model.

7.2   Future Directions

There are numerous future directions that can be pursued to better understand how the existing scaffold design and controlled growth factor delivery can be improved for more predictable periodontal tissue regeneration, and further extended into more general cases of bone-ligament regeneration. The primary techniques used in this work for scaffold design were 3D

printing and micropatterning. Three-dimensional (3D) printing—also referred to as additive manufacturing—allows for the use of a variety of materials, including metals and polymers, to create 3D structures with defined geometries. Formation of 3D constructs is achieved via printing with inkjet, laser-assisted, and extrusion-based techniques, with variability in the use of selected materials and final resolution capabilities. Designs generated for 3D printing come from computer-aided design (CAD) software or images from clinical scans obtained using computed tomography (CT), magnetic resonance imaging (MRI), or X-rays. Although the most common approach has been to use synthetic polymers to generate material "scaffolds", most recently bioprinting has allowed for direct printing of living cells in combination with materials—increasing their complexity and improving biological properties [1, 2]. This may serve as a future direction for investigating how growth factors and cells could be incorporated into scaffolds so as to allow for a more versatile platform of delivery with a focus on achieving proper tissue alignment [3]. More importantly, this may present a technique for creating scaffolds with encapsulated gene therapy vectors that can transduced cells *in vivo* over time as the scaffold degrades, without the need for pre-seeding with cells, thereby eliminating a potential barrier to clinical translation. Consideration of the regulatory requirements that pertain to such novel therapies is critical, thereby prioritizing treatments that are safer, more defined, and simpler in terms of the number of components used (i.e., limited need for additional steps such as cell seeding prior to implantation, limited use of virus-derived materials).

It is further important to anticipate and more thoroughly address the challenges that are likely to be encountered in the translation of this work to clinical applications. These are specific to the use of viral vectors, as well as human-derived cells not native to the host. As discussed earlier, the immobilization of viral vectors onto the polymer surface reduces the risk of systemic effects that would otherwise be more likely given the presence of virus that has potential to disperse. However, the presence of adenovirus still has potential to lead to infection of cells that were not the intended target, given the lack of cell-specific targeting that is currently only controlled for by saturating the virus-immobilized polymers with cells. A potential way of addressing this may be to use non-viral vectors for gene therapy, which have the disadvantage of having lower cell transduction efficiency, but at the same time avoid the main drawbacks of viral vectors (i.e., cytotoxicity, immunogenicity) that render them safer due to reduced pathogenicity and overall bio-safety [14]. Another translational barrier is the use of cells not originally derived

from the host (i.e., hPDL and hGF cells). Given that these are human-derived and have been shown to have high transduction efficiency using adenovirus, these cells were incorporated into the scaffold regions and transduced prior to implantation to ensure growth factor expression at the defect site, given that lack of cell seeding resulted in a lack of bone and PDL-like tissue formation at 3 weeks in the rat fenestration defect. To improve this aspect of scaffold design, it would be best to incorporate host-derived cells if cell seeding is required prior to implantation, such that the scaffold could be sterilized and ready for implantation into any patient given the availability of their native cells. Since it may be difficult to retrieve and expand hPDL and hGF cells from a human patient, it would be relevant to further investigate if another, more easily accessible patient-derived cell population could be obtained that would show high transduction efficiency with adenovirus or a non-viral gene therapy vector.

Potential incorporation of electrospun fibers into scaffold regions specific to areas intended for PDL regeneration may further improve the percentage of seeded cells (or native cells in cell-free scaffolds) that could be controllably aligned at the defect site [4-5]. Other techniques still utilizing additive manufacturing for achieving PDL-like tissue alignment may also be considered, such as the recently reported use of 3D-printed, angulated grooves reminiscent of PDL-like tissue orientation regions (i.e., parallel, oblique, and perpendicular) that were able to predictably promote cell alignment *in vitro* [6]. Given that the periodontium is comprised of multiple tissues, it is appropriate to use 3D-printed constructs that have defined areas for bone soft (i.e., periodontal ligament) and osseous tissue regeneration. Such materials include both biphasic and triphasic scaffold constructs, which have areas for the cementum/dentin interface, as well as the periodontal ligament/alveolar bone formation interface [7-10]. Further advantage of these compartments is that each can be used to deliver cells (i.e., dental, PDL, and bone stem/progenitor cells), and/or growth factors (i.e., bone morphogenetic protein (BMP), platelet-derived growth factor (PDGF)).

As was earlier described in Chapter 3, a first-in-human case report of a custom-designed, 3D-printed PCL scaffold for the treatment of a large peri-osseous defect was reported in combination with platelet-derived growth factor (PDGF-BB) delivery [11]. The scaffold was fabricated using selective laser sintering (SLS), which allows for material powder to be fused together to form a structure based on a CAD file of the scaffold that was designed from cone beam computed tomography (CBCT) scans of the patient defect. This novel approach provides a promising future application of 3D-printing for customized scaffold designs that can be tailored to

meet patient-specific needs based on defect site and location, with the added ability to deliver growth factors. However, given that the primary limitation of this study was the prolonged degradation of PCL, it would be beneficial to reduce the bulk of polymer used in future applications, while also incorporating more precise features for guiding PDL tissue alignment in addition to osseous tissue regeneration.

The ongoing evolution of 3D printers that are able to produce materials with higher resolution features and with the use of a variety of materials (including more rapidly degradable polymers such as PLGA) will enable the fabrication of scaffolds that are more precisely adaptable to patient defects, accounting for a variety of factors such as variations in material properties based on the expected defect milieu (i.e., transition from bone to ligament tissue) and intended rate of tissue regeneration at the site [12]. To date, 3D-printed materials with specific focus on bone regeneration have been more prevalent in oral based tissue engineering applications. Scaffold porosity is especially relevant in the design and fabrication of these constructs, as it is critical in ensuring adequate micro-architecture for tissue ingrowth at the defect site, in addition to proper vascularization and a tailored rate of biodegradation. 3D printing technology can further help customize pore size, morphology, and interconnectivity. For example, 3D printed glass-ceramic scaffolds with hexagonal designs show a high fatigue resistance compared to conventional architectures, with obtained strengths that are up to 150 times greater than values reported for composite or polymeric scaffolds, making these especially appropriate for use at load-bearing sites [13]. Improvement of the scaffold designs reported here based on these future directions has high potential for their continued evolvement for use in periodontal tissue engineering, with further translation into bone-ligament interface engineering.

7.3   References

[1]   Shafiee A and Atala A. Printing Technologies for Medical Applications. Trends in Molecular Medicine, 2016, Vol. 22, No. 3, p. 254–265.

[2]   Obregon F, Vaquette C, Ivanovski S, Hutmacher DW, Bertassoni LE. Three-Dimensional Bio-printing for Regenerative Dentistry and Craniofacial Tissue Engineering. J Dent. Res. 2015 Sep;94(9 Suppl):143S-52S.

[3]   Park CH, Rios HF, Taut AD, Padial-Molina M, Flanagan CL, Pilipchuk SP, Hollister SJ, Giannobile WV. Image-based, fiber guiding scaffolds: a platform for regenerating tissue interfaces. Tissue Eng Part C Methods. 2014;20(7):533-42.

[4]   Shang S, Yang F, Cheng X, Walboomers XF, Jansen JA. The effect of electrospun fibre alignment on the behavior of rat periodontal ligament cells, *Eur Cell Mater,* 2010;19:180-92.

[5]   Olvera D, Sathy BN, Carroll SF, Kelly DJ. Modulating microfibrillar alignment and growth factor stimulation to regulate mesenchymal stem cell differentiation, *Acta Biomater*, 2017:68:148-160.

[6]   Park CH, Kim KH, Lee YM, Giannobile WV, Seol YJ. 3D printed, microgroove pattern-driven generation of oriented ligamentous architectures, *Int J Mol Sci*. 2017;18(9).

[7]   Lee CH, Hajibandeh J, Suzuki T, Fan A, Shang P, Mao JJ. Three-dimensional printed multiphase scaffolds for regeneration of periodontium complex. *Tissue Eng Part A*. 2014 Apr;20(7-8):1342-51.

[8]   Park CH, Rios HF, Jin Q, Bland ME, Flanagan CL, Holister SJ, Giannobile WV. Biomimetic hybrid scaffolds for engineering human tooth-ligament interfaces. *Biomaterials*, 2010; 31(23):5945-52.

[9]   Ivanovski S, Vaquette C, Gronthos S, Hutmacher DW, Bartold PM. Multi-phasic scaffolds for periodontal tissue regeneration. *J Dent Res*. 2014;93(12):1212-21.

[10]   Costa PF, Vaquette C, Zhang Q, Reis RL, Ivanovski S, Hutmacher DW. Advanced tissue engineering scaffold design for regeneration of the complex hierarchical periodontal structure. *J Clin Periodontol.* 2014; 41(3):283-94.

[11]   Rasperini G, Pilipchuk SP, Flanagan CL, Park CH, Pagni G, Hollister SJ, Giannobile WV. 3D-printed Bioresorbable Scaffold for Periodontal Repair. J Dent Res. 2015 Sep;94(9 Suppl):153S-7S.

[12]   Youssef A, Hollister SJ, Dalton PD. Additive manufacturing of polymer melts for implantable medical devices and scaffolds. *Biofabrication*, 2017;9(1):012002.

[13]   Roohani-Esfahani SI, Newman P, Zreigat H, et al. Design and Fabrication of 3D printed Scaffolds with a Mechanical Strength Comparable to Cortical Bone to Repair Large Bone Defects. Sci Rep. 2016 Jan 19;6:19468.

[14]   Ramamoorth M and Narvekar A. Non Viral Vectors in Gene Therapy-An Overview. *J Clin Diagn Res.* 2015 Jan; 9(1): GE01–GE06.
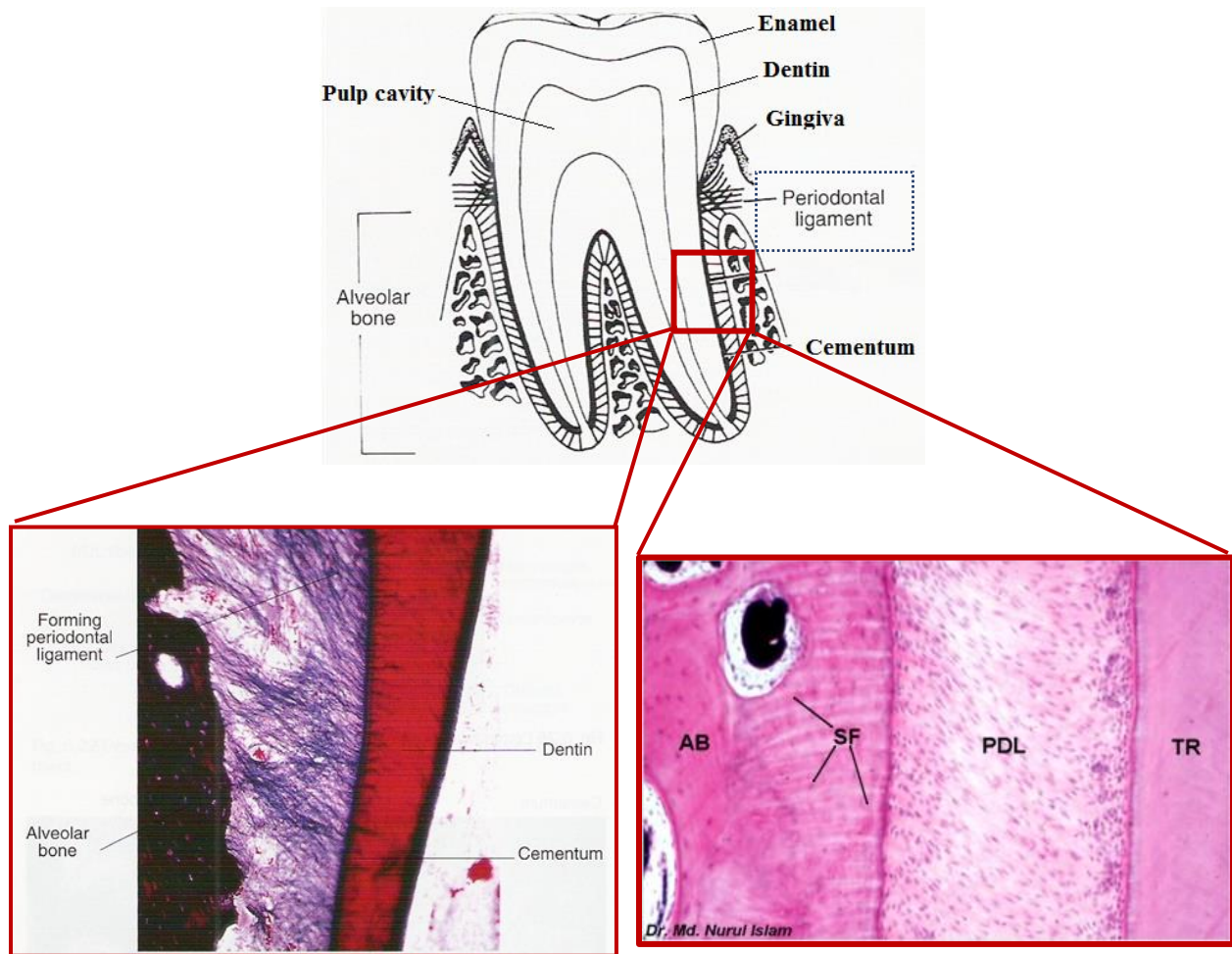
APPENDIX

Figure A1.1 Anatomy of the Periodontium.
Periodontal ligament (PDL) region shown between the tooth root (TR) and alveolar bone (AB), where Sharpey's fiber (SF) bundles (i.e., bundle bone region) are shown between the PDL and AB regions.

Images compiled from: Oral Histology Learning Modules from Syrian Clinic and School of Dental Sciences, Universiti Sains Malaysia.
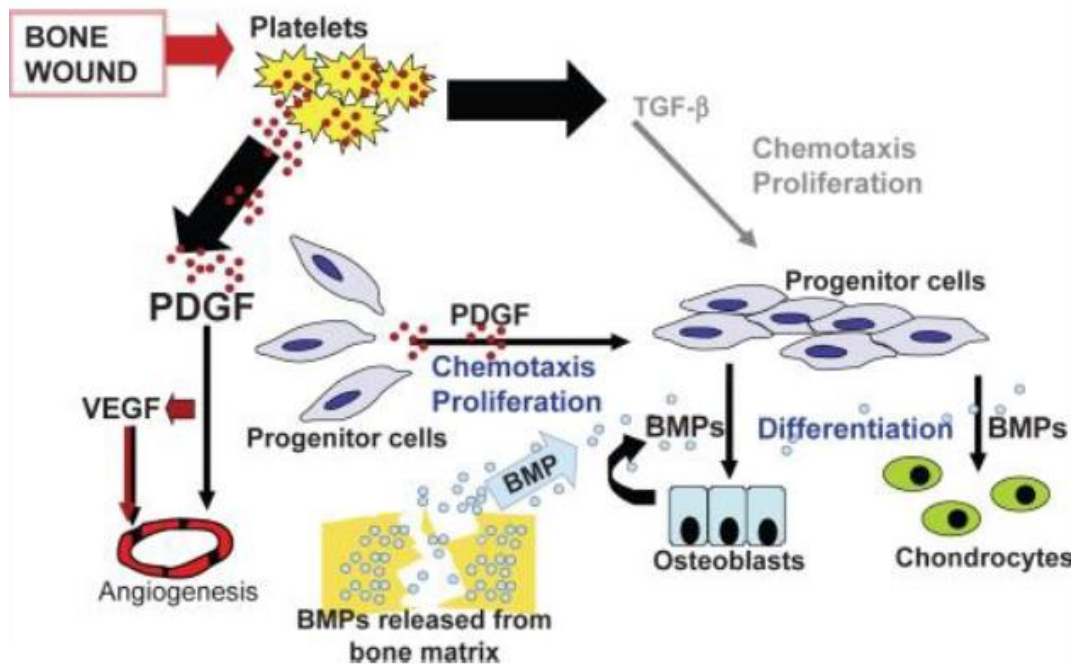
181

Figure A1.2 Wound Healing Process Involving BMP and PDGF
Overview of the wound healing process occurring after bone fracture, showing the cell signaling pathways and types of cells that proliferate as a result of fracture. Recruitment of osteoprogenitor cells occurs in response to bone morphogenetic protein (BMP)-related expression, with other key growth factors involved in angiogenesis and tissue repair, including platelet derived growth factor (PDGF), vascular endothelial growth factor (VEGF), and transforming growth factor beta (TGF).

Image used from: Ghodadra N and Singh K. Recombinant human BMP-2 in the treatment of bone fractures. Biologics; 2008, 2(3):345-54.

Table A1.1 Effects of growth factors on periodontal cells *in vitro.*

Growth factor	Cell type	Effect	Studies
PDGF	Cementoblasts	• Increased DNA synthesis and osteopontin mRNA expression	[51]
	Dental follicle cells	• Stimulated DNA synthesis and expression of CSF-1 and MCP-1	[181]
	Gingival fibroblasts	• Increased mitosis • No increase in proliferation or chemotaxis	[73, 182]
	Osteoblasts	• Increased proliferation and interleukin-6 transcription • Inhibited differentiation • Blocked osteopontin, osteonectin	[54-56]
	PDL cells	• Stimulated proliferation (with or without allograft) • Induced matrix synthesis and increased cell migration and mitosis	[52, 53, 65, 73]
BMP2	Cementoblasts	• Inhibited differentiation and mineralization	[183]
	Dental follicle cells	• Stimulated osteoblast/cementoblast differentiation • Increased mineralization and ALP	[184, 185]
	Gingival fibroblasts	• Decreased mitosis • At high doses, inhibited mineralization and OCN	[73, 186]
	Osteoblasts	• Increased proliferation, mineralization, and expression of ALP and OCN	[187]
	PDL cells	• Increased mineralization and expression of mineralization markers • At doses >10ng/mL, induced apoptosis/cytotoxicity • Stimulated osteoblast differentiation • Decreased mitosis	[72-74]
BMP-7	Cementoblasts	• Increased mineralization and mineralized tissue markers	[102]
	Dental follicle cells	• Increased mineralization and ALP expression	[184]
	Osteoblasts	• Increased proliferation, mineralization, and expression of ALP and OCN	[75, 76, 187]

	PDL cells	• Reduced proliferation • Induced ALP	[188]
FGF-2	Cementoblasts	• Stimulated DNA synthesis • Decreased mineralization and expression of OCN • Modulated expression of OPN	[189]
	Dental follicle cells	• Stimulated DNA synthesis and expression of CSF-1 and MCP-1	[181]
	Gingival epithelial cells	• Increased proliferation	[107]
	Gingival fibroblasts	• Increased proliferation	[190]
	Osteoblasts	• Promoted differentiation • Induced proliferation • Decreased mineralization gene expression	[105, 191]
	PDL cells	• Increased proliferation (alone and combined with DFDBA or FDBA), migration, and extracellular matrix production • Maintained differentiation potential • Stimulated OPN • Inhibited ALP expression, mineralization, and OCN	[103, 104]
GDF-5	CT fibroblasts	• Increased proliferation	[192]
	Dental follicle cells	• Reduced ALP activity	[193]
	Osteoblasts	• Increased early differentiation and matrix production • Modulated proliferation	[114, 192]
	PDL cells	• Increased proliferation and matrix synthesis • Decreased ALP activity	[113]
Teriparatide	PDL cells	• Modified proliferation & survival and expression of mineralized markers (dependent on maturation state)	[123, 124]
ALP: alkaline phosphatase, BMP: bone morphogenetic protein, CSF-1: colony stimulating factor-1, FGF-2: fibroblast growth factor-2, GDF-5: growth/differentiation factor-5, MCP-1: macrophage chemotactic protein-1, OCN: osteocalcin, OPN: osteopontin, PDGF: platelet-derived growth factor, PDL: periodontal ligament			

Table A1.2 Preclinical animal models of growth factor delivery for periodontal and implant applications

Growth factor	Model	Animal	Results	Studies
PDGF-BB	Furcation defect	Canine	• Stimulated PDL formation (early stage) • Promoted periodontal regeneration (late stage)	[64]
	GBR at implants	Canine	• With IGF-1, significantly increased histologic bone-implant contact and peri-implant bone fill • With IGF-1, increased early (3 week) bone formation at immediate implants • With ePTFE membrane and IGF-1, increased bone gain and histologic parameters versus membrane alone or membrane + DFDBA	[57, 65, 66]
	Periodontal defect	Canine	• After flap surgery, increased new bone, cementum and PDL • With IGF-1, promotes periodontal regeneration	[58-60, 63]
		Non-human primate	• Significantly increased new attachment	[61-63, 77]
	Ridge augmentation	Canine	• With block graft, increased histologic bone formation • With bone mineral and collagen membrane, supports lateral bone formation • With biphasic calcium phosphate and collagen membrane, supports GBR • With xenograft scaffold, promoted bone regeneration similar in quality to native bone • With xenograft, improved radiographic results when used without collagen membrane	[68, 69] [67]
rhBMP-2	Extraction socket	Rat	• Increased speed and quantity of bone formation • Induced proliferation and differentiation of mesenchymal cells	[84]
	Furcation defect	Feline	• Early ankylosis may resolve with polymer carrier	[194]

rhBMP-2	GBR at implants	Canine	• Resorbable and ePTFE membranes delay early (1 month) bone formation but may result in increased or similar 3-month bone formation vs. no membrane • Increased bone augmentation for implants placed in extraction sockets and for implant-site circumferential and fenestration defects • BMP2-coated implants provide increased bone formation, histologic bone apposition, and osseointegration • Improved late (3-month) bone formation for ACS versus PLGA carrier	[83, 96, 133, 148, 195]
	Periodontal defect	Non-human primate	• Increased bone and cementum regeneration	[77]
		Canine	• Increased quantity and speed of bone formation • Bone quantity formed correlated with residual bone height • Limited cementum regeneration • Induced ankylosis and root resorption • No benefit for calcium phosphate cement carrier	[78-80, 82, 83]
	Ridge augmentation	Rat	• Significant horizontal and vertical bone augmentation • ePTFE membranes improve bone contour • Increased bone formation with ACS+ bone graft material • Potential carriers: absorbable collagen sponge, hyaluronic acid polymer, • collagen-calcium hydroxyapatite-TCP complex, PLGA/gelatin sponge	[90, 92-94]
		Canine	• Increased histologic and radiographic bone formation, +/- bone graft • Increased incidence of seromas and wound failure • Possible decreased bone quality when combined with bone graft • With xenograft block, supported bone formation	[81, 91, 92, 122]

			• Late-stage implant stability comparable to native bone	
		Non-human primate	• Increased ridge width and bone quality in TCP/HA/ACS and CaP cement carriers	[196]
	Sinus augmentation	Canine	• Enhanced histologic bone formation	[85]
		Rabbit	• Increased bone volume for collagenated BCP/BCP carriers	[86]
		Goat	• Increased radiographic bone formation	[89]
		Non-human primate	• Increased vertical bone gain	[87]
		Mini-pig	• BMP-2 coatings did not improve peri-implant bone gain	[88]
BMP-4	Ridge augmentation	Rat	• Improved bone quality and comparable quantity versus BMP-2	[90]
BMP-7	Furcation defect	Canine	• Significantly increased histologic bone, cementum, and new attachment in class III furcations	[95]
	GBR at implants	Canine	• Implant-coating applications	[96]
		Non-human primate	• Stimulated cementum formation	[99]
	Ridge augmentation	Rat	• Increased bone formation in xenograft block versus control	[197]
	Sinus augmentation	Non-human primate	• Comparable radiographic and histologic bone formation and residual lateral wall defect reduction versus bone graft	[98, 198]
		Mini-pig	• With xenograft, increases speed and quality of osseointegration at simultaneous implants	[100, 101]
	Socket augmentation	Rabbit	• Histologic increased speed of healing by 4-6 weeks • Significantly increased ALP activity and calcium	[97]
FGF-2	Furcation defect	Canine	• Significantly increased regeneration of cementum, PDL, and bone vs. controls	[110, 111]
	GBR at implants	Canine	• Improves peri-implant GBR (β-TCP) • GDF-5 coating may increase bone formation (dose-dependent)	[199, 200]
	Implant coating	Rabbit	• Improved implant stability as determined by pull-out test	[119]

GDF-5	Periodontal defect	Canine	• Significantly increased perio. regeneration in PLGA (dose-dependent), β-TCP, ACS carriers, with bone formation for β-TCP stable up to 24 wks • Beta-TCP/PLGA carrier may cause ankylosis	[116-118, 201]
		Non-human primate	• Supported periodontal regeneration with β-TCP carrier	[115]
	Ridge augmentation	Canine	• With xenograft block, supported bone regeneration	[122]
	Sinus augmentation	Mini-pigs	• Enhanced bone formation with β-TCP	[120, 121]
Teriparatide	Extraction socket	Osteopenic rats	• Increased bone mineral density and anabolic effects	[125]
	GBR at implants	Canine	• Significantly improved bone formation •	[127, 128]
	Periodontal defect	Ovarectimized rats	• Preventative effects on periodontal bone loss	[126]

ACS: absorbable collagen sponge, ALP: alkaline phosphatase, BCP: biphasic calcium phosphate, BMP: bone morphogenetic protein, bTCP: beta tricalcium phosphate, ePTFE: expanded polytetrafluoroethylene, FGF: fibroblast growth factor, GBR: guided bone regeneration, GDF: growth/differentiation factor, HA: hydroxyapatite, IGF: insulin-like growth factor, PDGF: platelet-derived growth factor, PDL: periodontal ligament, PLA: polylactic acid, PGA: polyglycolic acid

Table A1.3 Clinical application of growth factor and protein delivery in periodontics, osseointegration, and pre-prosthetic surgical procedures

Growth factor/ protein	Indication	Evidence level	Efficacy and safety	References
PDGF-BB	Periodontal defects	★★ ★	• Gain in PD, CAL and BOP • Increasing of radiographic bone level	[50, 135-138]
	Furcation involvements	★	• Gain in PD, CAL and BOP • Increasing of radiographic bone level	
	Alveolar bone augmentation/preservation	★	• Accelerate the healing process	
BMP-2	Alveolar bone augmentation/preservation	★★	• Accelerate the healing process • Histological findings high proportion of newly formed bone	[141-144, 146-149]
BMP-7	Sinus augmentation	★★	• In combination with allogeneic/autologous bone graft: histologic findings similar to autologous bone and adequate vertical bone gain (BMP-2) • In combination with bovine-derived xenogeneic graft: histologic findings show less new bone compared to xenograft alone but adequate vertical bone gain (BMP-2, BMP-7)	
GDF-5	Periodontal defect	★	• Gain in CAL	[150, 151]
	Sinus augmentation	★	• Histologic results similar to autologous bone • Adequate vertical bone gain	
FGF-2	Periodontal defects	★	• Early radiographic bone fill	[152]
Teriparatide	Peri-implant bone	★	• Gain in PD and CAL • Increasing radiographic bone level • Greater bone-to-implant contact in the periosteal and medullary compartment • Minimal effect on cortical compartment • Slight higher bone-volume-per-tissue-volume	[154, 155]
Evidence level= (★) Slight clinical evidence; (★★) Moderate clinical evidence; (★★★) Robust clinical evidence; Clinical parameters= (PD) pocket depth; (CAL) clinical attachment level; (BOP) bleeding on probing				